AWARD NUMBER: W81XWH-15-1-0303

TITLE: Primary Blast Injury Criteria for Animal/Human TBI Models using Field Validated Shock Tubes

PRINCIPAL INVESTIGATOR: Dr. Namas Chandra

CONTRACTING ORGANIZATION: New Jersey Institute of Technology
Newark NJ 07102-1824

REPORT DATE: Sept. 2018

TYPE OF REPORT: Annual

PREPARED FOR: U.S. Army Medical Research and Materiel Command
                     Fort Detrick, Maryland 21702-5012

REPORT DOCUMENTATION PAGE

1. REPORT DATE	2. REPORT TYPE	3. DATES COVERED
September 2018	Annual	15 Aug 2017 – 14 Aug 2018

4. TITLE AND SUBTITLE
Primary Blast Injury Criteria for Animal/Human TBI Models using Field Validated Shock Tubes

5a. CONTRACT NUMBER
W81XWH-15-1-0303

5b. GRANT NUMBER
14059001

5c. PROGRAM ELEMENT NUMBER

6. AUTHOR(S)
Maciej Skotak, Kakulavarapu V. Rama Rao, Molly T. Townsend, Namas Chandra

E-Mail: namas.chandra@njit.edu

5d. PROJECT NUMBER

5e. TASK NUMBER

5f. WORK UNIT NUMBER

7. PERFORMING ORGANIZATION NAME(S) AND ADDRESS(ES)

New Jersey Institute of Technology
323 Martin Luther King Jr Blvd
Newark NJ 07102-1824

8. PERFORMING ORGANIZATION REPORT NUMBER

9. SPONSORING / MONITORING AGENCY NAME(S) AND ADDRESS(ES)

U.S. Army Medical Research and Materiel Command
Fort Detrick, Maryland 21702-5012

10. SPONSOR/MONITOR'S ACRONYM(S)

11. SPONSOR/MONITOR'S REPORT NUMBER(S)

12. DISTRIBUTION / AVAILABILITY STATEMENT

Approved for Public Release; Distribution Unlimited

13. SUPPLEMENTARY NOTES

14. ABSTRACT

Blast-induced Traumatic Brain Injury (bTBI) is a leading cause of morbidity in soldiers on the battlefield and training sites with long-term neurological and psychological pathologies. We characterized in details of the mechanisms triggered by loss of the blood-brain barrier (BBB) integrity: extravasation of exogeneous markers, depleted tight junction proteins (occludin and claudin-5), and blood serum levels of endogenous proteins. we established there exist complementary temporal trends. The expression of these proteins decreases in the brain tissue homogenates, which is accompanied by elevation of their levels in the blood serum. The effects of oxidative stress on the BBB integrity and repair were also evaluated. The influx of the exogeneous matter into the brain parenchyma triggers a cascade of inflammatory response. We developed a refined model of the rat head under shock wave loading. A comprehensive convergence study and extensive model refinement resulted in a model which reproduced spatial and temporal maps of the pressure, stress, and strain within the rat brain at three blast overpressures (100, 130, and 190 kPa). We demonstrated control over shock wave pressure profile and established a set of conditions where peak overpressure remains constant with gradation of impulse. This level of control is yet to be demonstrated in the available literature on the subject. The developed dose-response models indicate predicted mortality rate is shifted towards lower peak overpressures at higher impulse values. This means that both blast overpressure and impulse are critical in bTBI and not just BOP. This report covers findings of the year 3 of the project (tasks 8, 9 and 10) and it summarizes the findings of all the tasks 1 to 7 of years 1 and 2.

15. SUBJECT TERMS
Blast Induced Neurotrauma, Blast TBI, Primary blast brain injury, Blast overpressure, Impulse, Intracranial Pressure, Pressure measurement, Blood-brain barrier, Neuroinflammation, Oxidative stress, Finite element numerical models.

16. SECURITY CLASSIFICATION OF:			17. LIMITATION OF ABSTRACT	18. NUMBER OF PAGES	19a. NAME OF RESPONSIBLE PERSON USAMRMC
a. REPORT	**b. ABSTRACT**	**c. THIS PAGE**	Unclassified	185	**19b. TELEPHONE NUMBER** *(include area code)*
Unclassified	Unclassified	Unclassified			

Table of Contents

1. INTRODUCTION

The focus of our research is the role of compromised blood brain barrier (BBB) on the evolution of blast neuropathology after a single blast. We expanded our studies to incorporate inquiry into the mechanisms triggered by leaky BBB. First, we investigated the faith of the dislodged tight junction proteins (TJPs): occludin and claudin-5, and we established there exist complementary temporal trends. The expression of these proteins decreases in the brain tissue homogenates, which is accompanied by elevation of their levels in the blood serum. Additionally, we observed the leakage of S100β protein into the blood stream and concluded that the opening of the BBB has a temporary character. The concentration of this biomarker returned to baseline after 24 hours after reaching the maximum at 4 hours post blast exposure. Furthermore, we examined the mechanisms responsible for BBB permeability following moderate blast exposure (180 kPa). Several studies implicate oxidative stress resulting from the activation of the family of NADPH oxidases (NOX), responsible for superoxide production, as a mechanism for BBB disruption in various TBI models [1-3] and non-TBI neurological conditions [4-6]. We, therefore, examined the effect of apocynin that inhibits the assembly of different NOX subunits and renders NOX inactive, on BBB permeability following moderate blast exposure. First, we investigated the protein expression of NOX1 in vascular endothelial cells and found that NOX expression significantly increased 4h post injury. We next examined the effect of NOX inhibitor apocynin on superoxide production, tight junction protein (TJP) expression, EB extravasation and translocation of astrocytic protein GFAP from the brain to blood as well as albumin/CSF ratio as measures of BBB disruption. We found that apocynin significantly attenuated alterations in the above factors. We investigated the neuroinflammatory consequences of the blast exposure and identified the temporal pattern of the microglia activation. We hypothesized that microglia respond to the exogenous material transported to the brain parenchyma via compromised BBB, and the activation is reversible once all exogenous debris is cleared. Thus, we examined the temporal profiles of pro-inflammatory cytokines TNF-α and IL-1β in brain homogenates from hippocampus and thalamus in rats exposed to moderate blast injury (180 kPa). We found that both TNF-α and IL-1β displayed temporal changes in the expression.

We performed optimization and refinement of our numerical models and processing routines. Among three different models of the shock tube and its surroundings, it appears that a model of the shock tube with properly adjusted material constrains results in quality simulations. This is an important stem to optimize the computational efficiency in these studies. An unbiased mesh was used as the added fidelity did not result in an unacceptable increase in simulation time. A refinement of the brain model of the rat was performed, and additional mesh refinement was conducted to verify that simulation results were not artifacts of the mesh. Substantial revisions were made to the rat head and shock tube finite element models. A comprehensive convergence study and extensive model refinement resulted in a model which reproduced spatial and temporal maps of the pressure, stress, and strain within the rat brain at three blast overpressures (100, 130, and 190 kPa).

The control over shock wave profile characteristics is one of the many recent advances from our laboratory. This level of control over shock wave characteristics, to our knowledge, is yet to be demonstrated in the existing literature in the blast TBI research field. We have also established a set of dose-response curves correlating the mortality rates with peak overpressure and impulse of the incident shock wave, where extended impulse values were used. Resulting mortality rates indicate a shift towards lower peak overpressure at higher impulse values. We performed biomechanical loading evaluation on rats implanted with three sensors: two in the brain and a single sensor in the carotid artery. The measurements were performed at three nominal BOPs: 130, 180 and 230 kPa with variable impulse values and experimental results indicate intracranial pressures follow the incident shock wave pressure. The heads of rats were imaged using a micro-CT scanner to establish the precise location of the cannulas where pressure sensors were implanted. This information is then used in the development of the validated refined numerical model of the rat's head under shock wave loading conditions.

2. KEYWORDS

Blast Induced Neurotrauma, Blast TBI, Primary blast brain injury, Blast overpressure, Impulse, Intracranial Pressure, Pressure measurement, Blood-brain barrier, Neuroinflammation, Oxidative stress, Finite element numerical models.

3. ACCOMPLISHMENTS

Major Goals of the Project (Statement of Work with Timeline):

STATEMENT OF WORK	Year 1				Year 2				Year 3				Year 4			
Project Steps	Q1	Q2	Q3	Q4	Q1	Q2	Q3	Q4	Q1	Q2	Q3	Q4	Q1	Q2	Q3	Q4
SA 1: Develop Master Dose Response Curves for 10 week old SD rats																
Task 1: Evaluate Mortality Rates and Biomechanical Loading in Wide Range of Blast Intensities		▬														
Task 2: Determine the Biomechanical Loading of the Rat Brain During Simulated Blast		▬	▬													
Task 3: Numerical Simulation of Brain Injury			▬	▬												
Milestone 1: Master Dose Response Curve Developed					✛											
SA 2: Assess Pathologies in Mild-to-Moderate bTBI Range 24 hours After the Exposure																
Task 4: Evaluate the Lung Injuries Caused by Blast Exposure						▬										
Task 5: Assess Extent of Oxidative/Nitrosative Stress, BBB Damage and Neuroinflammation						▬	▬									
Task 6: Examine Plasma Membrane Damage Using Fluorescent Tracers							▬	▬								
Task 7: Evaluate Alterations in Brain Proteome After Primary Blast Exposure							▬	▬								
Milestone 2: Brain Injury/Blast Load Correlated with Biomarkers									✛							
SA 3: Examine the Effect of Blast Impulse on Master Dose-Response Curve																
Task 8: Establish Master *Impulse* Dose-Response Curve at Three Blast Overpressures									▬	▬						
Task 9: Examine Changes in Protein Expression Due to Changes in Blast Impulse										▬	▬					
Task 10: Determine Alterations of Loading in the Rat Brain Caused by Changes in Impulse										▬	▬					
Milestone 3: The Effects Associated With Blast Impulse Identified												✛				
SA 4: Establish Human Injury Criterion for Blast TBI - the Cross-Species Correlation Function																
Task 11: Identify Cross-Species Milt-To-Moderate bTBI via Numerical Simulations													▬	▬		
Task 12: Comprehensive Characterization of Blast Loading in PMHS Head Model														▬	▬	
Task 13: Devise Transfer Function to Correlate Rat and Human Blast Overpressure Conditions															▬	
Milestone 4: The Human Injury Criterion Established																✛

In the three years of the project, we have completed all the tasks included in the experimental design of years 1 and 2 (tasks 1 to 7) and majority of year 3 plan (work on task 9 is still ongoing). The major accomplishments in the current year are listed below:

1. Developed a dose-response master curves, which indicate <u>mortality rates are higher for the larger impulse values</u> at the same peak overpressure. This means that measuring only overpressure may not be enough to predict neurological outcome.
2. This report presents the most comprehensive map of the temporal evolution of pressure, stress, and strain within a rodent model of the brain when subjected to shock loading.
3. Extravasation of fluorescent markers identified biphasic temporal response of BBB damage
4. Extravasation indicated the regional vulnerability of the BBB
5. Demonstrated the role of oxidative stress and MMPs in the BBB damage
6. Demonstrated the depletion of tight junction proteins in the brain tissue and their increase in the blood
7. Comprehensive characterization of inflammatory response to a single blast
8. Demonstrated the efficacy of apocynin as a therapeutic to counter blood-brain barrier permeability following blast injury
9. Demonstrated for the first time the control over shock wave pressure characteristics: constant peak overpressure with variable impulse
10. Demonstrated for the first time the effects elicited by static electricity on the shock wave profile: the impulse values are diminished by 30%-50% for unprotected sensor operating conditions
11. This work is the first to consider validation of the numerical model by using precise sensor locations based on micro-CT scans of animal heads
12. Our numerical modeling validation is performed at more than a single blast overpressure using two intracranial pressure measurements
13. This work is the first rat numerical model to consider the exact experimental measurement locations in data reporting.

In the first two years of the grant, some of the key accomplishment achieved are added for the sake of completion.

We have made significant advances in the development and operation of shock tubes to replicate live-fire exposure from very low to extremely high blast loading conditions. Reproducing right shock pulse is the first step in understanding blast injury mechanisms. Many research groups do not adhere to this important step. Our design is the gold standard, now used in many government laboratories and universities.

- With the right field-validated blast loading, for the FIRST TIME, we developed and published load-response curve for rat models delineating none, mild, moderate, severe and lethal TBI based on blast overpressure and impulse (**Nature-Sci. Rep., 6:26992, 2016**). This work is a product of task 1 which significantly enhanced the quality of our earlier observations and has been cited 33 times.
- We also outlined how to achieve the right pulse by comparing live-fire measurements with shock tube data (**Mil. Med., 2018. 182, 105-113**). The data showed that a shock tube can produce the exact profile observed on a surrogate headform under a field shock.
- We further enhanced how to achieve the right conditions by using end plates and animal placements (**PLoS ONE, doi: 10.1371/jounal.pone.0161597, 2016**)
- Through many invited talks, poster presentations, DOD conferences we have now firmly established how to conduct shock tube testing for animal models.
- To understand the mechanisms of BINT (blast induced neurotrauma) in rats and in humans we need measure how external shock causes tissue-level loading. This tissue-level loading is the basis for "scale-up from rats to humans" that the MOMRP is interested in. For the FIRST TIME, we measured ICP (intracranial pressure) and carotid pressure in rats during blast loading at a very wide range of BOP. As shown in Figure 8 of the 2016 Annual Report, the measurements indicated that the ICP is similar to the applied profile. Such measurements in other species will help in the validation of computational models of rats. Currently, there are no FEM that are validated based on actual ICP measurements of rats under a variety of different blast conditions. Hence this is an important contribution for FEM validation and inter-species scaling.
- The work reported in the 2018 Annual Report will represent the most robustly validated numerical model of blast-induced TBI in a rodent. It is the first to be validated with multiple blast overpressures and offers a unique platform to investigate blast injury mechanisms. A manuscript based upon this work from Tasks 3 and 10 is currently under review.
- We showed unequivocally that blast pathology is very different from blunt or ballistic injuries. When blast attacks the head/brain, the shock wave traverses the brain and produces pathological changes from proximal to distal brain structures (i.e., prefrontal cortex to cerebellum, **J. Neurotrauma, 35:1-14, 2018**). Moreover, we for the first-time reported cell-specific responses in oxidative stress responsive factors in different brain regions following blast injury (Task 5) (see above manuscript).
- The results obtained on blood brain barrier permeability (Task 5) is a comprehensive piece of work, where we established, for the first time, a low threshold of BOP (35 kPa or 5 psi) wherein blood brain barrier permeability changes do not occur. These observations have never been reported before and has a significant bearing in understanding the relationship

6

between BOP and injury pathology. This work was published in **Nature-Sci. Rep., 8(1), 8681, (2018).**

- Our work in shows that blast injury is affected not only by blast overpressure but also impulse. We demonstrated for the first time the control over the impulse at arbitrarily chosen fixed peak overpressure. . This is an important finding, as only peak overpressure is reported in the field and laboratories. However, that is insufficient to determine the degree of injury severity to the soldiers. This work will be reported this year, and we are preparing a manuscript based on the data. In the scientific literature the impulse effects are neglected, and only in a small fraction of studies (10% out of 100 screened papers, **Front. Neurol. doi: 10.3389/fneur.2018.00052**) impulse values are reported.

- We identified piezoelectric pressure sensors are susceptible to electrostatic interference. These sensors (e.g. PCB 134A24) are widely used in the shock tube testing to measure the pressure experienced by animal models, and when exposed to electrostatic charges inherent to shock wave report erroneous pressure values. Manufacturers of these sensors were unaware of this effect in spite of decades of development and their own shock tube testing. These findings are summarized in **Front. Neurol.** (See above), which also serves as a guideline how to avoid pitfalls in pressure measurements while conducting shock tube testing, to guide other research groups.

- The follow up manuscript is in preparation, which will demonstrate quantitative effects associated with electrostatic interference on accuracy of reported pressure. In a nutshell, while peak pressures are mostly unaffected, the duration and impulse in extreme cases were decreased by 50%. We noted blast gauges used to monitor low-level blast exposure in training are susceptible to similar artifacts resulting in underreporting of peak overpressure and impulse values by the algorithm embedded in the blast gauge software. We shared our expertise in this area with the team of Dr. Kamimori (WRAIR), which helped improve the quality of the data collected in their studies on human subjects.

Task 3: Numerical Simulation of Brain Injury (completed)

Previous work conducted which used a numerical model to simulate the local stress and strain fields within the rat brain resulted in noisy signals which required filtering to result in an accurate intracranial pressure field [7]. This prompted a refinement of the numerical simulation. Substantial revisions were made to the rat head and shock tube finite element models. Details of the findings of these revisions were presented in two posters at the Institute for Brain and Neuroscience Research E-Poster Day and in an oral presentation at the Institute of Nuclear Medicine & Allied Sciences, the abstracts of which are included in the appendices. A comprehensive convergence study and extensive model refinement resulted in a model which reproduced spatial and temporal maps of the pressure, stress, and strain within the rat brain at three blast overpressures (100, 130, and 190 kPa).

Rat Lagrangian Model

A geometrical model of a ten-week old Sprague Dawley rat was generated by combining a magnetic resonance image (MRI) of a rat head, a micro-computed tomography (micro-CT) scan of the rat skull, and a geometrical representation of the rat body. The micro-CT scan of the rat skull was taken at a resolution of 35.6 μm (SkyScan 1275, Bruker microCT, Kontich Belgium) and was segmented into a solid mask (Simpleware ScanIP, Synopsys, Exeter, United Kingdom). The segmented mask was then imported with the MRI DICOM and co-registered. As different specimens were used, three-dimensional scaling was conducted to ensure accurate co-registration. The MRI images facilitated the segmentation of the soft tissues, which include the skin, brain, and the dura mater. A geometrical model representing the average dimensions of a 50th percentile rat body was combined with the segmented masks[8]. For simplicity, the geometrical model of the rat body was simulated as a skin material and did not have internal segmentation. The model is shown in Figure 1.
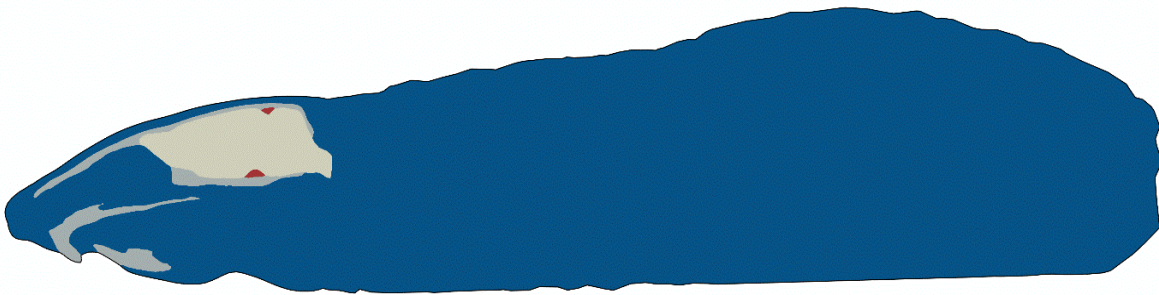

Figure 1 The internal segmentation of the rat Lagrangian model as observed with a mid-sagittal cut. The skin is depicted in blue, the skull in grey, the dura mater in red, and the brain in beige.

The model was meshed using a 10-node modified tetrahedral biased mesh, with an average minimum edge length of 0.75 mm and average maximum edge length of 1.25 mm at the regions of interest (Simpleware FE, Synopsys, Exeter, United Kingdom). This mesh density was selected based on the results of a convergence study, which highlighted that increasing the mesh density did not result in a substantial improvement in pressure predictions (defined to be a 5% change). Material properties used to approximate the mechanical response of the rat head tissues are included in Table 1.

Shock Tube Eulerian Model

A three-dimensional geometrical model was generated of the nine-inch shock tube, simulating a portion of the test region that was 3.3 m in length. The shock tube was modeled as an 8-node hexahedral Eulerian mesh with reduced integration and hourglass control with a minimum average mesh seed length of 6 mm at the region of interest (Abaqus/CAE, Dassault Systems, Vélizy-Villacoublay, France). The region of interest was 0.6 m in length which, when assembled, contained the full extent of the Lagrangian rat model. The air within the shock tube model was simulated as an equation of state at with ambient conditions (an air density of 1.225 kg/m^3 at 291 K) using the parameters in Table 1.

Table 1 Material properties used in the numerical simulation of shock.

		Linear Elastic		
	Elastic Modulus		Poisson's Ratio	
Skull[9, 10]	9500 MPa		0.3	
Soft Tissue[11]	16.7 MPa		0.42	
Dura[9]	20.0 MPa		0.45	
		Linear Viscoelastic		
	Long-Term Bulk Modulus	Poisson's Ratio	Shear Modulus	Relaxation Time Constant
Brain[12]	2.19 GPa	0.4999	1.05 MPa	0.02 s
		Ideal Gas Equation of State		
	Gas Constant		Specific Heat	
Air	287 J kg^{-1} K^{-1}		1010 J kg^{-1} K^{-1}	

Shock Simulation

The Lagrangian rat head was positioned within the Eulerian shock tube mesh so that it was in the center of the shock tube at the test section in a prone position. The entire body of the rat model was fixed in all rotational and translational degrees of freedom, to mirror the experimental methods of strapping down the rat body. The two domains were allowed to interact using Eulerian-Lagrangian contact. The Eulerian volume fraction was used to assign the elements which were filled with air, partially filled with air, or void of Eulerian material. This initial condition was based upon the surface generated at the interface between the Lagrangian part and the Eulerian material, as defined using an enhanced immersion boundary method. An initial step of 25 ms was conducted
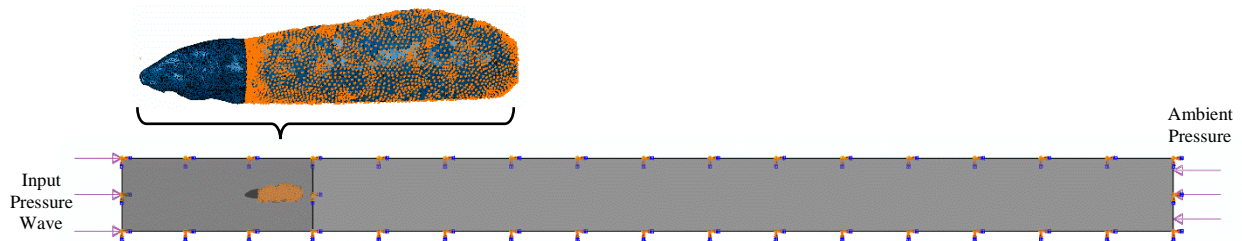

Figure 2 A lateral depiction of the input conditions used to simulate shock loading on the Lagrangian rat head. The shock tube Eulerian mesh is shown in grey. Pink arrows show the pressure loading locations. The left face, the opening of the shock tube model, is loaded with the pressure profiles shown in Figure 3. The right face is loaded with a constant pressure equivalent to the ambient pressure conditions. The orange and blue arrows indicate that a face is constrained in all degrees of freedom. This boundary condition was applied to the rat body, as shown in the above enlarged depiction of the Lagrangian model, and the walls of the Eulerian instance.

to initialize the system and to resolve this boundary condition, allowing the system to reach homeostasis (Abaqus/Explicit). During this step, the shock tube walls and the shock tube opening were constrained against all translational degrees of freedom. The exit of the shock tube experienced a distributed pressure load equal to ambient pressure (102.3 kPa).

At the end of this step, an explicit dynamic analysis was conducted to simulate the shock. These boundary conditions are summarized in Figure 2. The shock tube opening was subjected to a time-varying pressure load. This pressure load was calculated from the experimental pressure measurements taken at the location of the simulated shock tube opening. Eight pressure measurements were taken for each overpressure (four animals and two blasts per animal). The signals were normalized for arrival time, and the mean profile was taken. To ensure that the simulation was not affected by experimental variability, experimental consistency was examined. The average input pressure profiles used are depicted in Figure 3 with one standard deviation. As in the previous step, the translational degrees of freedom of the shock tube walls were constrained, and the exit of the shock tube was subjected to a pressure load equal to ambient pressure.
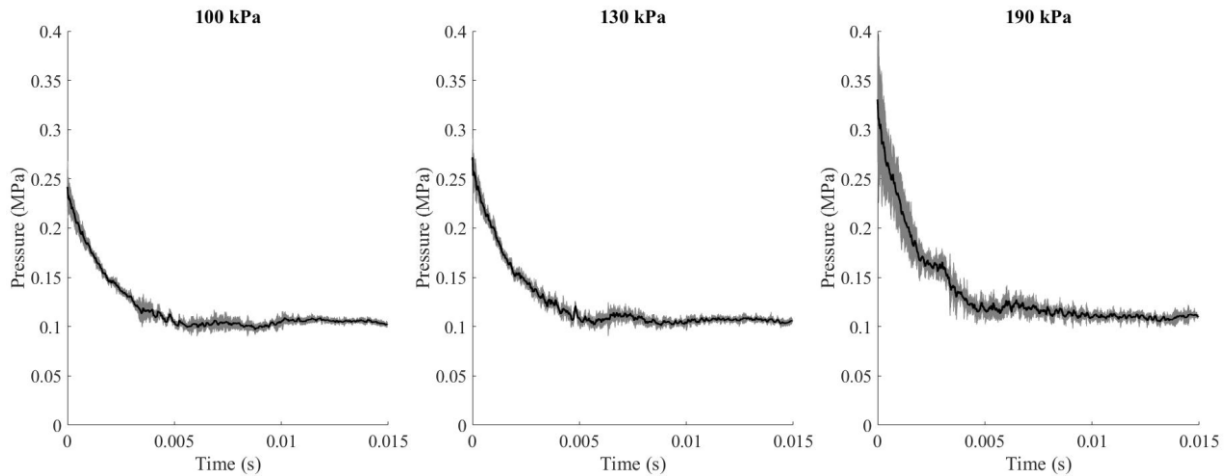
Figure 3 Input pressure profiles used in the simulation of the shock wave. The mean pressures are depicted in black and the standard deviation is included in grey.

Field variables were sampled from the solution at a variable sampling rate. This was done to ensure that adequate resolution was obtained in the solutions. The sampling rates are described in Table 2. From these points, it was found that the shock wave hit the rat head at 0.818, 0.807, and 0.780 ms, for the 100, 130, and 190 kPa blasts, respectively.

Table 2 The time points from which the simulation output was sampled.

Step:	Start Time (Step)	End Time (Step)	Start Time (Total)	End Time (Total)	Sampling Rate
Initialization	0 ms	25 ms	0 ms	25 ms	800 Hz
Shock	0 ms	0.78 ms	25 ms	25.78 ms	5 kHz
	0.78 ms	0.98 ms	25.78 ms	25.98 ms	1 MHz
	0.98 ms	5 ms	25.98 ms	30 ms	100 kHz
	5 ms	88.25 ms	30 ms	113.25 ms	10 kHz

Pressure Maps

The pressure within the rat brain was mapped temporally in Figures 4-6. To give perspective on the magnitude of the observed intracranial pressures these values are reported as a multiplicative

factor to the blast overpressure. For the lowest blast overpressure simulated, 100 kPa, the maximum pressures observed were on the order of three times higher than the blast overpressure (a maximum pressure of 300 kPa, Figure 4). The pressure begins to develop in the anterior region of the brain, beginning in the olfactory bulb, 64 μs, 51 μs, and 54 μs after the wave begins interacting with the headform for the 100, 130, and 190 kPa blast. This generates a pressure wave which traverses the brain which is of a lower magnitude, closer to the value of the incident waveform, indicated by a multiplier value of 1. This waveform traverses the brain very uniformly, followed by an underpressure in the anterior brain. The locations which see the highest intracranial pressures occurred in the brainstem in all blast overpressures. These high pressures are observed, in each case, over 1 ms after the shock wave has passed over the specimen. This location of interest, posterior to the cerebellum in the brain stem, is the location in which the brainstem passes through the foramen magnum. It was found that the pressure is transmitted through the skull and loads the brainstem with an additional pressure wave. Additionally, it can be observed that the pressure wave results in an oscillatory pressure. The pressure wave develops shortly after the shock wave interacts with the specimen, can be observed to decay approximately around 3-4 ms after the shock wave interacts with the specimen, and then increase again after 12.5 ms.
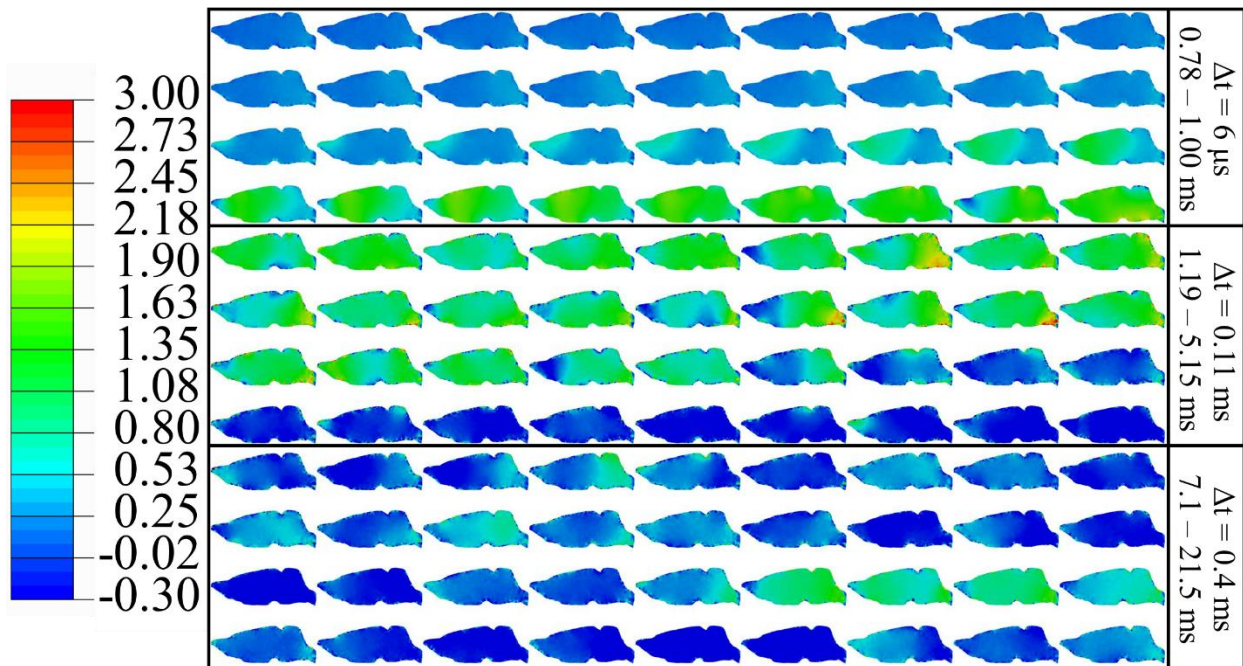

Figure 4 A temporal pressure map, reported as a multiple of the incident overpressure, of the mid-sagittal cut of a rat brain over the course of a 100 kPa shock wave. The earliest time point is in the upper left corner and time progresses at the time step Δt, moving left to right from the top to the bottom.
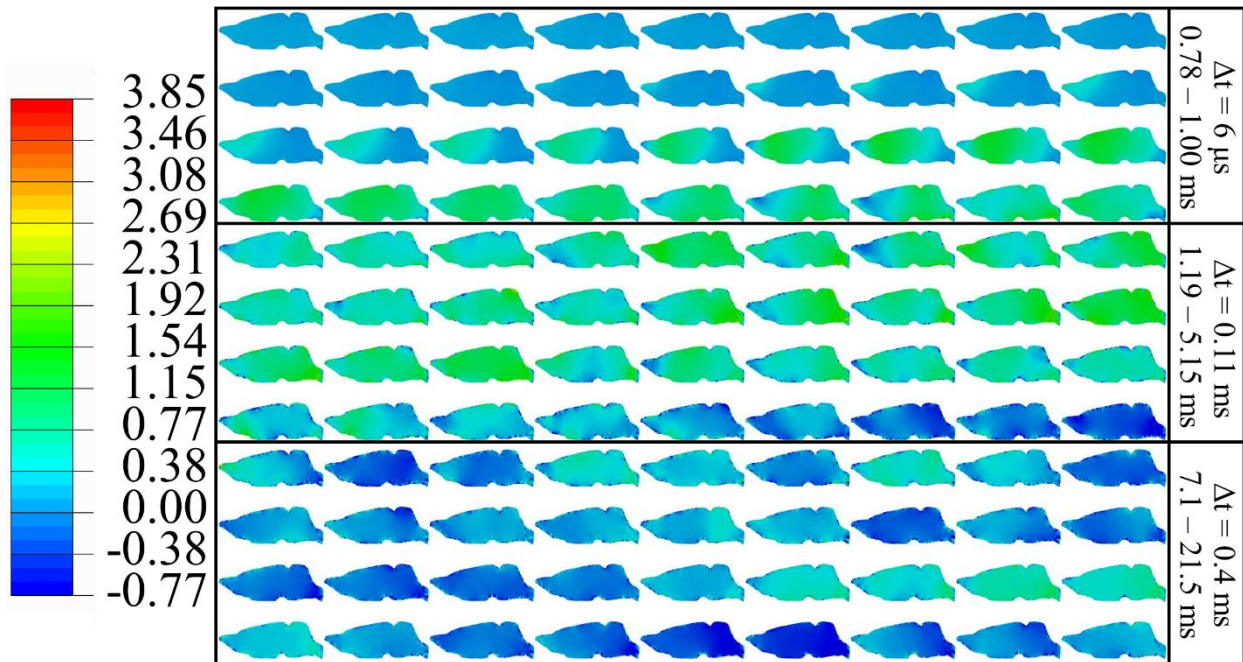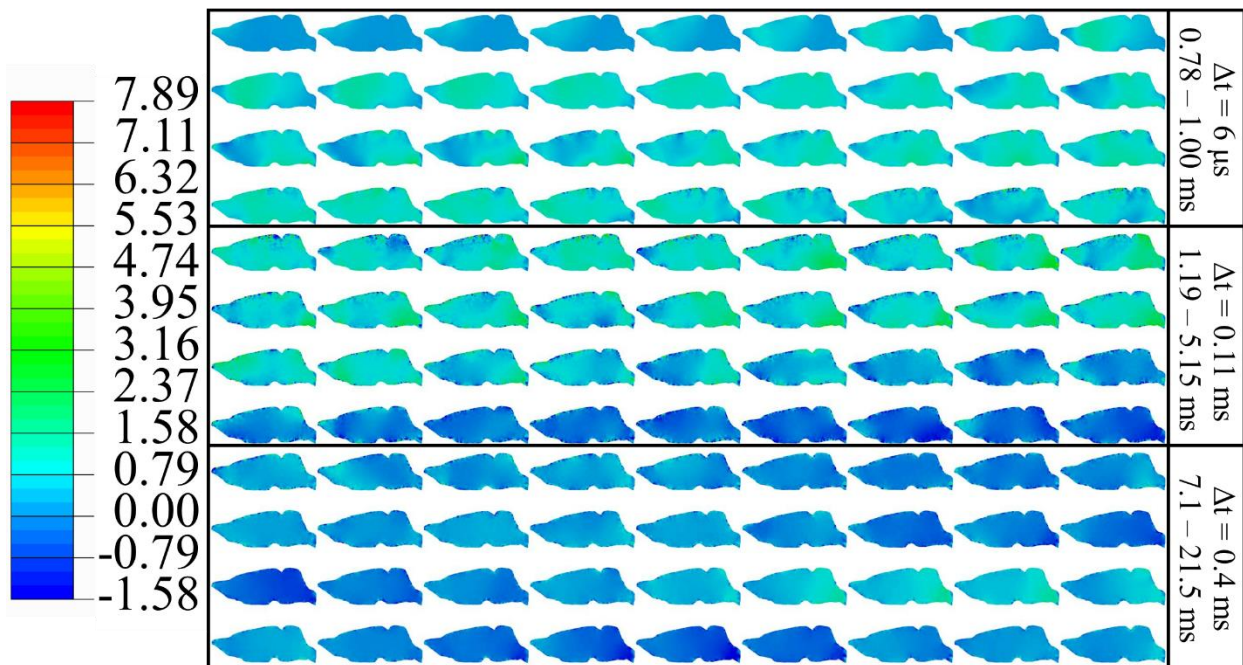
Figure 5 A temporal pressure map, reported as a multiple of the incident overpressure, of the mid-sagittal cut of a rat brain over the course of a 130 kPa shock wave. The earliest time point is in the upper left corner and time progresses at the time step Δt, moving left to right from the top to the bottom.

Figure 6 A temporal pressure map, reported as a multiple of the incident overpressure, of the mid-sagittal cut of a rat brain over the course of a 190 kPa shock wave. The earliest time point is in the upper left corner and time progresses at the time step Δt, moving left to right from the top to the bottom.

Stress Distribution

Figures 7-9 detail the temporal evolution of the von Mises stress in the mid-sagittal plane of a rat head for a 100, 130, and 190 kPa shock wave, respectively. The von Mises stress is reported in values of kPa. When comparing the spatial variation of the von Mises stress with the pressure waves in Figures 4-6, it is apparent that the von Mises stress is more diffuse and is of a lower magnitude than that of the pressure wave. The initial pressure wave does not appear to significantly induce a von Mises stress and peak von Mises stresses are not observed until the time point in which the pressure wave passes through the skull and loads the brainstem through the foramen magnum. Additionally, the von Mises stresses develop more at the periphery of the brain, converging toward the center of the brain. This supports the hypothesis that the skull is loading the brain with additional pressures and stresses. The development of the von Mises stresses in the brain appears to occur around the same time point as the pressure decay. However, this does not appear to have any correlation with the secondary increase in pressure observed in Figures 4-6. The magnitudes of the maximum von Mises stresses were not found to scale linearly with blast overpressure. When normalized with respect to the incident pressure wave, the maximum von Mises stresses for a 100, 130, and 190 kPa overpressure are 1.20, 1.46, and 1.58, respectively. These peak von Mises stresses appears to be greater on the ventral side of the brainstem.
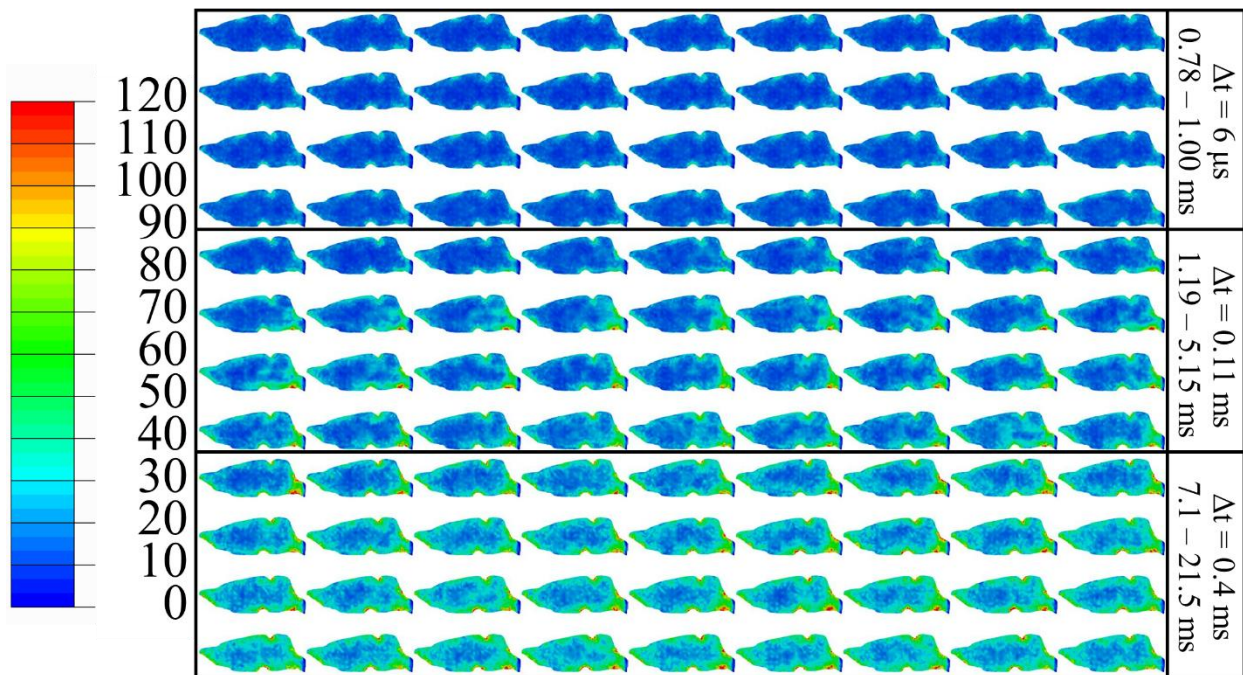

Figure 7 A temporal von Mises stress map, given in kPa, of the mid-sagittal cut of a rat brain over the course of a 100 kPa shock wave. The earliest time point is in the upper left corner and time progresses at the time step Δt, moving left to right from the top to the bottom.
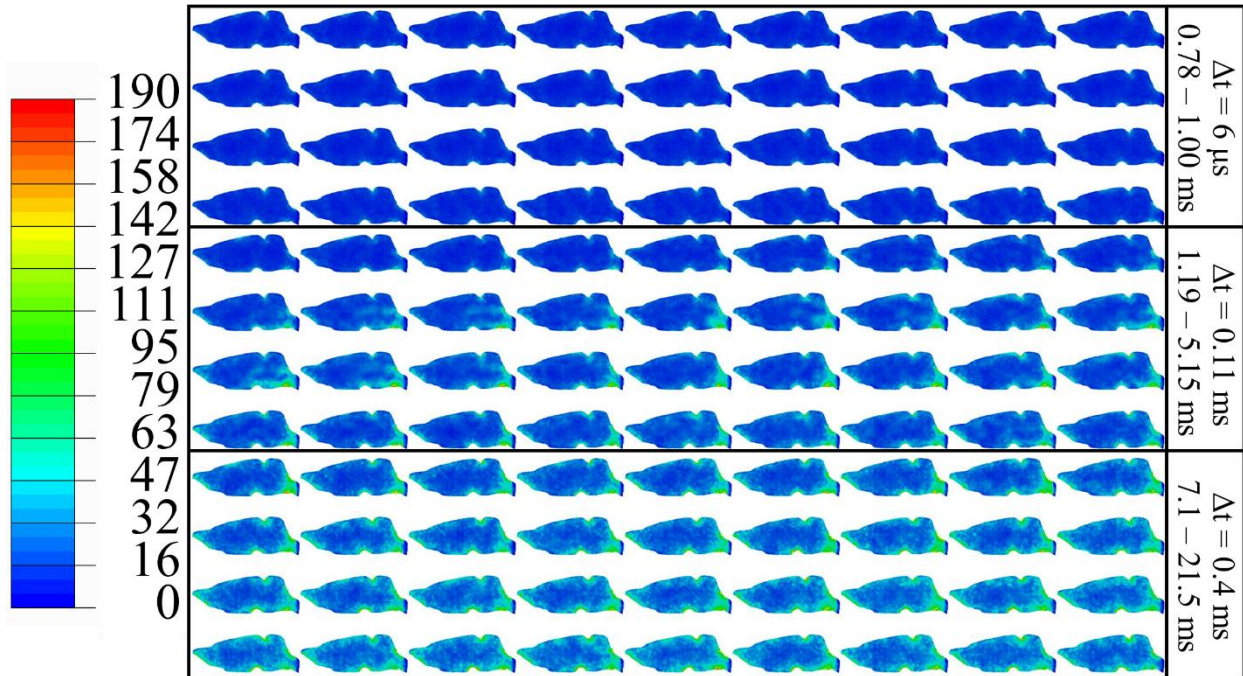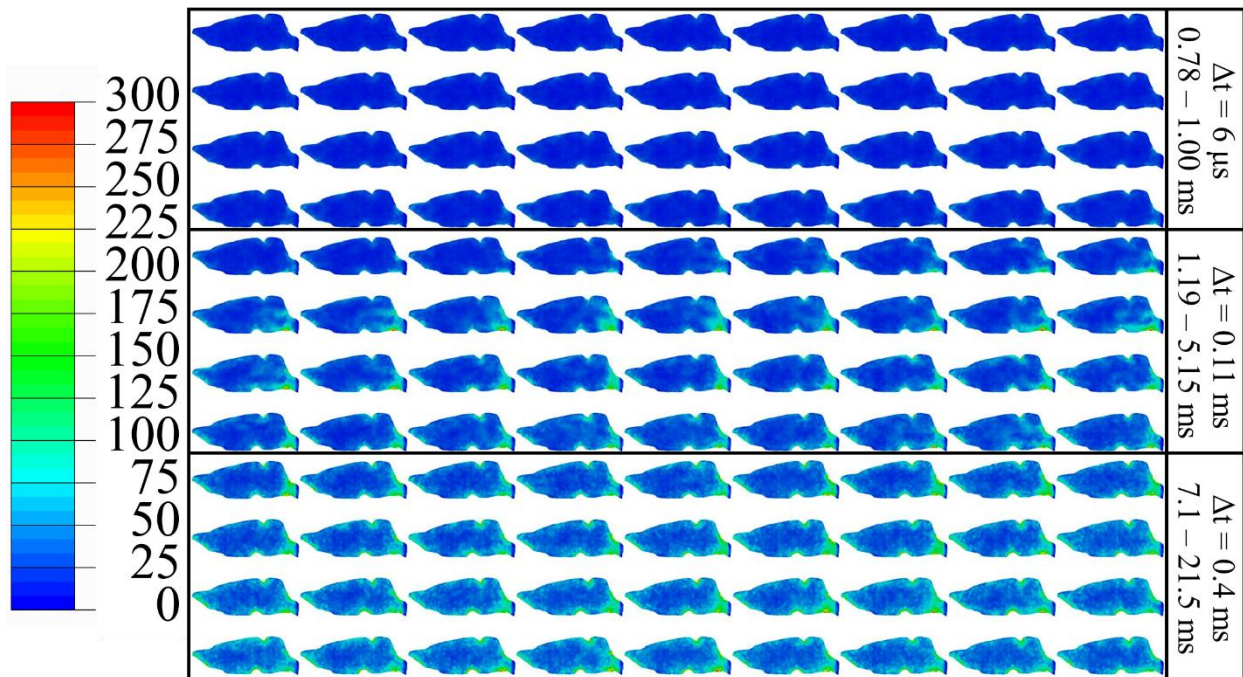
Figure 8 A temporal von Mises stress map, given in kPa, of the mid-sagittal cut of a rat brain over the course of a 130 kPa shock wave. The earliest time point is in the upper left corner and time progresses at the time step Δt, moving left to right from the top to the bottom.

Figure 9 A temporal von Mises stress map, given in kPa, of the mid-sagittal cut of a rat brain over the course of a 190 kPa shock wave. The earliest time point is in the upper left corner and time progresses at the time step Δt, moving left to right from the top to the bottom.

14

Strain Distribution

The temporal evolution of the maximum principal logarithmic strain in the mid-sagittal section of the rat brain is reported in Figures 10-12 for a 100, 130, and 190 kPa blast overpressure. When comparing the appearance of the strain maps with the pressure wave maps and the von Mises stress maps, it is apparent that the strain map more closely matches the diffuse nature of the von Mises stress. The pressure wave causes no notable strains to develop and the maximum strains were also observed at the posterior brainstem. It can be observed that the strains appear to be more pronounced on the ventral side of the brainstem, as seen in Figures 7-9 with the von Mises stresses. Additionally, the pattern of strain development closely follows that observed with the von Mises stresses. The strain pattern does not appear to be influenced by the passing of the initial pressure wave. The initial development of strains within the brain appear to occur shortly after the pressure wave begins to decay, but no apparent correlation is observed with the secondary pressure increase. The magnitude of the maximum logarithmic strain was found to increase with increased blast overpressure.
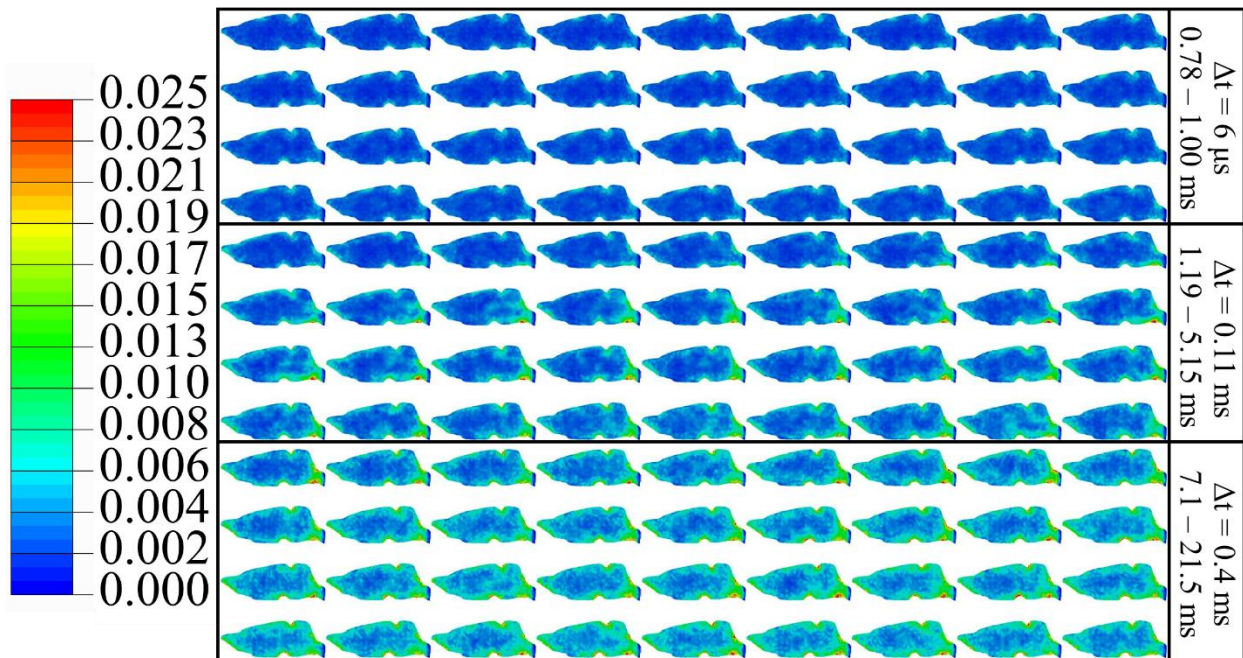

Figure 10 A temporal maximum principal logarithmic strain map of the mid-sagittal cut of a rat brain over the course of a 100 kPa shock wave. The earliest time point is in the upper left corner and time progresses at the time step Δt, moving left to right from the top to the bottom.
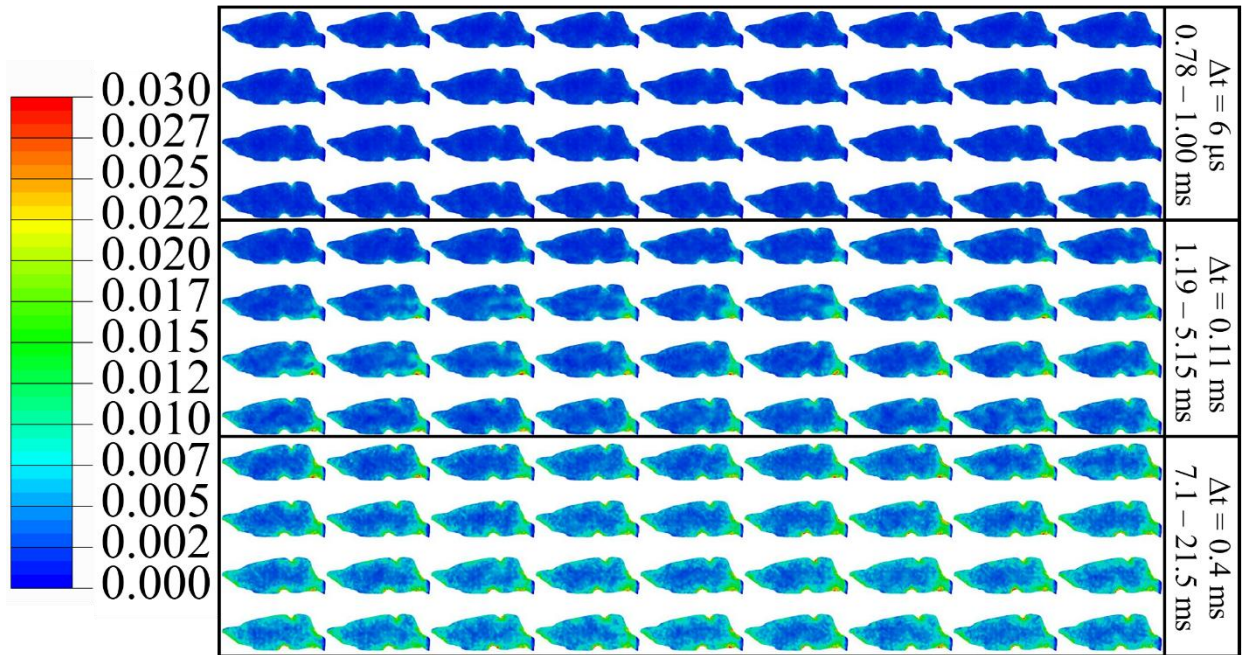
Figure 11 A temporal maximum principal logarithmic strain map of the mid-sagittal cut of a rat brain over the course of a 130 kPa shock wave. The earliest time point is in the upper left corner and time progresses at the time step Δt, moving left to right from the top to the bottom.
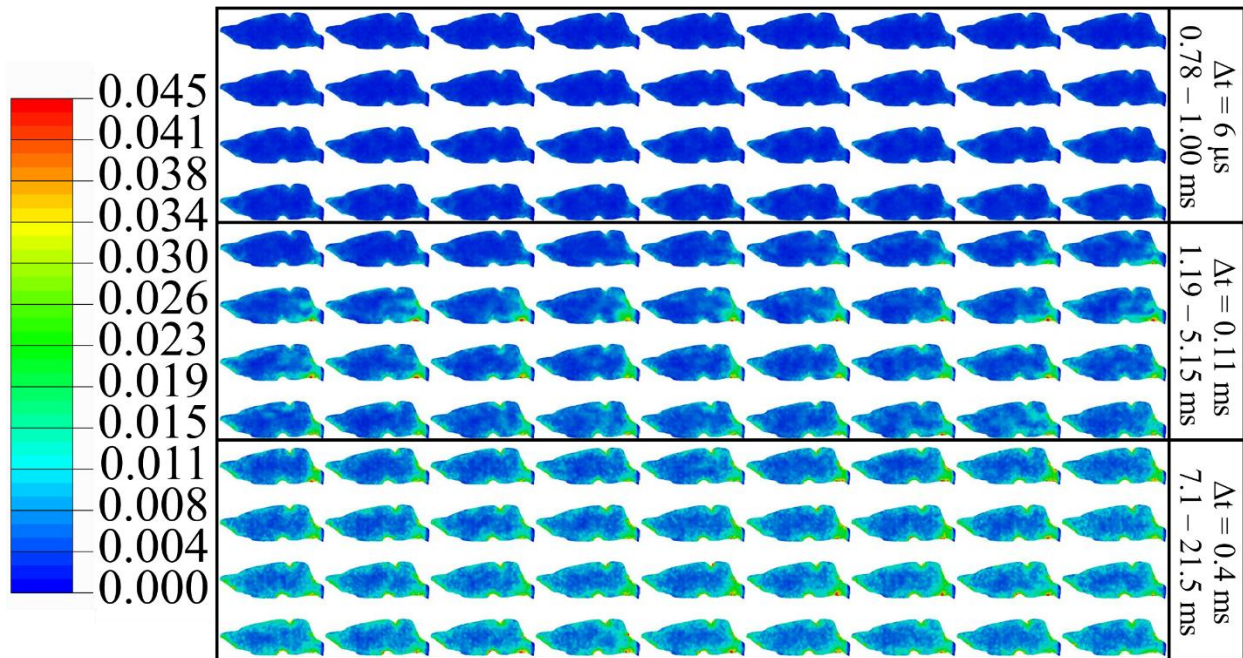

Figure 12 A temporal maximum principal logarithmic strain map of the mid-sagittal cut of a rat brain over the course of a 190 kPa shock wave. The earliest time point is in the upper left corner and time progresses at the time step Δt, moving left to right from the top to the bottom.

Reconstruction of Sensor Locations

To support model validation efforts, the locations of the ICP sensors were ascertained using micro-CT. After shock exposure and sacrifice, the test subjects were preserved in 4% paraformaldehyde for later imaging. The scans were taken with an image pixel size of 32.5 μm (SkyScan 1275, Bruker microCT), reconstructed (NRecon Reconstruction, Brucker microCT), and segmented into a solid mask (Simpleware ScanIP, Synopsys). These locations were scaled with respect to size of the cranial cavity and compared between the nine specimens. This highlighted the reproducibility of the experimental protocol. These locations were then selected to be the regions of interest from the simulation results when examining the local intracranial pressures, von Mises stresses, and the maximum principal logarithmic strains. The scaled sensor locations for the left, anterior and right, posterior sensors are included in Figure 13. It was observed that consistent spacing was maintained between the left, anterior and right, posterior sensors for all test subjects. The reconstructed images are included in Figures 14-22.
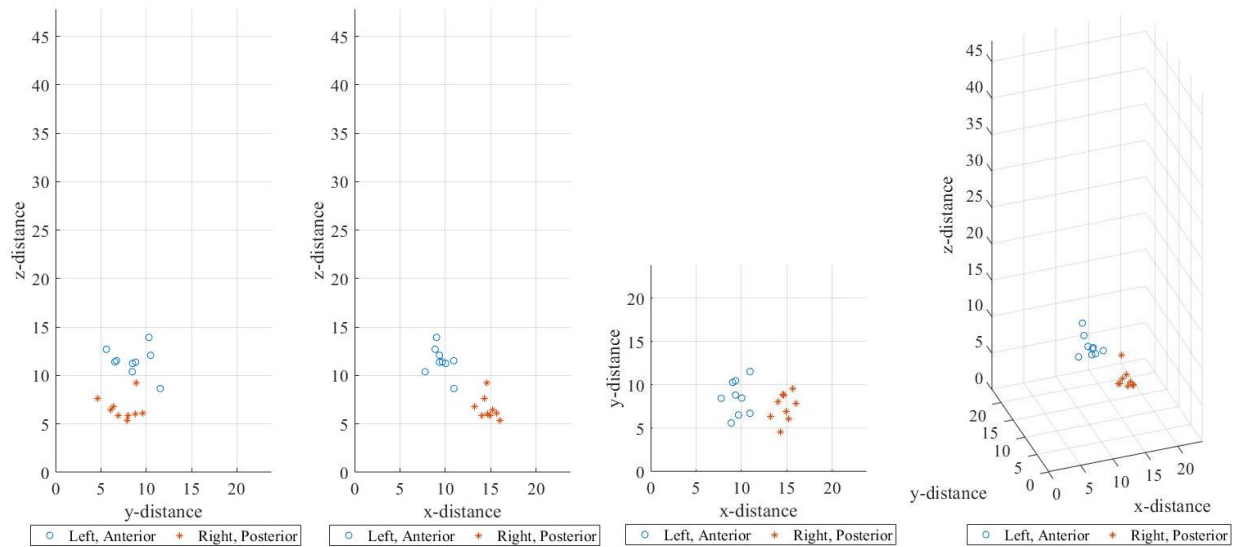

Figure 13 The sensor locations taken from micro-CT scans of the rat head. The field of view and the sensor locations are normalized to the dimensions the average skull size. Values of x-, y-, and z- distance are in mm.
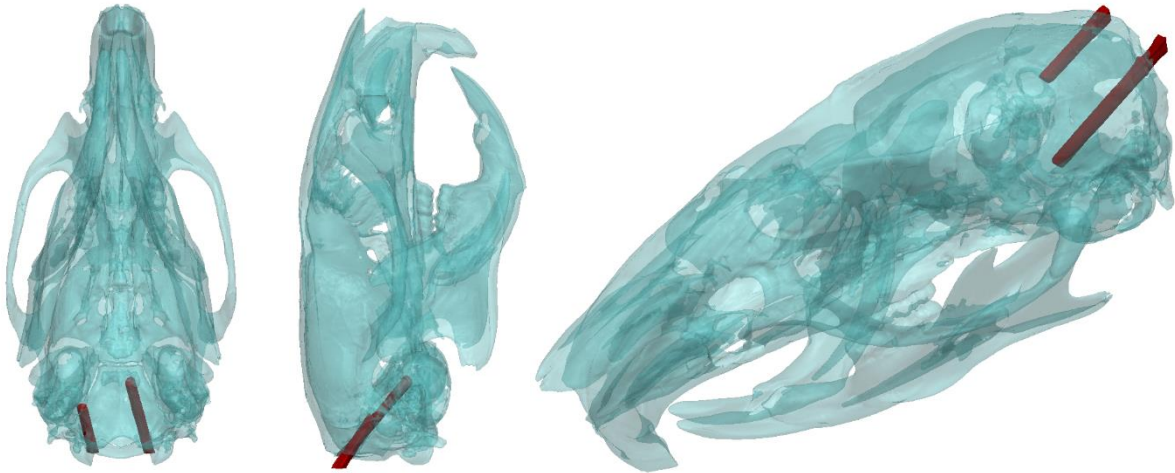
Figure 14 A depiction of the sensor location within test specimen 1 with a cranial, lateral, and isometric view. The skull is shown in blue and the cannulas are shown in red. This specimen was used in Task 2.

Figure 15 A depiction of the sensor location within test specimen 2 with a cranial, lateral, and isometric view. The skull is shown in blue and the cannulas are shown in red. This specimen was used in Task 2.

Figure 16 A depiction of the sensor location within test specimen 3 with a cranial, lateral, and isometric view. The skull is shown in blue and the cannulas are shown in red. This specimen was used in Task 2.

Figure 17 A depiction of the sensor location within test specimen 4 with a cranial, lateral, and isometric view. The skull is shown in blue and the cannulas are shown in red. This specimen was used in Task 2.
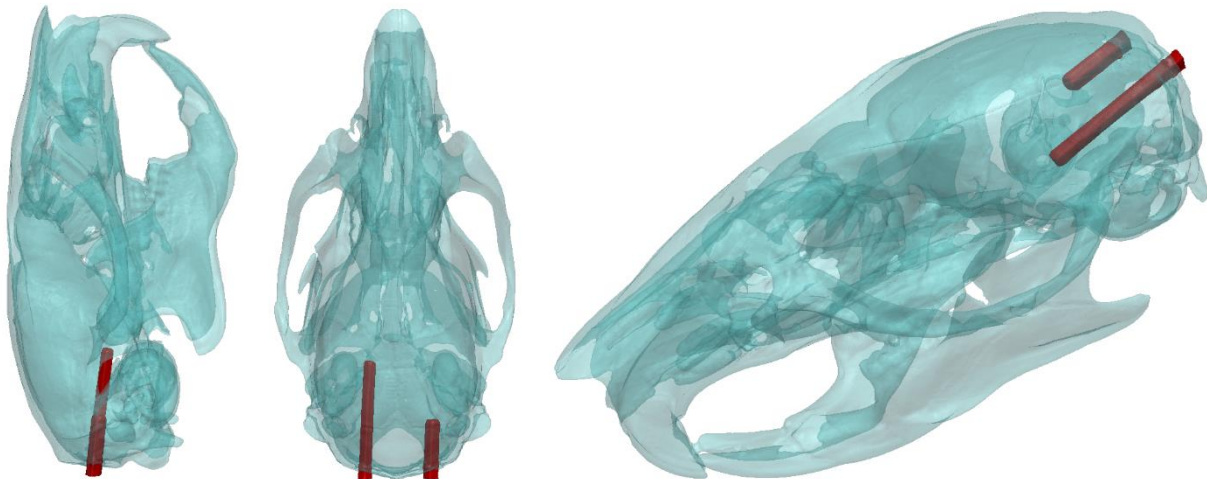

Figure 18 A depiction of the sensor location within test specimen 5 with a cranial, lateral, and isometric view. The skull is shown in blue and the cannulas are shown in red. This specimen was used in Task 8.

Figure 19 A depiction of the sensor location within test specimen 6 with a cranial, lateral, and isometric view. The skull is shown in blue and the cannulas are shown in red. This specimen was used in Task 8.
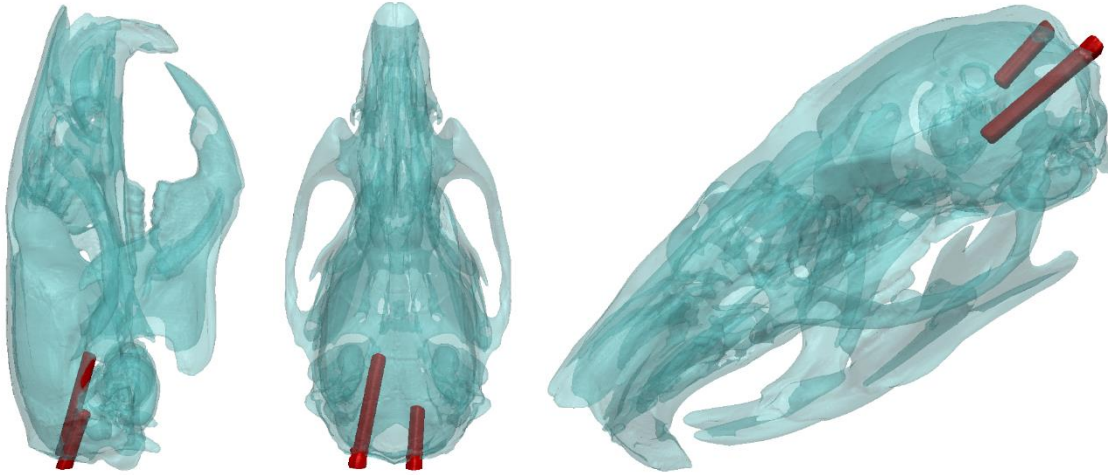
Figure 20 A depiction of the sensor location within test specimen 7 with a cranial, lateral, and isometric view. The skull is shown in blue and the cannulas are shown in red. This specimen was used in Task 8.

Figure 21 A depiction of the sensor location within test specimen 8 with a cranial, lateral, and isometric view. The skull is shown in blue and the cannulas are shown in red. This specimen was used in Task 8.
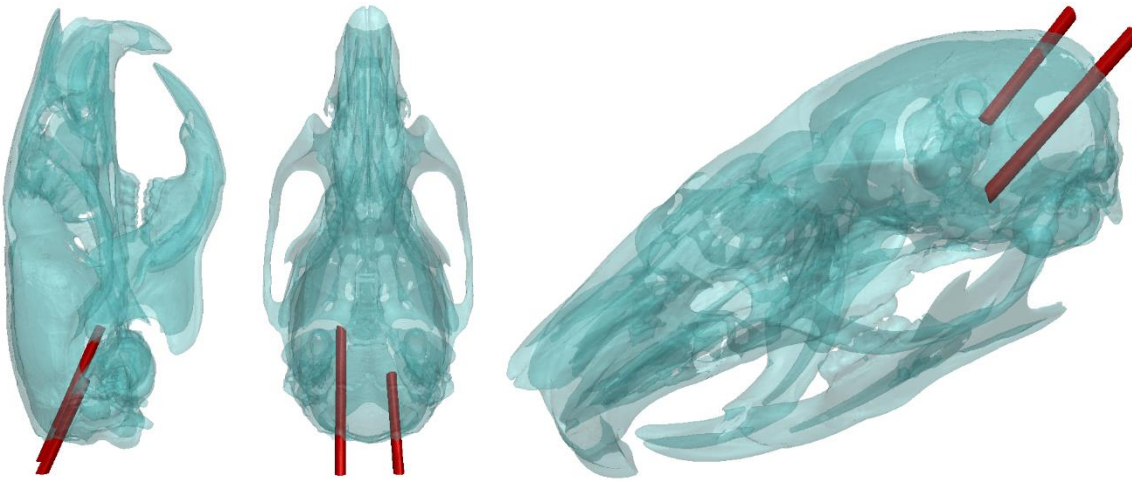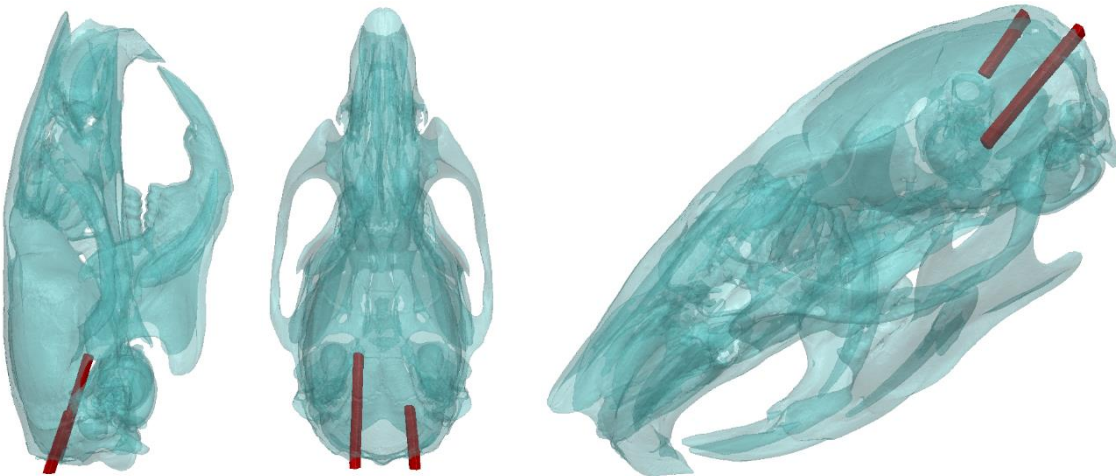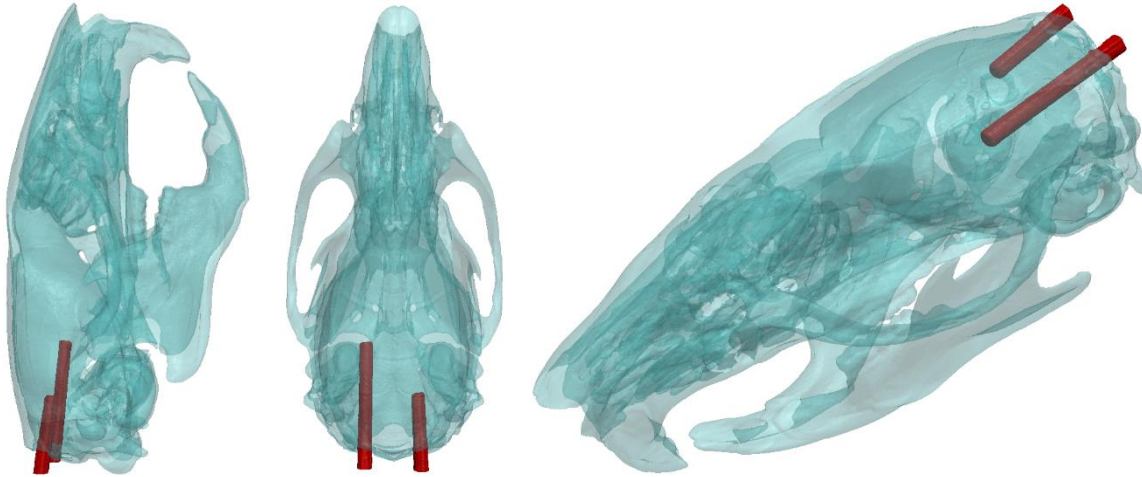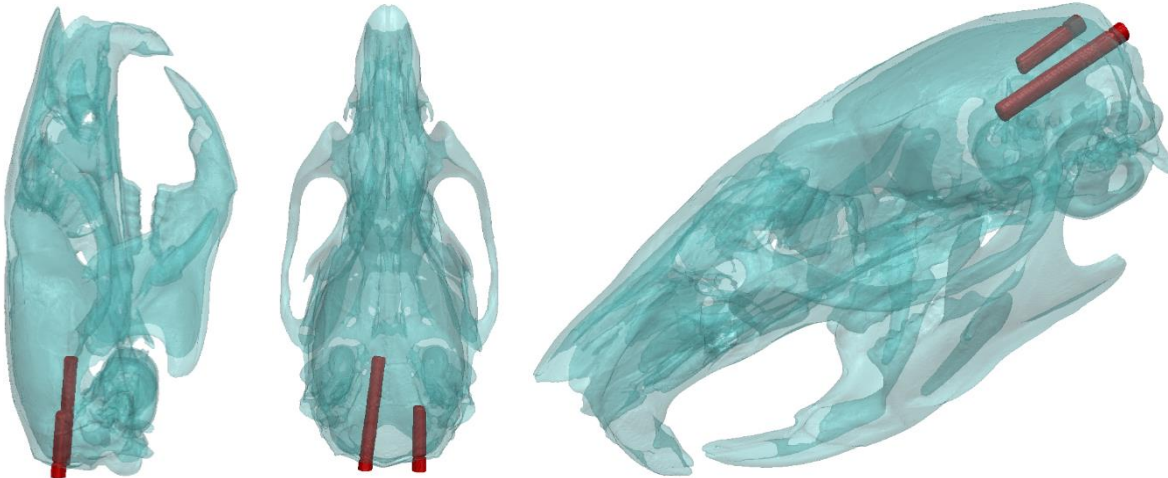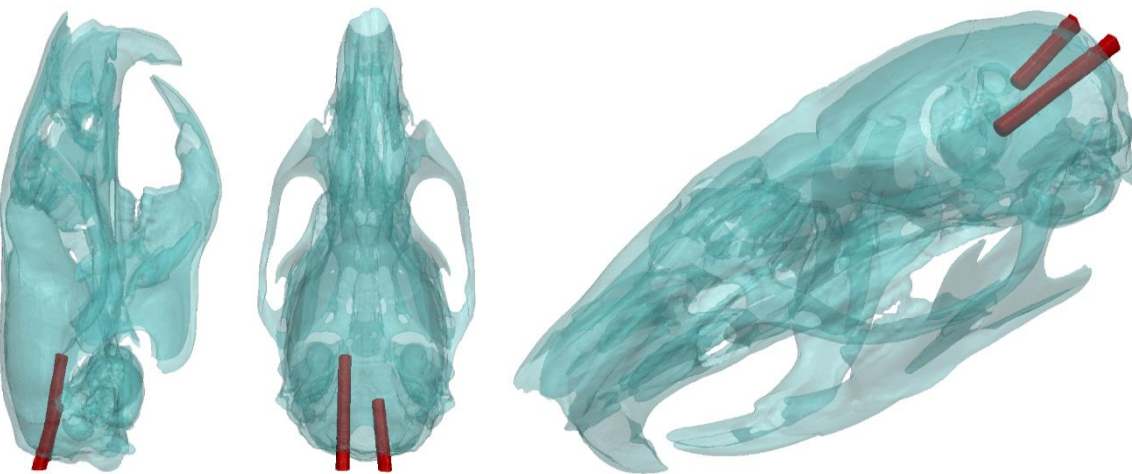

Figure 22 A depiction of the sensor location within test specimen 9 with a cranial, lateral, and isometric view. The skull is shown in blue and the cannulas are shown in red. This specimen was used in numerical simulations planned in the Task 8.

Temporal Relationship Between Mechanical Injury Markers

To compare the temporal evolution of the press, stress, and strain patterns in the rat brain, the normalized pressure, stress, and strain profiles were compared for the 190 kPa blast. Two locations were selected to compare, which correspond with the experimental ICP sensor locations. These locations, A and B, were selected to be the nodes which are closest to the sensor locations identified from micro-CT reconstruction of the rat skull/cannula complex. Location A was the sensor in the anterior left hemisphere and location B was the sensor in the posterior right hemisphere. The field variable outputs were plotted together, transformed to begin at zero when the shock loading step begins (t = 25 ms) and normalized with respect to the maximum value. This comparison is shown in Figure 23. It can be observed that the von Mises stress and the maximum principal logarithmic strain develop in the more anterior location earlier. Additionally, the increase of the von Mises stress and the logarithmic strain appears to coincide with the decrease of the intracranial pressure.
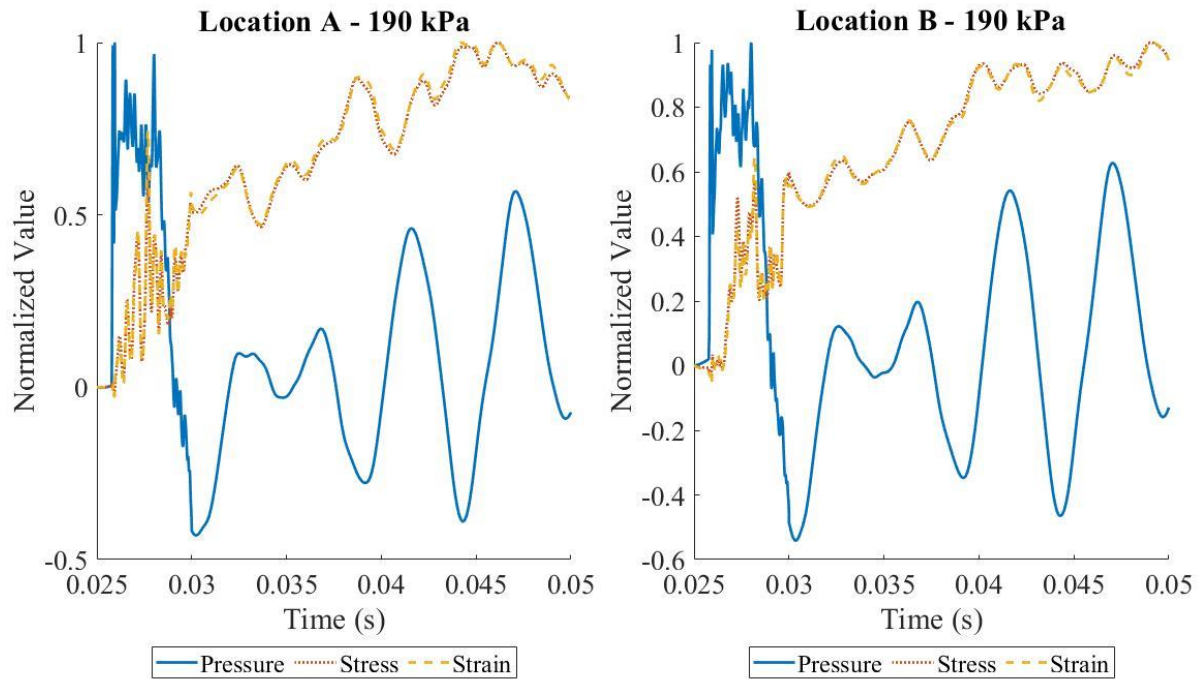

Figure 23 The transformed and normalized intracranial pressure, von Mises stress, and the maximum principal logarithmic strains at the left, anterior sensor location (A) and the right, posterior sensor location (B).

Task 5: Asses Extent of Oxidative/Nitrosative Stress, BBB Damage and Neuroinflammation (completed)

Changes in the protein expression of matrix metalloproteinases that contribute to BBB permeability changes in bTBI
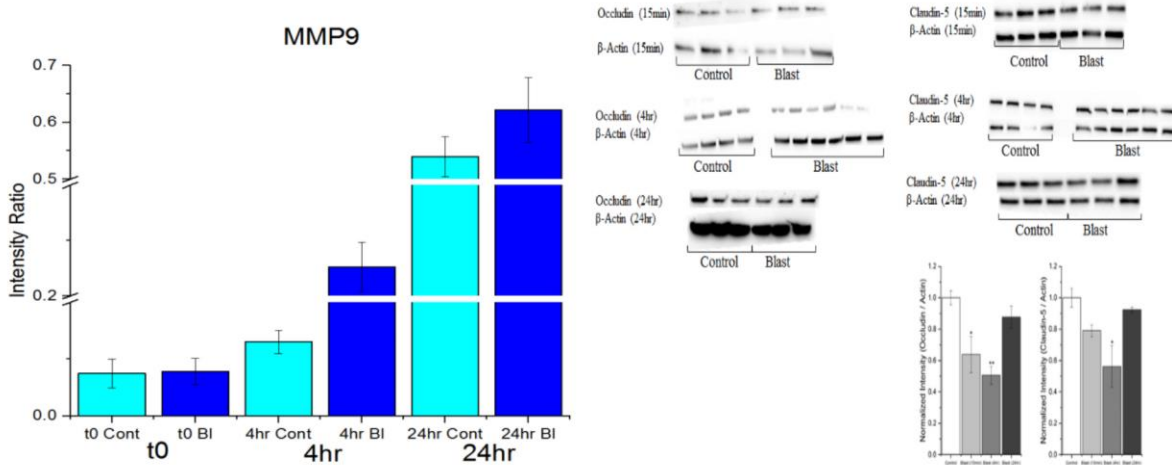

Figure 24 Western blots of MMP 9 (right panel) and tight junction proteins Occludin and Claudin-5 and respective quantitations. Proteins taken from control and blast (180 kPa BOP) cerebral brain homogenates fifteen minutes, four, and 24 four hours post-exposure and compared with levels of β-actin housekeeping protein. [*] indicates a difference in intensity. compared with control with a statistical significance of $p < 0.05$, [**] indicates $p < 0.01$.

A continuation of work on the spatial and temporal changes in the BBB permeability in rats subjected to different blast over pressures (70, 180, 240 kPa) examined changes in the matrix metalloproteinases (MMPs). MMPs, also called matrixins, comprise a family of enzymes that cleave protein substrates based on a conserved mechanism involving activation of a site-bound water molecule by a Zn^{2+} ion, and their activation may contribute to BBB permeability. There are several MMPs present in brain among which MMP-3 and MMP-9 are the most dominant. MMPs have been linked to BBB disruption since these proteases once released into the extracellular matrix degrade tight junction proteins which act as anchor between the two capillary endothelial cells to prevent the leakage of the barrier between blood and brain.

Protein levels of MMP9 significantly increase in moderate blast as a function of time and such increase correlate with the reduction in tight junction proteins

Quantitative measurements by Western blots of MMP9 in homogenates prepared from cerebral hemispheres from rats subjected to moderate blast at 180 kPa showed a progressive increase in its expression. Immediately following blast (t_0) there was no change in the expression of MMP9, whereas 4h post injury there was a significant increase, which
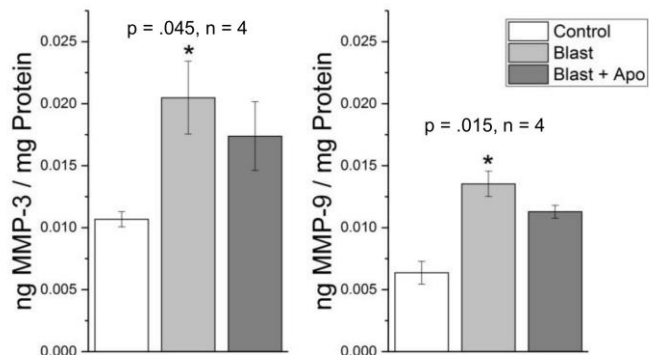

Figure 25 ELISA results for whole brain lysates for MMP-3 and MMP-9 (n=4). Statistically significant increases in blast groups were seen compared to controls ($p = 0.045$ and 0.015, respectively).

persisted up to 24 h (Figure 24). Noteworthy that the increase in MMP 9 expression inversely correlated with the reduction in the protein levels of tight junction proteins claudin 5 and occludin (Figure 24), suggesting that the degradation of tight junction proteins following blast may be mediated by MMP9, which could ultimately result in the BBB permeability. We conducted ELISAs for both MMP-9 and MMP-3 (figure 25), which have been implicated in the breakdown of the BBB and are present on neurovascular endothelial cells for control, injured, and injured groups treated with apocynin. It is important to note that in the case of both MMPs studied, apocynin treated groups did not show statistically significant differences from blast groups ($p > 0.05$), although it does seem as though there is a tendency towards decrease. This may indicate that upregulation of MMPs is not mediated by NOX (oxidative stress), but it is a response to some other mechanism, or a process disturbing the homeostasis in the brain parenchyma like influx of exogenous proteins after the BBB damage.
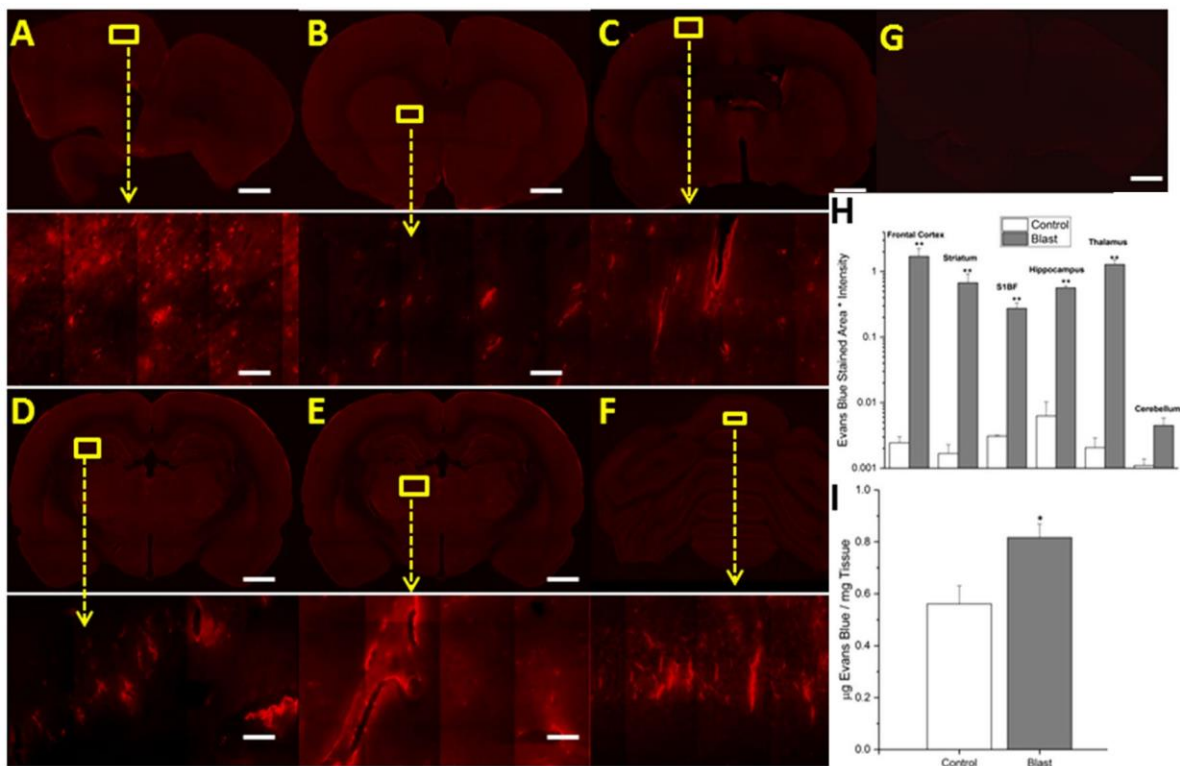
Figure 26 Fluorescent images of Evans blue extravasation. Images show 10x macro-shots as well as zoomed in 40x images in representative regions in the frontal cortex (**A**), striatum (**B**), somatosensory barrel-field cortex (**C**), hippocampus (**D**), thalamus (**E**) and cerebellum (**F**), 15 minutes following 180 kPa blast exposure. Control images were dramatically enhanced, yet still show limited visibility, due to the absence of extravasated dye. Frontal cortex was taken as a representative control image (**G**). Quantitation of extravasation is shown using a semilog plot to capture the differences (**H**). Absorption spectrophotometry results of Evans blue in control and injured rats (n = 5) (**I**). *Indicates a difference in intensity compared with control with a statistical significance of $p < 0.05$, **Indicates $p < 0.01$. Scale bar = 1 mm in coronal sections and 50 μm in 40x images.

Oxidative stress resulting from NADPH oxidase (NOX) activation contributes to BBB permeability

We have identified that blast injury results in oxidative stress mainly via the activation of NADPH oxidase (NOX), a superoxide producing enzymes in different brain regions (figure 26). Oxidative stress has been implicated as a secondary mechanism in BBB disruption in various blunt TBI as well as in other neurological disorders including stroke, meningitis and HIV infections. We examined the efficacy of apocynin, an antioxidant as well as agent that inhibits the activation of NOX on the extravasation of Evan's blue (EB) as measures of BBB permeability. Rats subjected to

Figure 27 Quantification of effect of apocynin on EB fluorescence in different brain regions 4 hours post injury.

moderate blast resulted in BBB disruption as indicated by extensive extravasation of EB (Figure 27) across different brain regions. Interesting that frontal cortex displayed maximum extravasation compared to other brain regions. Treatment of rats with apocynin 30 µM (i.p. injection) 30 min before blast injury showed a significant reduction in EB extravasation 4 h post-injury across all

the brain regions. These results strongly suggest that oxidative stress likely resulting by the activation of NOX contributes to BBB disruption. ELISA analysis of S100β, an astrocytic calcium-binding protein, on blood serum samples for animals exposed to moderate blast (180 kPa) at 4 and 24 hours post injury (figure 27) corroborate these findings. Immunohistochemistry was also done to determine the presence of monocytes in brain parenchyma in the frontal cortex, four hours after blast. Fluorescent co-stain for RECA-1 (endothelial cell marker) and CCR-2 (monocyte marker) was conducted for control and blast groups, qualitatively demonstrating increased presence of monocytes in the brain (fig. 28). These results clearly demonstrate a multiple mode of increased permeability of the BBB.
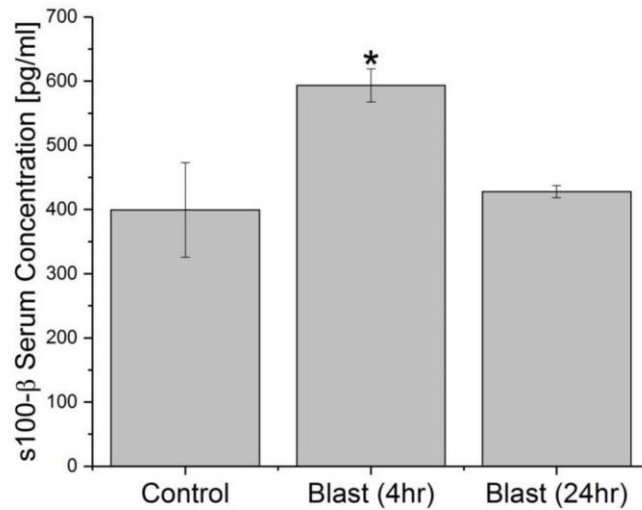
Figure 28 ELISA results for S100β in blood serum (n = 3). Statistically significant increase from control was seen in the blast groups four hours post injury (p=0.037), before returning to control values in 24 hours (p > 0.05).
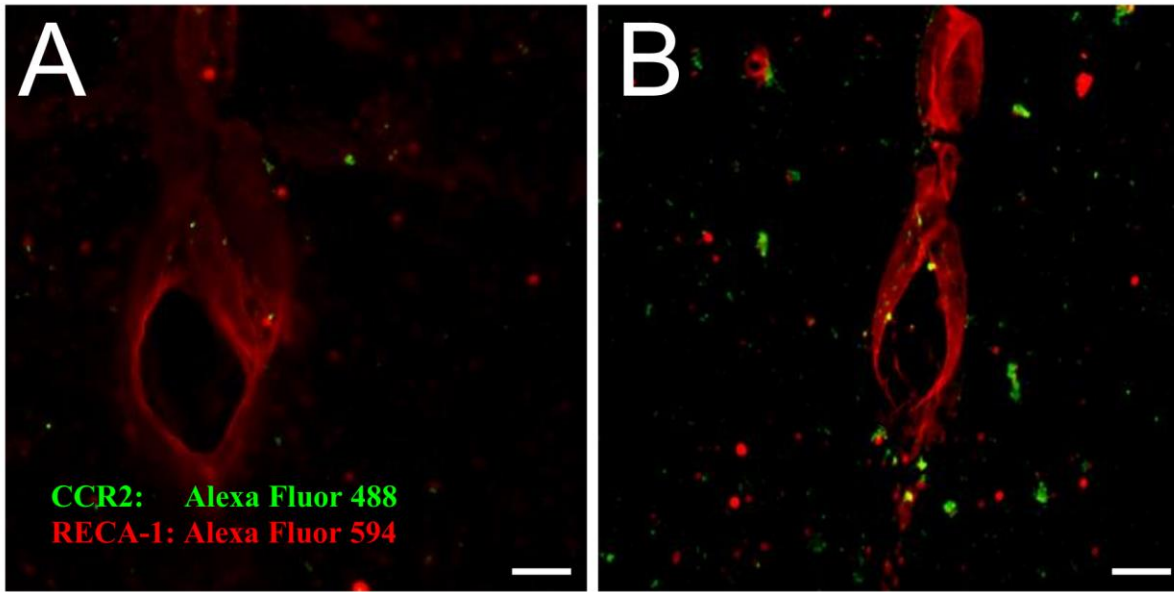
Figure 29 Immunohistochemistry in frontal cortex for endothelial cell marker (RECA-1) and monocyte marker (CCR2) at four hours post-exposure for control (A) and moderate (180 kPa BOP) blast (B). Scale bar equals 50μm.

Finally, to confirm our hypothesis that the tight junction proteins were indeed dislodged following the blast, an analysis via ELISA was conducted on brain lysates and serum samples for two tight-junction proteins, occludin and claudin-5. These results corroborate our early hypothesis; after the tight junctions are dislodged from their complexes on endothelial cells, they are taken up by circulation. However, by 24 hours, all the tight junction proteins that were taken up by the serum were excreted or otherwise removed from circulation.
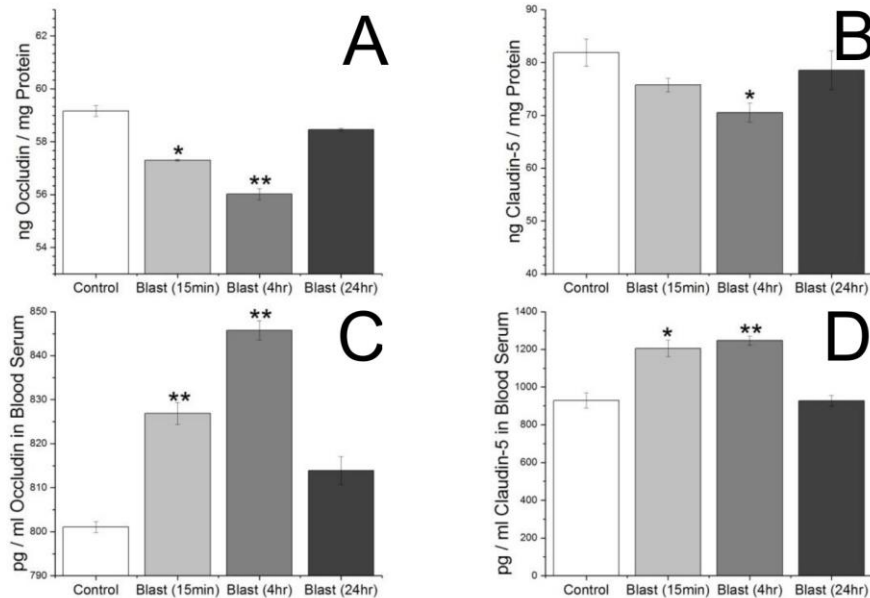
Figure 30 ELISA results for tight junction proteins occludin and claudin-5, respectively in brain (A & B) and blood serum (C & D). Assay conducted for blast (180 kPa BOP) samples fifteen minutes, four, and twenty-four hours post-exposure and compared with controls. [*] indicates a difference in intensity compared with control with a statistical significance of $p < 0.05$, [**] indicates $p < 0.01$.

Activation of microglia following blast TBI

The microglial activation is a frequent

sequela in animals exposed to blast. We found that in control animals (fig. 31A), microglia appear to be in their resting state (fully ramified) with their processes probing their microenvironment. Under normal physiological conditions these cells are evenly distributed throughout the brain. However, 4 hours following blast exposure microglia begin to migrate towards the blood vessel and activate, with apparent changes in morphology (amoeboid shape). This response is likely due to components of the blood entering the brain parenchyma through the compromised BBB. Once detected by the microglia, the cells activate and begin clearing the foreign material by phagocytosis. In figures 31B-D one can observe that microglia respond to blood vessels of all sizes indicating that BBB of arteries, arterioles and capillaries are all compromised. At 7 days following blast, microglia remain in their active state surrounding the blood vessels. The number of activated microglia surrounding each blood vessel decreased compared to the 4-hour time point. This may be due to the sealing of the BBB, which prevents additional foreign material from entering the brain
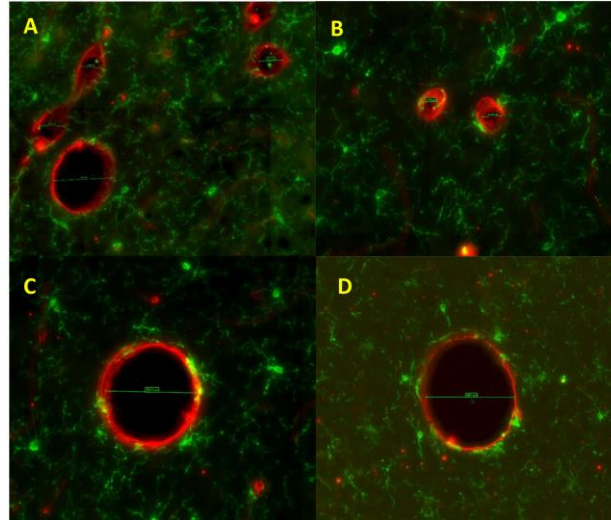
Figure 31 Fluorescent images of Iba (microglia) and RECA (rat endothelial cells) expression in the frontal cortex in control (A) and 4 hours of moderate blast in small (B) medium (C) and large (D) blood vessels. Note the change in microglia morphology surrounding the vessels of the blast group.
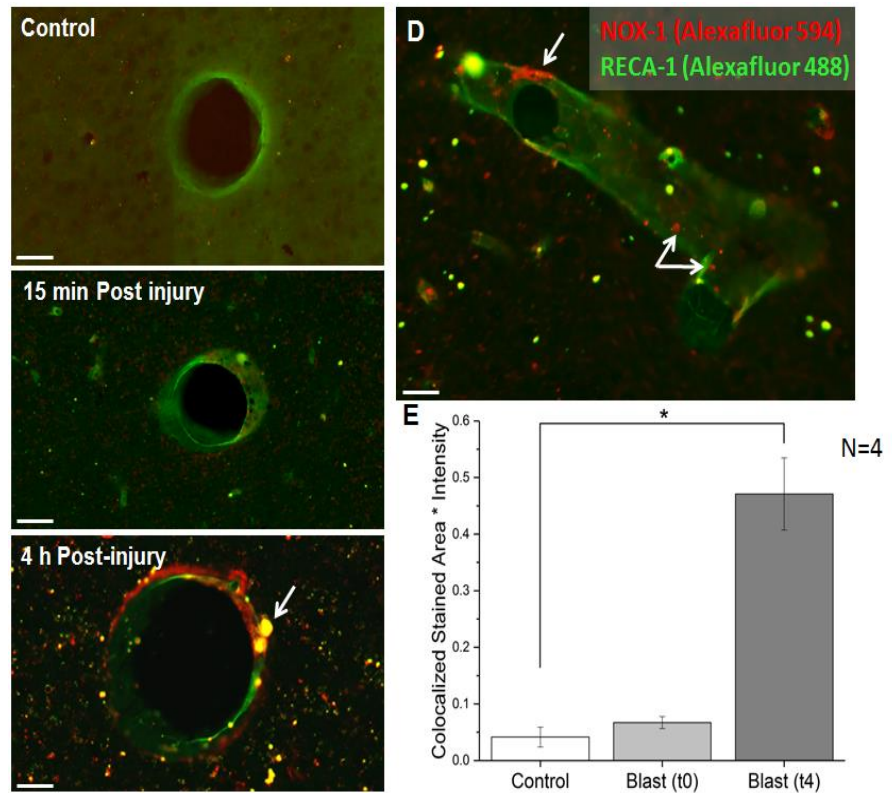
Figure 32 Colocalization of NOX-1 (red) and RECA-1 (green) in vascular endothelial cells in the frontal cortex. Control: little NOX-1 in vascular endothelial cells with an increase in colocalization fifteen minutes following blast. At four hours, there is a significant upregulation of NOX-1 in endothelial cells: yellow is indicating an overlap of NOX-1 and RECA-1. D. NOX-1 upregulation across the length of the vessel lumen (arrows). Quantitation of the colocalization shows a significant increase in blast groups, $p < 0.05$.

26

parenchyma. At this later time point, all the microglia surrounding large vessels return to their resting ramified state. This was not observed for small and medium vessels where microglia remained in their activated

NOX1 is upregulated in neurovascular endothelial cells

Previous studies in this laboratory identified increased levels of NOX1 and NOX2 in neurons, astrocytes, and microglia following moderate blast injury (180 kPa) across the cerebral hemisphere and cerebellum. In the present study, we examined the levels of NOX1 in brain endothelial cells in the frontal cortex in vascular endothelial cells. The double immunofluorescence for NOX1 and RECA-1 (endothelial cell marker) showed a significant increase in amount of colocalization following moderate blast (Fig. 32). Fifteen minutes post-exposure, a statistically insignificant increase in colocalized NOX1 compared to controls was observed. Four hours after blast, which previous work from this group has shown as the peak time for BBB permeability following blast injury, we observed a robust increase (ten-fold) in NOX1 concentration in vascular endothelial cells.

Apocynin significantly reduces superoxide production following blast injury

Several groups have demonstrated that activation of NOX results in increased superoxide production. After demonstrating the increase in NOX1 concentration in neurovasculature in the frontal cortex, we sought to determine if this results in an increase of superoxide production. *In-vivo* levels of superoxide were measured using DHE and we observed a clear increase in superoxide produced in the frontal cortex, which corroborated well with the upregulation of NOX1 (Fig. 33). Differences between control and blast groups and blast and treatment groups were found to be statistically significant.

Apocynin significantly reduces tight junction degradation following blast injury

To determine the degree of BBB breakdown following blast injury, ELISA was conducted for tight junction proteins occludin and claudin-5 for control, blast, and blast + apocynin groups (Fig. 34). Occludin decreased by 20.31% four hours post-blast compared to controls but barely changed in animals treated with apocynin. The difference between the blast group and the treatment group was also significant. Claudin-5 decreased by 12.40% four hours post-blast compared to controls, but like occludin, displayed only a negligible decrease in the treatment group. The difference between blast and treatment groups was statistically significant.
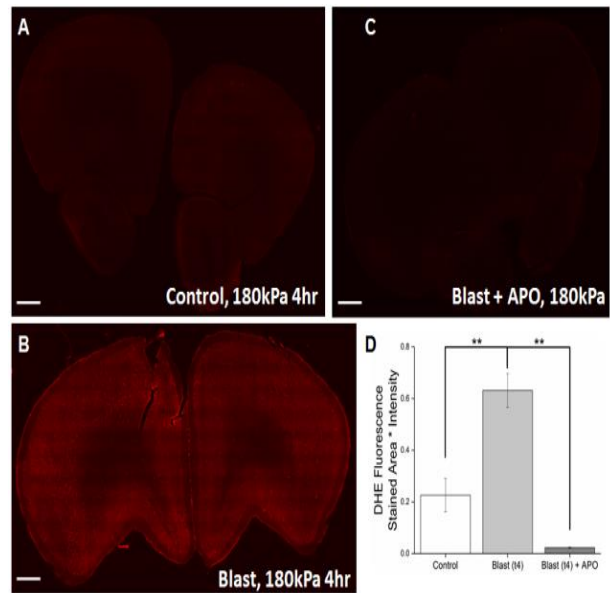
Figure 33 DHE stain to observe superoxide concentration in the frontal cortex: A control (basal level of superoxide). B superoxide increase 4 hours following blast exposure, C. return to basal levels with pretreatment of apocynin. D quantitation of DHE fluorescence intensity for the three groups. [**] $p < 0.01$.

Apocynin significantly decreases blood-brain barrier permeability following blast injury

The extent of extravasation was evaluated in the frontal cortex at both fifteen minutes and four hours post-blast injury (Fig. 35). Our group previously displayed that extravasation of Evans blue was significant at both times post-moderate blast injury and our current results support that. Significant extravasation was observed in both injured and treatment groups at the acute stage, with no statistically significant difference between them. EB presence in the brain parenchyma

Figure 34 ELISA results for matrix metalloproteinases. A & B show results for MMP-3 and 9, respectively, in control and blast groups. Levels of MMPs were taken four and 24 hours after exposure and compared against controls. C & D show results for MMP-3&9, respectively, in control, blast, and treatment groups. [*] indicates a difference in intensity with a statistical significance of $p < 0.05$, [**] indicates $p < 0.01$.

increased by 1300-fold four hours following moderate blast over the control in the frontal cortex and over the blast + apocynin group (75-fold, $p < 0.01$). There was no statistically significant difference between the control group and the treated group. Four animals were used per group in this phase of the study.
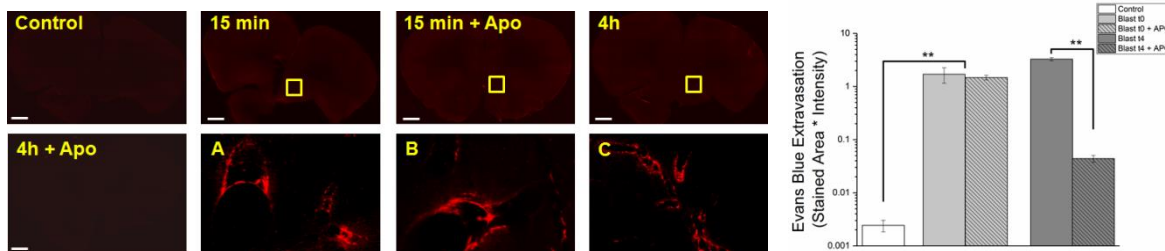
Figure 35 Fluorescent images of Evans blue extravasation. Images show frontal cortex from control animal, with almost no observable extravasation of leakage, Sections from 180kPa BOP, acutely (15 minutes) show significant leakage, apocynin treatment completely blocked EB extravasation. 4 h post-exposure showed greater leakage than 15m post injury A, B, C show zoomed in, 20x images from images. Quantitation of extravasation intensity shows a statistical significance of $p < 0.01$.

Moderate blast induces translocation of glial fibrillary acidic protein into the blood stream

Concentration of GFAP, an astrocyte specific protein in brain (which is not present in blood under normal conditions) in the blood plasma was determined via ELISA (Fig. 36). Statistically significant increase in GFAP concentration was seen compared to controls in both blast and treatment groups 15 minutes after injury, but no difference between blast and treatment group. At four hours post-blast, there is a further increase in GFAP concentration in blood plasma, but with apocynin, the values drop back to control levels. Intergroup comparison reveals a statistically significant difference between blast and treatment groups four hours after injury.
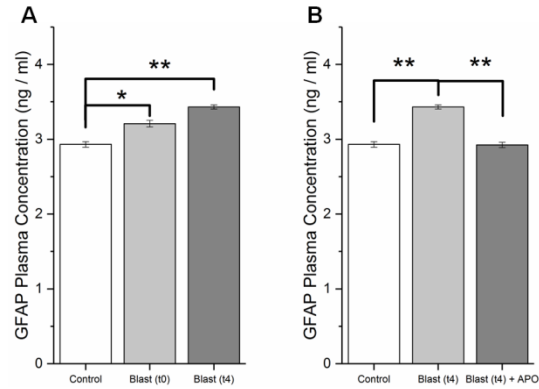
Figure 36 ELISA results for GFAP concentration in blood plasma. A compares control levels with levels 15 minutes and 4 hours following blast and B compares control levels with levels 4 hours following blast with and without apocynin pretreatment. [*] indicates a difference in intensity with a statistical significance of $p < 0.05$, [**] indicates $p < 0.01$.

CSF-Plasma ratio of albumin increases following moderate blast injury

To determine the ratio of albumin in the CSF (which should be negligible in normal conditions) and blood plasma, another ELISA was conducted on both samples (**Fig. 6**). While an increase in the CSF-Plasma albumin ratio was observed acutely (fifteen minutes post-blast) for both blast and treatment groups, statistical significance was not achieved in either. Four hours following blast, a statistically significant increase over control was observed in the injured group. Comparison between blast and treatment group at this point also revealed statistically significant difference. These studies together strongly suggest that NOX-derived oxidative stress plays a major role in BBB disruption following moderate blast injury.
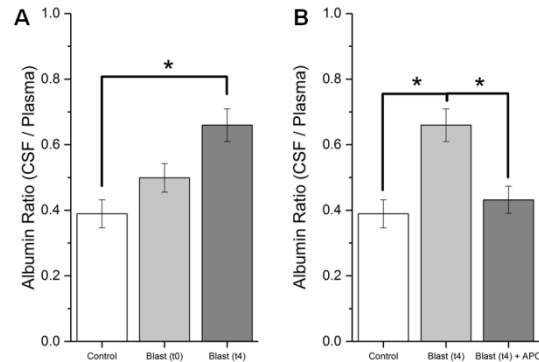
Figure 37 ELISA results for albumin concentration in CSF and blood plasma, as presented as a ratio between the two. A compares control levels with levels 15 minutes and 4 hours following blast and B compares control levels with levels 4 hours following blast with and without apocynin pretreatment. [*] indicates a difference in intensity with a statistical significance of $p < 0.05$.

Moderate blast increases the production of proinflammatory cytokines

In the previous progress report, we reported that microglial activation occurred in animals exposed to moderate blast (180 kPa). One event associated with microglial activation is increased production of proinflammatory cytokines. Here we examined the temporal profiles of two proinflammatory cytokines TNF-α and IL-1β in homogenates from hippocampus and thalamus brain regions found to me more vulnerable to blast injury. Levels of IL-1β moderately increased 4h post injury and declined to control levels by 24h, however showed a progressive increase at 7- and 15-days post-injury (Figure 38) in hippocampus. Thalamus showed much robust increase in

IL-1β production compared to hippocampus but showed a similar time course of increase as that of hippocampus. Like IL-1β, levels of TNF-α also showed a biphasic response of increase in both hippocampus and thalamus (Fig. 38). These results indicate that moderate blast increases the production of proinflammatory cytokines and such increase is likely mediated by activation of microglia.

Task 6. Examine plasma membrane permeability using fluorescent tracers (completed)

Figure 38 ELISA results for IL-1β and TNF-α in hippocampus and thalamus lysates in animals exposed to moderate blast (180 kPa).

We evaluated alterations in cell plasmalemmal permeability following blast exposure using a shock tube at two peak overpressures (180 kPa and 240 kPa) and a single time point post-injury (30 min). Animals were sacrificed using transcardial perfusion, brains extracted and sectioned on a vibratome into 50 micrometer thick slices. We assessed the patterns of neural cells acutely permeabilized due to blast based on neuroanatomical locale, phenotype, and extent of damage. We hypothesized that blast shockwave directly elicits biophysical plasmalemmal disruptions in specific neural cellular populations that are dependent on brain region. We found that blast exposure caused immediate increases in cell membrane

Figure 39 Lucifer Yellow positive cells in the frontal cortex of brain in rats exposed to a single blast with 180 kPa peak overpressure (left, middle) versus control (right).

permeability predominantly in the cortical region. However, large numbers of Lucifer Yellow positive (LY+) cells in were present in both contralateral and ipsilateral regions with respect to injection site (fig. 39), and quantification of cell numbers lead to the conclusion this method is not sensitive to discriminate between controls and injury groups. As an alternative, we performed characterization of blood serum samples from the same cohort of animals probing for proteins associated with neuronal cells. Blood serum samples from control and 24h, 3days and 7 days after

moderate blast injury (180 kPa) were immunoblotted for neuron-specific enolase (NSE), a specific marker of neurons that appears in blood circulation only after neuronal membrane damage. Results showed that NSE levels in serum did not change significantly suggesting that neuronal plasma membrane damage did not occur in animals exposed to blast injury (Figure 40).

Task 8: Establish Master Impulse Dose-Response Curve at Three Blast Overpressures (completed)

The effect of the electrostatic charges on the pressure profile and impulse

We performed a set of experiments where incident pressure was measured and pressure sensors (PCB 134A24) were used in protected and unprotected configuration. Tests were performed at a single nominal shock wave intensity (130 kPa), and the effect of the static electricity along the shock tube was evaluated. Measurements were repeated four times and shock wave evolution was monitored using six pressure sensors (fig. 41, for details of the experimental setup see figures 1 in references [13] and [14]). The quantification of the BOP and impulse was performed to capture the effect of static electricity on the signal quality in the unprotected mode. It turns out that pressure profiles recorded using unprotected sensors result in impulse values with values lower by 30-50% (figure 42).

Calibration of the shock tube to control the impulse at three blast overpressures
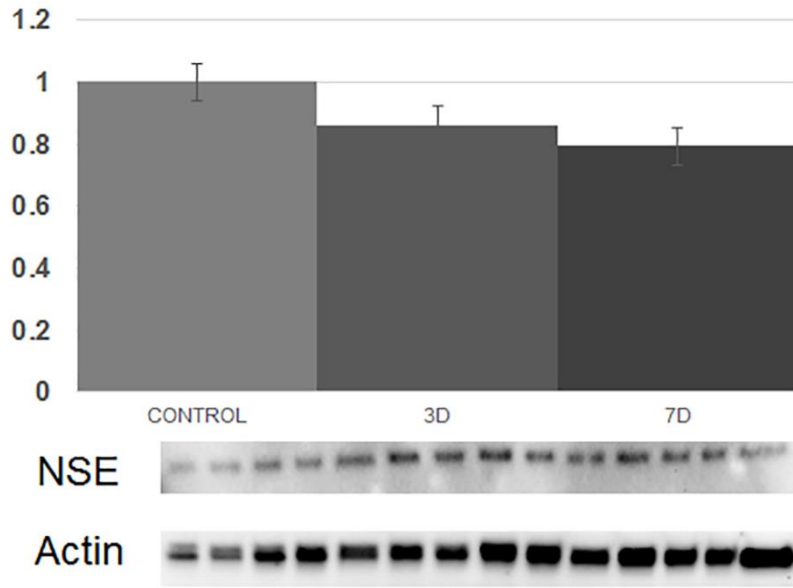
Figure 40 Levels of Neuron Specific Enolase (NSE), a marker of neuronal plasma membrane integrity in serum samples obtained from animals of control, 3 and 7days post blast injury (180 kPa).
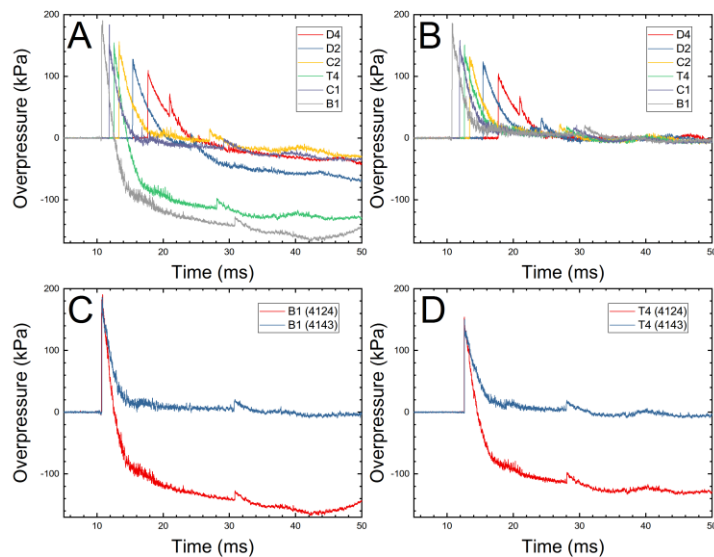
Figure 41 The effect of the baseline drift on the quality of the recorded shock wave profiles. The same set of sensors was tested in the unprotected (A) and protected (B) configurations. The comparison of individual pressure-time traces for sensors B1 (C) and T4 (D) is presented. It is evident there is severe signal degradation which will results in underestimation of the duration and impulse values.

The control over shock wave profile characteristics is one of the many recent advances from our laboratory, a feature which, to our knowledge, was not demonstrated in any other published work to date. Considering the deleterious effects of the static electricity on the impulse we had to perform a set of experiments to re-calibrate the operational parameters of the 9-inch shock tube and establish a set of experimental conditions to select the location in the shock tube where the shock wave profile has the same peak overpressure and increasing duration (impulse). We used helium and nitrogen as driver gases, three operational breech configurations and four membrane thicknesses and
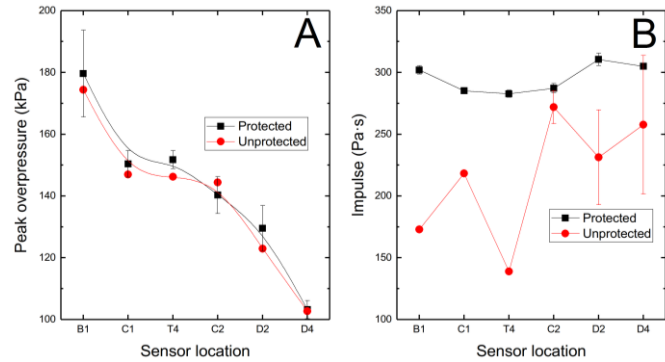
Figure 42 The effect of static electricity on the peak overpressure (A) and impulse (B). Tests were performed at a nominal blast intensity of 130 kPa. The peak overpressure is unaffected, while pressure histories recorded using unprotected pressure sensors result in diminished impulse values.

In panel A:
$y = 0.016x^2 + 1.88x$
$R^2 = 0.98$

$y = 0.002x^2 + 1.43x$
$R^2 = 0.99$
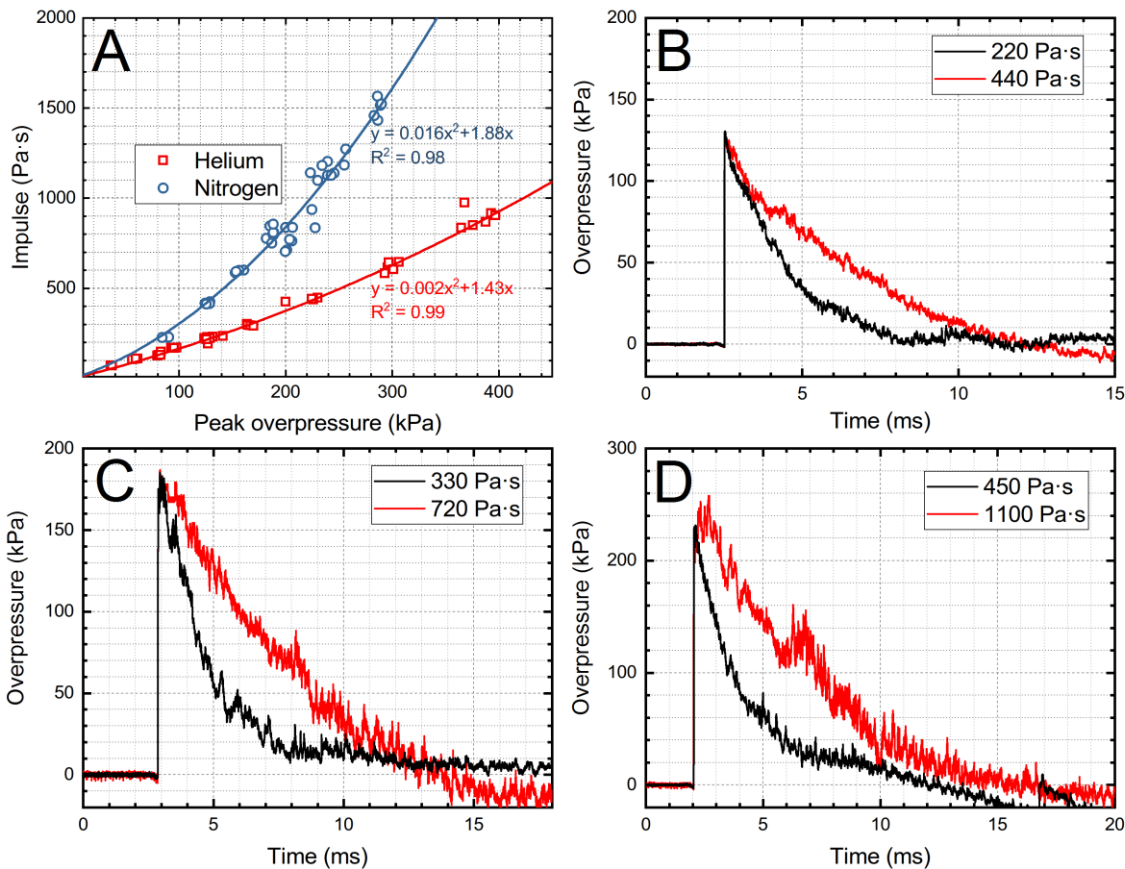
Figure 43 The BOP-impulse calibration. A. Two calibration curves for helium and nitrogen used as a basis for the development of the master impulse dose-response curves and BOP-impulse selection for biochemical and biomechanical evaluation. Representative curves illustrating controlled variable impulse at three nominal BOPs: B. 130 kPa, C. 180 kPa and D. 230 kPa.

repeated four times, for a total of 96 tests (2 x 3 x 4 x 4 = 96). Shock wave profile evolution was monitored by 6 pressure sensors distributed along the shock tube, and total of 576 profiles were generated (96 x 6 = 576). The data analysis consisted of quantification of four characteristics of the shock wave: 1) peak overpressure, 2) rise time, 3) duration and 4) impulse. The evaluation of time domain parameters (rise time and duration) included reading: 1) the time at 10% and 90% of the pressure increase of the shock front (for the rise time) and 2) onset of the pressure increase and intersection of the pressure decay with neutral (baseline) pressure (for the duration). The data points were fitted with two polynomial functions to establish low impulse and high impulse curves (figure 43) with the following six nominal BOP-impulse combinations selected for further tests: 1) 130 kPa-220 Pa·s, 2) 130 kPa-440 Pa·s, 3) 180 kPa-330 Pa·s, 4) 180 kPa-720 Pa·s, 5) 230 kPa-450 Pa·s, and 6) 230 kPa-1100 Pa·s.

Master impulse dose-response curves

The final step in the process of dose-response curves generation was the exposure of 150 animals to a single shock wave with precisely known peak overpressure and impulse values obtained from shock tube calibration experiments. The results are presented in figure 44. It is obvious that
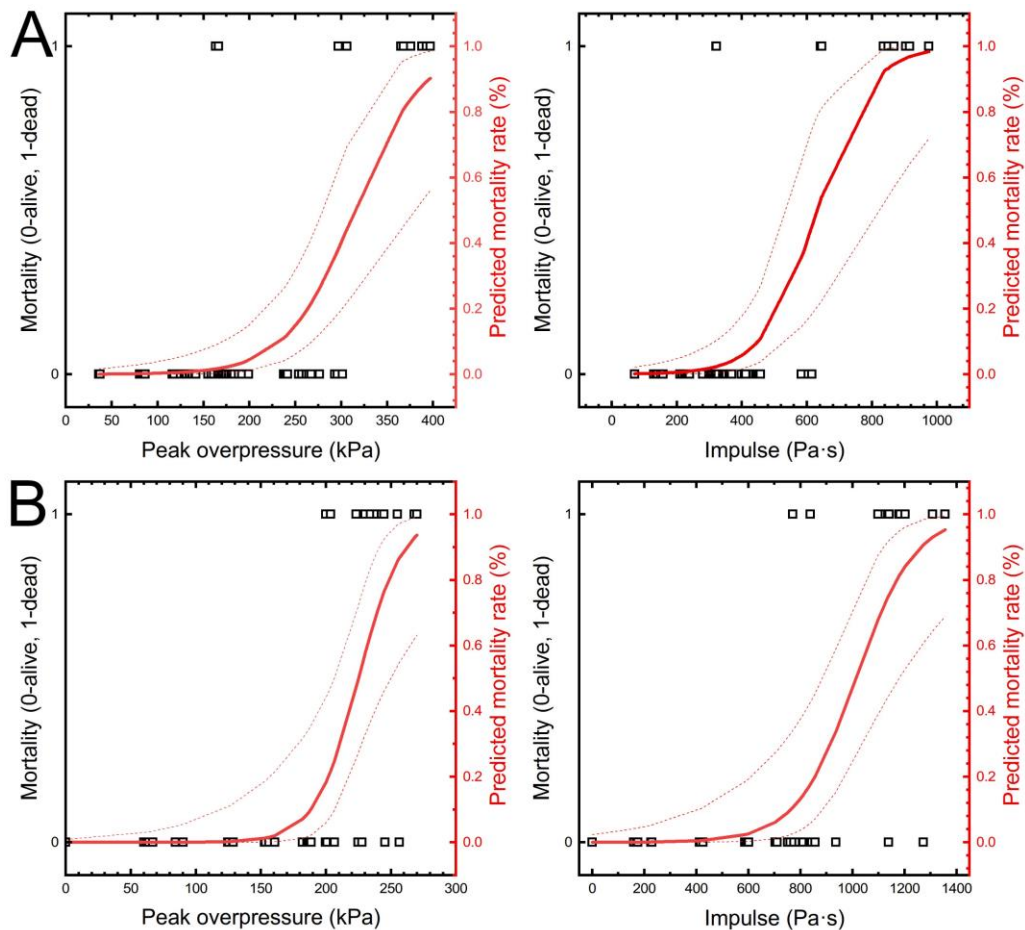
Figure 44 The two dose-response curves developed for short (A) and long (B) duration impulse using a cohort of 150 animals. Rats were exposed to a single shock wave with predefined characteristics, based on the two calibration curves (see fig. 43), and 24-hour survival was evaluated (0-alive, 1-dead). The data were fitted using binary logistic regression for BOP and impulse as mortality predictors. For long duration impulse (B) the shift towards lower BOPs is apparent.

mortality rates for long duration impulse are shifted towards lower peak overpressures (figure 44B): the 10%-90% predicted mortality rate (PMR) function are in the 230-400 kPa (figure 44A) and 190-260 kPa (figure 44B) peak overpressure for short and long impulse, respectively.

Task 9: Examine the changes in protein expression due to changes in blast impulse 24 hours after primary blast exposure (20% complete)

In this ongoing study as part of Specific Aim 3 we performed biomarker identification and examined by ELISA the levels of glial fibrillary acidic protein (GFAP), an astrocyte marker that is released into blood stream after astrocyte end feet damage. Blood samples were collected from control and animals exposed to moderate blast (180 kPa, immediately and 4 hours after injury) and levels of GFAP were examined by quantitative ELISA. Blast injury caused significant increase in plasma levels of GFAP immediately following blast and continued to show elevation until 4 hours after blast injury (Figure 45). These results not only indicate evidence of blood brain barrier breakdown following blast, but also that astrocytes undergo cellular (plasma membrane) damage following blast injury.
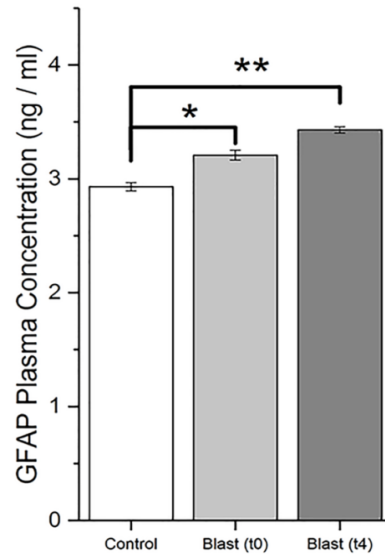
Figure 45 Levels of glial fibrillary acidic protein (GFAP) a marker of astrocytes in plasma samples obtained from animals of control, immediately and 4 hours after blast injury (180 kPa).

As part of proteomic analysis to identify different protein biomarkers following changes in blast impulse, we performed studies initially screening the levels of neuronal synaptic vesicle markers
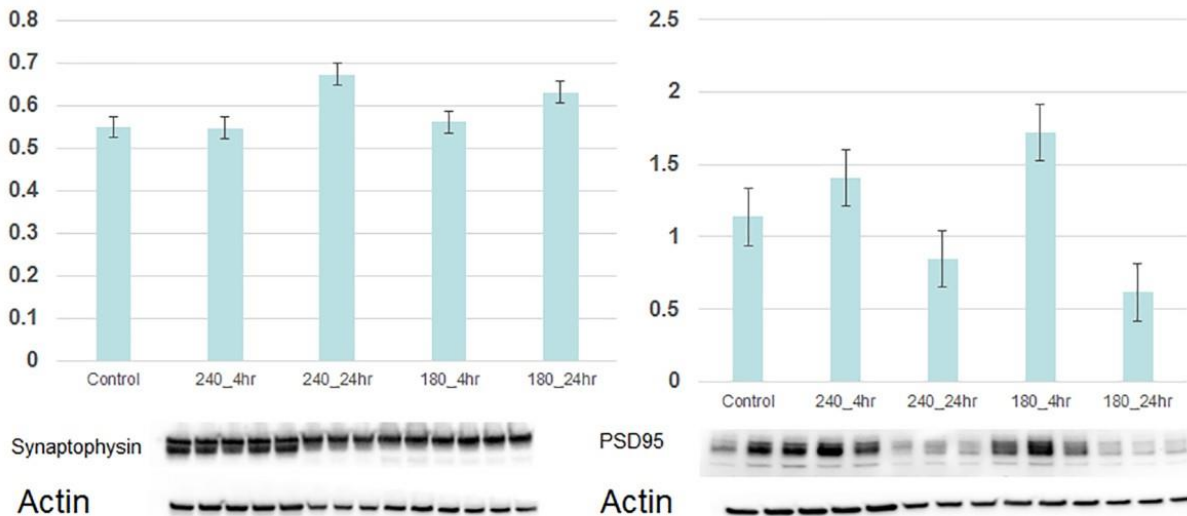
Figure 46 Levels of synaptophysin and PSD-95, markers of pre-and-post synaptic vesicles as a function of different BOPs. Note that there is an inverse correlation of changes between synaptophysin and PSD-95 24 hours post injury at 180 and 240 kPa.

synaptophysin and post-synaptic density protein of 95 kDa (PSD-95), markers of pre-and-post synapses in hippocampus of animals exposed to 2 BOPs (180 kPa and 240 kPa) and 24 hours after injury. Accordingly, lysates from hippocampus were used to determine the protein levels of synaptophysin (marker of presynaptic vesicles) and PSD95 (marker of post-synaptic vesicles) by immunoblot analysis. Results show differential changes in synaptophysin and PSD-95 as a function of different blast overpressures, in that synaptophysin protein levels showed strong tendency of increase at 24h post injury at both BOPs (180 and 240 kPa). However, PSD-95 protein levels show an increase as early as 4 h post injury, but their levels significantly reduced 24 hours after blast (Figure 46). These data strongly suggest: 1) blast injury causes post-synaptic vesicle protein changes earlier than pre-synaptic vesicle proteins and that while there appears to be an inverse correlation between pre-and-post synaptic vesicle protein changes 24 hours post-injury. Further studies are being carried out investigating proteomic analysis of synaptic vesicle changes following changes in blast impulse.

Task 10: Determine Alterations of Loading in the Rat Brain Caused by Changes in Impulse (completed)

We performed biomechanical loading evaluation on rats implanted with three sensors: two in the brain and a single sensor in the carotid artery (Figure 47). The measurements were performed at three nominal BOPs: 130, 180 and 230 kPa with variable shock wave impulse (Figure 48). The heads of rats were imaged using micro-CT scanner to establish precise location of the cannulas where pressure sensors were implanted. This information will be used in the development of the refined numerical model of the rat's head under shock wave loading conditions. The parametric studies of the material properties were completed, and manuscript submitted to AMBE journal
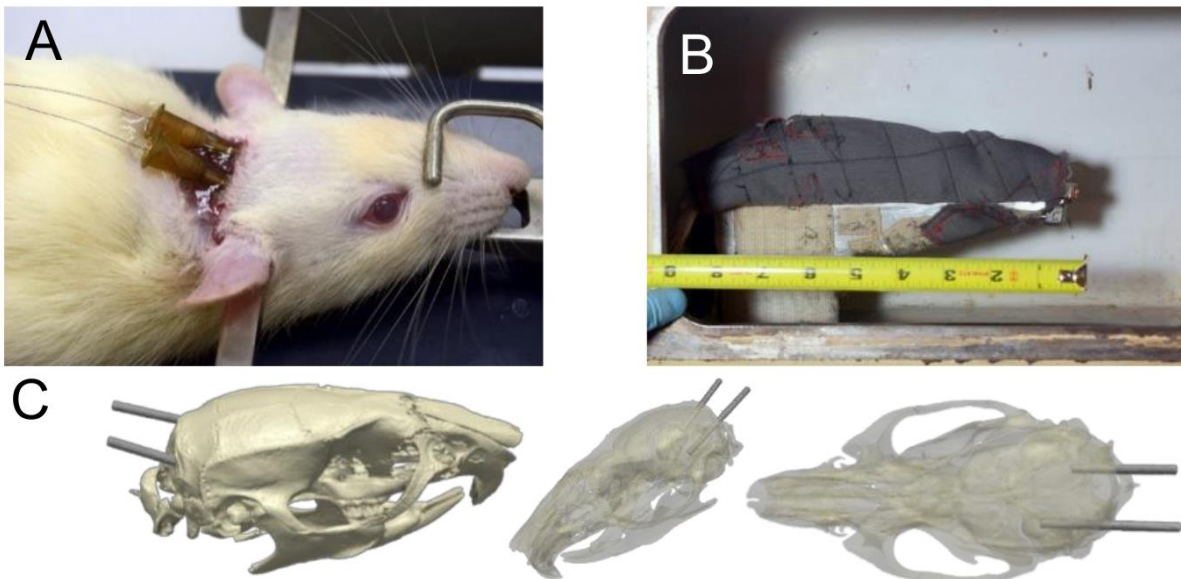
Figure 47 A. The specimen with cannulas inserted into the left and right hemispheres. B. The specimen secured in the cotton wrap within the shock tube in the prone position. C. Three-dimensional reconstruction of the μCT of the rat skull, showing the positions of the cannulas within the cranial cavity.

(currently under review). With the conclusion of Task 3 and Task 8, work has begun to apply the computational model and analysis techniques used to examine the effect of changing impulse. Six simulations are underway for this task, simulating low impulse blasts at overpressures of 130, 180, 230 kPa at low and high impulse values. The simulations have been constructed in an identical

manner as those reported in Task 3. The waveforms which are being used for these simulations are included in Figure 48D and E. Precluding unforeseen numerical solution instabilities or simulation artifacts resulting from the higher energy waveforms, results are anticipated to be completed for the Q1 Quarterly Report for Year 4.
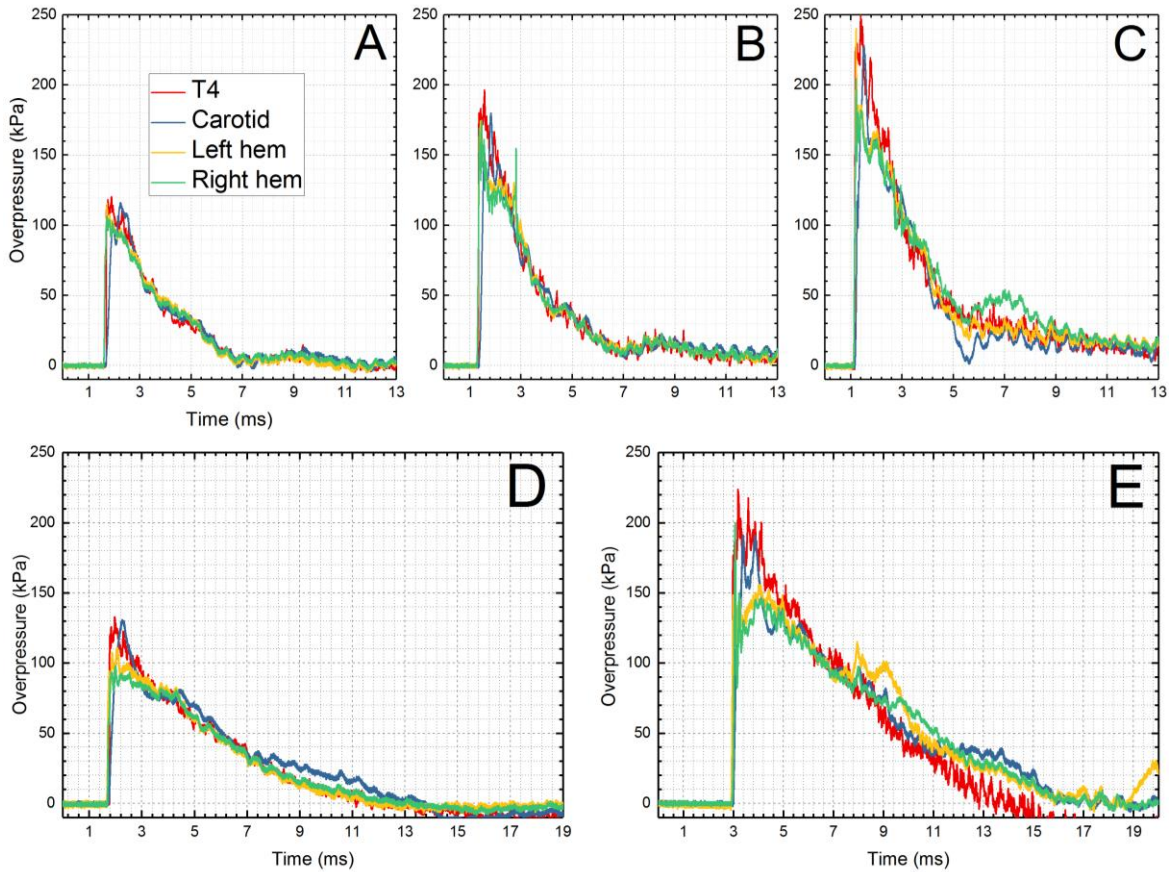
Figure 48 The biomechanical loading evaluation – the impulse effect. Double ICP and carotid artery pressure sensors were used to measure the pressures of rats exposed to the "low impulse" (with nominal BOP of: A. 130, B. 180, and C. 230 kPa) or "high impulse" (nominal BOP: D. 130 kPa, and E. 180 kPa). The durations in each group are illustrated.

References

1.   Ferreira AP, Rodrigues FS, Della-Pace ID, Mota BC, Oliveira SM, de Campos Velho Gewehr C, et al. HOE-140, an antagonist of B2 receptor, protects against memory deficits and brain damage induced by moderate lateral fluid percussion injury in mice. Psychopharmacology (Berl). 2014;231(9):1935-48. Epub 2013/11/10. doi: 10.1007/s00213-013-3336-x. PubMed PMID: 24202114.
2.   Cooney SJ, Bermudez-Sabogal SL, Byrnes KR. Cellular and temporal expression of NADPH oxidase (NOX) isotypes after brain injury. Journal of neuroinflammation. 2013;10(1):917.
3.   Choi BY, Jang BG, Kim JH, Lee BE, Sohn M, Song HK, et al. Prevention of traumatic brain injury-induced neuronal death by inhibition of NADPH oxidase activation. Brain research. 2012;1481:49-58.
4.   Kahles T, Kohnen A, Heumueller S, Rappert A, Bechmann I, Liebner S, et al. NADPH oxidase Nox1 contributes to ischemic injury in experimental stroke in mice. Neurobiology of disease. 2010;40(1):185-92.
5.   de la Monte SM, Wands JR. Molecular indices of oxidative stress and mitochondrial dysfunction occur early and often progress with severity of Alzheimer's disease. Journal of Alzheimer's disease. 2006;9(2):167-81.
6.   Zekry D, Epperson TK, Krause KH. A role for NOX NADPH oxidases in Alzheimer's disease and other types of dementia? IUBMB life. 2003;55(6):307-13.
7.   Skotak M, Chandra N. Primary Blast Injury Criteria for Animal/Human TBI Models using Field Validated Shock Tubes. New Jersey Institute of Technology: New Jersey Institute of Technology, Newark, NJ, 07102, 2016 W81XWH-15-1-0303 Contract No.: AD1033280.
8.   Misistia A. Rodent testing device surrogate for shockwave blast testing: New Jersey Institute of Technology; 2015.
9.   Baumgartner D, Lamy M, Willinger R, Choquet P, Goetz C, Constatinesco A, et al. Finite element analysis of traumatic brain injuries mechanisms in the rat. IRCOBI Conference2009. p. 97-108.
10.   Hua Y, Akula P, Kelso M, Gu L. Characterization of Closed Head Impact Injury in Rat. Biomed Research International. 2015;2015. doi: 10.1155/2015/272976.
11.   Gadd CW, Nahum AM, Schneider DC, Madeira RG. Tolerance and properties of superficial soft tissues in situ. SAE Technical Paper, 1970 0148-7191.
12.   Gefen A, Gefen N, Zhu QL, Raghupathi R, Margulies SS. Age-dependent changes in material properties of the brain and braincase of the rat. Journal of Neurotrauma. 2003;20(11):1163-77. doi: 10.1089/089771503770802853. PubMed PMID: WOS:000186784600002.
13.   Kuriakose M, Skotak M, Misistia A, Kahali S, Sundaramurthy A, Chandra N. Tailoring the Blast Exposure Conditions in the Shock Tube for Generating Pure, Primary Shock Waves: The End Plate Facilitates Elimination of Secondary Loading of the Specimen. PLoS One. 2016;11(9):e0161597. Epub 2016/09/08. doi: 10.1371/journal.pone.0161597. PubMed PMID: 27603017; PubMed Central PMCID: PMCPMC5014318.
14.   Skotak M, Alay E, Chandra N. On the accurate Determination of shock Wave Time-Pressure Profile in the experimental Models of Blast-induced neurotrauma. Frontiers in neurology. 2018;9:52.

What opportunities for training and professional development has the project provided?

Similarly, to previous years, a group of undergraduate students participated in projects developed as sub-sections of the project. Undergraduate students worked in the capacity of 20 hours per week under the supervision of graduate students, laboratory technicians, and senior researchers. Students gained practical knowledge of the techniques used in the characterization of blast TBI: 1) biochemistry: brain sectioning, immunostaining, and Western blot, 2) pressure measurements and 3) computer simulations: development of 3D models and hands on experience with FEM software, as well as analytical techniques used in these research areas. Results were presented during poster session on July 27, 2018, as a part of 11th International Undergraduate Summer Symposium organized by NJIT. The following students participated in the Undergraduate Summer Experience: Swathi Pavuluri, Sushni Mukkamalla, Waleed Mujib, Ajay Gandhi, Sainithin Kuntakukkala, Aayush Verma, Rahul Shah, Kaylah Ruiz, Dhruv Patel, Shahbaz Choudry, and Osama Mahgob

How were the results disseminated to communities of interest?

- Manuscripts:
    1. KV Rama Rao, S. Iring, D. Younger, M. Kuriakose, M. Skotak, E. Alay, R. K. Gupta, and N. Chandra. "A Single Primary Blast-Induced Traumatic Brain Injury in a Rodent Model Causes Cell-Type Dependent Increase in Nicotinamide Adenine Dinucleotide Phosphate Oxidase Isoforms in Vulnerable Brain Regions." *Journal of neurotrauma* 35, (2018) 2077-2090.
    2. M. Skotak, E. Alay, and N. Chandra. "On the accurate Determination of shock Wave Time-Pressure Profile in the experimental Models of Blast-induced neurotrauma." *Frontiers in neurology* 9 (2018) 52.
    3. M. Kuriakose, KV. Rama Rao, D. Younger, and N. Chandra. "Temporal and Spatial Effects of Blast Overpressure on Blood-Brain Barrier Permeability in Traumatic Brain Injury." *Scientific reports* 8, 1 (2018) 8681.
    4. G. Ordek, A.S. Asan, E. Cetinkaya, M. Skotak, V. R. Kakulavarapu, N. Chandra, and M. Sahin. "Electrophysiological Correlates of Blast-Wave Induced Cerebellar Injury." *Scientific Reports* 8, (2018) 13633.
    5. Daniel Younger, M. Murugan, KV Ramarao, L.-J. Wu, and N. Chandra, "Microglia Receptors in Traumatic Brain Injury", Molecular Neurobiology, accepted.
- Conference presentations; see section 6. Products.

What do you plan to do during the next reporting period to accomplish the goals?

In the year 4 of the project, we are planning to complete the examination of the protein changes related to the effect of *impulse*. We collected brain samples, and the results of the analysis will be reported in the following quarterly reports.

The focus of the research effort for year 4 deliverables is the development of the interspecies scaling laws. We have established the foundation for the numerical simulations (rat and human 3D models, ICP measurements for the rat), and will supplement these with the experimental data using post-mortem human specimen (PMHS). We will conduct blast exposure using PMHS heads mounted on Hybrid III mechanical necks. The intracranial space of PMHS heads will be backfilled with ballistic gel, which is a validated surrogate material for human brain considering similarities in acoustic properties of the brain and ballistic gel. Brain surrogate is needed to replace the brain tissue damaged because of autolysis progressing post-mortem rapidly.

The PMHS specimens will be instrumented to measure surface reflected pressure, surface deformation using strain gauges, and ICP. Each specimen will be exposed at least three times (n=3) at a single specified incident peak overpressure, and for a given condition at least three different pressures will be used.

4. IMPACT

What was the impact on the development of the principal discipline(s) of the project?

1. Computational models of bTBI require a robust definition of the constitutive material models of biological tissues, which are difficult to characterize, leading to a range of values reported in literature that span multiple orders of magnitude. We systematically evaluated the sensitivity of the intracranial pressure (ICP) and maximum principal strain to variations in the material model of the brain through a combined computational and experimental approach. A FEM model of a rat was created to simulate an experimental shock wave exposure. The time-independent and time-dependent properties of the brain were parametrically varied. An effective long-term bulk modulus values of 80 MPa exhibited the best match with experimental measurements of ICP. This work will establish a validated set of material properties and aid the development of numerical models where experimental validation is not available and serve as a basis for the development of interspecies scaling laws.

2. We identified piezoelectric pressure sensors are susceptible to electrostatic interference. These piezoelectric sensors (e.g. PCB 134A24) are widely used in the field and shock tube testing to measure the pressure experienced by animal models, and when exposed to electrostatic charges inherent to shock wave report erroneous pressure values. Manufacturers of these sensors were unaware of this effect in spite of decades of development and their own shock tube testing. These findings are summarized in the paper published in Frontiers of Neurology (M. Skotak, E. Alay, N. Chandra, *Front. Neurol. 9:52.* (2018), doi: 10.3389/fneur.2018.00052), which also serves as a guideline how to avoid pitfalls in pressure measurements while conducting shock tube testing. The follow up manuscript is in preparation, which will demonstrate quantitative effects associated with electrostatic interference on accuracy of reported pressure. In a nutshell, while peak pressures are mostly unaffected, the duration and impulse are decreased by a factor of 30% to 50%.

3. The effect of impulse on survival and brain pathology. We demonstrated for the first time the control over the impulse at arbitrarily chosen fixed peak overpressure (year 3 contribution). We performed a series of calibration tests which permit generation of shock waves with Friedlander waveform at fixed BOP and various impulse. Our data indicate that at 180 kPa and 230 kPa BOP at *high* impulse results in 20% and 80% mortality rate, respectively, while mortality rates are nearly 0% at these BOPs and *low* impulse. The impulse is an important parameter of the etiology of bTBI, and it is nearly neglected by research community, i.e. there are no reports investigating effects associated with impulse in the recent literature. More importantly, impulse values are only rarely reported. We have screened a pool of 100 papers selected from existing literature on animal and *in vitro* models of bTBI covering the last 20 years of research to identify reporting standards regarding shock wave parameters. This survey gives an overview and revealed the following trends: in most of the published work (97%), peak overpressure is reported as the most important parameter (see Table S1 in Supplementary Material in M. Skotak, E. Alay, N. Chandra, *Front. Neurol. 9:52.* (2018), doi: 10.3389/fneur.2018.00052). Interestingly, little attention is devoted to other characteristics of the shock wave waveform: the duration (51%), *impulse (18%)*, the sampling frequency (46%).

What was the impact on technology transfer?

Nothing to report.

What was the impact on other disciplines?

We noted blast gauges used to monitor low-level blast exposure in training are susceptible to similar artifacts like commercially available pressure sensors. Those artifacts result in underreporting of peak overpressure and impulse values by the quantification algorithm embedded in the blast gauge software. We shared our expertise in this area with the team WRAIR team lead by Dr. Kamimori (personal communication and white paper), which helped improve the quality of the data collected in their studies.

What was the impact on society beyond science and technology?

Nothing to report.

5. CHANGES/PROBLEMS

The Project Director/Principal Investigator (PD/PI) is reminded that the recipient organization is required to obtain prior written approval from the awarding agency Grants Officer whenever there are significant changes in the project or its direction. If not previously reported in writing, provide the following additional information or state, "Nothing to Report," if applicable:

Changes in approach and reasons for change

Nothing to Report.

Actual or anticipated problems or delays and actions or plans to resolve them
Describe problems or delays encountered during the reporting period and actions or plans to resolve them.

A modification to year 4 use of human skull instead of PMHS was requested for increasing the total number of experiments and better scientific correlation with animal data. The request was denied.

Changes that had a significant impact on expenditures
Describe changes during the reporting period that may have had a significant impact on expenditures, for example, delays in hiring staff or favorable developments that enable meeting objectives at less cost than anticipated.

None.

Significant changes in use or care of human subjects, vertebrate animals, biohazards, and/or select agents
Describe significant deviations, unexpected outcomes, or changes in approved protocols for the use or care of human subjects, vertebrate animals, biohazards, and/or select agents during the reporting period. If required, were these changes approved by the applicable institution committee (or equivalent) and reported to the agency? Also specify the applicable Institutional Review Board/Institutional Animal Care and Use Committee approval dates.

Significant changes in use or care of human subjects

None.

Significant changes in use or care of vertebrate animals.

None.

Significant changes in use of biohazards and/or select agents

None.

6. PRODUCTS

List any products resulting from the project during the reporting period. If there is nothing to report under a particular item, state "Nothing to Report."

- **Publications, conference papers, and presentations**
  Report only the major publication(s) resulting from the work under this award.

  Journal publications (all published):

  1. KV Rama Rao, S. Iring, D. Younger, M. Kuriakose, M. Skotak, E. Alay, R. K. Gupta, and N. Chandra. "A Single Primary Blast-Induced Traumatic Brain Injury in a Rodent Model Causes Cell-Type Dependent Increase in Nicotinamide Adenine Dinucleotide Phosphate Oxidase Isoforms in Vulnerable Brain Regions." *Journal of neurotrauma* 35, (2018) 2077-2090.
  2. M. Skotak, E. Alay, and N. Chandra. "On the accurate Determination of shock Wave Time-Pressure Profile in the experimental Models of Blast-induced neurotrauma." *Frontiers in neurology* 9 (2018) 52.
  3. M. Kuriakose, KV. Rama Rao, D. Younger, and N. Chandra. "Temporal and Spatial Effects of Blast Overpressure on Blood-Brain Barrier Permeability in Traumatic Brain Injury." *Scientific reports* 8, 1 (2018) 8681.
  4. G. Ordek, A.S. Asan, E. Cetinkaya, M. Skotak, V. R. Kakulavarapu, N. Chandra, and M. Sahin. "Electrophysiological Correlates of Blast-Wave Induced Cerebellar Injury." *Scientific Reports* 8, (2018) 13633.
  5. Daniel Younger, M. Murugan, KV Ramarao, L.-J. Wu, and N. Chandra, "Microglia Receptors in Traumatic Brain Injury", Molecular Neurobiology, accepted.

  Books or other non-periodical, one-time publications.

  Nothing to Report.

Other publications, conference papers, and presentations.

Conference presentations:
1. Neuroscience 2017, the Society for Neuroscience Annual Meeting, Washington D.C, November 11-15, 2017:
   a. Namas Chandra, KV RamaRao, Stephanie Iring, Daniel Younger, Aswati Aravind, Bryan Pfister, Matthew Kuriakose, Maciej Skotak, "Blast-Induced Traumatic Brain Injury Displays a Unique Pattern of Spatial Neuropathology" Session 392: 07102-1982.
   b. Aswati Aravind, Pfister BJ, Kakulavarapu V. Rama Rao, Mathew Long, Namas Chandra, "Characterization of Combined Model of Blast and Blunt" Session 141: 141.01-CC1.
2. 5th National Symposium on Shockwaves, Chandigarh, India, February 26-28, 2018
   a. Poonam Rana, Rama Rao V. Kakulavarapu, Matthew Kuriakose, Subash Khushu[2] Richa Trivedi, Raj Gupta, Namas Chandra "Experimental Model of Blast Shows Whole-brain and Regional Variations in Histopathology and Metabolomics profile".
   b. Richa Trivedi, Priyanka Sharma, Maria M D'souza, Namas Chandra, Subash Khushu, Raj K Gupta, Ajay K Singh "Altered Diffusion Indices of the Rat Brain Parenchyma after Mild Blast Induced Traumatic Neurotrauma (BINT)".
   c. Molly Townsend, Priyanka Sharma, Maciej Skotak, Ajay Kumar Singh, Maria D'Souza Subhash Khushu, Raj Gupta and Namas Chandra "Validation of a compressed-gas driven shocktube against free-field shocks and a computational model".
   d. Maria M D'Souza, Richa Trivedi, Amit Bagchi, Namas Chandra, Raj Gupta, Subhash Khushu, and Ajay Kumar Singh "Role of Advanced Imaging Methods in Mild Traumatic Brain Injury".
   e. Namas Chandra, Ajay K Singh, Subash Khushu and Raj Gupta. "Blast Induced Neurotrauma-Current state of clinical and experimental progress".
3. Military Health Sciences Research Symposium, Kissimmee, FL, August 20-23, 2018:
   a. Daniel Younger, Rama Rao V. Kakulavarapu, Arunreddy Ravula, Namas Chandra "Microglia Interaction with Blood Brain Barrier following Blast TBI: Role of Inflammasome".
   b. Matthew Kuriakose, Rama Rao V. Kakulavarapu, Namas Chandra "Synergistic Role of Oxidative Stress and Blood Brain Barrier Permeability as Potential as Potential Mechanisms in Blast-induced Neurotrauma".
   c. Molly Townsend, Maciej Skotak, Namas Chandra, "Computational and Experimental Methods to Understand Traumatic Brain Injury Mechanisms".
4. Institute of Brain and Neuroscience Research, Graduate Student/Post-Doctoral Showcase, NJIT Newark, March 29, 2018:
   a. Debrina Roy, Molly Townsend, Maciej Skotak, Namas Chandra, "Development, Convergence, and Validation of a Rat Finite Element Model Applicable to the Investigation of Blast-Induced Traumatic Brain Injury".
   b. Molly Townsend, Namas Chandra, "The limitations of a modeling shockwave development in a shocktube using commercially available finite element tools".
   c. Madhuvika Murugan, Vijayalakshimi Santhakumar, Namas Chandra "Mechanisms underlying epileptogenisis following blast induced traumatic brain injury in rat model".
5. The 3rd Annual Rutgers Brain Health Institute Symposium, Raritan Valley College, Branchburg, NJ, December 1, 2017:
   a. Madhuvika Murugan, Bogumila Swietek, Vijayalakshmi Santhakumar, Namas Chandra "Mechanisms underlying epileptogenesis following blast induced traumatic brain injury in rat model".
   b. Madhuvika Murugan, Daniel Younger, Maciej Skotak, Rama Rao, Bryan Pfister, Namas Chandra "Blast and brain injury research at the Center for Injury Biomechanics materials and medicine at NJIT".
6. Mid Atlantic Brain Symposium, Piscataway, NJ, April 17, 2018:
   a. Madhuvika Murugan, Maciej Skotak, K.V. Rama Rao, Molly Townsend, Bryan Pfister, Namas Chandra "Multidisciplinary Approach to Understand the Pathology of Blast induced Traumatic Brain Injury".
7. Biomedical Engineering Society Annual Meeting, Phoenix, AZ, October 11-14, 2017:
   a. N. Chandra, K.V. Rama Rao, S. Iring, D. Younger, A. Aravind, B. Pfister, M. Skotak, "Blast-induced Traumatic Brain Injury Displays a Unique Pattern of Spatial Resolution of Brain NADPH oxidase".
   b. A. Asan, G. Ordek, E. Cetinkaya, V. Kakulavarapu, M. Skotak, N. Chandra, M. Sahin, „Assessment of Cerebellar Injury in Rats Using Evoked Potentials and a Behavioral Task".
8. 2017 International State of the Science Meeting, Arlington, VA, March 12-14, 2018:
   a. Namas Chandra, Rama Rao V. Kakulavarapu, Maciej Skotak, and Matthew Kuriakose, "Blood-brain barrier permeability is a sensitive neurological marker for single and repeated occupational low-level blast exposures in a rodent model".

- **Website(s) or other Internet site(s)**
  List the URL for any Internet site(s) that disseminates the results of the research activities. A short description of each site should be provided. It is not necessary to include the publications already specified above in this section.

<div style="border:1px solid black; padding:10px;">

Nothing to Report.

</div>

- **Technologies or techniques**
  Identify technologies or techniques that resulted from the research activities. In addition to a description of the technologies or techniques, describe how they will be shared.

<div style="border:1px solid black; padding:10px;">

Nothing to Report.

</div>

- **Inventions, patent applications, and/or licenses**
  Identify inventions, patent applications with date, and/or licenses that have resulted from the research. State whether an application is provisional or non-provisional and indicate the application number. Submission of this information as part of an interim research performance progress report is not a substitute for any other invention reporting required under the terms and conditions of an award.

- **Other Products**

What individuals have worked on the project?
Provide the following information for: (1) PDs/PIs; and (2) each person who has worked at least one-person month per year on the project during the reporting period, regardless of the source of compensation (a person month equals approximately 160 hours of effort). If information is unchanged from a previous submission, provide the name only and indicate "no change."

Name: Namas Chandra
Project Role: PI/PD
Researcher Identifier:
Nearest person month worked: 2
Contribution to Project: Design of the research, data interpretation

Name: Maciej Skotak
Project Role: Research Scientist
Researcher Identifier: 0000-0003-2584-7294
Nearest person month worked: 6
Contribution to Project: Exposure of animals, supervision of students & staff, data analysis, proteomics, manuscript and report preparation

Name: RamaRao Venkata Kakulavarapu
Project Role: Research Scientist
Researcher Identifier:
Nearest person month worked: 6
Contribution to Project: Overseeing of biochemistry analysis, supervision of students and staff, manuscript and report preparation

Name: Molly Townsend
Project Role: Research Scientist
Researcher Identifier:
Nearest person month worked: 6
Contribution to Project: Development of the rat model, shock tube numerical simulations, data analysis, supervision of students

Name: Eren Alay
Project Role: Laboratory technician
Researcher Identifier:
Nearest person month worked: 6
Contribution to Project: Assistance with exposure of animals, shock wave experimentation, data analysis and quantification

Name: Sudeepto Kahali
Project Role: Graduate student
Researcher Identifier:
Nearest person month worked: 3
Contribution to Project: Development of the rat model, shock tube numerical simulations

Name: Ravula Arun Reddy
Project Role: Graduate student
Researcher Identifier:
Nearest person month worked: 4
Contribution to Project: Biochemical analysis, staining of brain sections

Name: Matthew Kuriakose
Project Role: Graduate Student
Researcher Identifier:
Nearest person month worked: 6
Contribution to Project: Assistance with shock wave experimentation, exposure of animals, biochemistry work, data analysis, manuscript preparation

Name: Daniel Younger
Project Role: Graduate Student
Researcher Identifier:
Nearest person month worked: 6
Contribution to Project: Assistance with shock wave experimentation, exposure of animals, biochemistry work, data analysis, manuscript preparation

Name: Smit Shah
Project Role: Graduate student
Researcher Identifier:
Nearest person month worked: 3
Contribution to Project: Western blot, immunohistochemistry, ELISA, sectioning of brain sections, data quantification

Name: Sainithin Kuntakukkala
Project Role: Graduate student
Researcher Identifier:
Nearest person month worked: 4

Contribution to Project: Western blot, immunohistochemistry, sectioning of brain sections, data quantification

Name: Ryan Rattazzi
Project Role: Undergraduate student
Researcher Identifier:
Nearest person month worked: 2
Contribution to Project: Assistance with shock tube experiments, data analysis

Name: George Fahmy
Project Role: Undergraduate student
Researcher Identifier:
Nearest person month worked: 1
Contribution to Project: Assistance with shock tube experiments, data analysis

Name: Rahul Shah
Project Role: Undergraduate student
Researcher Identifier:
Nearest person month worked: 2
Contribution to Project: Development of the rat model, shock tube numerical simulations

Has there been a change in the active other support of the PD/PI(s) or senior/key personnel since the last reporting period?
If there is nothing significant to report during this reporting period, state "Nothing to Report."

If the active support has changed for the PD/PI(s) or senior/key personnel, then describe what the change has been. Changes may occur, for example, if a previously active grant has closed and/or if a previously pending grant is now active. Annotate this information so it is clear what has changed from the previous submission. Submission of other support information is not necessary for pending changes or for changes in the level of effort for active support reported previously. The awarding agency may require prior written approval if a change in active other support significantly impacts the effort on the project that is the subject of the project report.

No.

What other organizations were involved as partners?

Nothing to Report.

7. SPECIAL REPORTING REQUIREMENTS

COLLABORATIVE AWARDS: For collaborative awards, independent reports are required from BOTH the Initiating PI and the Collaborating/Partnering PI. A duplicative report is acceptable; however, tasks shall be clearly marked with the responsible PI and research site. A report shall be submitted to **https://ers.amedd.army.mil** for each unique award.

QUAD CHARTS: If applicable, the Quad Chart (available on https://www.usamraa.army.mil) should be updated and submitted with attachments.

8. APPENDICES

Primary Blast Injury Criteria for Animal/Human TBI Models using Field Validated Shock Tubes
14059001
W81XWH-15-1-0303

PI: Namas Chandra   **Org:** New Jersey Institute of Technology   **Award Amount:** 3,330,279

Study/Product Aim(s)

• Shock tube calibration to establish control over shock wave characteristics
• Develop master *impulse* dose-response curve
• Evaluat the biomechanical loading in the rat brain caused by the extended impulse
• Characterize the protein changes associated with exposure to the short and long impulse

Approach

We established the low impulse and high impulse curves, and six nominal BOP-impulse combinations were selected for further tests: 1) 130 kPa-220 Pa·s, 2) 130 kPa-440 Pa·s, 3) 180 kPa-330 Pa·s, 4) 180 kPa-720 Pa·s, 5) 230 kPa-450 Pa·s, and 6) 230 kPa-1100 Pa·s. Biomechanical loading was established via ICP measurements at these conditions. The mortality increased significantly at high-impulse blast compared to low-impulse based on the dose-response model data. The analysis of the proteome in the low- and high-impulse groups is currently ongoing.
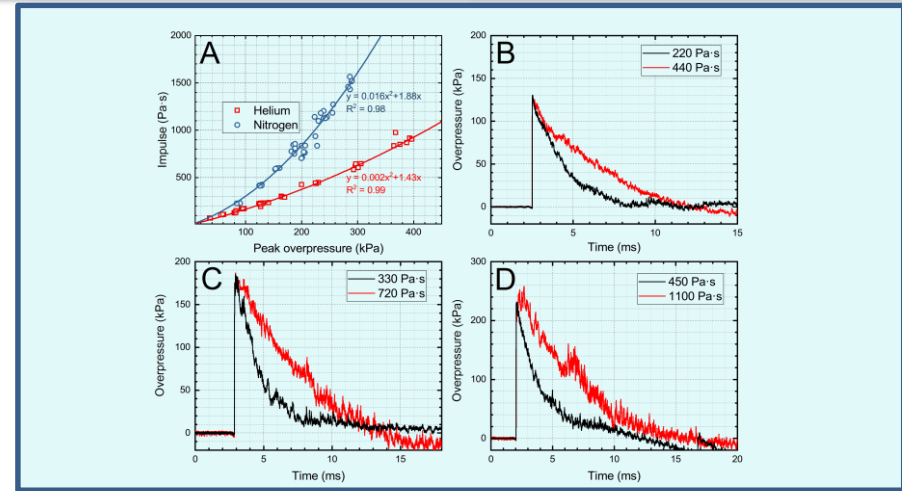
Accomplishment: The BOP-impulse calibration: A. curves used for development of the master *impulse* dose-response curves and biomechanical evaluation. Representative curves illustrating controlled variable impulse at three nominal BOPs: B. 130 kPa, C. 180 kPa and D. 230 kPa.

Timeline and Cost

Activities CY	16	17	18	19
Master dose response curves				
Assess mild-moderate bTBI				
Effect of impulse on master curves				
Establish HIC for bTBI (x-species)				
Estimated Budget ($K)	$1,064	$728	$773	$764

Updated: September 15th, 2018

Goals/Milestones (3 years only)

CY16 Goal: Develop Master Dose Response Curves for 10 w/o SD rats
☑ Evaluate Mortality & Biomechanical Loading in Wide Range of BOP
☑ Determine Biomechanical Loading of Rat Brain in Simulated Blast
☑ Numerical Simulation of Brain Injury

CY17 Goal: Assess Pathologies of bTBI 24 hours After Exposure
☑ Evaluate the Lung Injuries Caused by Blast Exposure
☑ Assess Oxidative/Nitrosative Stress, BBB Damage and Inflammation
☑ Evaluate Alterations in Brain Proteome After Primary Blast Exposure

CY18 Goal: Effect of Blast Impulse on Master Dose-Response Curve
☑ Establish Master Impulse Dose-Response Curve at Three BOPs
☐ Protein Expression Due to Changes in Blast Impulse
☑ Effect of Changes in Impulse on Loading in the Rat Brain

Comments/Challenges/Issues/Concerns
• Timeline change: N/A.
• Spending change: N/A.

Budget Expenditure to Date
Projected Expenditure: 100%
Actual Expenditure: 90%

On the Accurate Determination of Shock Wave Time-Pressure Profile in the Experimental Models of Blast-Induced Neurotrauma

Maciej Skotak, Eren Alay and Namas Chandra*

Department of Biomedical Engineering, New Jersey Institute of Technology, Newark, NJ, United States

Measurement issues leading to the acquisition of artifact-free shock wave pressure-time profiles are discussed. We address the importance of in-house sensor calibration and data acquisition sampling rate. Sensor calibration takes into account possible differences between calibration methodology in a manufacturing facility, and those used in the specific laboratory. We found in-house calibration factors of brand new sensors differ by less than 10% from their manufacturer supplied data. Larger differences were noticeable for sensors that have been used for hundreds of experiments and were as high as 30% for sensors close to the end of their useful lifetime. These observations were despite the fact that typical overpressures in our experiments do not exceed 50 psi for sensors that are rated at 1,000 psi maximum pressure. We demonstrate that sampling rate of 1,000 kHz is necessary to capture the correct rise time values, but there were no statistically significant differences between peak overpressure and impulse values for low-intensity shock waves (Mach number <2) at lower rates. We discuss two sources of experimental errors originating from mechanical vibration and electromagnetic interference on the quality of a waveform recorded using state-of-the-art high-frequency pressure sensors. The implementation of preventive measures, pressure acquisition artifacts, and data interpretation with examples, are provided in this paper that will help the community at large to avoid these mistakes. In order to facilitate inter-laboratory data comparison, common reporting standards should be developed by the blast TBI research community. We noticed the majority of published literature on the subject limits reporting to peak overpressure; with much less attention directed toward other important parameters, i.e., duration, impulse, and dynamic pressure. These parameters should be included as a mandatory requirement in publications so the results can be properly compared with others.

Keywords: shock wave, shock tube, peak overpressure, impulse, sampling frequency, electrostatic charges, baseline drift

INTRODUCTION

The blast-induced traumatic brain injury (bTBI) is a signature "invisible wound" among active military personnel partaking in war theaters in Iraq and Afghanistan (1–3). Specifically, the mild TBI (mTBI) remains an important public health problem: 2000–2016 period, the Department of Defense reported more than 360,000 cases of combat- and non-combat-related head injuries of which 82.4%

were mTBI (4, 5). A recent analysis of literature related to studies performed on veterans returning from deployment indicates the "at least half of the TBIs related to the wars in Iraq and Afghanistan appears to be blast related" (6). Human studies provide an array of health outcomes associated with mTBI, ranging from anxiety, depression, post-traumatic stress disorder, and post-concussive symptoms (7), but it is difficult to correlate precisely these symptoms with exposure to blast without knowledge about levels and frequency of exposure. This situation was partially ameliorated by the deployment of Blast Gauge™ system (8), which aids in the retrieval of this crucial information about overpressure "dosage" (a waveform exceeding the predefined threshold is recorded with 100 kHz sampling frequency) and in turn, allows reconstruction of specific incidents involving blasts (9). A large amount of collected data, issues with data interpretation and lack of associated medical history has inhibited the development of correlations between exposure levels with outcomes (10).

Animal models are, thus used to gain an insight into etiology of brain trauma and to study underlying molecular mechanism. The success of these studies in bTBI research area relies on a number of factors, and the two chief ones are: (1) appropriate exposure condition, equivalent to those experienced in the field and (2) proper animal restraint to eliminate injuries other than those classified as primary bTBI (exposure to shock wave only) (11, 12). In the laboratory setting, the shock tubes are used to recreate bTBI etiology in animal models (13–15). The importance of animal location on the characteristics of the loading conditions has been recently demonstrated (16): in general, animals mounted for testing inside of the shock tube are exposed to shock wave resulting in primary blast TBI (17). Animal models tested inside experience a higher level of loading caused by static pressure, simply because higher peak overpressures and durations can be achieved inside when compared with the outside. This difference is demonstrated in reported durations in the published literature where unlike inside the shock tube, overpressure durations longer than 2 ms have not been reported outside of the shock tube (18–22). Furthermore, acceleration of the rodent head, and body caused by dynamic pressure (jet effect) of expanding shock wave (classified as tertiary blast injury) are characterized by increased level of injury compared with primary blast TBI (23).

The distinction between primary and other types of TBI is important to allow comparison of results between laboratories. However, this comparison will not be complete if shock wave-associated parameters are not measured and disclosed in the reports. We have screened a pool of 100 papers selected from existing literature on animal and *in vitro* models of bTBI covering the last 20 years of research to identify reporting standards regarding shock wave parameters. This survey gives an overview and revealed the following trends: in a majority of the published work (97%), peak overpressure is reported as the most important parameter (see Table S1 in Supplementary Material for details). Interestingly, little attention is devoted to other characteristics of the shock wave waveform: the duration (51%), impulse (18%), the sampling frequency (46%), and finally the rise time, which is essentially neglected (2%). Only in very few papers, all four of these parameters were provided (20, 24–27), including or not sampling rates used in these studies.

In this paper, we discuss issues related to overpressure measurements: the importance of pressure transducer calibration, the effect of sampling frequency on the quantification of shock waveform characteristics, and preventive measures to avoid signal corruption. Electromagnetic interference and mechanical vibration are two aggravating factors that lead to an acquisition of incorrect waveforms with exaggerated peak overpressure values and baseline drifts, which might lead to erroneous duration and impulse values. We present preventive measures, which are illustrated with examples of experimental data.

MATERIALS AND METHODS

The Shock Tubes
Both large (28-inch square cross section) and small (9-inch square cross section) scale shock tubes at the New Jersey Institute of Technology have modular design and the following characteristics (**Figure 1**): (1) adjustable volume breech, (2) variable length transition section, (3) the 6 m long test section, equipped with bullet-proof glass windows for high-speed video observation of the specimen during the shock wave exposure, and (4) the reflector end-plate. In all experiments described in this contribution, the compressed helium was filled into the fixed volume breech, which is separated from the main body of the shock tube by Mylar membranes [for a detailed description of the principles of operation an informed reader is referred to Ref. (28, 29)].

Overpressure Measurement
A series of pressure sensors distributed along the length of the shock tube was used to measure pressure-time profiles of incident shock wave (**Figure 1B**) (28). The incident pressure was measured using high-frequency Tourmaline pressure transducers model 134A24 (1,000 psi maximum pressure, resonant frequency ≥1,500 kHz, 0.2 μs rise time, PCB Piezotronics, Depew, NY, USA). These sensors use 402 charge amplifiers, which are connected in series with pressure transducers *via* 3-inch-long low-noise cable with 10–32 coaxial jacks. In headform exposure experiments, we used high-frequency ICP® model 102B06 pressure transducers (500 psi maximum pressure, resonant frequency ≥500 kHz, and ≤1.0 μs rise time, PCB Piezotronics, Depew, NY, USA). All data were recorded at 1.0 MHz sampling frequency, and the typical acquisition time ranged from 50 to 200 ms. The 134A series sensors have 1/2–20 thread and require mounting holes of larger diameter; we used 5/8–18 tapped threaded holes, which are blinded with appropriate screws when not in use. Sensors are mounted in 0.25-inch thick steel brackets with rubber feet to prevent the transfer of the vibrations from the shock tube wall. Brackets with sensors are clamped to the shock tube wall, which prevents their displacement by pressure during shock wave experiments (**Figure 1A**, inset). There are 11 pressure sensor mounting openings in the shock tube designated as An, Bn, Cn, or Dn, depending on which module of the shock tube these sensors are located, where the number $n = 1, 2, 3,...$ indicates the consecutive sensor count for that specific module (**Figure 1B**). There are an additional nine ports in the test section located in the
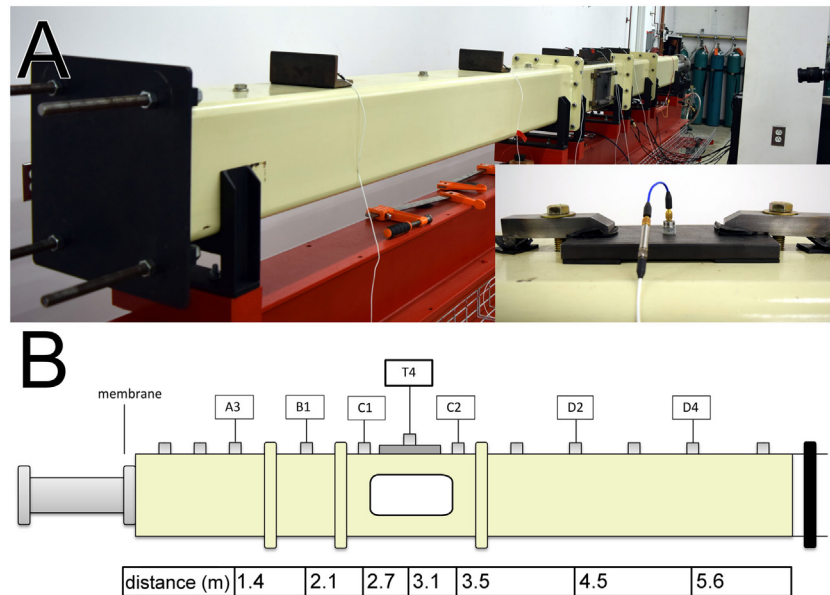
FIGURE 1 | The 9-inches square cross section shock tube: the rear view with the reflector plate and sensor brackets distributed along the shock tube **(A)**. The inset depicts PCB 134A24 sensor (connected *via* 3 in long low-noise cable to a series 402 charge amplifier) in the modified sensor mounting system with rubberized brackets and steel clamps preventing vertical movement of the sensor caused by the pressure of the passing shock wave. Schematic representation of the shock tube with sensor labeling and sensor distances from the membrane mounting port in the breech **(B)**. Only ports used in experiments described therein are indicated in the diagram.

C module of the shock tube and denoted as Tn (for $n = 1$–9). Typically, only six to seven sensors are used at the same time to capture a representative snapshot of the evolution of the shock wave profile.

Pressure Sensor Calibration

Pressure sensor calibration methodology developed in our lab relies on the measurement of the shock wave velocity which is related to the overpressure using Rankine–Hugoniot relationship:

$$\Delta P = \frac{\left(M^2 - 1 \right) 2 \gamma_i P_{at}}{\gamma_i}, \qquad (1)$$

where ΔP—overpressure, M—Mach number, γ_i—specific heat ratio (1.4 for nitrogen, 1.66 for helium), P_{at}—atmospheric pressure.

Typically, an array of seven sensors is mounted in a straight-line along the shock tube axis spanning the distance of 10 inches (first to last, **Figure 2A**). Sensors are mounted using tapped holes in a single steel plate and mounted in the test section and the plate is secured in place using clamps, to prevent vertical displacement. This is an important precaution for accurate measurement of the sensor output (in volts) which is used to calculate calibration constant. The shock wave velocity is calculated based on the arrival time between sensors and typically a combination of 21 measurements is used. The average velocity is used to calculate corresponding experimental overpressure, ΔP from Eq. 1. The voltage output from the sensor divided by ΔP gives calibration factor.

Electrostatic Interference

The baseline drift caused by electrostatic charges was recorded using six pressure sensors (PCB 134A24) distributed along the 9-inch cross section shock tube. Silicone grease (Dow Corning, four Electrical Insulating Grease, McMaster-Carr, cat. no. 1204K12) was purchased and applied to the sensing surface of the sensors to eliminate the baseline drift.

The electrostatic charges leaking into the data acquisition system were observed in experiments with the headform instrumented with 10 PCB 102B06 sensors. These sensors are mounted flush with the surface of the headform and signal cabling is extending from the interior of the headform through the metallic plate (base), the neck and then is lead on the outside of the shock tube. We have routinely observed signal corruption in the event of compromised electrical insulation of the coaxial signal cable caused by shock wave impact and loosening of connector nut. This was also investigated using a dummy sensor setup. Briefly, a 1/4-inch stainless steel tubing was insulated with electrical insulation tape and inserted in the bolt. The entire assembly was mounted in the A3 port in the shock tube (Figure S1 in Supplementary Material), and connected to the data acquisition system.

The Effect of Sampling Frequency

The effect of sampling frequency on characteristic parameters of the shock wave was evaluated using three sampling frequencies: 10, 100, and 1,000 kHz (**Figure 3**). A single sampling frequency was set in the DAQ and all experiments were performed using a single shock wave with a nominal intensity of 130 kPa in the test section (T4 sensor, **Figure 1B**). All tests were repeated four

FIGURE 2 | An array of seven pressure transducers (PCB 134A24) mounted on a plate in the test section and ready for calibration shots **(A)**. The plate is protected against vertical displacement using two clamps with rubber padding. Comparison of the factory calibration factors and those obtained using experiments performed in-house **(B)**. Data for sensors with long experimental life are outlined with a black rectangle (sensor nos. 1–8). Discrepancies in calibration factor values of below 5% were noted for brand new sensors (sensor nos. 9–18). Pressure transducers are connected *via* 3 in long low-noise cable to the charge amplifier *via* 10–32 jacks, and then *via* long low-noise cable to the data acquisition system.

times and the signal was recorded by six pressure sensors located along the shock tube. A total of 72 waveforms was analyzed ($3 \times 4 \times 6 = 72$), which included quantification of peak overpressure, rise time, duration, and impulse.

Sensor Misalignment

The effect of sensor misalignment with respect to the shock tube wall on the pressure profile was tested using sensor located in a T4 position in two configurations: (1) sensor was protruding by 0.25 inch into the shock tube and (2) sensor was receded from the flush position by 0.25 inch. A single shock wave with 130 kPa nominal peak overpressure was generated and compared with an adjacent sensor (denoted as T1, located five inches downstream of the T4 sensor). All measurements were repeated four times and peak overpressure was quantified.

Statistical Analysis

Data from experiments performed at different experimental conditions were pooled together and checked for normality using Ryan–Joiner test (similar to Shapiro–Wilk) in Minitab 17.0 (Minitab Inc., State College, PA, USA). Then a multiple comparison two-tailed *t*-test (statistical significance threshold was set at $p < 0.05$) was performed with Bonferroni correction on data for evaluation of the effect of sampling frequency and sensor misalignment. All data are presented as a mean and SD.

RESULTS AND DISCUSSION

Sensor Calibration

The accurate measurements of shock waves rely solely on the characteristics of the sensing element in the pressure transducer, appropriate calibration, and sampling frequency [details of pressure profile evolution in the shock tube are discussed extensively

in Ref. (28)]. Tourmaline is among the most popular materials employed as a sensing element in pressure transducers. Its piezoelectric properties were recognized more than 80 years ago with some of the earliest publications on the subject issued in the early 1930s (30), while its crystallographic structure was determined in the early 1950s of the twentieth century (31). This coincided with the extensive development work on pressure transducers (32). Typically, two pressure calibration methods can be employed in the manufacturing facility (33): (1) using Aronson pressure generator (34) and (2) in the shock tube. However, to check the characteristic frequency of the sensor and its rise time in response to shock loading, only a shock tube can be used since loading rates of Aronson's apparatus are insufficient for this purpose.

Typically, sensor calibration performed in the factory establishes maximum pressure and linear dependency between the applied pressure and voltage output from the sensor. Standard parts and equipment used for this purpose are hardly ever replicated in the laboratory, particularly if long signal cables are used. The differences between factory calibration setup and instrumentation used in the laboratory have to be checked to account for possible discrepancies in sensor response caused by impedance and triboelectric effects associated with cabling of different length. The methodology used in our lab relies on the measurement of the shock wave velocity which is related to pressure using Rankine–Hugoniot relationship. **Figure 2B** presents the discrepancies between factory calibration factors, and those obtained using the procedure developed in-house. For brand new sensors (number 9–18), the discrepancies are less than 7%; however, we must stress our method of calibration covers 0–60 psi range, which lies within practical interest for studying of blast TBI. Older sensors (3 years old, after hundreds of exposures), possibly due to wear and tear and some differences in manufacturing showed somewhat larger differences (sensitivity loss up to −10%) in calibration factors with two on the extreme
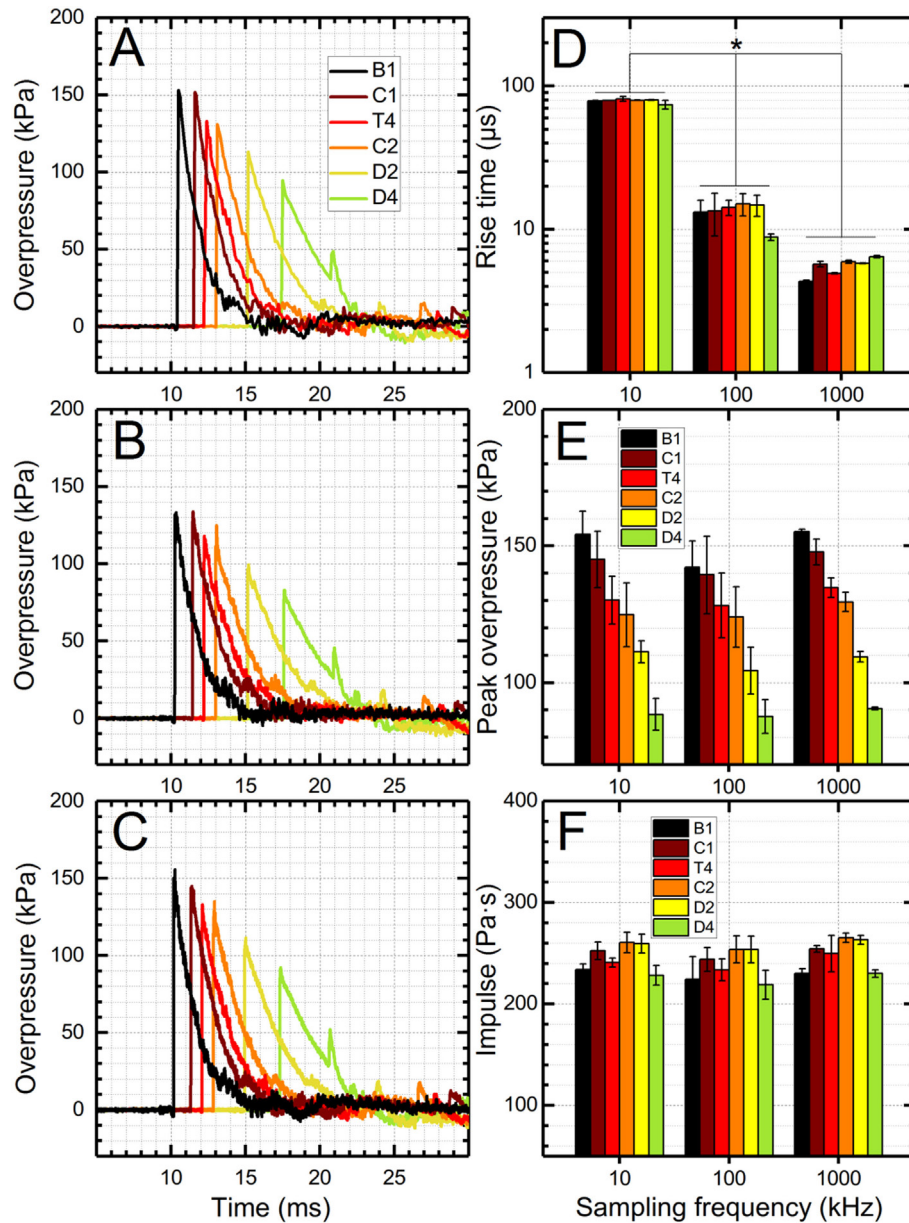
FIGURE 3 | The effect of sampling frequency on the quality of shock wave pressure profiles. Representative pressure profiles recorded using a sampling frequency of 10 kHz **(A)**, 100 kHz **(B)**, and 1,000 kHz **(C)**. Rise time values calculated from respective data sets depend strongly on the sampling frequency **(D)**, while peak overpressure and impulse values are independent of the sampling frequency **(E,F)**, for sampling frequencies used in this study. Statistical significance between respective groups is marked with asterisk ($p < 0.05$).

end where the discrepancy was almost −40% (for sensors 1 and 2 in **Figure 2B**). We have not observed any consistent trends in the calibration factor differences, and it would appear it is a case-by-case occurrence. This observation, combined with a random occurrence of larger deviations in calibration factor values, necessitates this type of sensor evaluation, and justifies the additional time spent on these tests. For new sensors, the calibration is thus recommended before routine use, while experimentally observed loss of sensitivity and history of particular sensor should dictate the need for additional calibration.

Sampling Rate

The sampling rate is an important experimental variable to capture the shape of the pressure profile. Since there are no universal measurement and reporting standards on shock wave parameters and data acquisition settings in the blast-induced neurotrauma (BINT) research field, a broad variety of sampling rates are typically reported, ranging from 10 kHz to 10 MHz (20, 24, 25, 28, 35–41). However, in a majority of publications, this parameter is omitted from reporting whatsoever, either because it was reported earlier in the original report on the characterization

of the blast generating device, or simply because it is treated as a trivial test parameter. Not only is the sampling frequency important for capturing the shape of the pressure profile, it is also an important factor in optimizing the output file size, along with the number of recorded channels and acquisition time. Moreover, it is unknown what sampling frequencies are adequate to accurately capture the shock wave profile traveling at supersonic speeds. To address these questions and establish adequate thresholds, we have performed a series of experiments where three sampling frequencies were used: 10, 100, and 1,000 kHz (**Figure 3**). We used a single shock wave with a nominal intensity of 130 kPa in the test section (T4 sensor, **Figure 1B**). At first glance, there are no significant differences between the three sampling frequencies (**Figures 3A–C**), but differences have become obvious after quantification of three basic shock wave characteristics: rise time, peak overpressure, and impulse. The most significant changes are with respect to the rise time (**Figure 3D**): only at 1,000 kHz sampling rate it is captured accurately. Note, that time resolution at this frequency is 1 µs which is adequate to capture rise times on the order of 4–5 µs which are typical for moderate intensity shock waves (Mach number below 2) based on our experience to date (28). Interestingly, sampling frequency as low as 10 kHz still allows accurate capture of peak overpressure and impulse values. This is simply because in this case, the shock wave with 5-ms duration traveling at 400 m/s velocity is a 2-m long (head to tail) mass of compressed air traveling in the 6 m long shock tube. With this sampling frequency, 10 data points per millisecond will be captured resulting in 50 data points for the 5 ms duration, which appears adequate to capture pressure-time outline without significant errors. However, when shorter duration shock waves are of interest, i.e., below 1 ms, which is characteristic of shock waves generated outside the shock tube, the sampling frequency needs to be increased to more than 1 MHz (20, 41).

Electrostatic Interference

We have performed more than 7,000 tests during the longevity of the shock wave testing laboratories at the University of Nebraska-Lincoln and then at New Jersey Institute of Technology. The shock tube walls have been painted to protect against rusting, but the downside is the paint also diminished dissipation of static electricity generated by the propagating shock wave. The PCB 134A24 tourmaline sensors mounted on the walls of both shock tubes for measurements of incident pressure suffer from a severe baseline drift which occurs as early as 1 ms after the shock front passage (**Figure 4**). The pressure reading reaches unrealistic values depending on the location of the sensor: nearly 5,400 kPa for the A3 sensor, and below −100 kPa for the D2 and D4 sensors; the unrealistic negative overpressure of less than 100 kPa are observed at 360 ms for sensors A3-T4. The maximum positive pressure for the A3 sensor is higher than burst pressure recorded for this test (5,200 kPa) and values of negative overpressure below −100 kPa are physically impossible to attain (vacuum pressure of outer space is below 10^{-7} kPa). These values demonstrate some other phenomenon is affecting pressure sensor readings. Considering extreme temperature variations on the order of hundreds of degrees are necessary to cause baseline drift in this class of pressure sensors, it leaves only electromagnetic radiation
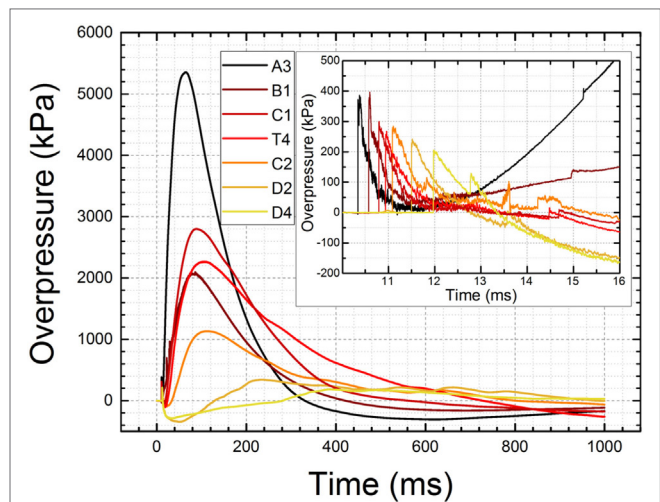
FIGURE 4 | The baseline drift recorded by seven PCB 134A24 pressure sensors distributed along the shock tube (see **Figure 1** for details). The data were recorded at 1 MHz frequency for 1 s (1 million data points per channel) for a shock wave with a nominal intensity of 250 kPa (a T4 sensor located in the test section). The burst pressure was 5,309 kPa (770 psi) for this test while erroneous peak pressure is 5,360 kPa for sensor A3 located at 1.43 m distance from the breech. The inset illustrates the shock wave profiles and baseline drift within 7 ms time frame. Note unrealistic negative pressure levels of −150 kPa reported by sensors D2 and D4.

as the source of observed anomalous readings and baseline drifts. These baseline drifts while apparently not interfering with measurements of the shock front characteristics (rise time and peak overpressure) adversely affect the estimation of the shock wave duration and hence lead to the erroneous calculation of the impulse values. We have performed additional verification that the static electricity is associated with shock wave passage using a dummy sensor (Figure S1 in Supplementary Material). The voltage variations were observed and coincided with a shock wave initiation.

The PCB Tourmaline Pressure Bars series 134A24 high-pressure, fast rise time sensors, with ranges up to 20,000 psi, are best suited for applications which require high-frequency measurements of the incident or reflected shock wave pressures like those found in studies of plasma physics and hypersonics. These sensors are factory protected against baseline drifts caused by high temperatures which exist near the epicenter of explosions or other high-pressure phenomena where heat is generated (42, 43), by a layer of a thermal insulator like vinyl tape. This method of sensor protection has proven ineffective against the level of static electricity generated in our shock tubes. We decided to resort to another compound with similar electrical insulation properties, commercially available silicone grease. Application of a thin 2–3 mm layer on the sensing surface of the sensors prevents baseline drifts and other adverse effects associated with static electricity as illustrated by overpressure profiles presented in **Figure 5**. It is obvious the baseline drift is virtually eliminated with this method. Periodic inspection and reapplication of the grease is necessary in order to record high quality, repeatable shock wave pressure profiles.

The second type of manifestation of the static electricity has become obvious during the testing of the effect of the shock wave loading conditions at different locations in the shock tube using the headform instrumented with PCB 102B06 (**Figure 6B**, inset). The sensor is connected to the low-noise data cable *via*
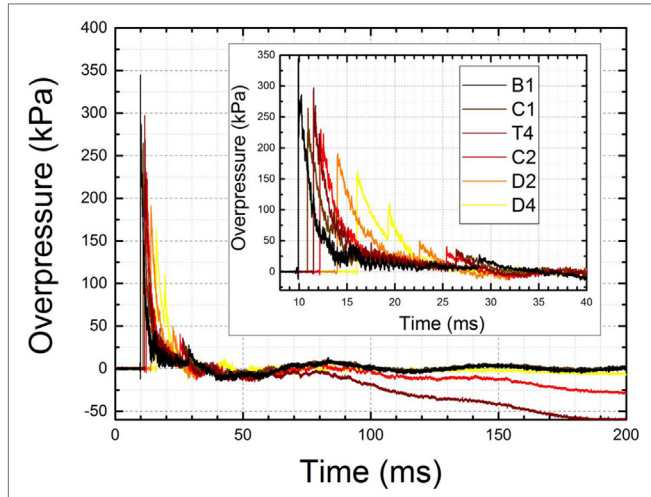
FIGURE 5 | Baseline drift was eliminated with an aid of silicone insulator grease applied on the tip of the sensors. The baseline shows no signs of drifts toward positive or negative range over 200 ms of signal. Some baseline drift is observed for sensors T4 and C2, most likely due to gradual deterioration of silicone insulator layer caused by repeated exposure. The inset shows enlarged shock wave profiles recorded by six sensors for the nominal intensity of 250 kPa (T4 sensor).

10-32 plug (PCB 002C10 low-noise cable) and then to the signal conditioner using a BNC connector *via* expansion terminal. Repeated exposure to the shock wave with 70–210 kPa intensity caused vibration of the headform which resulted in loosening of a connector between the pressure sensor and data cable. This in turn caused loss of electrical insulation of the data line running in the middle of the cable and results in a static electricity surge, i.e., a large number of high-intensity spikes randomly embedded in the pressure signal (**Figure 6**). Fast Fourier Transform analysis performed on this signal revealed three high-frequency bands: 50, 70, and 130 kHz. Due to relatively small amount of the signal contamination, in this case, it was possible to salvage the pressure data by running low-pass filter. However, in extreme cases, the loosening of 10–32 jacks resulted in unrecoverable levels of static electricity flooding the data channel (**Figure 6B**). The only remedy for this type of artifact is to secure the 10–32 plug with an electrical insulation tape to prevent the disconnection and a breach in electrical insulation.

The Effect of Vibration on Pressure Signal Quality

The peak overpressure is the only parameter consistently reported among shock wave characteristics (peak overpressure, rise time, duration, impulse, and sampling frequency). Sensor mounting and mechanical vibrations have the tremendous effect on the signal quality of the shock front and peak overpressure is an extremely sensitive parameter prone to misinterpretation. We observed sensors mounted on the top wall of the shock tube are being pushed upwards by the pressure of the passing shock
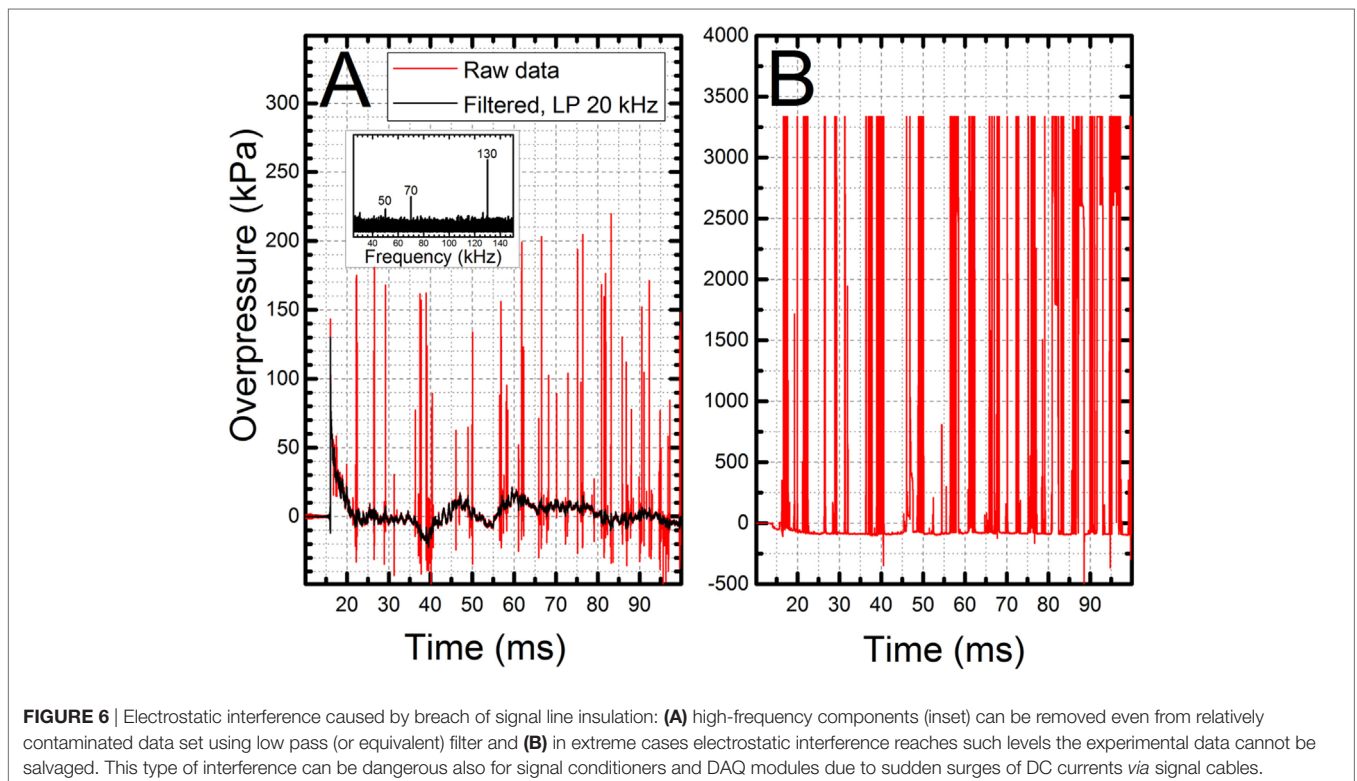
FIGURE 6 | Electrostatic interference caused by breach of signal line insulation: **(A)** high-frequency components (inset) can be removed even from relatively contaminated data set using low pass (or equivalent) filter and **(B)** in extreme cases electrostatic interference reaches such levels the experimental data cannot be salvaged. This type of interference can be dangerous also for signal conditioners and DAQ modules due to sudden surges of DC currents *via* signal cables.

wave: this is obvious on the high-speed videos (not shown) and the results in the corrupted initial part of the shock wave signal as seen in **Figure 7**. The upward motion of the sensor and its return to the resting position lasts only approximately 200 µs for the shock wave with 280 kPa peak overpressure (**Figure 7B**). The resulting signal is corrupted by the sensor translation within the opening of the mounting port. We have noticed this particular artifact present on numerous occasions in our data, and decided to install clamps on both sides of the pressure brackets to prevent the displacement of the bracket-pressure sensor assembly (**Figure 1A**, inset). However, to explore the origin of the exaggerated peak overpressure values in the controlled and systematic way, we decided to mount one of our sensors receded by 0.25 inch, and compare results with two other configurations where the sensor is mounted flush (default configuration for all experiments) and protruding by 0.25 inch (**Figure 8**). In both cases of non-flush sensor mounting, there is an excessive pressure buildup which lasts less than 100 µs (**Figures 8A,B**). Quantification of peak overpressure for $n = 4$ repeated trials indicates that the receded configuration results in a higher overestimation of peak overpressure (**Figure 8C**), and observed changes are statistically significant ($p < 0.05$). However, non-optimal sensor location cannot explain vibrations in the signal (**Figure 7**), which is likely associated with the impact of the sensor by the shock wave, and unrestricted displacement path while free-floating in the air. It would appear sensor vibration upon the initial shock wave impact leads to gross overestimation of the peak overpressure, while not affecting other characteristics. Literature survey related to reporting and existing standards of pressure measurements revealed some research groups were aware of the consequences

of the improper sensor mounting. For example, Kochanek and co-workers mentioned in their recent work that "surface flush gauges were used for the shock measurements because it is known that a gauge protruding or recessed by less than 1 mm will affect measurements" (17). Examples of waveforms with a sharp spike at the beginning of the shock wave are scattered through the literature. Chavko and colleagues report that when they measured the pressure with a miniature fiber-optic sensor made by Fiso, they detected "a lower pressure spike than the spike measured with the PCB probe." It would appear both sensors were not mounted perfectly flush, which was not recognized at the time and the difference in spike intensity was explained by mere differences in sampling rate, which was 40 kHz for Fiso sensor and 500 kHz for PCB sensors or by their specific characteristics (44). Similarly, the presence of high-intensity spikes in the reflected pressure measured at the end of the closed shock tube was interpreted as a peak reflected overpressure (45, 46), most likely incorrectly based on our experimental data (**Figure 8**).

However, while consequences of non-flush mounting are recognized, far less attention is dedicated to proper signal analysis and preventive measures when high-frequency artifacts are present in the signal. For example, a quick glimpse on the overpressure profiles published by Svetlov and co-workers reveals that in their experiments, this artifact leads to twofold overestimation of the peak overpressure [see **Figure 2** in Ref. (47)], i.e., it was erroneously reported as 358 kPa, while, in fact, it was merely 180 kPa. Only in some instances where the sharp spike is present in the data correct peak pressure was reported, i.e., as the highest pressure resulting from the exponential decay part of the waveform (48).
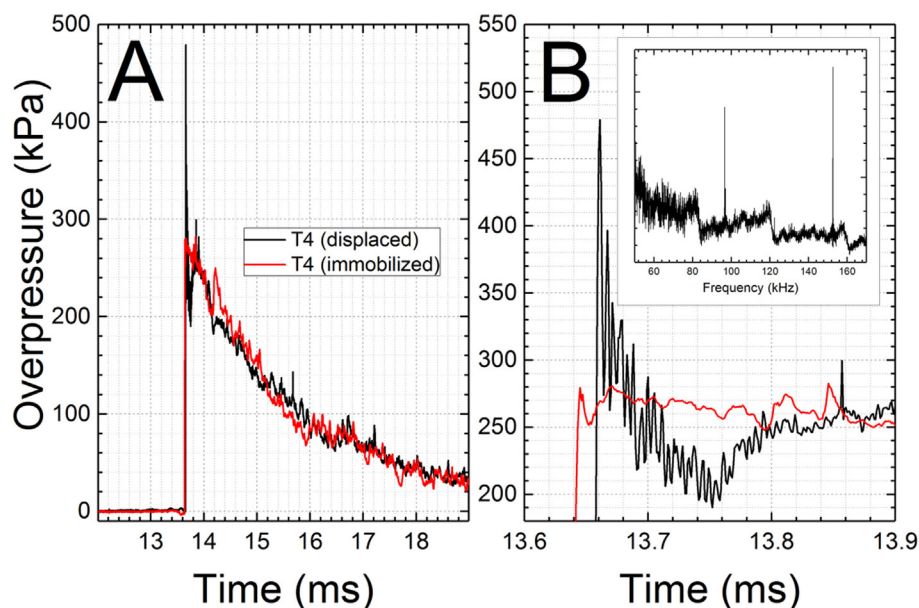
FIGURE 7 | High-frequency signal observed in experiments where the sensor and the mounting bracket were pushed upwards by the passing shock wave. Comparison of the recorded overpressure with the artifact associated with the sensor [T4 (displaced)] and the signal with eliminated artifact **(A)**. Two brackets were used to prevent the displacement of the sensor resulting in clean waveform [T4 (immobilized)]. The magnified part of the pressure history reveals the presence of high-frequency noise and excessive peak pressure level **(B)**. Inset: FFT results of the pressure signal with artifact reveal characteristic frequencies: 96 and 152 kHz.

FIGURE 8 | The effect of sensor misalignment with the shock tube wall on the resulting pressure profile. The exaggerated peak overpressure values are observed when the sensor is: receding **(A)** or protruding **(B)** from the shock tube wall. Quantification results ($n = 4$) for both tested scenarios demonstrate peak overpressure values are higher for receded sensor configuration than when the sensor was protruding **(C)**. These differences are statistically significant ($p < 0.05$). Nominal shock wave intensity of 130 kPa measured in the test section (T4 location) was used for these tests. Schematic representation of two sensor configurations resulting in peak overpressure artifacts is presented **(D)**. The distance between shock tube wall and sensing surface was the same in both cases ($d = 0.25$ in). Statistically significant differences are indicated with an asterisk ($p < 0.05$).

CONCLUSION

We have discussed two important experimental variables, mechanical vibration and electromagnetic interference on the quality of a waveform recorded using state-of-the-art high-frequency pressure sensors. The importance proper implementation of preventive strategies, understanding of pressure measurement artifacts, and data interpretation with examples provided in this paper will help the community at large avoid these mistakes. In order to facilitate interlaboratory data comparison on the BINT research area, common reporting standards should be developed. We noticed the majority of published literature on the subject limits reporting to peak overpressure, with much less attention directed toward other important parameters, i.e., duration and especially impulse, which should be included as mandatory in future contributions. We have demonstrated sampling frequency as low as 10 kHz can be used to capture correctly the shape of the shock wave with a few milliseconds duration. However, shock waves with shorter durations might require higher sampling rates, and a sampling rate of 1,000 kHz is typically necessary to capture the rise time, which might be an important parameter depending upon the design of the study. We have also demonstrated sensor calibration is a significant quality measure, particularly for sensors with an extended lifetime. While there were only slight differences between factory and in-house generated calibration factors, we must stress the importance of this step to obtain correct pressure values. It is extremely important in the recording of peak overpressure values, which seem to be very prone to errors.

AUTHOR CONTRIBUTIONS

MS and EA performed experiments and data analysis, MS and NC wrote the manuscript.

FUNDING

SUPPLEMENTARY MATERIAL

The Supplementary Material for this article can be found online at http://www.frontiersin.org/articles/10.3389/fneur.2018.00052/full#supplementary-material.

REFERENCES

1. Moore DF, Jaffee MS. Military traumatic brain injury and blast. *Neuro Rehabil* (2010) 26(3):179–81. doi:10.3233/NRE-2010-0553
2. Hoge CW, McGurk D, Thomas JL, Cox AL, Engel CC, Castro CA. Mild traumatic brain injury in U.S. soldiers returning from Iraq. *N Engl J Med* (2008) 358(5):453–63. doi:10.1056/NEJMoa072972
3. Elder GA, Cristian A. Blast-related mild traumatic brain injury: mechanisms of injury and impact on clinical care. *Mt Sinai J Med* (2009) 76(2):111–8. doi:10.1002/msj.20098
4. DePalma RG, Cross GM, Beck L, Chandler D. Epidemiology of mTBI (mild traumatic brain injury) due to blast: history, DOD/VA data bases: challenges and opportunities. *Proc NATO RTO-MP-HFM-207 Symposium on a Survey of Blast Injury across the Full Landscape of Military Science*. Washington, DC (2011).
5. *DoD Worldwide Numbers for TBI*. (2017). Available from: http://dvbic.dcoe.mil/dod-worldwide-numbers-tbi
6. Greer N, Sayer N, Koeller E, Velasquez T, Wilt TJ. Outcomes associated with blast versus nonblast-related traumatic brain injury in US military service members and veterans: a systematic review. *J Head Trauma Rehabil* (2017). doi:10.1097/HTR.0000000000000304
7. Vanderploeg RD, Belanger HG, Horner RD, Spehar AM, Powell-Cope G, Luther SL, et al. Health outcomes associated with military deployment: mild traumatic brain injury, blast, trauma, and combat associations in the Florida National Guard. *Arch Phys Med Rehabil* (2012) 93(11):1887–95. doi:10.1016/j.apmr.2012.05.024
8. Ostertag MH, Kenyon M, Borkholder DA, Lee G, da Silva U, Kamimori G. The blast gauge™ system as a research tool to quantify blast overpressure in complex environments. *ASME 2013 International Mechanical Engineering Congress and Exposition*. San Diego, California: American Society of Mechanical Engineers (2013). p. A17–13.
9. Wiri S, Needham C. Reconstruction of improvised explosive device blast loading to personnel in the open. *Shock Waves* (2016) 26(3):279–86. doi:10.1007/s00193-016-0644-1
10. Bennett S, Fintelman G, Patchell M, Webb A, Wynen B, Costello J, et al. Project cerebro: an evaluation of blast gauges in the Australian Defence Force. *J Mil Vet Health* (2015) 23(3):27–30.
11. Phillips Y, Richmond DR. Primary blast injury and basic research: a brief history. In: Zatchuck R, Jenkins D, Bellamy R, Quick C, editors. *Textbook of Military Medicine Part I Warfare, Weapons, and the Casualty. Vol. 5, Conventional Warfare. Ballistic, Blast, and Burn Injuries*. Washington, DC: TMM Publications (1991). p. 221–240.
12. DePalma RG, Burris DG, Champion HR, Hodgson MJ. Blast injuries. *N Engl J Med* (2005) 352(13):1335–42. doi:10.1056/NEJMra042083
13. Cernak I. The importance of systemic response in the pathobiology of blast-induced neurotrauma. *Front Neurol* (2010) 1:151. doi:10.3389/fneur.2010.00151
14. Cernak I, Savic J, Ignjatovic D, Jevtic M. Blast injury from explosive munitions. *J Trauma Acute Care Surg* (1999) 47(1):96–103. doi:10.1097/00005373-199907000-00021
15. Richmond DR, Gaylord CS, Damon EG, Taborelli R. DASA-AEC-Lovelace foundation blast-simulation facility. *Defense Nuclear Agency (Formerly Defense Atomic Support Agency)*. Washington, DC: Department of Defense (1966). Technical Progress Report No. DASA-1853.
16. Sundaramurthy A, Alai A, Ganpule S, Holmberg A, Plougonven E, Chandra N. Blast-induced biomechanical loading of the rat: an experimental and anatomically accurate computational blast injury model. *J Neurotrauma* (2012) 29(13):2352–64. doi:10.1089/neu.2012.2413
17. Garman RH, Jenkins LW, Switzer RC III, Bauman RA, Tong LC, Swauger PV, et al. Blast exposure in rats with body shielding is characterized primarily by diffuse axonal injury. *J Neurotrauma* (2011) 28(6):947–59. doi:10.1089/neu.2010.1540
18. Irwin RJ, Lerner MR, Bealer JF, Mantor PC, Brackett DJ, Tuggle DW. Shock after blast wave injury is caused by a vagally mediated reflex. *J Trauma* (1999) 47(1):105–10. doi:10.1097/00005373-199907000-00023
19. Awwad HO, Gonzalez LP, Tompkins P, Lerner M, Brackett DJ, Awasthi V, et al. Blast overpressure waves induce transient anxiety and regional changes in cerebral glucose metabolism and delayed hyperarousal in rats. *Front Neurol* (2015) 6:132. doi:10.3389/fneur.2015.00132
20. Miller AP, Shah AS, Aperi BV, Budde MD, Pintar FA, Tarima S, et al. Effects of blast overpressure on neurons and glial cells in rat organotypic hippocampal slice cultures. *Front Neurol* (2015) 6:20. doi:10.3389/fneur.2015.00020
21. Effgen GB, Hue CD, Vogel E III, Panzer MB, Meaney DF, Bass CR, et al. A multiscale approach to blast neurotrauma modeling: part II: methodology for inducing blast injury to in vitro models. *Front Neurol* (2012) 3:23. doi:10.3389/fneur.2012.00023
22. Alay E, Skotak M, Misistia A, Chandra N. Dynamic loads on human and animal surrogates at different test locations in compressed-gas-driven shock tubes. *Shock Waves* (2017):1–12. doi:10.1007/s00193-017-0762-4
23. Gullotti DM, Beamer M, Panzer MB, Chen YC, Patel TP, Yu A, et al. Significant head accelerations can influence immediate neurological impairments in a murine model of blast-induced traumatic brain injury. *J Biomech Eng* (2014) 136(9):091004. doi:10.1115/1.4027873
24. Cernak I, Merkle AC, Koliatsos VE, Bilik JM, Luong QT, Mahota TM, et al. The pathobiology of blast injuries and blast-induced neurotrauma as identified using a new experimental model of injury in mice. *Neurobiol Dis* (2011) 41(2):538–51. doi:10.1016/j.nbd.2010.10.025
25. Saljo A, Arrhen F, Bolouri H, Mayorga M, Hamberger A. Neuropathology and pressure in the pig brain resulting from low-impulse noise exposure. *J Neurotrauma* (2008) 25(12):1397–406. doi:10.1089/neu.2008.0602
26. Lu J, Ng KC, Ling G, Wu J, Poon DJF, Kan EM, et al. Effect of blast exposure on the brain structure and cognition in *Macaca fascicularis*. *J Neurotrauma* (2012) 29(7):1434–54. doi:10.1089/neu.2010.1591
27. Huber BR, Meabon JS, Martin TJ, Mourad PD, Bennett R, Kraemer BC, et al. Blast exposure causes early and persistent aberrant phospho- and cleaved-tau expression in a murine model of mild blast-induced traumatic brain injury. *J Alzheimers Dis* (2013) 37(2):309–23. doi:10.3233/jad-130182
28. Kuriakose M, Skotak M, Misistia A, Kahali S, Sundaramurthy A, Chandra N. Tailoring the blast exposure conditions in the shock tube for generating pure, primary shock waves: the end plate facilitates elimination of secondary loading of the specimen. *PLoS One* (2016) 11(9):e0161597. doi:10.1371/journal.pone.0161597
29. Holmberg AD. *Development and Characterization of Shock Tubes for Laboratory Scale Blast Wave Simulation*. University of Nebraska-Lincoln (2010).
30. Fox GW, Underwood M. On the piezoelectric properties of tourmaline. *J Appl Phys* (1933) 4(1):10–3. doi:10.1063/1.1745137
31. Wooster W. Physical properties and atomic arrangements in crystals. *Rep Prog Phys* (1953) 16(1):62. doi:10.1088/0034-4885/16/1/302
32. Walter PL. Air-blast and the science of dynamic pressure measurements. *Sound Vib* (2004) 38(12):10–7.

33. Lally J, Cummiskey D. Dynamic pressure calibration. *Sensors* (2003) 20(4):15–21.

34. Aronson P, Waser R. *Pressure-Pulse Generator for the Calibration of Pressure Gages*. White Oak, MD: DTIC Document (1963).

35. Ahlers ST, Vasserman-Stokes E, Shaughness MC, Hall AA, Shear DA, Chavko M, et al. Assessment of the effects of acute and repeated exposure to blast overpressure in rodents: toward a greater understanding of blast and the potential ramifications for injury in humans exposed to blast. *Front Neurol* (2012) 3:32. doi:10.3389/fneur.2012.00032

36. Cho HJ, Sajja V, Vandevord PJ, Lee YW. Blast induces oxidative stress, inflammation, neuronal loss and subsequent short-term memory impairment in rats. *Neuroscience* (2013) 253:9–20. doi:10.1016/j.neuroscience.2013.08.037

37. Rubovitch V, Ten-Bosch M, Zohar O, Harrison CR, Tempel-Brami C, Stein E, et al. A mouse model of blast-induced mild traumatic brain injury. *Exp Neurol* (2011) 232(2):280–9. doi:10.1016/j.expneurol.2011.09.018

38. Skotak M, Wang F, Alai A, Holmberg A, Harris S, Switzer RC, et al. Rat injury model under controlled field-relevant primary blast conditions: acute response to a wide range of peak overpressures. *J Neurotrauma* (2013) 30(13):1147–60. doi:10.1089/neu.2012.2652

39. Svetlov SI, Prima V, Glushakova O, Svetlov A, Kirk DR, Gutierrez H, et al. Neuro-glial and systemic mechanisms of pathological responses in rat models of primary blast overpressure compared to "composite" blast. *Front Neurol* (2012) 3:15. doi:10.3389/fneur.2012.00015

40. Tompkins P, Tesiram Y, Lerner M, Gonzalez LP, Lightfoot S, Rabb CH, et al. Brain injury: neuro-inflammation, cognitive deficit, and magnetic resonance imaging in a model of blast induced traumatic brain injury. *J Neurotrauma* (2013) 30(22):1888–97. doi:10.1089/neu.2012.2674

41. Yeoh S, Bell ED, Monson KL. Distribution of blood-brain barrier disruption in primary blast injury. *Ann Biomed Eng* (2013) 41(10):2206–14. doi:10.1007/s10439-013-0805-7

42. De Vries J, Petersen E. Autoignition of methane-based fuel blends under gas turbine conditions. *Proc Combust Inst* (2007) 31(2):3163–71. doi:10.1016/j.proci.2006.07.206

43. Mathieu O, Kopp M, Petersen E. Shock-tube study of the ignition of multi-component syngas mixtures with and without ammonia impurities. *Proc Combust Inst* (2013) 34(2):3211–8. doi:10.1016/j.proci.2012.05.008

44. Chavko M, Watanabe T, Adeeb S, Lankasky J, Ahlers ST, McCarron RM. Relationship between orientation to a blast and pressure wave propagation inside the rat brain. *J Neurosci Methods* (2011) 195(1):61–6. doi:10.1016/j.jneumeth.2010.11.019

45. Courtney E, Courtney A, Courtney M. Shock tube design for high intensity blast waves for laboratory testing of armor and combat materiel. *Defence Technol* (2014) 10(2):245–50. doi:10.1016/j.dt.2014.04.003

46. Courtney AC, Andrusiv LP, Courtney MW. Oxy-acetylene driven laboratory scale shock tubes for studying blast wave effects. *Rev Sci Instrum* (2012) 83(4):045111. doi:10.1063/1.3702803

47. Svetlov SI, Prima V, Kirk DR, Gutierrez H, Curley KC, Hayes RL, et al. Morphologic and biochemical characterization of brain injury in a model of controlled blast overpressure exposure. *J Trauma* (2010) 69(4):795–804. doi:10.1097/TA.0b013e3181bbd885

48. Reneer DV, Hisel RD, Hoffman JM, Kryscio RJ, Lusk BT, Geddes JW. A multi-mode shock tube for investigation of blast-induced traumatic brain injury. *J Neurotrauma* (2011) 28(1):95–104. doi:10.1089/neu.2010.1513

Conflict of Interest Statement: The authors declare that the research was conducted in the absence of any commercial or financial relationships that could be construed as a potential conflict of interest.

A Single Primary Blast-Induced Traumatic Brain Injury in a Rodent Model Causes Cell-Type Dependent Increase in Nicotinamide Adenine Dinucleotide Phosphate Oxidase Isoforms in Vulnerable Brain Regions

Kakulavarapu V. Rama Rao,[1] Stephanie Iring,[1] Daniel Younger,[1] Matthew Kuriakose,[1]
Maciej Skotak,[1] Eren Alay,[1] Raj K. Gupta,[2] and Namas Chandra[1]

Abstract

Blast-induced traumatic brain injury (bTBI) is a leading cause of morbidity in soldiers on the battlefield and in training sites with long-term neurological and psychological pathologies. Previous studies from our laboratory demonstrated activation of oxidative stress pathways after blast injury, but their distribution among different brain regions and their impact on the pathogenesis of bTBI have not been explored. The present study examined the protein expression of two isoforms: nicotinamide adenine dinucleotide phosphate (NADPH) oxidase 1 and 2 (NOX1, NOX2), corresponding superoxide production, a downstream event of NOX activation, and the extent of lipid peroxidation adducts of 4-hydroxynonenal (4HNE) to a range of proteins. Brain injury was evaluated 4 h after the shock-wave exposure, and immunofluorescence signal quantification was performed in different brain regions. Expression of NOX isoforms displayed a differential increase in various brain regions: in hippocampus and thalamus, there was the highest increase of NOX1, whereas in the frontal cortex, there was the highest increase of NOX2 expression. Cell-specific analysis of changes in NOX expression with respect to corresponding controls revealed that blast resulted in a higher increase of NOX1 and NOX 2 levels in neurons compared with astrocytes and microglia. Blast exposure also resulted in increased superoxide levels in different brain regions, and such changes were reflected in 4HNE protein adduct formation. Collectively, this study demonstrates that primary blast TBI induces upregulation of NADPH oxidase isoforms in different regions of the brain parenchyma and that neurons appear to be at higher risk for oxidative damage compared with other neural cells.

Keywords: astrocytes; blast injury; 4-hydroxynonenal; microglia; neuron; NADPH oxidase; oxidative stress; traumatic brain injury

Introduction

Traumatic brain injury (TBI) resulting from different episodes of head trauma is one of the leading causes of morbidity and death in both military personnel and civilian populations. TBI causes approximately 1.5 million deaths and hospitalizations annually in the United States.[1–3] Blast-induced TBI (bTBI) is the most prevalent form of brain injury in soldiers in combat zones because of the widespread use of high explosives in the war zones, and an increasing number of cases has also been reported in civilian populations with the use of improvised explosive devices by insurgents.[4,5]

Among many pathological factors associated with either primary mechanical injury or secondary biochemical cascades, oxidative stress has been shown to play a major role in various models of TBI.[6,7] The main inducers of oxidative stress are reactive oxygen species (ROS), which include superoxide (O2•−), hydroxyl radical (HO•), and hydrogen peroxide (H_2O_2).[8,9] ROS are normally produced in several metabolic reactions, including redox-reactions (oxidation/reduction), oxidative phosphorylation, and in a normal

[1]Center for Injury Biomechanics, Materials, and Medicine, Department of Biomedical Engineering, New Jersey Institute of Technology, Newark, New Jersey.
[2]Department of Defense Blast Injury Research Program Coordinating Office, United States Army Medical Research and Materiel Command, Fort Detrick, Maryland.

process of electron transport chain reactions. There are a number of enzymes that produce free radicals during their catalytic reactions, which include the nicotinamide adenine dinucleotide phosphate (NADPH) oxidase family, cytochrome P450 (CYP450), cyclooxygenase (COX), lipoxygenase (LOX), and xanthine oxidase.

The NADPH oxidase (NOX) is a multi-subunit enzyme that catalyzes the reduction of molecular oxygen and oxidation of NADPH to generate superoxide radicals ($O_2^{\bullet-}$). NOX is comprised of subunits that are both plasma membrane-bound (cytochrome b_{558}, composed of p22phox and gp91phox) and cytoplasmic (p40phox, p47 phox, and p67 phox), which spans across the lipid bilayers.[10,11] A number of NOX isoforms were identfied in the brain, which include NOX1, NOX2, and NOX4, and their cellular distribution is highly dependent on the cell type. Neurons express both NOX1 and NOX2, microglia are enriched with NOX2, while only small amounts of NOX isoforms were identified in astrocytes.[12]

Extensive experimental evidence suggests NOX plays a significant role in the pathophysiology of various forms of TBI. NOX has been shown to be upregulated in a brain in a controlled cortical impact model of trauma[13] and closed head injury models.[14–16] We have previously reported increased protein expression of NOX1 in a rodent model of a single blast injury at different blast overpressure exposures.[17,18] While these studies establish a primary role of NOX1 in the pathophysiology of various forms of TBI, no studies have been performed to determine the spatial and temporal resolution of NOX family of enzymes in the brain and their role in the pathophysiology of bTBI. It is hypothesized that in bTBI, a single blast overpressure exposure is capable of biomechanically loading the whole brain, which may trigger a cascade of biochemical events consistent with regional vulnerabilities.

The present study therefore examined the spatial resolution of two isoforms of NOX (NOX1 and NOX2) and their cellular distribution and changes in rats exposed to moderate blast TBI. Levels of superoxide and formation of protein adducts of 4-hydroxynonenal (4HNE) were also determined. Based on the evidence that blast overpressure waves travel through the whole brain, we hypothesize that blast-induced NOX-related oxidative stress will be diffuse across the brain. Moreover, we hypothesize that different neural cell types have differential susceptibility to the oxidative stress-inducing effect of the primary blast.

Methods

Animals

Adult 10-week-old male Sprague-Dawley (Charles River Laboratories) rats weighing 320–360 g were used in all the studies. The animals were housed with free access to food and water in a 12-h dark-light cycle at 22°C. All procedures followed the guidelines established in the *Guide for the Care and Use of Laboratory Animals* and were approved by Rutgers University Institutional Animal Care and Use Committee before experiments. Rats were divided into two groups (sham controls and animals exposed to a moderate blast of 180 kPa).

A total number of 24 rats was used in this study as follows: immunoblotting (three controls and three blast injured); immunofluorescence studies (four controls and four blast-injured); superoxide production studies (five controls and five blast-injured). For immunofluorescence studies, each brain tissue was processed to obtain several sections (>10) from frontal cortex, striatum, hippocampus, thalamus, and cerebellum. Each of those sections were used for identification of NOX1 and NOX2 isoforms in neurons, astrocytes, and microglia by double immunofluorescence analysis. Similarly, for superoxide production, several sections from different brain regions of animals (five control and five blast-injured) were used for regional analyses.

Blast injury

Rats were exposed to a single blast wave at the Center of Injury Biomechanics, Materials and Medicine (New Jersey Institute of Technology, Newark) in the 9-inch square cross section shock tube as described previously.[18,19] The primary shockwave generated in
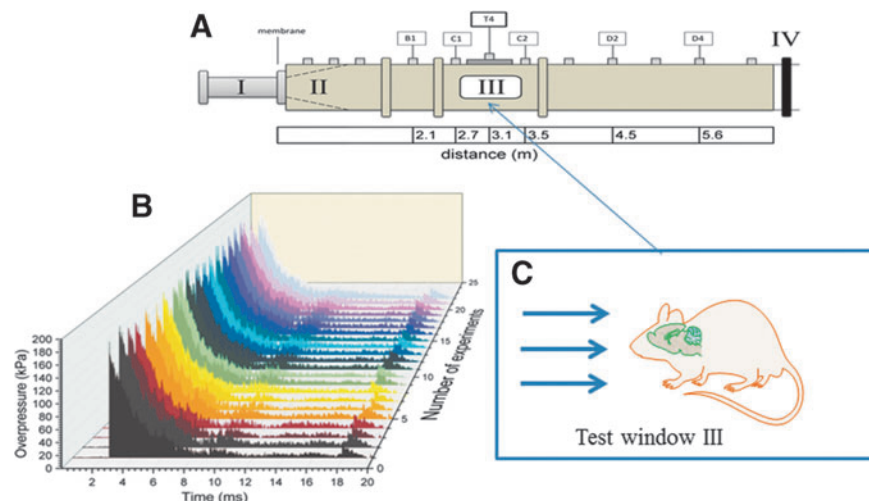
FIG. 1. Schematic depiction of the shock tube. (**A**) Schematic of 9×9 inch square, 30 feet long shock tube with section I-Breech with high pressure helium gas separated from section II by different thickness of mylar sheets that generate pure shockwave in section III where the specimens are located. Section IV is past the section and is a design requirement; the pressure-time cycle is identical to live fire tests with actual C-4 (or trinitrotoluene equivalent) explosives at specified standoff distance. (**B**) Composite of actual experimental profiles that generate 180 kPa with only about five kPa variation in peak pressure and less than a millisecond in duration. The front of the pressure rise indicates shock-wave conditions. (**C**) Schematic of rodent model in prone position facing the shock front. The shock travels in the rostral-caudal direction traversing the pre-frontal cortex, striatum, hippocampus, thalamus, visual cortex, and cerebellum within a period of a millisecond with minimal attenuation of pressure loading. Color image is available online at www.liebertpub.com.neu

this shock tube has been validated against the pressure-time profiles measured experimentally in the live-fire explosion experiments[10] and against theoretical pressure-time profiles associated with the detonation of C4 explosive (see Kuriakose and colleagues[20] for details).

All rats were anesthetized with a mixture of ketamine (100 mg/kg) and xylazine (10 mg/kg) at 10:1 ratio administered via intraperitoneal injection. Rats underwent a single exposure to 180 ± 5 kPa peak overpressure (duration: 6.5 ± 0.5 msec, impulse: 320 ± 20 kPa·msec) and euthanized 4 h post-TBI. All rats were mounted in the middle of the shock tube (2.8 meters from the breech, and 3 meters from the exit) in a prone position—i.e. were strapped securely to the aluminum plate using a cotton cloth wrapped around the body (see Mishra and associates,[18] Fig. 1B). The cloth provides no protection against the shockwave, but prevents any excessive head motion.[19] Sham control rats received anesthesia and noise exposure but without blast exposure—i.e., anesthetized animals were placed next to the shock tube, and then a single blast was fired.

As a quality control measure, we have also monitored a high-speed video recording to capture any substantial head and body motion during the blast so as to exclude the impact of tertiary bTBI. After blast injury, animals were monitored closely for any signs of trauma-related distress (e.g., apnea). For immunoblot analysis, rats were anesthetized and transcardially perfused with phosphate buffered saline (PBS, pH 7.0) whereas for immunofluorescence studies, rats were first perfused with PBS followed by 4% paraformaldehyde (PFA); brains were then isolated and cryoprotected in 30% sucrose.

Western blotting

Before evaluating spatial resolution of NOX1 and NOX2 protein changes in different brain regions by immunofluorescence, we first examined their levels in cerebral hemisphere and cerebellum by immunoblot. After perfusion with PBS, brains were excised from the cranial vaults, the whole left hemisphere and cerebellum were separately homogenized in ice-cold conditions using CellLytic-M (Sigma) using sonicator with probe amplitude set to 45%. Samples were then centrifuged at $14,000 \times g$ at 4°C. The protein concentration in the samples was estimated by bicinchoninic acid (BCA) method (Thermo Scientific, Rockford, IL).

Subsequently, 10–20 μg of protein per lane was loaded into 4–15% SDS-PAGE gradient gels (Bio Rad). Proteins separated according to their molecular size were then transferred onto polyvinylidene difluoride (PVDF) membranes using Turbo Protein Transfer instrument (Bio Rad Laboratories) according to manufacturer instructions. Membranes were blocked with 5% milk dissolved in Tris-Buffered saline containing 0.1% Tween-20 (TBS-T) and incubated overnight at 4°C with NOX 1 antibody (Sigma-Aldrich) or NOX2 antibody (Novus Biologicals) or 4HNE (Abcam, Cambridge, MA) at a dilution of 1:1000. Bands were visualized using Western Pico Chemiluminescence Substrate (Thermo Scientific) on Chemi Doc Imaging System (Bio Rad Laboratories). For densitometric quantitation of Western blots, images were digitized using a BioRad GS800 calibrated densitometer, and analyzed with BioRad Quantity One software.

Immunofluorescence and microscopy

To evaluate the spatial changes of NOX1 and NOX2 proteins in different brain regions, as well as to identify cell-specific changes in discrete brain regions, we performed double-immunofluorescence studies of two isoforms of NOX with NeuN, glial fibrillary acidic protein (GFAP) and Iba1, markers of neurons, astrocytes, and microglia, respectively, in frontal cortex, striatum, hippocampus, thalamus, and cerebellum. Briefly, 4 h post-injury, both sham and TBI animals were transcardially perfused with phosphate buffered saline (PBS) followed by 4% paraformaldehyde (PFA). After perfusion, the brains were removed from cranial vaults and incubated in 4% PFA for an additional 48 h and cryoprotected by immersing in 30% sucrose. Brains were then dissected into 2 mm thick sections using rat brain slicer (Kent Scientific Corp.) and embedded in OCT (Optimal Cutting Temperature) media and frozen quickly in isopentane cooled to liquid nitrogen temperature. Frozen sections were stored at −80°C until ready for sectioning.

Brain sections (20 μm thick) were prepared from the frozen tissue blocks, using Leica CM3050 cryostat, and immunofluorescence was performed. Briefly, tissue sections mounted on glass slides prepared from four individual animals in each group were washed with 10 mM PBS, fixed in ice-cold methanol (100%) solution for 10 min at −20°C. The tissue sections were blocked with 10% donkey serum at room temperature for 1 h in PBS containing 0.03% Triton X-100. Fixed tissues were incubated overnight at 4°C with respective primary antibodies to NOX1, NOX2, GFAP, NeuN, and Iba1. The details on the source, clonality, and the dilution of each antibody used are provided in Table 1.

Double immunofluorescence was performed using donkey-antirabbit Alexafluor 594 for NOX1 or NOX2 and donkey-antimouse Alexafluor 488 for GFAP, donkey-antirabbit Alexafluor 488 for NeuN, and donkey-antigoat Alexafluor 488 for Iba1. The specificity of each antibody staining was validated by excluding each primary antibody (negative controls) and visualized for any nonspecific fluorescence. The primary antibody specificity, however, was not validated independently by blocking the binding to tissue with the corresponding antigen. Slides containing different brain regions were digitized (20x magnification) using Leica Aperio Versa 200 fluorescent microscope and slide scanner. Fluorescence intensities in each region were quantitated using AreaQuant software (Leica Biosystems) and expressed as average fluorescence intensity/unit area.

Superoxide production

Superoxide (O_2^-) levels in different brain regions were measured using dihydroethidium (DHE) following the method of Kim and co-workers.[21] Briefly, control and blast-induced animals (five controls and five animals immediately after blast) were injected with 5 mg/kg DHE (Molecular Probes, MA), dissolved in dimethylsulfoxide (DMSO) intraperitoneally, and 4 h after blast, animals were

TABLE 1. ANTIBODIES USED IN THE CURRENT STUDY

Antibody	Source	Catalog number	Host-species	Dilution
NADPH oxidase 1	Sigma-Aldrich Inc.	SAB420097-200UL	Rabbit (polyclonal)	1:400
NADPH oxidase 2	Invitrogen Inc.	PA5-34600	Rabbit (Polyclonal)	1:250
Glial fibrillary acidic protein (GFAP)	ThermoFisher Scientific Inc.	MA5-12023	Mouse (Monoclonal)	1:400
NeuN	Abcam	AB104224	Mouse (Monoclonal)	1:400
Iba1	Invitrogen Inc.	PA5-18039	Goat (Polyclonal)	1:250

NADPH, nicotinamide adenine dinucleotide phosphate.

transcardially perfused first with PBS followed by 4% PFA, brains excised, and 50 μm thin sections of different brain regions were prepared using Leica VT 1000S vibratome and mounted. DHE immunofluorescence in each region was visualized by digitizing the images using Leica Aperio Versa 200 slide scanner. Fluorescent intensities in each region were quantitated using AreaQuant software (Leica Biosystems) and expressed as average fluorescence intensity/unit area.

Image acquisition and analysis

Slides with mounted coronal sections from the brain were imaged at 20x magnification using a Leica Aperio Versa 200 digital pathology scanner. Control sections were used as reference for adjusting the exposure times and gray scale balance for optimal image quality; once set, these parameters were fixed and used for image acquisition of the reminder of both control and experimental groups. Three channels were collected for each coronal section. Blue: 405 nm (DAPI), red: 594 nm (NOX1), and green: 488 nm (cell specific marker GFAP [astrocytes], Iba1 [microglia], and NeuN [neurons]). We then manually outlined the regions of interest in different brain structures, and the fluorescence intensities in each brain region were quantitated using FLAreaQuantV1 algorithm (Leica Biosystems) and expressed as average fluorescence intensity/unit stained area.

For each channel, we set a minimum intensity threshold value using control sections as reference that will exclude any background fluorescence caused by nonspecific binding of fluorescent secondary antibody, and the same threshold values were used to quantify both control and experimental groups. A maximum intensity threshold was also set to remove any oversaturation from excess fluorescent dye. The algorithm outputs the area of positive staining for each brain region, the average intensity of each channel, and intensity profile of each protein.

Statistical analysis

Data are presented as mean $\pm$ standard error of the mean (SEM). Between-group comparisons were made by one-way analysis of variance (ANOVA) with a *post hoc* test (Bonferroni) to determine individual group differences. Differences between means were assessed at the probability level of $p \leq 0.05$, 0.01, and 0.001. GraphPad Prism 6.0 software was used in all analyses and preparation of plots.

Results

Moderate blast over pressure increases the protein levels of NOX1 and NOX2

Previous studies in this laboratory identified increased oxidative and nitrosative stress factors in the cerebral cortex in rats exposed to mild bTBI.[17,18] This study evaluated further the effect of moderate blast (180 kPa peak overpressure) on the early evolution of the protein expression of NOX isoforms (NOX1 and NOX2). Immunoblot analysis of NOX1 and NOX2 in the whole cerebral hemisphere showed a significant increase (87% and 52%, respectively, $p < 0.05$) (Fig. 2). To assess the diffuse nature of primary blast (shockwave) in the posterior region of the brain, NOX1 and NOX2 protein levels were also determined in the cerebellum, and we found that similar to cerebral hemisphere, cerebellar levels of NOX1 and NOX2 protein were significantly increased (60% and 40%, respectively, $p < 0.05$) (Fig. 2).

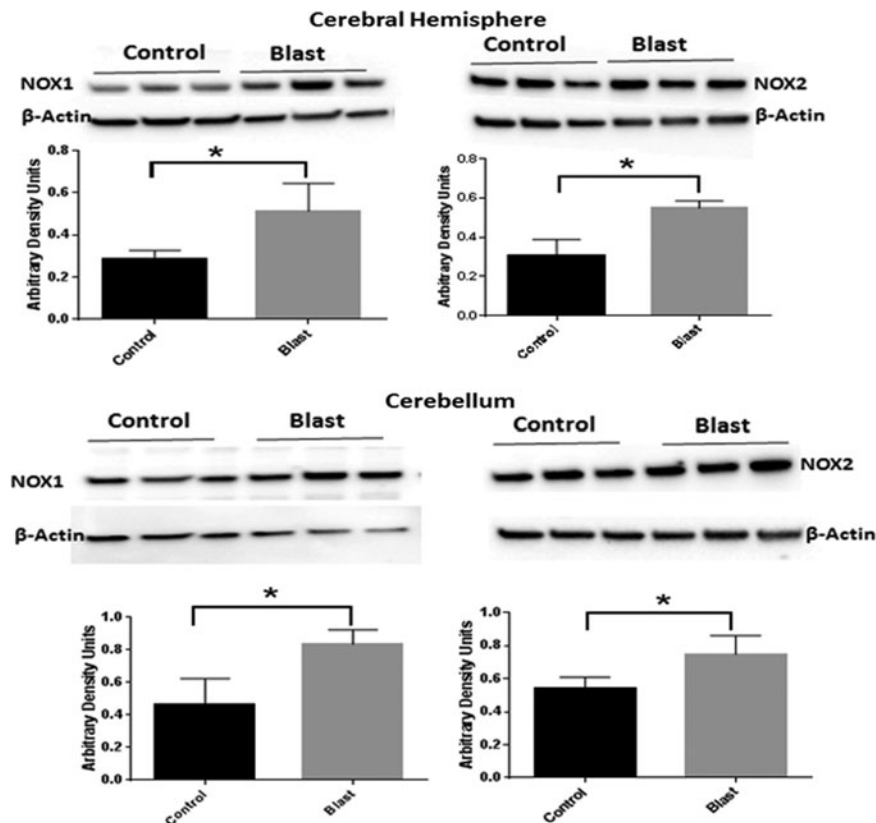**FIG. 2.** Blast increases the expression of nicotinamide adenine dinucleotide phosphate oxidase (NOX) isoforms. Immunoblots of NOX1 and NOX2 isoforms in the cerebral hemisphere and cerebellum 4 h after blast at 180 kPa blast over pressure. There was a significant increase (80%) in NOX1 in both cerebral hemispheres and cerebellum, while NOX2 increased by 83% in cerebral hemispheres and 38% in cerebellum. $n = 3$, *$p < 0.05$.
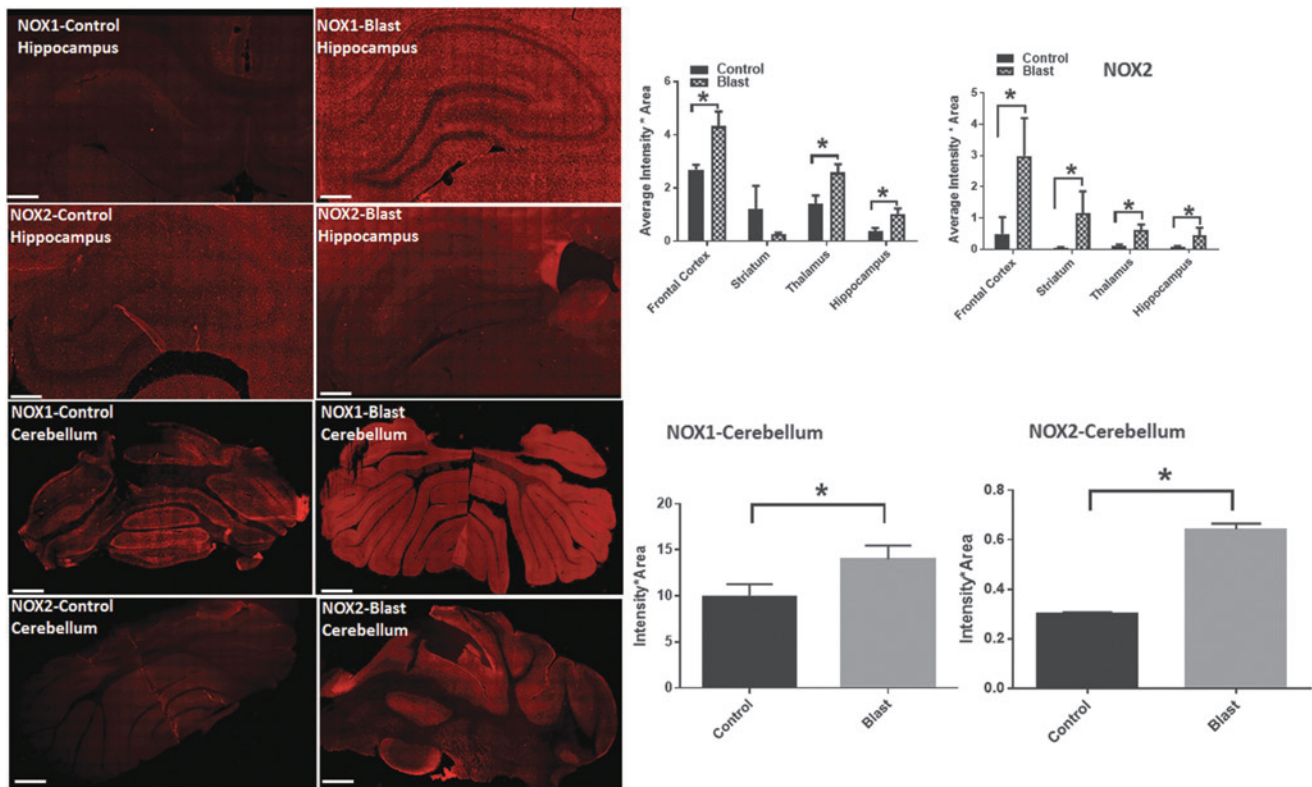
FIG. 3. Nicotinamide adenine dinucleotide phosphate oxidase (NOX) isoforms show a differential increase in different brain regions. Fluorescence intensities (red) of NOX1 and NOX2 in the hippocampus and cerebellum from control and blast-injury animals. Quantification of fluorescence intensities in different brain regions show a striking increase in NOX1 in the hippocampus of blast-injured animals compared with controls. Intensities of NOX2 display a higher increase in the frontal cortex compared with other regions. $n = 4$. *$p < 0.01$–0.05. Fluorescent intensities NOX1 in the cerebellum display a striking increase (96%) compared with NOX2 (38%). Color image is available online at www.liebertpub.com.neu

Differential changes in NOX isoforms expression in different brain regions

We next examined regional variations in NOX1 and NOX2 protein levels in the following brain structures: frontal cortex, striatum, hippocampus, thalamus, and cerebellum. The rationale in examining these regions is as follows: (a) NOX1 and NOX 2 isoforms are ubiquitously expressed in all brain regions, (b) the effect of shockwave propagation over the entire brain is not known, and (c) to use NOX1 and NOX2 as markers to evaluate whether there exists any selective vulnerability of various brain structures, a phenomenon that has not been investigated previously.

Under primary blast loading conditions, the pathological changes were found throughout the brain as indicated by changes in the fluorescent intensities of NOX1 and NOX 2 in different brain regions. Interestingly. various regions displayed a differential response. Thus, NOX1 levels in the frontal cortex showed a 49% increase; hippocampus showed the highest degree of increase (107%) followed by thalamus displaying a 90% increase (Fig. 3). Total NOX1 levels did not change in the striatum and somatosensory barrel cortex (S1BF) (data not shown).

The regional variations in the levels of NOX2 are slightly different from that of NOX1. Total NOX2 levels were highest in the frontal cortex (>two-fold) followed by the striatum and hippocampus that showed the lowest increase (Fig. 3). NOX isoform expression was also increased in other discrete brain regions from rostral and caudal areas, among which theCA1 region of a hippocampus displayed the biggest increase (Table 2).

Different neural cell types display differential vulnerability to oxidative damage

To evaluate cellular vulnerability to oxidative damage resulting from primary blast, changes in NOX1 expression patterns in astrocytes, neurons, and microglia were determined by double immunofluorescence staining. In addition, simultaneous

TABLE 2. PROTEIN LEVELS OF NICOTINAMIDE ADENINE DINUCLEOTIDE PHOSPHATE OXIDASE ISOFORM EXPRESSION IN DIFFERENT BRAIN REGIONS (FROM ROSTRAL TO CAUDAL AREAS) IN CONTROL AND ANIMALS FOUR HOURS AFTER EXPOSED TO MODERATE BLAST (180 KPA)

Region	NOX 1 (% over Control)	NOX2 (% over Control)
Hippocampus CA1	411%	+142%
Hippocampus CA3	265%	+203%
Dentate gyrus	605%	+20%
Corpus callosum	−77%	−65%
Cingulate cortex	+0.4%	−12.8%
Amygdala	+89%	+51.8%
Hypothalamus	+69%	+33.13

NOX, nicotinamide adenne dincleotide phosphate.
Note that highest increase in NOX expression was found in the CA1 region of the hippocampus that correlates with the known vulnerability to oxidative damage.
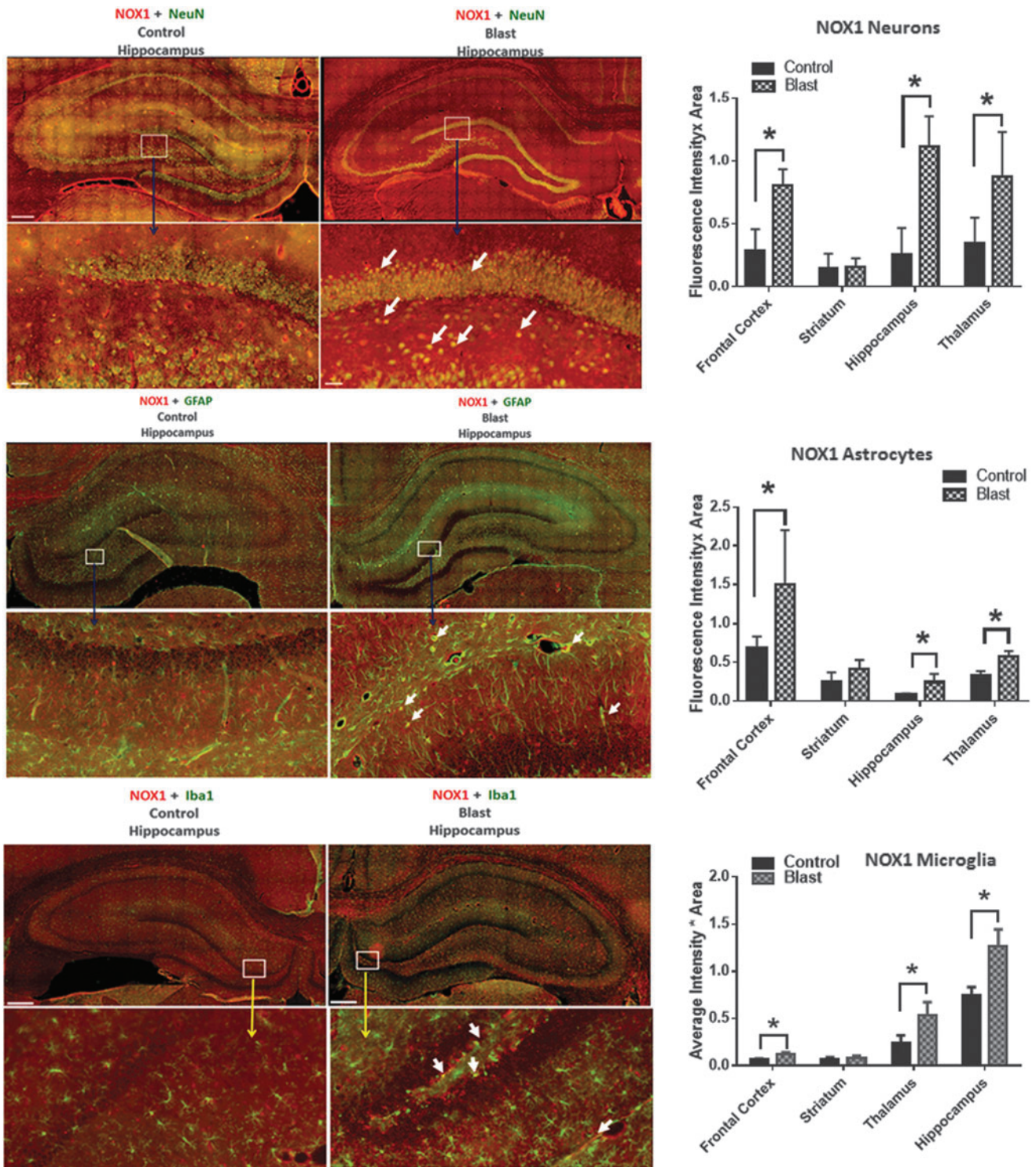
FIG. 4. Nicotinamide adenine dinucleotide phosphate oxidase (NOX)1 shows greater co-localization in neurons. Representative merged images showing the co-localization of NOX1 with NeuN, GFAP and Iba1 in the hippocampus indicating neuronal, astrocytic, and microglia localization, respectively, of NOX1 in control and blast-injured animals. Majority of increase in NOX1 with respect to corresponding controls is in neurons compared with astrocytes and microglia. Quantification of florescence intensities in different brain regions show a striking increase in NOX1 fluorescence in neurons in the hippocampus of blast-injured animals compared with controls. $n = 4$, $*p < 0.01$–0.05. Color image is available online at www.liebertpub.com.neu

quantification of NOX immunofluorescence using cell-specific markers will provide an insight into changes in its expression in different neural cells including astrocytes, neurons, and microglia.

Cell-specific analysis of increase in NOX1 and NOX2 levels after bTBI compared with their baseline expression (controls) indicate that neurons display a higher increase compared with astrocytes and microglia. In addition, NOX1 and NOX2 increases were more pronounced in neurons in the hippocampus and thalamus, respectively, compared with the frontal cortex. These conclusions were deduced based on the double immunofluorescence analysis showing co-localization of NOX1 with NeuN (a marker protein for neurons), with GFAP (a marker for astrocytes) and with Iba1 (a marker for microglia). (Fig. 4 and 5).

Primary blast also significantly affects posterior brain structures including the cerebellum

Primary blast caused diffused pathological changes not only in the perpendicular direction (deeper brain structures, hippocampus, thalamus) but also in the parallel direction to the wave propagation from the pre-frontal cortex to the cerebellum. The total tissue levels of NOX1 in the cerebellum not only increased, but this increase was highest in neurons (Fig. 6). Such higher expression of NOX1 in neurons compared with other neural cells also correlates with the known fact that the cerebellum contains the highest density of neurons compared with other brain regions.[22,23] Similar to NOX1, elevated levels of NOX2

expression were also found to be mainly co-localized with neurons (Fig. 7).

Primary blast increases superoxide levels in different brain regions

The activation of a variety of NOX isoforms is usually associated with the increased production of superoxide.[12,24] Because the present study showed increased protein levels of NOX isoforms, we then sought to examine whether increased NOX protein after blast has a functional significance. Accordingly, *in vivo* levels of superoxide in the frontal cortex, hippocampus, thalamus, and cerebellum were measured using DHE. Hippocampus displayed a robust level of the increase in superoxide (>10 fold, $p < 0.001$) followed by thalamus and frontal cortex. It is noteworthy that the extent of the rise in superoxide production in the hippocampus and thalamus (Fig. 8) correlated well with the increased degree of NOX expression. In addition, a pre-treatment of animals with apocynin, which is known to block the assembly of different NOX subunits, completely inhibited the increase in superoxide production indicating an essential role of NOX in brain superoxide production after moderate blast.

Primary blast results in oxidative damage and lipid peroxidation products in different brain structures

Several reports indicate the TBI resulting from different etiologies, including primary blast and blunt injuries, display oxidative stress during the evolution of its symptoms.[7,25–27] Accordingly,
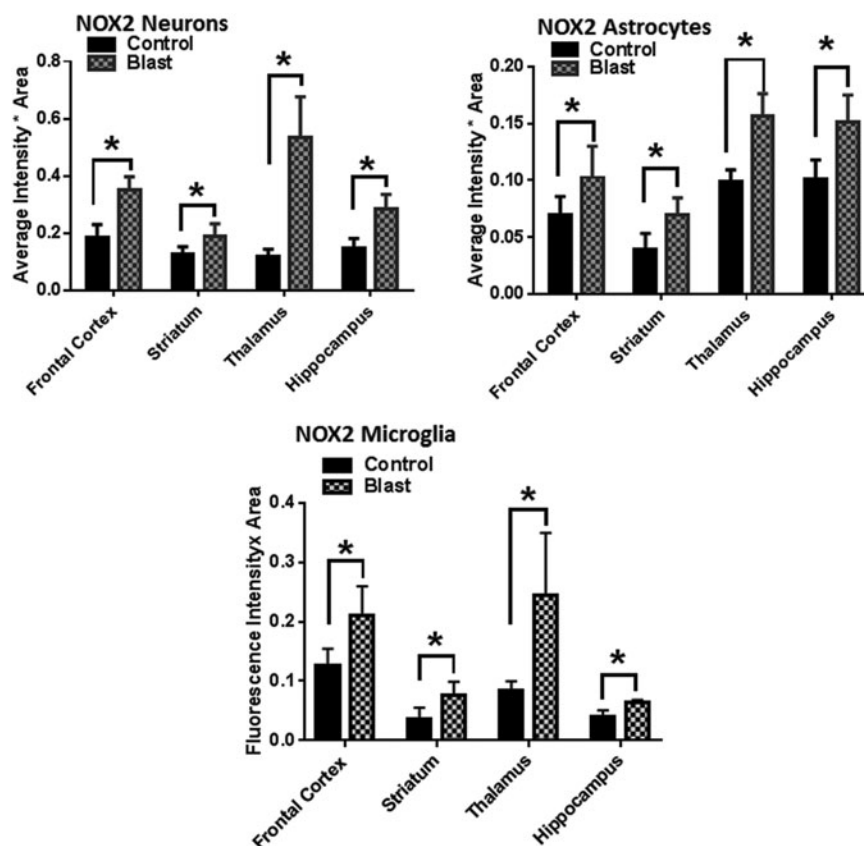
FIG. 5. Neurons show the highest increase in nicotinamide adenine dinucleotide phosphate oxidase (NOX)2 expression. Quantification of florescence intensities in different brain regions show a striking increase in NOX2 fluorescence in the hippocampus and thalamus of blast-injured animals compared with other brain regions. $n = 4$, $*p < 0.01–0.05$.
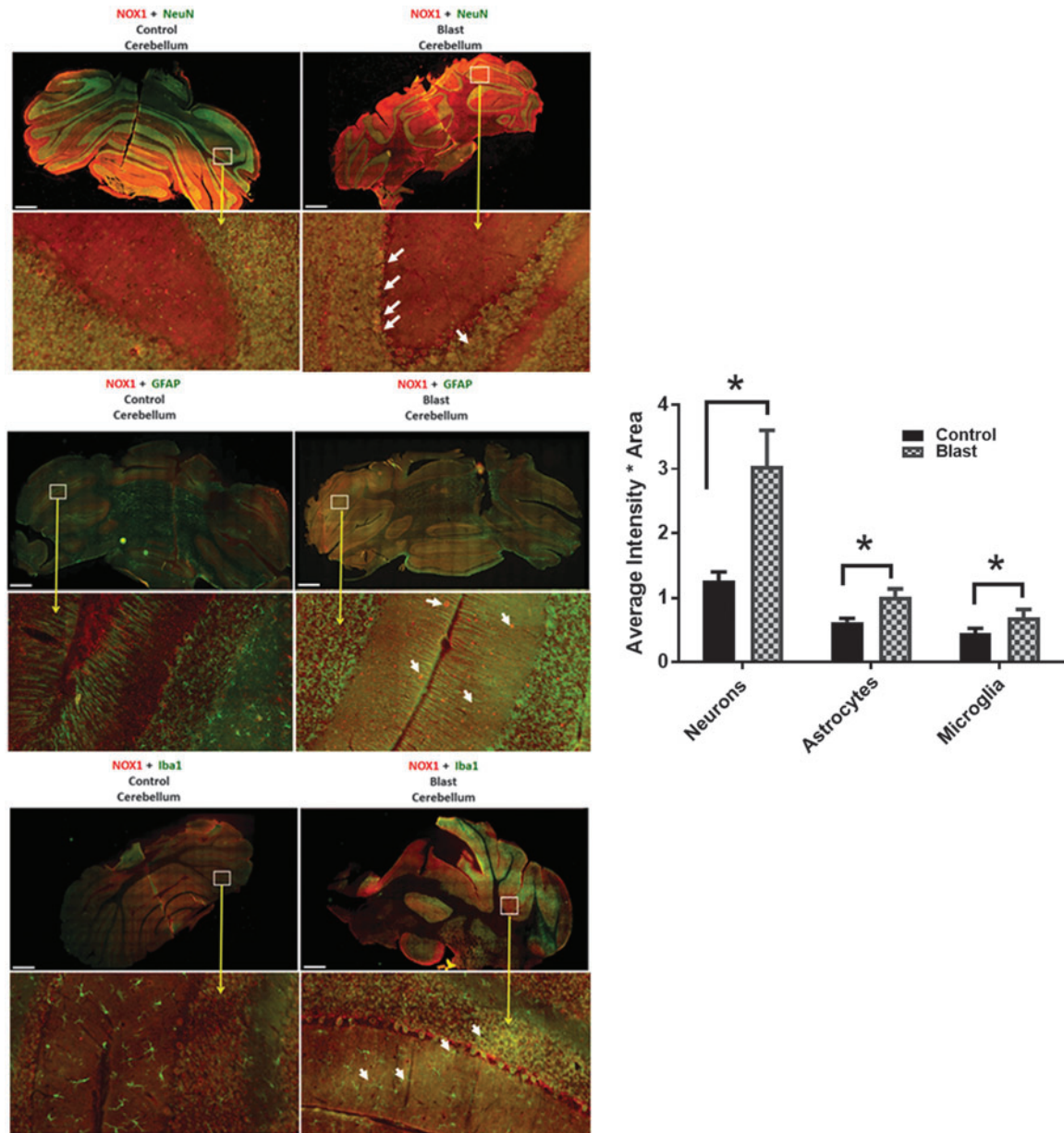
FIG. 6. Cerebellum displays an increased nicotinamide adenine dinucleotide phosphate oxidase (NOX)1 expression in neurons compared with astrocytes and microglia. Representative merged images showing the co-localization of NOX1 with NeuN, GFAP, and Iba1 in the cerebellum indicating neuronal, astrocytic, and microglia localization, respectively, of NOX1 in control and blast-injured animals. $n = 4$, $*p < 0.01–0.05$. Color image is available online at www.liebertpub.com.neu

several pathways are involved directly in the induction of oxidative stress including the activation of NOX[15,28–30] and alterations of antioxidant defense mechanisms (a reduction in superoxide dismutase, catalase, glutathione peroxidase).[9,31]

One of the major downstream effects of oxidative stress in many neurological disorders and TBI is the formation and accumulation of lipid peroxidation products.[32–35] Lipid peroxidation is a process under which oxidants such as free radicals attack various lipids containing carbon double bonds, and the resulting aldehyde products such as 4HNE generated by the lipid peroxidation directly modify amino acid structures in proteins and form adducts.[36]

Superoxide is one of the free radicals that can directly oxidize lipids to aldehydes that leads to the formation of protein adducts and activation of NOX produces excess levels of superoxide.[25,37,38]

Because the present study clearly showed an increase in NOX proteins and increased levels of superoxide after bTBI, we sought to examine the levels of 4HNE adducts in discrete brain regions in rats subjected to moderate blast (180 kPa, 4 h). Immunoblot analysis of 4HNE products identified two major bands corresponding to molecular weights of 70 and 100 kDa, which showed a trend toward an increase in cerebral hemispheres, hippocampus, thalamus, and cerebellum; however, such changes were not significant (Fig. 9).

Discussion

This study demonstrates that protein levels of superoxide producing enzymes NOX1 and NOX2 were significantly increased to different levels in various brain regions in rats exposed to moderate
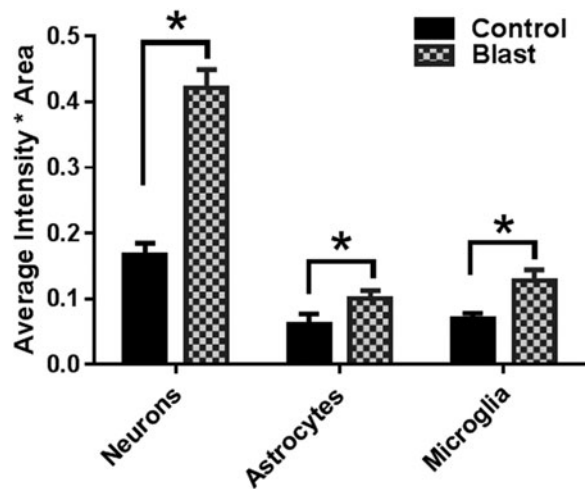
FIG. 7. Nicotinamide adenine dinucleotide phosphate oxidase-2 (NOX)2 displays a greater increase in neurons compared with astrocytes and microglia. Similar to NOX1, the majority of NOX2 is localized in neurons compared with astrocytes and microglia. $n = 4$, $*p < 0.01–0.05$.

primary blast overpressure. Increased NOX expression was accompanied by increased superoxide production and a strong tendency toward increased HNE adduct formation in two proteins. Together these observations strongly indicate that there is an increase in oxidative stress and oxidative damage occurring in the early phase after a single exposure to a shockwave. This work is motivated by two related questions: (1) does the blast TBI affect different brain regions equally assuming homogeneous spatial distribution of biomechanical loading, and (2) does the extent of the damage vary between different brain regions containing disparate ratios of neural cells (neurons, astrocytes, and microglia)? Hence,

we focused on the role of two different forms of superoxide producing enzymes and their downstream oxidative damage markers to understand both the spatial and cellular effects.

The bTBI has an unique pattern of biomechanical phenotype in that the external forces are dictated by the size and shape of the interacting body—in this instance, skull and brain structures. Further, the magnitude of forces generated depends on the contact area and interaction time that in turn determine the overall biomechanical loads at the tissue level. This loading triggers secondary biochemical cascades depending on the local tissue content. The cascade of secondary events usually develops over a period of hours to days that ultimately lead to additional neuropathological sequela.[39–41] Among many causal factors implicated in the pathophysiology of bTBI, oxidative stress represents an important early pathological outcome resulting from either the activation of free radical producing enzymes or downregulation of antioxidant defense mechanisms.[7,26,27,42]

NOX is a superoxide producing enzyme and different isoforms of NOX, including NOX1, NOX2, and NOX4 have been identified in the brain.[12] Studies reported increased activation of different isoforms of NOX in various forms of TBI. Accordingly, in a mouse model of controlled cortical impact (CCI), increased NOX2 expression was observed at 24–48 h after injury[43] whereas Byrnes and associates[44] found a delayed increase in NOX2 activity one month post-injury. In a rat model of CCI, however, increased NOX activity was observed as early as 1 h post-injury.[44] Increased NOX expression was also found in different animal models of fluid percussion injury.[14.45.46] In addition, apocynin, an inhibitor of NOX activation, showed protective effects on various models of blunt TBI.[16,46] Together these studies highlight the critical role of NOX in the pathology of TBI.

While studies have established the importance of NOX in the pathophysiology of blunt TBI, there are limited studies of NOX in bTBI.[47–49] This could in part be because of the lack of a true understanding the role of biomechanical loading in blast injury from
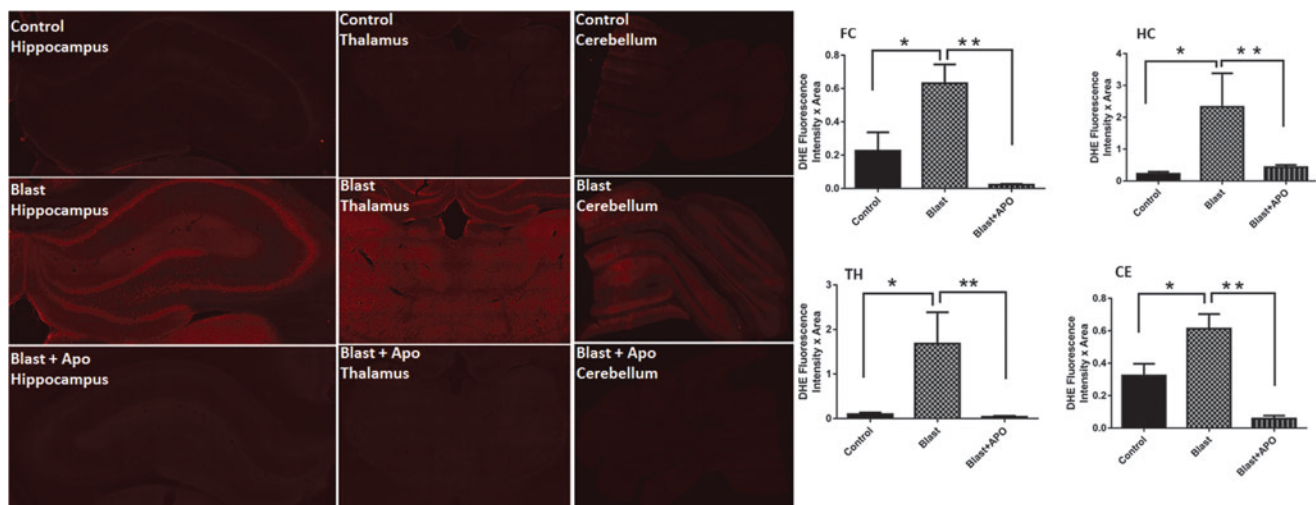
FIG. 8. Primary blast increases superoxide levels in different brain regions. Representative fluorescent intensities (red) of dihydroethidium (DHE, dye that recognizes superoxide production) in hippocampus, thalamus and cerebellum in control, Blast-injured and blast+ apocynin. Quantification of fluorescence intensities in different brain regions shows a striking increase in DHE fluorescence in the hippocampus of blast-injured animals compared with controls indicating high levels of superoxide production in the hippocampus. Note that a pre-treatment with apocynin (APO), an inhibitor of nicotinamide adenine dinucleotide phosphate oxidase (NOX) activation, completely blocks the DHE fluorescence increase indicating that the superoxide increase is mediated by activation of NOX. $n = 5$ $*p < 0.01–0.05$. Color image is available online at www.liebertpub.com.neu
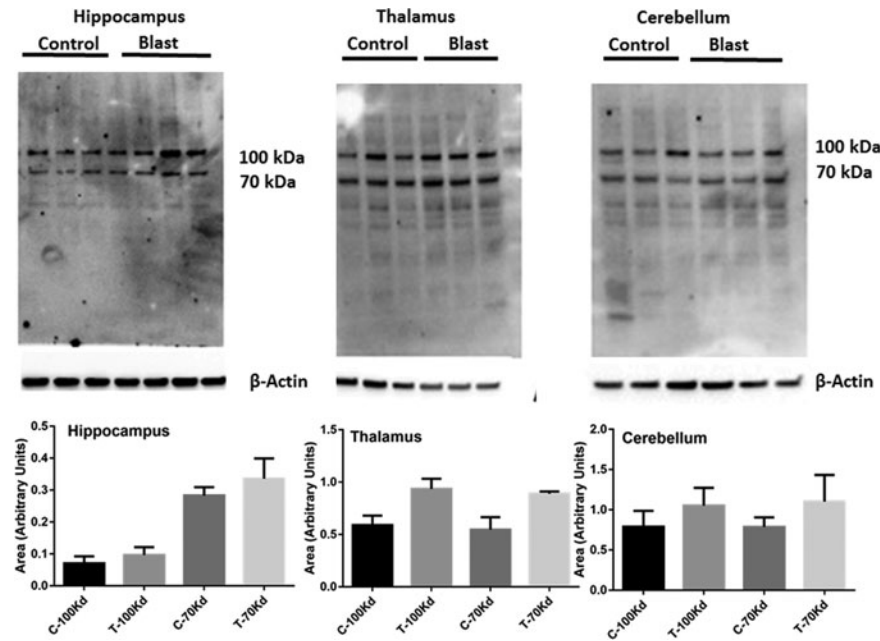
FIG. 9.   Primary blast displays a strong tendency to increase 4HNE protein adducts. Immunoblot analysis of 4HNE in lysates from the hippocampus, thalamus, and cerebellum 4 h after blast at 180 kPa blast overpressure is shown. Two proteins of 100 and 70 kDa show a strong tendency to increase in the hippocampus and thalamus. $n = 3$.

limited availability of a field validated shock tube that simulates battlefield injuries. In the present study, we therefore characterized the spatial resolution of two isoforms of NOX (NOX1 and NOX2) in various brain regions and their localization in neurons, astrocytes, and microglia 4 h after blast injury in a field validated shock tube.[10,19,20]

A generalized increase in NOX protein levels by immunoblots in the present study is comparable to our previous reports indicating its upregulation in the homogenates of a cerebral cortex in rats exposed to different blast overpressures.[17,18] Further, using immunofluorescence analysis, the present study identified regional variations in the expression pattern of NOX 1 in that the highest increase is found in the hippocampus followed by the thalamus. Interestingly, the frontal cortex showed higher expression in NOX2 compared with that in the hippocampus and thalamus. Other fine brain structures, including motor cortex, amygdala, and hypothalamus, also showed a significant increase in both the isoforms of NOX with the exception that NOX2 levels were significantly lower in a motor cortex (Table 2).

Interestingly, in the present study, a single blast exposure also affected distal brain structures, including the cerebellum, suggesting that blast injury propagation is highly diffusive in nature. While it is interesting to observe differential vulnerability of various brain structures to blast injury, in blast, a high-velocity shockwave traverses across and through the entire body loading all the regions almost simultaneously within a matter for 5–10 milliseconds. Recent experimental evidence in animal models and human cadaveric heads has shown that the shockwaves are capable of passing through the skin and skull and load all the brain structures.[10]

In addition to regional variations observed in NOX levels, we also found a cellular heterogeneity in the expression of NOX isoforms. Thus, blast injury displayed a robust increase in the levels of both isoforms of NOX in neurons compared to astrocytes and microglia with respect to their baseline values (controls). Studies have shown that all neural cells express different isoforms of NOX, including

NOX1, NOX2, and NOX4.[50] In addition, within the neurons, NOX1 is abundantly expressed in cerebellar granule cells,[51] while NOX2 has been shown to be expressed in both cerebellar granule cells as well as hippocampal neurons.[52] In addition to NOX1, the present study found a striking increase in NOX2 in neurons of the hippocampus, thalamus, and cerebellum compared with microglia.

Our results are in slight contrast to other reports wherein NOX2 is abundantly expressed in microglia.[44,53–55] While the reason for apparent abundance of NOX2 in neurons in our study is not known, studies report that NOX2 upregulation in hippocampal pyramidal neurons drives neuropathology associated with psychosocial stress in rats.[56,57] Further, studies also report that cellular injury to neurons after stroke resulted in an early upregulation of NOX2 in neurons (3–6 h after injury) whereas NOX2 was upregulated in microglia at later time points (72 h post-injury).[58,59] Such temporal difference in the expression pattern of NOX2 between neurons and microglia is reasonable because neurons may be far more vulnerable acutely in the evolution of the injury process whereas microglial activation could be a relatively late phenomenon.

Superoxide is a major free radical produced in the brain by a variety of reactions, including disturbances in mitochondrial oxidative phosphorylation, increased production of arachidonic acid as a consequence of activation of phosphilipase A2 (PLA2), activation of xanthine oxidase as well as by the activation of NOX.[60–63] Increased superoxide production has been shown in different models of TBI.[64–67] The present study observed a striking increase in superoxide production in the hippocampus, thalamus, and frontal cortex, areas where corresponding increases in NOX levels were found. Moreover, our studies showing a complete absence of $O_2^{\bullet-}$ in animals treated with apocynin (an inhibitor of NOX activation) before the exposure to blast injury reinforces the finding that the increase in $O_2^{\bullet-}$ is indeed mediated by NOX activation. Our results are also in agreement with previous studies showing protective effects of apocynin in attenuating oxidative damage in different models of TBI.[15,16,30,47,68,69]

While in the present study, the superoxide levels were found to be strikingly increased in different brain regions, the levels of 4HNE adducts showed a trend toward the increase in two proteins with average molecular weights of 70 and 100 kDa, but did not show statistically significant changes. The reason behind the lack of significant changes is not known. The 4HNE products, however, can be formed via peroxidation of unsaturated fatty acids not only by superoxide radical but also by a variety of other reactive oxygen species, including hydroxyl, peroxyl as well as a varety of cyclic compounds.[70] It is therefore likely that lipid peroxidation reaction and subsequent 4HNE formation may not have achieved a threshold as to show significant changes at 4 h after blast because reactive oxygen species other than superoxide (e.g., hydroxyl radicals among others) may not have been increased in the early phase of blast injury.

Despite an observed increase in factors conducive to oxidative damage in neurons, in the present study, we did not observe neuro-degeneration nor apoptotic cell death as investigated by fluorescent staining for Fluorojade C and cleaved caspase-3 4 h after blast injury (data not shown). Perhaps a 4 h window of blast injury may be too early to detect neuronal death. It is also likely that moderate blast may not cause neuronal death because of the diffuse nature of the shockwave unlike blunt injuries where neuronal death was observed close to the epicenter in the acute phase of injury.[71]

The selective vulnerability of neurons to oxidative damage may be dictated not only by the propagation of primary shockwave, the so-called direct mechanical impact throughout the brain regions, but also in part influenced by the cellular density and cell types distribution in different brain regions. Recently, it has been shown that the cerebellum and hippocampus contain the highest density of neurons compared with a cerebral cortex although relative mass of the hippocampus and cerebellum is far lesser than cerebral cortex.[23,72] In the present study, our observation of the highest increase in NOX levels in neurons in the hippocampus and cerebellum after blast suggests that neuron rich regions may be at higher risk for oxidative damage than other brain regions. This is further supported by our observation of a striking increase in superoxide levels in the hippocampus after blast. Also, within the hippocampus, studies have shown that neurons in CA1 region are more vulnerable to superoxide than CA3 neurons.[73,74]

Moreover, it is interesting to note that NOX1 showed a greater increase in CA1 region compared with CA3 (Table 2). Such higher level of neuronal oxidative damage in discrete brain regions may also depend on a number of other factors, including vascular density and associated metabolic supply and consumption of glucose and oxygen, neuronal excitability, and synaptic transmission.[75] In support of this tenet, it has been shown that the density (and perhaps subsequent nutrient supply) of brain capillaries was far less in the CA1 region of the hippocampus compared with the CA3 region, which likely places the CA1 region at higher risk for ischemia and hypoxia.[76]

The precise mechanism by which bTBI increases NOX isoform expression is not known. A shock-wave passage throughout the brain during a transient period could initiate a mechanical disturbance to plasma membrane structures within the brain parenchyma. It is reasonable, considering the small size of the rat brain and relatively thin skull, to assume the shockwave loading of the brain is uniform within brain structures investigated in this work (frontal cortex, striatum, hippocampus, and thalamus and cerebelllum). The uniformity of the pressure field within the rat brain under blast loading conditions was demonstrated in a numerical model[77] and was validated via intracranial pressure measurements by our group (data not published). If this is true—i.e. the mechanical forces created by the shockwave are distributed uniformly, and considering the brain's highly anisotropic and heterogeneous organization—our data suggest the extent of the local damage would depend on the composition and microarchitecture of a specific brain region (Fig. 10).
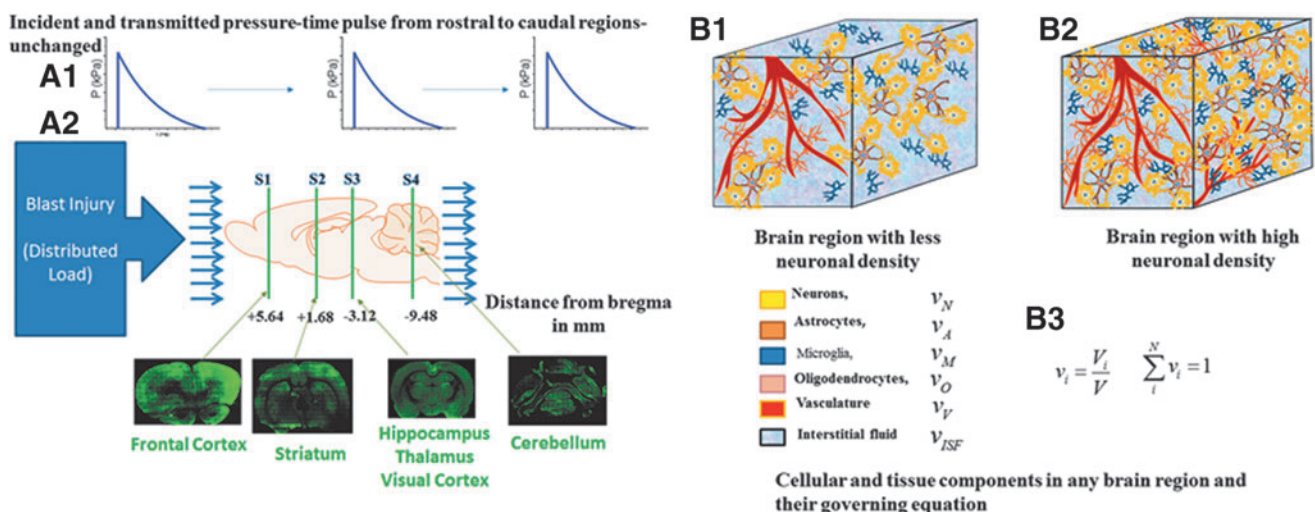
FIG. 10. Schematic of experimental blast injury model and effective loading and tissue-specific response. (**A**) The top panel shows the blast overpressure-time pulse applied to the rostral to caudal to rostral regions of the rodent brain travels with minimal change because of very short duration of less than a millisecond. The bottom panel shows different regions S1 to S4 analyzed in this study (**B**) A given brain volume comprises the six components (neurons, astrocytes, microglia, oligodendrocyte, vasculature, and interstitial/cerebrospinal fluid) that can vary from region to region. The mechanical properties of the representative volume given in B3 indicate that the effective mechanical stresses in the volume and hence the neural components will be determined by the differential volume fraction of that cell type. The different nicotinamide adenine dinucleotide phosphate oxidase expressions seen in this work are hypothesized to be driven by this differential cell volume fraction. Color image is available online at www.liebertpub.com.neu

Conclusion

Our studies demonstrate that moderate blast injury causes an increase in NOX isoforms in various brain regions to a differential degree. Increased NOX isoforms correlated with a concomitant rise in superoxide levels in corresponding regions that show a higher increase in NOX expression indicating oxidative damage. In addition, protein oxidation product 4HNE showed a strong tendency to increase in different brain regions. Further, higher increase in NOX isoforms in neurons compared with other brain cells strongly suggests neurons are by far the most vulnerable to oxidative damage in the early evolution of injury pathology.

Acknowledgments

Author Disclosure Statement

No competing financial interests exist.

References

1. Bochicchio, G.V., Lumpkins, K., O'Connor, J., Simard, M., Schaub, S., Conway, A., Bochicchio, K., and Scalea, T.M. (2008). Blast injury in a civilian trauma setting is associated with a delay in diagnosis of traumatic brain injury. Am. Surg. 74, 267–270.

2. DuBose, J.J., Barmparas, G., Inaba, K., Stein, D.M., Scalea, T., Cancio, L.C., Cole, J., Eastridge, B., and Blackbourne, L. (2011). Isolated severe traumatic brain injuries sustained during combat operations: demographics, mortality outcomes, and lessons to be learned from contrasts to civilian counterparts. J. Trauma 70, 11–16.

3. Reid, M.W. and Velez, C.S. (2015). Discriminating military and civilian traumatic brain injuries. Mol. Cell. Neurosci. 66, 123–128.

4. Wallace, D. (2009). Improvised explosive devices and traumatic brain injury: the military experience in Iraq and Afghanistan. Australas. Psychiatry 17, 218–224.

5. Singleton, J.A., Gibb, I.E., Hunt, N.C., Bull, A.M., and Clasper, J.C. (2013). Identifying future 'unexpected' survivors: a retrospective cohort study of fatal injury patterns in victims of improvised explosive devices. BMJ Open 3.

6. Bayir, H., Kochanek, P.M., and Kagan, V.E. (2006). Oxidative stress in immature brain after traumatic brain injury. Dev. Neurosci. 28, 420–431.

7. Cornelius, C., Crupi, R., Calabrese, V., Graziano, A., Milone, P., Pennisi, G., Radak, Z., Calabrese, E.J., and Cuzzocrea, S. (2013). Traumatic brain injury: oxidative stress and neuroprotection. Antioxid. Redox. Signal 19, 836–853.

8. Koppula, S., Kumar, H., Kim, I.S., and Choi, D.K. (2012). Reactive oxygen species and inhibitors of inflammatory enzymes, NADPH oxidase, and iNOS in experimental models of Parkinson's disease. Mediators Inflamm. 2012, 823902.

9. Lewen, A. and Hillered, L. (1998). Involvement of reactive oxygen species in membrane phospholipid breakdown and energy perturbation after traumatic brain injury in the rat. J. Neurotrauma 15, 521–530.

10. Chandra, N., Sundaramurthy, A., and Gupta, R.K. (2017). Validation of laboratory animal and surrogate human models in primary blast injury studies. Mil. Med. 182, 105–113.

11. Carbone, F., Teixeira, P.C., Braunersreuther, V., Mach, F., Vuilleumier, N., and Montecucco, F. (2015). Pathophysiology and treatments of oxidative injury in ischemic stroke: focus on the phagocytic NADPH oxidase 2. Antioxid. Redox. Signal 23, 460–489.

12. Infanger, D.W., Sharma, R.V., and Davisson, R.L. (2006). NADPH oxidases of the brain: distribution, regulation, and function. Antioxid. Redox. Signal 8, 1583–1596.

13. Cooney, S.J., Bermudez-Sabogal, S.L., and Byrnes, K.R. (2013). Cellular and temporal expression of NADPH oxidase (NOX) isotypes after brain injury. J. Neuroinflammation 10, 155.

14. Ferreira, A.P., Rodrigues, F.S., Della-Pace, I.D., Mota, B.C., Oliveira, S.M., de Campos Velho Gewehr, C., Bobinski, F., de Oliveira, C.V., Brum, J.S., Oliveira, M.S., Furian, A.F., de Barros, C.S., dos Santos, A.R., Ferreira, J., Fighera, M.R., and Royes, L.F. (2014). HOE-140, an antagonist of B2 receptor, protects against memory deficits and brain damage induced by moderate lateral fluid percussion injury in mice. Psychopharmacology (Berl) 231, 1935–1948.

15. Choi, B.Y., Jang, B.G., Kim, J.H., Lee, B.E., Sohn, M., Song, H.K., and Suh, S.W. (2012). Prevention of traumatic brain injury-induced neuronal death by inhibition of NADPH oxidase activation. Brain Res. 1481, 49–58.

16. Song, S.X., Gao, J.L., Wang, K.J., Li, R., Tian, Y.X., Wei, J.Q., and Cui, J.Z. (2013). Attenuation of brain edema and spatial learning deficits by the inhibition of NADPH oxidase activity using apocynin following diffuse traumatic brain injury in rats. Mol. Med. Rep. 7, 327–331.

17. Abdul-Muneer, P.M., Schuetz, H., Wang, F., Skotak, M., Jones, J., Gorantla, S., Zimmerman, M.C., Chandra, N., and Haorah, J. (2013). Induction of oxidative and nitrosative damage leads to cerebrovascular inflammation in an animal model of mild traumatic brain injury induced by primary blast. Free Radic. Biol. Med. 60, 282–291.

18. Mishra, V., Skotak, M., Schuetz, H., Heller, A., Haorah, J., and Chandra, N. (2016). Primary blast causes mild, moderate, severe and lethal TBI with increasing blast overpressures: experimental rat injury model. Sci. Rep. 6, 26992.

19. Skotak, M., Wang, F., Alai, A., Holmberg, A., Harris, S., Switzer, R., and Chandra, N. (2013). Rat injury model under controlled field-relevant primary blast conditions: acute response to a wide range of peak overpressures. J. Neurotrauma 30, 1147–1160.

20. Kuriakose, M., Skotak, M., Misistia, A., Kahali, S., Sundaramurthy, A., and Chandra, N. (2016). Tailoring the blast exposure conditions in the shock tube for generating pure, primary shock waves: the end plate facilitates elimination of secondary loading of the specimen. PLoS One 11, e0161597.

21. Kim, J.H., Jang, B.G., Choi, B.Y., Kim, H.S., Sohn, M., Chung, T.N., Choi, H.C., Song, H.K., and Suh, S.W. (2013). Post-treatment of an NADPH oxidase inhibitor prevents seizure-induced neuronal death. Brain Res. 1499, 163–172.

22. Herculano-Houzel, S., Mota, B., and Lent, R. (2006). Cellular scaling rules for rodent brains. Proc. Natl. Acad. Sci. U. S. A. 103, 12138–12143.

23. Fu, Y., Rusznak, Z., Herculano-Houzel, S., Watson, C., and Paxinos, G. (2013). Cellular composition characterizing postnatal development and maturation of the mouse brain and spinal cord. Brain Struct. Funct. 218, 1337–1354.

24. Fernandez, V., Barrientos, X., Kipreos, K., Valenzuela, A., and Videla, L.A. (1985). Superoxide radical generation, NADPH oxidase activity, and cytochrome P-450 content of rat liver microsomal fractions in an experimental hyperthyroid state: relation to lipid peroxidation. Endocrinology 117, 496–501.

25. Cernak, I., Savic, V.J., Kotur, J., Prokic, V., Veljovic, M., and Grbovic, D. (2000). Characterization of plasma magnesium concentration and oxidative stress following graded traumatic brain injury in humans. J. Neurotrauma 17, 53–68.

26. Rodriguez-Rodriguez, A., Egea-Guerrero, J.J., Murillo-Cabezas, F., and Carrillo-Vico, A. (2014). Oxidative stress in traumatic brain injury. Curr. Med. Chem. 21, 1201–1211.

27. Abdul-Muneer, P.M., Chandra, N., and Haorah, J. (2015). Interactions of oxidative stress and neurovascular inflammation in the pathogenesis of traumatic brain injury. Mol. Neurobiol. 51, 966–979.

28. Angeloni, C., Prata, C., Dalla Sega, F.V., Piperno, R., and Hrelia, S. (2015). Traumatic brain injury and NADPH oxidase: a deep relationship. Oxid. Med. Cell. Longev. 2015, 370312.

29. Lu, X.Y., Wang, H.D., Xu, J.G., Ding, K., and Li, T. (2014). NADPH oxidase inhibition improves neurological outcome in experimental traumatic brain injury. Neurochem. Int. 69, 14–19.

30. Ma, M.W., Wang, J., Zhang, Q., Wang, R., Dhandapani, K.M., Vadlamudi, R.K., and Brann, D.W. (2017). NADPH oxidase in brain injury and neurodegenerative disorders. Mol. Neurodegener. 12, 7.

31. Muir, J.K., Tynan, M., Caldwell, R., and Ellis, E.F. (1995). Superoxide dismutase improves posttraumatic cortical blood flow in rats. J. Neurotrauma 12, 179–188.

32. Butterfield, D.A. and Reed, T.T. (2016). Lipid peroxidation and tyrosine nitration in traumatic brain injury: insights into secondary injury from redox proteomics. Proteomics Clin. Appl. 10, 112.

33. Cristofori, L., Tavazzi, B., Gambin, R., Vagnozzi, R., Vivenza, C., Amorini, A.M., Di Pierro, D., Fazzina, G., and Lazzarino, G. (2001). Early onset of lipid peroxidation after human traumatic brain injury: a fatal limitation for the free radical scavenger pharmacological therapy? J. Investig. Med. 49, 450–458.

34. Roof, R.L., Hoffman, S.W., and Stein, D.G. (1997). Progesterone protects against lipid peroxidation following traumatic brain injury in rats. Mol. Chem. Neuropatho.l 31, 1–11.

35. Wada, K., Alonso, O.F., Busto, R., Panetta, J., Clemens, J.A., Ginsberg, M.D., and Dietrich, W.D. (1999). Early treatment with a novel inhibitor of lipid peroxidation (LY341122) improves histopathological outcome after moderate fluid percussion brain injury in rats. Neurosurgery 45, 601–608.

36. Arlt, S., Beisiegel, U., and Kontush, A. (2002). Lipid peroxidation in neurodegeneration: new insights into Alzheimer's disease. Curr. Opin. Lipidol. 13, 289–294.

37. Banakou, E. and Dailianis, S. (2010). Involvement of Na+/H+ exchanger and respiratory burst enzymes NADPH oxidase and NO synthase, in Cd-induced lipid peroxidation and DNA damage in haemocytes of mussels. Comp. Biochem. Physiol. C. Toxicol. Pharmacol. 152, 346–352.

38. Stanger, O., Renner, W., Khoschsorur, G., Rigler, B., and Wascher, T.C. (2001). NADH/NADPH oxidase p22 phox C242T polymorphism and lipid peroxidation in coronary artery disease. Clin. Physiol. 21, 718–722.

39. Chandra, N. and Sundaramurthy, A. (2015). Acute pathophysiology of blast injury-from biomechanics to experiments and computations: implications on head and polytrauma. In: *Brain Neurotrauma: Molecular, Neuropsychological, and Rehabilitation Aspects*. Kobeissy, F.H. (ed): Boca Raton, FL.

40. Courtney, A. and Courtney, M. (2015). The complexity of biomechanics causing primary blast-induced traumatic brain injury: a review of potential mechanisms. Front. Neurol. 6, 221.

41. Bandak, F.A., Ling, G., Bandak, A., and De Lanerolle, N.C. (2015). Injury biomechanics, neuropathology, and simplified physics of explosive blast and impact mild traumatic brain injury. Handb. Clin. Neurol. 127, 89–104.

42. Chong, Z.Z., Li, F., and Maiese, K. (2005). Oxidative stress in the brain: novel cellular targets that govern survival during neurodegenerative disease. Prog. Neurobiol. 75, 207–246.

43. Dohi, K., Ohtaki, H., Nakamachi, T., Yofu, S., Satoh, K., Miyamoto, K., Song, D., Tsunawaki, S., Shioda, S., and Aruga, T. (2010). Gp91phox (NOX2) in classically activated microglia exacerbates traumatic brain injury. J. Neuroinflammation 7, 41.

44. Byrnes, K.R., Loane, D.J., Stoica, B.A., Zhang, J., and Faden, A.I. (2012). Delayed mGluR5 activation limits neuroinflammation and neurodegeneration after traumatic brain injury. J. Neuroinflammation 9, 43.

45. Luo, T., Wu, J., Kabadi, S.V., Sabirzhanov, B., Guanciale, K., Hanscom, M., Faden, J., Cardiff, K., Bengson, C.J., and Faden, A.I. (2013). Propofol limits microglial activation after experimental brain trauma through inhibition of nicotinamide adenine dinucleotide phosphate oxidase. Anesthesiology 119, 1370–1388.

46. Ferreira, A.P., Rodrigues, F.S., Della-Pace, I.D., Mota, B.C., Oliveira, S.M., Velho Gewehr Cde, C., Bobinski, F., de Oliveira, C.V., Brum, J.S., Oliveira, M.S., Furian, A.F., de Barros, C.S., Ferreira, J., Santos, A.R., Fighera, M.R., and Royes, L.F. (2013). The effect of NADPH-oxidase inhibitor apocynin on cognitive impairment induced by moderate lateral fluid percussion injury: role of inflammatory and oxidative brain damage. Neurochem. Int. 63, 583–593.

47. Cho, H.J., Sajja, V.S., Vandevord, P.J., and Lee, Y.W. (2013). Blast induces oxidative stress, inflammation, neuronal loss and subsequent short-term memory impairment in rats. Neuroscience 253, 9–20.

48. Readnower, R.D., Chavko, M., Adeeb, S., Conroy, M.D., Pauly, J.R., McCarron, R.M., and Sullivan, P.G. (2010). Increase in blood-brain barrier permeability, oxidative stress, and activated microglia in a rat model of blast-induced traumatic brain injury. J. Neurosci. Res. 88, 3530–3539.

49. Lucke-Wold, B.P., Naser, Z.J., Logsdon, A.F., Turner, R.C., Smith, K.E., Robson, M.J., Bailes, J.E., Lee, J.M., Rosen, C.L., and Huber, J.D. (2015). Amelioration of nicotinamide adenine dinucleotide phosphate-oxidase mediated stress reduces cell death after blast-induced traumatic brain injury. Transl. Res. 166, 509–528 e1.

50. Sorce, S. and Krause, K.H. (2009). NOX enzymes in the central nervous system: from signaling to disease. Antioxid. Redox. Signal. 11, 2481–2504.

51. Coyoy, A., Olguin-Albuerne, M., Martinez-Briseno, P., and Moran, J. (2013). Role of reactive oxygen species and NADPH-oxidase in the development of rat cerebellum. Neurochem. Int. 62, 998–1011.

52. Park, K.W. and Jin, B.K. (2008). Thrombin-induced oxidative stress contributes to the death of hippocampal neurons: role of neuronal NADPH oxidase. J. Neurosci. Res. 86, 1053–1063.

53. Surace, M.J. and Block, M.L. (2012). Targeting microglia-mediated neurotoxicity: the potential of NOX2 inhibitors. Cell. Mol. Life Sci. 69, 2409–2427.

54. Guilarte, T.R., Loth, M.K., and Guariglia, S.R. (2016). TSPO finds NOX2 in microglia for redox homeostasis. Trends Pharmacol. Sci. 37, 334–343.

55. Kumar, A., Barrett, J.P., Alvarez-Croda, D.M., Stoica, B.A., Faden, A.I., and Loane, D.J. (2016). NOX2 drives M1-like microglial/macrophage activation and neurodegeneration following experimental traumatic brain injury. Brain Behav. Immun. 58, 291–309.

56. Sorce, S., Schiavone, S., Tucci, P., Colaianna, M., Jaquet, V., Cuomo, V., Dubois-Dauphin, M., Trabace, L., and Krause, K.H. (2010). The NADPH oxidase NOX2 controls glutamate release: a novel mechanism involved in psychosis-like ketamine responses. J. Neurosci. 30, 11317–11325.

57. Schiavone, S., Jaquet, V., Sorce, S., Dubois-Dauphin, M., Hultqvist, M., Backdahl, L., Holmdahl, R., Colaianna, M., Cuomo, V., Trabace, L., and Krause, K.H. (2012). NADPH oxidase elevations in pyramidal neurons drive psychosocial stress-induced neuropathology. Transl. Psychiatry 2, e111.

58. Zhang, Q.G., Raz, L., Wang, R., Han, D., De Sevilla, L., Yang, F., Vadlamudi, R.K., and Brann, D.W. (2009). Estrogen attenuates ischemic oxidative damage via an estrogen receptor alpha-mediated inhibition of NADPH oxidase activation. J. Neurosci. 29, 13823–13836.

59. Yoshioka, H., Niizuma, K., Katsu, M., Okami, N., Sakata, H., Kim, G.S., Narasimhan, P., and Chan, P.H. (2011). NADPH oxidase mediates striatal neuronal injury after transient global cerebral ischemia. J. Cereb. Blood Flow Metab. 31, 868–880.

60. Siesjo, B.K., Agardh, C.D., and Bengtsson, F. (1989). Free radicals and brain damage. Cerebrovasc. Brain Metab. Rev. 1, 165–211.

61. Jesberger, J.A. and Richardson, J.S. (1991). Oxygen free radicals and brain dysfunction. Int. J. Neurosci. 57, 1–17.

62. Evans, P.H. (1993). Free radicals in brain metabolism and pathology. Br. Med. Bull. 49, 577–587.

63. O'Connell, K.M. and Littleton-Kearney, M.T. (2013). The role of free radicals in traumatic brain injury. Biol. Res. Nurs. 15, 253–263.

64. Brown, S.A. and Hall, E.D. (1992). Role of oxygen-derived free radicals in the pathogenesis of shock and trauma, with focus on central nervous system injuries. J. Am. Vet. Med. Assoc. 200, 1849–1859.

65. Mattson, M.P. (1996). Calcium and free radicals: mediators of neurotrophic factor and excitatory transmitter-regulated developmental plasticity and cell death. Perspect. Dev. Neurobiol. 3, 79–91.

66. Deng-Bryant, Y., Singh, I.N., Carrico, K.M., and Hall, E.D. (2008). Neuroprotective effects of tempol, a catalytic scavenger of peroxynitrite-derived free radicals, in a mouse traumatic brain injury model. J. Cereb. Blood Flow Metab. 28, 1114–1126.

67. Willmore, L.J. and Ueda, Y. (2009). Posttraumatic epilepsy: hemorrhage, free radicals and the molecular regulation of glutamate. Neurochem. Res. 34, 688–697.

68. Zhang, Q.G., Laird, M.D., Han, D., Nguyen, K., Scott, E., Dong, Y., Dhandapani, K.M., and Brann, D.W. (2012). Critical role of NADPH oxidase in neuronal oxidative damage and microglia activation following traumatic brain injury. PLoS One 7, e34504.

69. Loane, D.J. Stoica, B.A., Byrnes, K.R., Jeong, W., and Faden, A.I. (2013). Activation of mGluR5 and inhibition of NADPH oxidase improves functional recovery after traumatic brain injury. J. Neurotrauma 30, 403–412.

70. Schaur, R.J., Siems, W., Bresgen, N., and Eckl, P.M. (2015). 4-Hydroxy-nonenal-A bioactive lipid peroxidation product. Biomolecules 5, 2247–2337.

71. Raghupathi, R. (2004). Cell death mechanisms following traumatic brain injury. Brain Pathol. 14, 215–222.

72. Herculano-Houzel, S., Ribeiro, P., Campos, L., Valotta da Silva, A., Torres, L.B., Catania, K.C., and Kaas, J.H. (2011). Updated neuronal scaling rules for the brains of Glires (rodents/lagomorphs). Brain Behav. Evol. 78, 302–314.

73. Wang, X. and Michaelis, E.K. (2010). Selective neuronal vulnerability to oxidative stress in the brain. Front. Aging Neurosci. 2, 12.

74. Wang, X., Pal, R., Chen, X.W., Limpeanchob, N., Kumar, K.N., and Michaelis, E.K. (2005). High intrinsic oxidative stress may underlie selective vulnerability of the hippocampal CA1 region. Brain Res. Mol. Brain Res. 140, 120–126.

75. Friedman, J. (2011). Why is the nervous system vulnerable to oxidative stress? in: *Oxidative Stress and Free Radical Damage in Neurology*. Gadoth, N., Göbel, H.H. (eds). Humana Press: New York, pps. 19–27.

76. Cavaglia, M., Dombrowski, S.M., Drazba, J., Vasanji, A., Bokesch, P.M., and Janigro, D. (2001). Regional variation in brain capillary density and vascular response to ischemia. Brain Res. 910, 81–93.

77. Tan, X., Przekwas, A.J. and Long, J.B. (2013). Validations of virtual animal model for investigation of shock/blast wave TBI, in: *ASME 2013 International Mechanical Engineering Congress and Exposition.* American Society of Mechanical Engineers, pps. V03AT03A011–V003AT003A011.

Address crrespondence to:
Kakulavarapu V. Rama Rao, PhD
Namas Chandra, PhD, PE
Center for Injury Biomechanics, Materials and Medicine
Department of Biomedical Engineering
New Jersey Institute of Technology
111 Lock Street
Newark, NJ 07102

E-mail: kakulava@njit.edu;
kakulavarapuvenkata41@gmail.com;
namas.chandra@njit.edu

SCIENTIFIC REP⚙RTS

Temporal and Spatial Effects of Blast Overpressure on Blood-Brain Barrier Permeability in Traumatic Brain Injury

Matthew Kuriakose, Kakulavarapu V. Rama Rao, Daniel Younger & Namas Chandra

Blast-induced traumatic brain injury (bTBI) is a "signature wound" in soldiers during training and in combat and has also become a major cause of morbidity in civilians due to increased insurgency. This work examines the role of blood-brain barrier (BBB) disruption as a result of both primary biomechanical and secondary biochemical injury mechanisms in bTBI. Extravasation of sodium fluorescein (NaF) and Evans blue (EB) tracers were used to demonstrate that compromise of the BBB occurs immediately following shock loading, increases in intensity up to 4 hours and returns back to normal in 24 hours. This BBB compromise occurs in multiple regions of the brain in the anterior-posterior direction of the shock wave, with maximum extravasation seen in the frontal cortex. Compromise of the BBB is confirmed by (a) extravasation of tracers into the brain, (b) quantification of tight-junction proteins (TJPs) in the brain and the blood, and (c) tracking specific blood-borne molecules into the brain and brain-specific proteins into the blood. Taken together, this work demonstrates that the BBB compromise occurs as a part of initial biomechanical loading and is a function of increasing blast overpressures.

Blast-induced traumatic brain injuries (bTBIs) are the signature wounds in military and civilian populations due to the increased use of improvised explosive devices and asymmetric warfare in military conflicts and acts of terrorism, domestically and overseas[1–3]. Despite the increase in studies related to bTBI in recent years, there is only a limited understanding of how blast waves interact with the brain and cause injury, which has precluded the establishment of comprehensive diagnostic criteria for bTBI and the potential of therapeutic strategies. A recent survey reported that more than 30 phase III clinical trials aimed at targeting TBI have failed[4–7]. Understanding how blast-induced neurotrauma displays a temporal and spatial evolution of neuropathology in various regions of the brain is critical for the identification of injury mechanisms and the development of preventative measures and treatments for bTBI patients. Among many mechanisms of injury, damage to the BBB has been identified as a potential candidate and has been the focus of several clinical and experimental investigations aimed to establish injury baselines and to determine the timelines for therapeutic interventions for neurotrauma[8,9].

The blood-brain barrier (BBB) is a highly, selectively-permeable membrane that separates the brain from the circulatory system. The BBB is dynamically modulated by cellular interactions between endothelial cells, the tight junctions that join them, pericytes, and astrocytes that support the endothelial capillaries[10–16]. Many neurological disorders including stroke[17–20], Alzheimer's disease[21,22], Parkinson's disease[14,23], HIV-1 encephalitis[16,24], epilepsy[25,26], and multiple sclerosis[27–29] display impaired BBB permeability. BBB disruption is also one of the most frequently investigated mechanisms of injury in blunt TBI and has been commonly used to evaluate the degree and extent of injury[30–34]. Several groups have reported abnormal opening of the BBB in closed cortical injuries[35–37], weight drop models[38,39], and blast models[34,40–45]. Reported results are derived from different probing methodologies, with different injury models, at different injury intensities, in different spatial regions of the brain. A limited number of studies has implicated increased BBB permeability in the pathology of blast-induced traumatic brain injury but, to the author's knowledge, no such investigation has resolved the temporal and spatial resolution of BBB changes in bTBI, especially as a function of increasing biomechanical blast loadings. While a number of groups have assessed the BBB permeability following blast[42,46–49], it is important to note that not all

Center for Injury Biomechanics, Materials and Medicine (CIBM3), Department of Biomedical Engineering, New Jersey Institute of Technology, Newark, NJ, 07102-1982, USA. Correspondence and requests for materials should be addressed to K.V.R.R. (email: kakulava@njit.edu) or N.C. (email: namas.chandra@njit.edu)
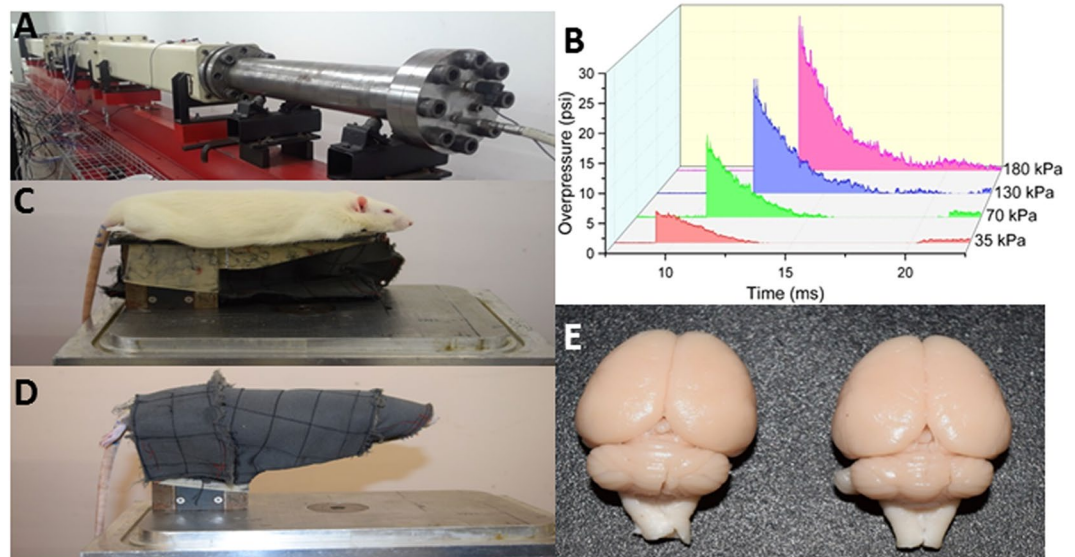
Figure 1. The shock tube housed in the blast laboratory in the Center for Injury Biomechanics, Materials, and Medicine at NJIT. (**A**) The 9-inch, square cross-section, 6 meters long shock tube instrumented with pressure sensors along the top of the shock tube. (**B**) Representative pressure-time profiles acquired from pressure sensors in the shock tube at the four overpressures used in this study. (**C**) Rat holder mounted in the test section of the shock tube, with rat placed in the prone position (top) and (**D**) tightly wrapped in a harness to minimize head and body motion during the blast (bottom). (**E**) Control (left) and injured (right) brains following perfusion-fixation. All blood in the neurovasculature has been washed away, as seen from the white appearance of brains, confirming that all tracers measured has leaked from the vessels into the brain parenchyma.

blast models impart the same type of injury on experimental animals and, for this reason, authors compared the results of this work only to models that feature pure, primary blast injury void of secondary and tertiary effects[50,51].

In this study, rats were exposed to a range of shock waves in a field-validated shock tube and permeability of the BBB was assayed by extravasation of Evans blue (which binds to albumin, a 66 kDa protein abundant in blood) and sodium fluorescein (a 376 Da molecule) in the frontal cortex, striatum, somatosensory barrel-field cortex, hippocampus, thalamus, and cerebellum. Rats were exposed to sub-mild (35 kPa), mild (70 kPa), mild-moderate (130 kPa), and moderate (180 kPa) blast overpressures; these classifications were based on a 24-hour survival dose-response of rodent models based on our previous results (see Fig. 2 of ref.[52]). Also, the Department of Defense (DOD) Instruction 6490.11 dated September 18, 2012 has established policies, responsibilities and procedures for mTBI occurring in the battlefield. When service members are involved in a potential concussive event, they are separated for medical observations and mandatory rest period. DOD defines potential concussive events as the presence of service members within 50 m of a blast or exposure to more than a single blast in a year[1]. Based on theoretical analysis, the peak blast overpressure of 180 kPa can occur at a distance of about 10 m for 100 kg TNT explosive. The same blast will produce 130 kPa BOP in about 12 m, 70 kPa in a distance of 16 m and 35 kPa in a distance of 23 m[53]. We had achieved these field blast loadings using operating characteristics like membrane thickness, transition length, driver gas, driver volume, and end plates[54]. Additionally, three different time-points post-injury (15 min, 4 hr, and 24 hr) were chosen in order to develop a temporal profile of BBB opening and to identify the extent of barrier breach.

Results

Primary blast induces breakdown of the blood-brain barrier. The blast injury model developed at NJIT, capable of reproducing field-relevant blast overpressures and previously characterized[52,55–57] was used throughout this study (Fig. 1A,B). All test animals were mounted in the custom-made rat holder and placed in the test section of the shock tube (Fig. 1C). Rats were immobilized with the head restrained in order to ensure no confounding head movements or possible acceleration/deceleration that can be artifacts of this study (Fig. 1C,D). Rats were exposed to a single blast exposure of varying overpressures (see above) and subjected to transcardial perfusion (with phosphate buffered saline)-fixation (with 4% paraformaldehyde) within 15 min from exposure of animals to blast loading, which was the earliest time point that was assessed for BBB extravasation. The extent of extravasation of both sodium fluorescein and Evans blue was evaluated in all selected regions of the brain (Figs 2 and 3). These quantitative results support the hypothesis that blast-induced BBB opening allows for extravasation of molecules of 69 kDa or smaller immediately following injury (biomechanical loading) and, given an increase in molecular mass, extravasation of tracers was less widespread.

The fluorescence detection method of extravasation was also validated with absorption spectrophotometry for Evans blue. Animals (n = 6) exposed to 180 kPa shock wave showed an average of 45.6% increase in the tissue

Figure 2. Fluorescent images of Evans blue extravasation. Images show 10x macro-shots as well as zoomed in 40x images in representative regions in the frontal cortex (**A**), striatum (**B**), somatosensory barrel-field cortex (**C**), hippocampus (**D**), thalamus (**E**) and cerebellum (**F**), 15 minutes following 180 kPa blast exposure. Control images were dramatically enhanced, yet still show limited visibility, due to the absence of extravasated dye. Frontal cortex was taken as a representative control image (**G**). Quantitation of extravasation is shown using a semilog plot in order to capture magnitudinal differences (**H**). Absorption spectrophotometry results of Evans blue in control and injured rats (n = 5) (**I**). *Indicates a difference in intensity compared with control with a statistical significance of $p < 0.05$, **Indicates $p < 0.01$. Scale bar = 1 mm in coronal sections and 50 μm in 40x images.

content of EB than control animals wherein the precise concentration of EB present in tissue was derived from a standard curve made of seven different EB dilutions (Fig. 2I).

Different brain regions express different degrees of BBB permeability following moderate blast injury. After exposing animals to moderate blast (180 kPa), differential damage was observed in six different regions immediately following trauma (~15 min). In almost every region studied, statistically significant differences ($p < 0.01$), as determined by ANOVA followed by Tukey test, in the levels of both extravasated dyes was observed, highlighting the diffuse nature of bTBI (Figs 2 and 3). The quantitative values of the fluorescence intensities of EB (as measured by intensity x stained area) between control and blast injury groups in different brain regions are as follows: frontal cortex (control 0.002432, blast 1.699085, 700-fold, $p = 0.006$), striatum (control 0.001674, blast 0.675456, 400-fold, $p = 0.001$), somatosensory-barrel field cortex (control 0.003094, blast 0.274115, 90-fold, $p = 0.009$), hippocampus (control 0.006258, blast 0.564796, 90-fold, $p = 0.001$), thalamus (control 0.002056, blast 1.282525, 600-fold, $p = 0.002$) and cerebellum (control 0.001102, blast 0.00448, 4-fold, $p > 0.05$); and for sodium fluorescein: frontal cortex (control 0.004555, blast 1.91963, 400-fold, $p = 0.008$), striatum (control 0.005134, blast 1.822249, 300-fold, $p = 0.008$), somatosensory barrel-field cortex (control 0.001584, blast 0.429447, 250-fold, $p = 0.009$), hippocampus (control 0.00794, blast 0.630788, 80-fold, $p = 0.009$), thalamus (control 0.003556, blast 1.767197, 500-fold, $p = 0.004$) and cerebellum (control 0.004479, blast 0.055629, 30-fold, $p > 0.05$). The most robust changes occurred in the frontal cortex, striatum, and thalamus for both tracers while minimal to no statistically significant extravasation was observed in the cerebellum, which aligns well with results from previous investigations[34,58]. In every other region analyzed, there is at least a tenfold difference in the amount of extravasated dyes compared to controls in the acute time period.

BBB permeability varies as a function of time following moderate blast injury. In order to determine the time-course for blood-brain barrier permeability following blast, groups of (n = 4–6 for each time point) rats were sacrificed at specified times post-injury (15 min, 4 hours, 24 hours). While the amount of extravasation was significant for both sodium fluorescein and Evans blue immediately after blast, there was an even greater increase in tracer penetration four hours following the blast exposure (Figs 4 and 5). Increases over controls were as follows for Evans blue at 4 hours, respectively (four hour blast values followed by fold-increase and 24 hour blast values followed by fold increase): frontal cortex (3.270751, 1300-fold, 0.005012, 2-fold), striatum (1.681731,
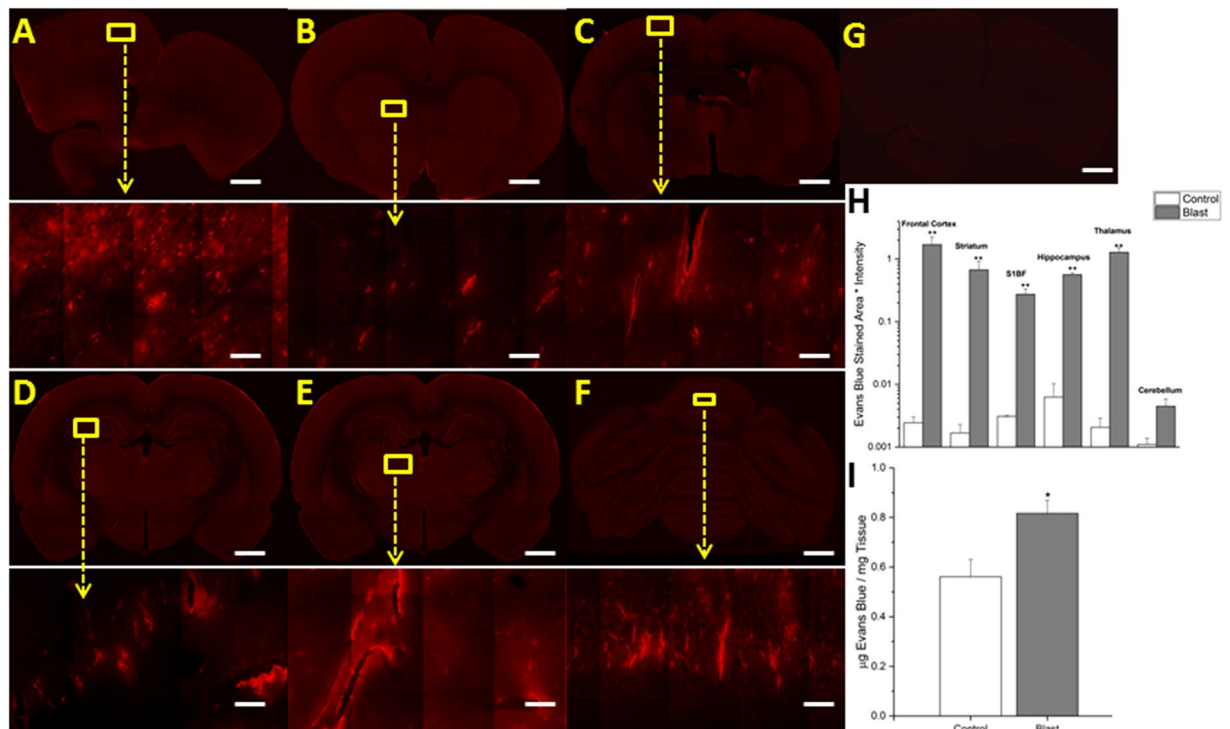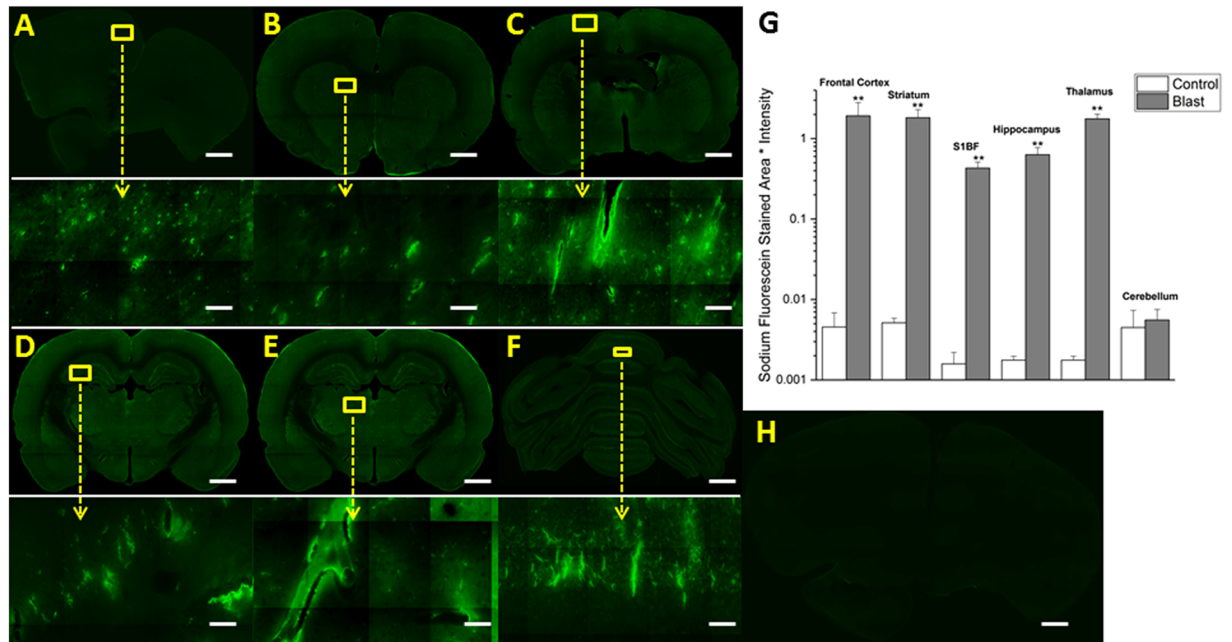
Figure 3. Fluorescent images of sodium fluorescein extravasation. Images show 10x macro-shots as well as zoomed in 40x images in representative regions in the frontal cortex (**A**), striatum (**B**), somatosensory barrel-field cortex (**C**), hippocampus (**D**), thalamus (**E**) and cerebellum (**F**) 15 minutes following 180 kPa blast exposure. Quantitation of extravasation is shown using a semilog plot in order to capture magnitudinal differences (**G**). Control images were dramatically enhanced, yet still show limited visibility, due to the absence of extravasated dye. Frontal cortex was taken as a representative image (**H**). **Indicates a difference in intensity compared with control with a statistical significance of $p < 0.01$. Scale bar = 1 mm in coronal sections and 50 μm in 40x images.
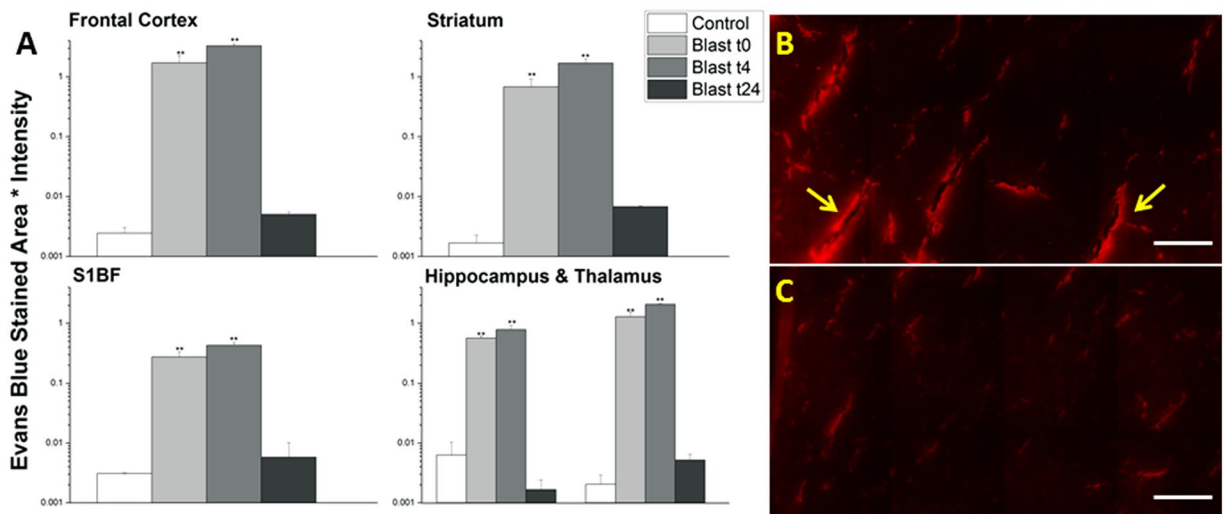
Figure 4. Quantitation of extravasation of Evans blue for 15 minutes (t0), 4 (t4), and 24 (t24) hours post-180 kPa blast exposure in frontal cortex, striatum, somatosensory barrel-field cortex, hippocampus, and thalamus using a semilog plot in order to capture magnitudinal differences (**A**). The frontal cortex was chosen for illustrative purposes and to qualitatively depict the difference between 4 (**B**) and 24 hrs (**C**). Arrows indicate areas of leakage from the vessels, which are more pronounced in 4 hours than any other time point studied in this investigation. **Indicates a difference in intensity compared with control with a statistical significance of $p < 0.01$. Scale bar = 100 μm.

1000-fold, 0.006758, 4-fold), somatosensory barrel-field cortex (0.427674, 150-fold, 0.005808, 1-fold), hippocampus (0.781473, 120-fold, 0.00166, <1-fold), and thalamus (2.080952, 1000-fold, 0.005169, 2-fold) and for sodium fluorescein: frontal cortex (3.365124, 700-fold, 0.014903, 3-fold), striatum (1.966033, 400-fold, 0.00229, <1-fold),
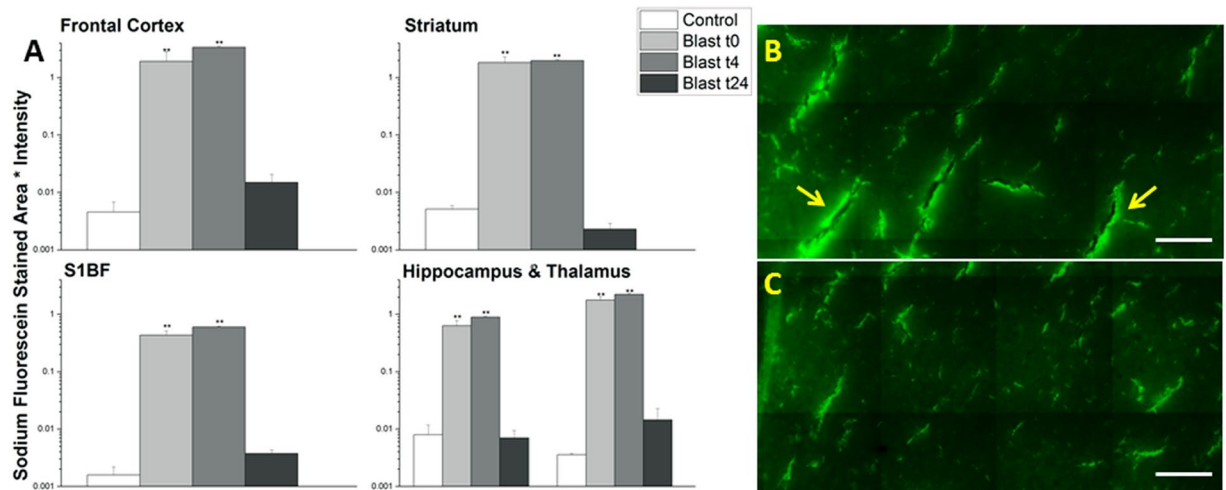
Figure 5. Quantitation of extravasation of sodium fluorescein for 15 minutes (t0), 4 (t4), and 24 (t24) hours post- 180 kPa blast exposure in frontal cortex, striatum, somatosensory barrel-field cortex, hippocampus, and thalamus using a semilog plot in order to capture magnitudinal differences (**A**). The frontal cortex was chosen for illustrative purposes and to qualitatively depict the difference between 4 (**B**) and 24 hrs (**C**). Arrows indicate areas of leakage from the vessels, which are more pronounced in 4 hours than any other time point studied in this investigation. **indicates a difference in intensity compared with control with a statistical significance of $p < 0.01$. Scale bar = 100 μm.

somatosensory barrel-field cortex (0.596185, 400-fold, 0.003732, 2-fold), hippocampus (0.885597, 100-fold, 0.006966, <1-fold), and thalamus (2.223883, 600-fold, 0.014472, 4-fold). Interestingly, 24 hours post-injury, the extravasation of EB and NaF returned back to that of control levels (Figs 4 and 5) suggesting possible resealing occurring at or before 24 hours.

As an alternate means to investigate BBB disruption as well as to examine possible mechanisms of BBB permeability change following blast, levels of tight junction proteins (TJPs) occludin and claudin-5 were determined in lysates from cerebral hemispheres by quantitative ELISAs. Statistically significant reductions in tight junction protein abundance were observed at this time point, which serves as further evidence of the compromised BBB (Fig. 6). Noteworthy that such reduction in TJPs in brain lysates is accompanied by a concomitant increase in their levels in serum samples obtained from the same animals that are used for evaluation of brain levels of tight junction proteins. These data not only strongly suggest that shockwave propagated from blast is able to dislodge TJPs from the cerebral vasculature but also that these proteins translocate to blood.

The extent of BBB permeability displays a tendency to increase as a function of blast overpressure. In order to determine the effects of blast overpressure on BBB permeability, groups of (n = 3) rats were exposed to mild shockwaves of 35, 70, and 130 kPa BOPs and sacrificed immediately after blast. While no measurable extravasation was induced at 35 kPa, there is clear evidence of leakage starting at 70 kPa (Figs 7 and 8) and extravasation quantitation for both tracers showed a tendency to increase with increasing overpressure. The fluorescence intensity increases over controls and were as follows for Evans blue at 35, 70 and 130 kPa, respectively as determined by post-ANOVA Tukey test: frontal cortex (0.014762, 6-fold, 0.826735, 340-fold, 0.898087, 370-fold), striatum (0.00983, 5-fold, 0.118309, 70-fold, 0.355441, 200-fold), somatosensory barrel-field cortex (0.0036, 1-fold, 0.101135, 30-fold, 0.215851, 70-fold), hippocampus (0.0.007685, 1-fold, 0.15515, 25-fold, 0.15437, 25-fold), and thalamus (0.003252, 2-fold, 0.380609, 180-fold, 0.773843, 380-fold) and for sodium fluorescein: frontal cortex (0.030414, 7-fold, 1.146571, 250-fold, 1.91895, 260-fold), striatum (0.012241, 2-fold, 0.201411, 40-fold, 0.545131, 100-fold), somatosensory barrel-field cortex (0.003914, 2-fold, 0.132123, 80-fold, 0.256239, 160-fold), hippocampus(0.013312, 1-fold, 0.172132, 20-fold, 0.205551, 25-fold), and thalamus (0.00404, 1-fold, 0.181371, 50-fold, 0.302787, 85-fold).

Primary blast induces translocation of astrocytic marker s100-β into blood stream and monocyte infiltration into brain. In order to more strongly display the presence of brain-specific proteins in circulation following blast injury, an ELISA was conducted for s100-β at 4 and 24 hours post-moderate blast (180 kPa) in serum samples (n = 3, Fig. 9). At four hours post-injury, concentration of s100-β rose from 399 pg/ml to 594 pg/ml, a statistically significant increase of 48.8% (post-ANOVA Tukey test, $p = 0.037$). However, after 24 hours, the protein levels in serum fall to 427 pg/ml, an increase of only 7% from control values (Tukey test, $p > 0.05$).

Similarly, as an alternative means to demonstrate the presence of blood-borne macromolecules/cells in the brain parenchyma, double immunofluorescence staining was performed for CCL2 (monocyte marker) and RECA-1 (endothelial cell marker) at 4 hours post-moderate blast in the frontal cortex (n = 3, Fig. 10). Results indicate that, qualitatively, the presence of monocytes around blood vessels increased following blast compared to controls.
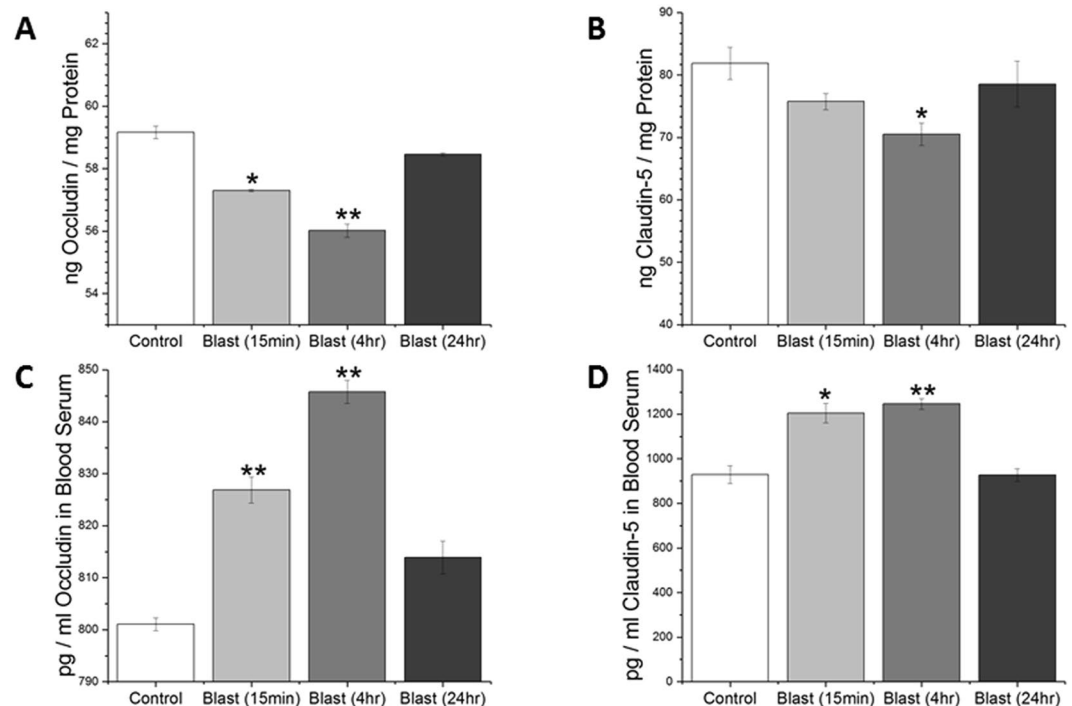
Figure 6. ELISA results for tight junction proteins occludin and claudin-5, respectively in brain (**A,B**) and blood serum (**C,D**). Assay conducted for blast (180 kPa BOP) samples fifteen minutes, four, and twenty four hours post-exposure and compared with controls. *Indicates a difference in intensity compared with control with a statistical significance of $p < 0.05$, **Indicates $p < 0.01$.

Discussion

This work focused on establishing spatial and temporal relationships of the BBB permeability as a function of overpressure in blast-induced traumatic brain injury. Through the use of two tracers (Evans blue and sodium fluorescein) injected intravenously in the lateral tail vein of the rat, the degree of the BBB disruption following injury was functionally assayed. At the sub-mild overpressure (35 kPa) very limited extravasation of dyes was observed. A breach in the BBB was first observed at a mild blast overpressure (70 kPa) which revealed a significant increase in barrier permeability almost immediately after blast (~15 min). In addition to extravasation of tracers (NaF and EB), absorption spectrophotometry was used to demonstrate the breakdown of the BBB by the presence of EB in brain parenchyma. The results of the absorption spectrophotometry offer interesting piece of corroboratory information; unlike gross blunt injuries, where there is a substantial amount of extravasated tracers recorded[59,60], in this mild-moderate blast injury, a difference of only about 250 picograms of EB was observed between injured and control groups (Fig. 2).

It is interesting to note that the extravasation of the tracers showed a significant increase as early as 15 min following the blast, strongly supporting the hypothesis that direct biomechanical loading of the primary blast was able to disrupt the BBB (Figs 2 and 3). We should note that there is no physical impact of external objects such as in CCI or weight drop models, nor a specific fluid pressure in subdural space as in fluid percussion model. However, while the degree of BBB disruption appears large when compared to controls (which was negligible), the physiological as well as neurological state of the animal were not altered based on visual observation of the animal's status including unaltered gait, righting and startle reflexes (data not shown). This strongly suggests that this injury can be classified as a subtle, tissue-level mechanical disruption of vasculature. Therefore, caution must be exercised when comparing these results with those from blunt injury models, where injury severity is greater and degree of extravasation is larger but the injury is highly local, mostly restricted to the site of external impact or fluid pressure[35,36,61]. As noted earlier, the degree of the BBB permeability increased further at 4 hours post-injury (Figs 4 and 5), which not only indicates the persistence of the BBB disruption but also indicates that, in addition to direct biomechanical loading (shock loads that lasts for a transient period of approximately 3 milliseconds), some secondary mechanisms may be activated post-injury and contribute to BBB disruption for hours after initial trauma.

While several secondary mechanisms have been implicated in the degradation of the BBB including oxidative stress[12,30,33,43], matrix metalloproteinase activity and neuroinflammation[12,33,38,62], pericyte detachment[15,63–65], astrocytic end-feet swelling and detachment[66–69], among others, precise involvement of one or more of these mechanisms contributing to BBB disruption in bTBI remains to be determined. Previous studies have cited maximum degree of damage to the BBB following mild-moderate TBI (although not blast) occurring between 4–6 hours of injury[8,35,39]. The lack of a detailed time course of BBB disruption in blast injury is a primary motivation for this work and a greater understanding of the temporal nature of the evolution of pathology and
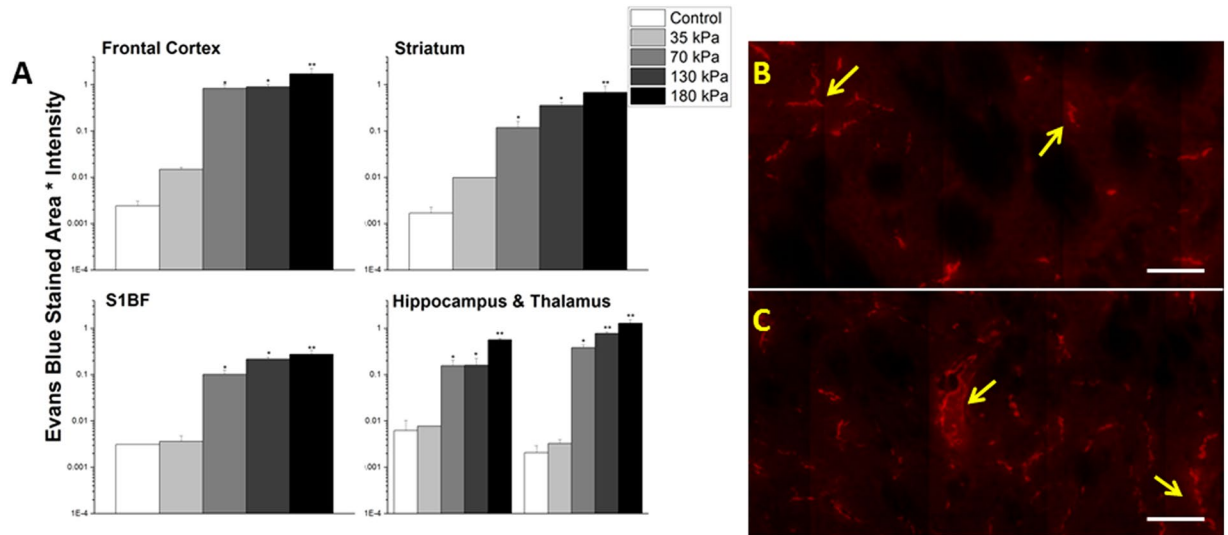
Figure 7. Quantitation of extravasation of Evans blue for 35, 70, 130, and 180 kPa blast overpressures, 15 minutes post-exposure in frontal cortex, striatum, somatosensory barrel-field cortex, hippocampus, and thalamus using a semilog plot in order to capture magnitudinal differences (**A**). The striatum was chosen for illustrative purposes and to qualitatively depict the difference between 70 (**B**) and 130 kPa (**C**). Leaks appear longer and more intense with increasing overpressure in the same brain regions. *Indicates a difference in intensity compared with control with a statistical significance of $p < 0.05$, **Indicates $p < 0.01$. Scale bar = $100 \mu m$.
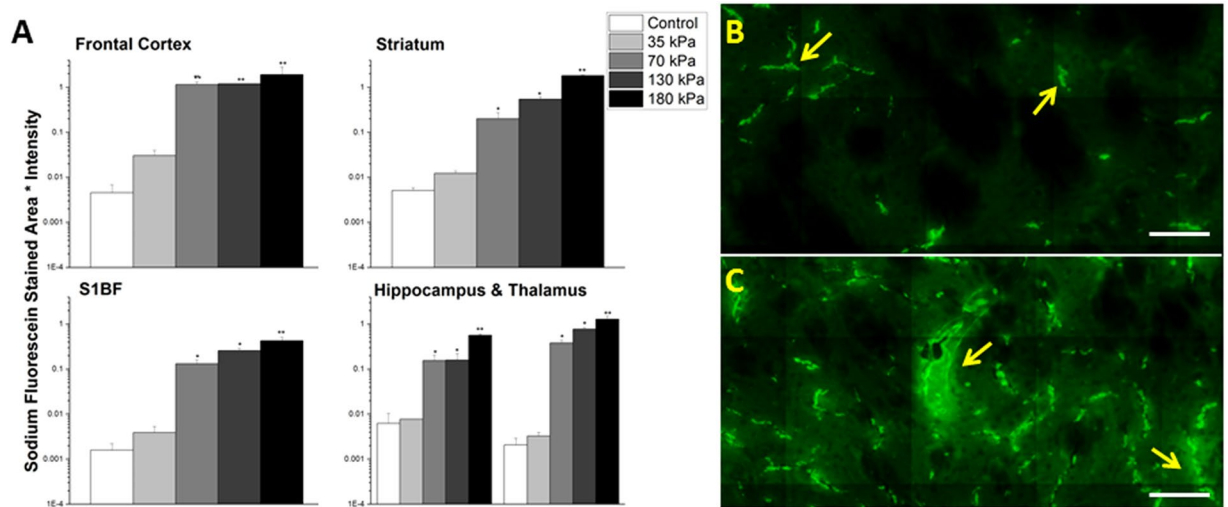
Figure 8. Quantitation of extravasation of sodium fluorescein for 35, 70, 130, and 180 kPa blast overpressures, 15 minutes post-exposure in frontal cortex, striatum, somatosensory barrel-field cortex, hippocampus, and thalamus using a semilog plot in order to capture magnitudinal differences (**A**). The striatum was chosen for illustrative purposes and to qualitatively depict the difference between 70 (**B**) and 130 kPa (**C**). Leaks appear longer and more intense with increasing overpressure in the same brain regions. *Indicates an intensity compared with control with a statistical significance of $p < 0.05$, **Indicates $p < 0.01$. Scale bar = $100 \mu m$.

contributions of precise mechanisms during the time-course of BBB disruption in blast-induced neurotrauma will aid in diagnostic and therapeutic discoveries[70].

The integrity of the tight junctions was also assessed in the current study immediately following moderate blast, four, and twenty-four hours post injury. Tight junctions are water-tight seals that connect adjacent endothelial cells across the brain vasculature[11,13]. These complexes are comprised of several proteins that anchor the tight junction to the surface of endothelial cells and represent a strong mechanical junction that is the foundation of the BBB. Several groups have studied the integrity of the tight junctions as a means to assess the state of the BBB[30,44,56,71,72]. In the present study, the abundance of tight junction proteins (occludin and claudin-5) was evaluated quantitatively via ELISA (Fig. 6A,B). In the acute phase of injury (~15 mins), a reduction in tight junction protein abundance was observed in both occludin ($p = 0.012$) and claudin-5 ($p > 0.05$). Although the reduction
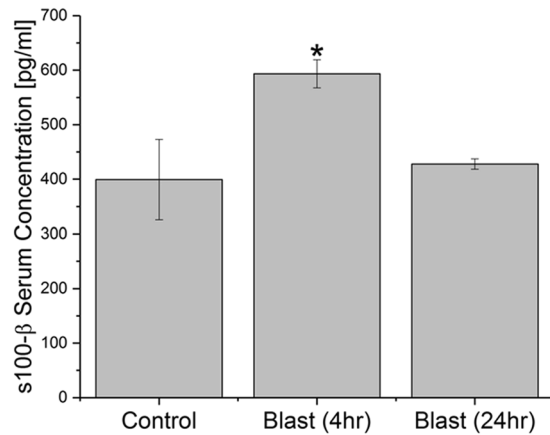
Figure 9. Concentration of s100-β in blood serum. Assay conducted for blast (180 kPa BOP) samples four and twenty four hours post-exposure and compared with controls. *Indicates a difference in intensity compared with control with a statistical significance of $p < 0.05$.
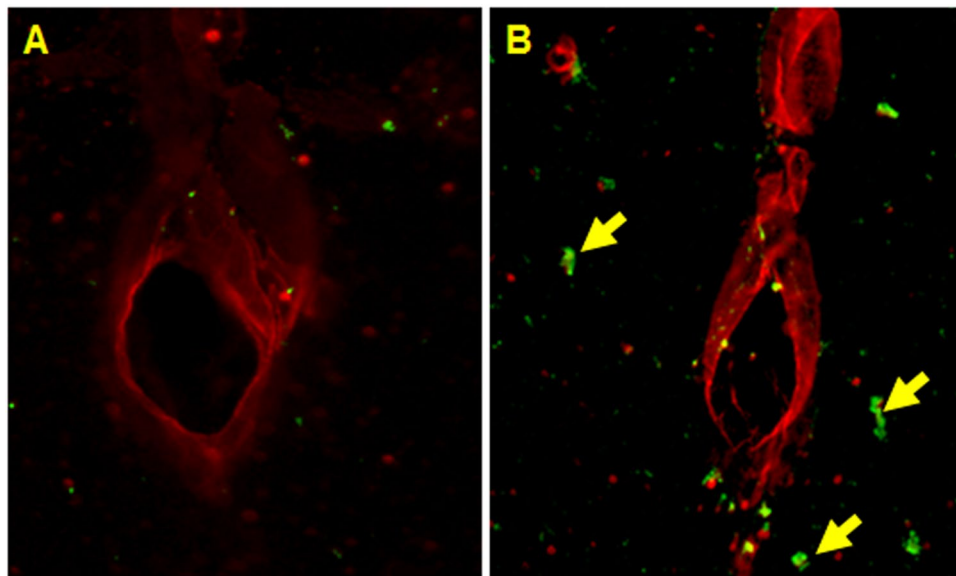
Figure 10. Double immunofluorescence of endothelial cell marker (RECA-1, red) and monocyte marker (CCL2, green) at four hours post-exposure in frontal cortex in animals from control (**A**) and moderate (180 kPa BOP) blast injury (**B**). Scale bar = 50 μm.

in claudin-5 was not statistically significant, it displays a strong tendency to decrease. These results strongly support our tenet that a direct mechanical loading may be able to break and dislodge tight junction complexes and cause subsequent reduction in integrity of the BBB, which may have manifested in the extravasation of the dyes. Further, at four hours post-blast, levels of occludin and claudin-5 were reduced ($p = 0.002$, $p = 0.035$, respectively) suggesting that, in addition to direct mechanical forces, secondary factors that are likely activated 4 hours post-injury also contribute to the reduction in TJPs. Such sustained decrease in these proteins may in part be responsible for greater compromise in BBB integrity 4 hours post-injury observed in the present study. While several factors have been implicated in the breakdown of tight junction proteins, oxidative stress and increased matrix metalloproteinase activity have been shown to contribute to the disruption of the BBB[12,30]. Moreover, restoration of the levels of occludin and claudin-5 observed in the present study within twenty-four hours post-blast corroborates the absence of extravasation seen at 24 hours post-blast.

While the reduction in the brain levels of tight junction proteins suggest a possibility of their dislodging by direct impact of the shockwaves, we sought to examine the accountability of these proteins in the blood stream, since it is likely that once dislodged, these proteins may be translocated into blood stream. Therefore, we estimated the levels of these proteins in serum samples by quantitative ELISA. Interestingly, we observed a close, inverse correlation on the levels of these proteins between brain homogenates and serum (Fig. 6C,D). Fifteen minutes post-injury, there was a significant increase in the amount of occludin ($p = 0.012$) and claudin-5

(p = 0.011) detected in the blood serum compared to controls. The amount of detected tight junction proteins further increased four hours post-injury (p < 0.001, p = 0.002) for occludin and claudin-5, respectively. These results not only corroborate the ELISA results in the brain tissue, but also give strong support to the assertion that the tight junction proteins are being mechanically dislodged from the tight junction complexes and being taken up into circulation. Moreover, a complete recovery of these TJPs to the control levels in brain and blood 24 hours post-injury corroborates well with the absence of any extravasation of EB or NaF which together indicate the possibility of resealing of the BBB at this time point.

Several studies report that increased levels of astrocytic protein s100-β in the blood indicate the breakdown of the BBB[12,30,40,73–75]. The current study shows increased s100-β in serum from animals exposed to blast provides additional support to our extravasation studies and together represent the involvement of astrocytic defects in the compromise of BBB following blast injury.

To demonstrate infiltration of any blood-borne cells entering the brain parenchyma, an immunofluorescence stain was performed to identify the presence of monocytes in the vicinity of vascular endothelial cells using CCL2 and RECA-1, respectively (n = 3, Fig. 10). CCL2 is a monocyte chemoattractant protein which presents on blood monocytes and is integral in monocyte mobilization while RECA-1 is a common vascular endothelial marker[76–78]. The increased number of CCL2 staining in the frontal cortex near blood vessels indicates that monocytes are leaking from the blood into the brain parenchyma four hours post-injury. This qualitatively supports the extravasation results for Evans blue and sodium fluorescein.

In the current study, differential degree of BBB permeability was observed spatially across different brain regions. Such differential blood-brain barrier permeability may, in part, be due to variations in the vascular architecture (density, size, orientation) in different brain regions. Cavaglia's group characterized the variation in neurocapillary density in the adult rat hippocampus and cortical structures[79]. The hippocampal CA1 region revealed a significantly lower capillary density compared to CA3, but a much more extensive blood-brain barrier leakage. This may instinctively point to an inverse relationship between vascular density and BBB vulnerability; however Cavaglia's studies also showed that neocortical regions have a much higher vascular density compared to neighboring gray/white matter junctions. Since gray matter regions (frontal cortex, thalamus, etc.) have a higher vascular density than the white matter regions, the mechanical shock loading in the acute phase of injury in conjunction with the onset of secondary mechanisms during latter stages may damage the brain regions containing higher vascular densities more than others. Supporting this tenet, our results and many other studies reveal higher degree of BBB damage in the frontal cortex (Figs 2 and 5)[34,43,58,72]. In addition to vascular density (number of vessels, vessel length, etc.), it is also possible that vascular orientation and cellular architecture may also be, in tandem, responsible for the observed spatial variation of BBB permeability. From a purely biomechanical perspective, a combination of vascular architecture and, to some extent, perivascular attachment to astrocytes may dictate the response to the sudden physical motion of capillaries leading to the mechanical disruption of tight junctions.

While it is strongly assumed that the propagation of shock uniformly travels and loads the whole brain, absence of BBB damage in cerebellum is interesting. The lack of functional BBB damage in the cerebellar regions has been reported by several groups, but there is still uncertainty to its cause[34,58,80]. Several groups have shown vascular volume in the cerebellum to be higher than that in the cerebrum[81–83], but Holash et. al determined that this difference was due to the inclusion of pia vasculature[84]. Without pial vessels (which have a BBB quite different from the parenchymal vessels in terms of tight junction distribution and astrocytic ensheathment[85]), the vascular volume of the cerebellum and cerebrum are comparable. Most extravasation studies use intravascular tracers, which do not discriminate between pial and intraparenchymal vessels in the cerebellum. The authors speculate that the lack of extravasation in the cerebellum based on these methods is due to the presence of the pial vessels, but more work needs to be done to validate this hypothesis (ie. isolating parenchymal vessels).

Further, in the current study, based on the high magnification images (Figs 2, 3, 4, 5, 7 and 8) it is tempting to speculate that larger diameter blood vessels had greater leakage compared to smaller ones. Hypothetically, given a larger cross-sectional area, these vessels bear a greater brunt of the passing shock wave and hence are more damaged than their smaller counterparts. It is also possible that these larger vessels only appear to leak more because of a greater vascular volume: more vessel content, the more blood is able to leak out in the presence of a vascular rupture. In this case, vessels of all sizes would experience a similar mechanical load from the shock wave and show a similar pattern of leakage (with only differences in leakage volume, proportional to vessel size), which is consistent with the results of this study. When a shock/stress wave encounters vasculature, the biomechanical forces will be proportional to the projected area and the difference in acoustic impedance between the different materials that make up the local tissue construct. The resistance to deformation will be proportional to the structural integrity of the vasculature vis-à-vis the surrounding cellular architecture. As different subregions of the brain have different architectures and biomechanical characteristics, the forces, the deformation and hence the BBB leakage will be a function of the specific region under question even if the loading is identical.

After 24 hours following mild blast, a statistically significant decrease in extravasation was observed in all brain regions, which represents possible evidence of a BBB resealing in combination with the restoration of TJPs (Figs 4, 5, 6). A recent study also reported a reduction in BBB damage 24 hours after injury in mice exposed to moderate blast (100 kPa)[86]. This, however, may not preclude continued presence of phenotypic changes of the TBI in brain structures since vascular leakage of various blood born substances into the parenchyma may trigger secondary events such as microglial activation leading to neuroinflammation.

At all time-points, in all regions, the total amount of extravasated sodium fluorescein tracer was greater than Evans blue, an intuitive result given the difference in size between these two tracers. One needs to be careful in interpreting the results in terms of fold increase since the baseline data for the smaller molecule, sodium fluorescein, was higher than the larger Evans blue. In no region was there a collection of sodium fluorescein in the absence of Evans blue, meaning that in the current work, there was an insignificant number of breaches in the BBB which could accommodate the 376 Da sodium fluorescein but not the larger 69 kDa Evans blue.

The present study showing a strong tendency of higher extravasation in animals exposed to 130 kPa compared to 70 kPa in the acute phase of the injury suggests the BBB permeability changes are directly proportional to increasing BOP, at least in the acute phase of the injury. Interesting that 4 hours post-injury such magnitude of difference in the extravasation of EB and NaF as a function of BOP is absent. While the reason for this is not known, the authors speculate that differences in these injuries become more apparent after the acute phase of injury and such significant changes may be masked once secondary mechanisms begin to occur (4 hours), which may uniformly exacerbate injury conditions since, in the immediate phase of injury (~15 min), all leakage of the BBB is attributed to the mechanical insult of the shock wave. Therefore, the resulting biomechanical injury may not be grossly different between mild and moderate overpressures at time interval (4 h) where secondary mechanisms begin to occur. Indeed, such differential changes in BBB permeability have also been reported in other investigations[52,56], which may superimpose the mechanical injury with the influences of secondary biochemical mechanisms (e.g., oxidative stress, neuroinflammation).

Our efforts to establish a sub-mild injury model of bTBI led to the identification of 35 kPa as a BOP that does not show any tracer extravasation. However, the BBB permeability changes are significant with a minimal BOP of 70 kPa and increased further as a function of increasing BOPs (Figs 7 and 8). These results indicate that the mechanical loading sustained at 35 kPa is insufficient to cause the significant damage to the BBB that was seen at 70 kPa and higher overpressures. Therefore, 70 kPa BOP offers a basal injury threshold for the BBB permeability changes to occur under primary blast loading. These studies together demonstrate that BBB permeability is a sensitive phenotypic marker for mTBI in the acute phase of the injury wherein a direct mechanical disruption is able to cause vascular rupture. Accordingly, alterations in the integrity of BBB may be considered a prognostic event to scale the injury severity (i.e., sub-mild to mild vs moderate TBI) as well as the extent of pathological outcomes in blast TBI.

In summary, this work addresses a clear gap in knowledge in the understanding of the BBB permeability in the pathophysiology of blast-induced traumatic brain injury. The results and conclusions presented herein should provide the baseline for future studies attempting to connect the BBB permeability and the pathophysiological progression of bTBI. However, while the authors maintain that these results are reproducible in age-matched rats exposed under the same loading conditions, it is important that the described experimental model is replicated as closely as possible in order to reproduce these results. For example, non-primary injuries will likely be observed if animals are located outside or near the end of the shock tube or if animals are not properly fixed and thus may reveal an altered injury profile.

Materials and Methods

Animal Preparation. A total of 88 adult, 10-week old male Sprague Dawley rats (Charles River Laboratories) weighing between 300–350 g were used throughout this study, in accordance with protocols approved by Rutgers University Institutional Animal Care and Use Committee (IACUC). Animals were housed at 22 °C with free access to food and water in a 12 hour dark-light cycle. Animals were divided among sham and injured groups for four different blast overpressures and three different time-points post-injury. All methods used throughout the study were performed in accordance with protocols, guidelines, and regulations approved by Rutgers University IACUC.

Exposure to Blast and Tracer Injections. Rats were exposed to a single shock wave at the Center for Injury Biomechanics, Materials, and Medicine (New Jersey Institute of Technology) in the modular, field-validated shock tube described in previous publications[54–56,87]. Based on preliminary findings, we observed an obvious difference between sham and blast groups, where an $n = 4$ was sufficient to achieve a power value of 0.9 ($\alpha = 0.05$ and combined SD of 0.819) based on power analysis. An $n = 1–2$ was added in case of mortality or inadequate perfusion. As we continued the study, we maintained an $n = 5–6$ for all blast groups (for 70 and 130 kPa groups, only three animals were used, but statistical significance was achieved). Prior to blast exposure, animals were anesthetized with 5% isoflurane, released in a chamber containing 95% air and 5% CO_2, until unresponsive to noxious stimulation. At this point the rats were mounted and immobilized on a custom rat-holder in the test section of the shock tube. Sham animals were anesthetized and received noise exposure, but kept outside of the shock tube, away from the shock wave. Exposed animals were subjected to a single blast of 35, 70, 130, or 180 kPa peak overpressure and euthanized via transcardial perfusion-fixation at prescribed time-points (15 mins, 4 hrs, 24 hrs). Tracers were injected two hours prior to euthanasia (animals in the 15 min group received injections prior to blast exposure). Sodium fluorescein was administered via the lateral tail vein (376 Da, 20% dissolved in phosphate-buffered saline [PBS], 0.02 g/mL, 0.7 mL delivered) at the same time Evans blue was (69 kDa when bound to albumin, 2% solution dissolved in PBS, 0.002 g/ml, 0.7 mL delivered). Two hours were given as to give sufficient time for the tracers to circulate the body multiple times and perfuse even deeper neurovasculature across all experimental groups. Other groups have used both these dyes to assess BBB permeability up to four hours following tracer administration[34,88,89]. Half-life of EB in circulation was confirmed to be > four hours, while the same is true for NaF half-life[90–92], instilling confidence that allowing two hours for circulation and extravasation for these tracers is adequate.

As a quality control measure, high-speed video was monitored and recorded with a Photron FASTCAM Mini UX100 operating at a framerate of 5000 fps to capture any substantial head/body movement during blast, in order to exclude the effects of secondary/tertiary injury from this study. Approximately two seconds of video footage were recorded per exposure and then saved via PFV (Photron FASTCAM Viewer) 3.3.5 software. Incident overpressure at the location of the animals in the test section of the shock tube was recorded at 1.0 MHz sampling frequency by a custom LabView program running on in-house built data acquisition system based on National Instruments PXI-6133 32 MS Memory S Series Multifunction DAQ Modules and PXIe-1082 PXI Express Chassis. PCB Piezotronics (Depew, NY) model 134A24 pressure sensors were used in all experiments.

Tissue Preparation, Absorption Spectrophotometry, and *Ex-Vivo* Imaging and Analysis. Rats were perfusion-fixed two hours following tracer administration. Prior to perfusion, blood serum was extracted from the heart (left ventricle, approximately 3 ml volume). Rats were transcardially perfused with phosphate buffered saline (PBS) and brains fixed with 4% paraformaldehyde (PFA). Brains were then liberated from cranial vaults, immersed in 4% PFA for an additional 48 hours and cryoprotected through immersion in 30% sucrose. Appearance of brains can be seen in Fig. 1E, wherein the brains were completely devoid of blood in the vasculature, indicating a complete saline perfusion. Brains were then dissected into 100 micron sections using Rat Brain vibratome (Kent Scientific Corp.) and mounted on glass slides. Regions of interest included the frontal cortex, striatum, somatosensory barrel-field cortex, hippocampus, thalamus, and cerebellum. Each animal offered 30 sections across five regions that were analyzed. Slides contained between two to three sections, resulting in over 200 slides scanned throughout this study. Slides containing different brain regions were digitized (10x magnification) using Leica Aperio Versa 200 digital pathology grade slide scanner. Fluorescent intensities were quantified after excitation at 488 nm (sodium fluorescein), 50 ms exposure, and 594 nm (Evans blue), 125 ms exposure, using AreaQuant software specifically designed for this imaging application (Leica Biosystems) and expressed as average fluorescence intensity/unit area. This imaging technique allows for visualization of micro-structural details and digital scanning affords the ability to image large brain regions with no loss of resolution. In order to quantify fluorescence intensities, regions of interest were manually outlined in different brain section. For each channel (green 488 nm and red 594 nm), a minimum intensity threshold value was selected to exclude any background fluorescence from our calculation. The AreaQuant algorithm then determines if the intensity value of each pixel enclosed in the outlined region exceeds the minimum intensity threshold and outputs the total area of positive stain for each brain regions, the average intensity in each channel, and the expression profile of the tracers.

As a means to validate the results of fluorescent image quantitation, absorption spectrophotometry was conducted on homogenized frontal cortices extracted from control and acutely injured rats (n = 5, 180 kPa). Rats were sacrificed via saline perfusion (no fixation) and brains were extracted, sectioned, and frozen in dry ice. Absorption was measured and standard curve generated from seven gradient dilutions of Evans Blue. Experimental samples were plotted against the curve ($R^2 = 0.998$) using SpectraMax i3 (Molecular Devices) microplate reader and SoftMax Pro 6.5 software. Output concentration was converted into micrograms per mg of brain tissue.

ELISA. As a means of alternative evidence for BBB disruption, tight junction protein changes were examined in the cerebral hemisphere by ELISA and immunoblot. Following perfusion with PBS, brains were excised from the skull and cerebrum was homogenized in CellLytic-M (Sigma) using sonicator with probe amplitude set to 45% on ice. Samples were then centrifuged at 14,000 g at 4 °C. The protein concentration in the samples was estimated by bicinochoninic acid (BCA) method (Thermo Scientific, Rockford, IL). Subsequently, samples were diluted in PBS and loaded onto ELISA plate (LSBio, Seattle, WA). Serum samples were also loaded onto same plate for tight junction protein quantification and separate serum ELISAs were run for s100-β. Plates were read in microplate reader (Spectra Max i3, Molecular Devices) at wavelength of 450 nm. All the Steps of ELISA procedure (washings, incubation time etc) were conducted in accordance with manufacturer instructions and samples plotted against a standard curve made up of eight samples ($R^2 = 0.995, 0.999$ for occludin and claudin-5 respectively) using SoftMax Pro 6.5 software.

Immunofluorescence. In order to further establish blood-to-brain leakage following blast injury, double-immunofluorescence studies for RECA-1 and CCL2 were performed in the frontal cortex, four hours post-injury (n = 3) as a means to detect infiltration of monocytes into the brain parenchyma. Following transcardial perfusion-fixation, tissue was cryoprotected in sucrose, and 20 μm thick sections were cut using Leica 1000 S vibratome. Sections were mounted on glass slides and washed with 10 mM PBS, fixed in ice-cold methanol (100%) solution for ten minutes at −20 °C. The tissue sections were blocked with 10% donkey serum at room temperature for 1 hour in PBS containing 0.03% Triton X-100. Fixed tissues were incubated overnight at 4 °C with respective primary antibodies to RECA-1 (Mouse monoclonal, Abcam, 1:50) and CCL2 (Rabbit polyclonal, Abcam, 1:50). Double immunofluorescence was performed using Alexafluor 594 for RECA-1 and Alexafluor 488 for CCL2. Slides containing different brain regions were digitized (20x magnification) using Leica Aperio Versa 200 fluorescent microscope and slide scanner.

Statistical Analysis. Data are presented as mean + standard error of the mean. Statistical significance was determined using one-way analysis of variance (ANOVA) to compare mean fluorescence intensities of different brain regions for sodium fluorescein and Evans blue with a Tukey pairwise test done to determine differences between individual time-point and overpressure groups. Statistical comparisons were also made for each blast overpressure and each time-point post injury. Normalcy and population variance homogeneity were assessed with Shapiro-Wilk and Levene's tests respectively. Differences between means were assessed and probability levels of $p < 0.05$ were considered statistically significant. Minitab 17 Statistical Software was used for all analyses and Origin 2017 was used for generation of bar plots. Bar plots presented are in semi-log scale in order to capture magnitudinal differences between groups. Fluorescent images were taken using Aperio Versa software and analysis and export done via ImageScope software (LEICA Corp.).

References

1. Ling, G. S. *et al.* Traumatic brain injury in modern war. *Sensing Technologies for Global Health, Military Medicine, and Environmental Monitoring III* **8723**, 87230K. International Society for Optics and Photonics. (2013).
2. Mathews, Z. R. & Koyfman, A. Blast injuries. *The Journal of emergency medicine* **49**, 573–587 (2015).
3. Moore, B. Blast injuries-a prehospital perspective. *Australasian Journal of Paramedicine* **4** (2015).

4. Loane, D. J. & Faden, A. I. Neuroprotection for traumatic brain injury: translational challenges and emerging therapeutic strategies. *Trends in Pharmacological Sciences* **31**, 596–604, https://doi.org/10.1016/j.tips.2010.09.005 (2010).
5. Maas, A. I., Roozenbeek, B. & Manley, G. T. Clinical trials in traumatic brain injury: past experience and current developments. *Neurotherapeutics* **7**, 115–126 (2010).
6. Narayan, R. K. *et al.* Clinical trials in head injury. *Journal of neurotrauma* **19**, 503–557 (2002).
7. Schouten, J. W. Neuroprotection in traumatic brain injury: a complex struggle against the biology of nature. *Current opinion in critical care* **13**, 134–142 (2007).
8. Chodobski, A., Zink, B. J. & Szmydynger-Chodobska, J. Blood–brain barrier pathophysiology in traumatic brain injury. *Translational stroke research* **2**, 492–516 (2011).
9. Hayes, R. L. & Dixon, C. E. In *Seminars in Neurology*. 25–31 (© by Thieme Medical Publishers, Inc.) (1994).
10. Abbott, N. J. Inflammatory mediators and modulation of blood-brain barrier permeability. *Cell. Mol. Neurobiol.* **20**, 131–147, https://doi.org/10.1023/a:1007074420772 (2000).
11. Abbott, N. J., Patabendige, A. A., Dolman, D. E., Yusof, S. R. & Begley, D. J. Structure and function of the blood-brain barrier. *Neurobiol Dis* **37**, 13–25, https://doi.org/10.1016/j.nbd.2009.07.030 (2010).
12. Abdul-Muneer, P. M., Chandra, N. & Haorah, J. Interactions of oxidative stress and neurovascular inflammation in the pathogenesis of traumatic brain injury. *Mol Neurobiol* **51**, 966–979, https://doi.org/10.1007/s12035-014-8752-3 (2015).
13. Ballabh, P., Braun, A. & Nedergaard, M. The blood–brain barrier: an overview: structure, regulation, and clinical implications. *Neurobiology of disease* **16**, 1–13 (2004).
14. Hawkins, B. T. & Davis, T. P. The blood-brain barrier/neurovascular unit in health and disease. *Pharmacological reviews* **57**, 173–185 (2005).
15. Obermeier, B., Daneman, R. & Ransohoff, R. M. Development, maintenance and disruption of the blood-brain barrier. *Nat Med* **19**, 1584–1596, https://doi.org/10.1038/nm.3407 (2013).
16. Zlokovic, B. V. The blood-brain barrier in health and chronic neurodegenerative disorders. *Neuron* **57**, 178–201 (2008).
17. Abbruscato, T. J., Lopez, S. P., Roder, K. & Paulson, J. R. Regulation of blood-brain barrier Na, K, 2Cl-cotransporter through phosphorylation during *in vitro* stroke conditions and nicotine exposure. *Journal of pharmacology and experimental therapeutics* **310**, 459–468 (2004).
18. Iłzecka, J. The structure and function of blood-brain barrier in ischaemic brain stroke process. *Annales Universitatis Mariae Curie-Sklodowska. Sectio D: Medicina* **51**, 123–127 (1996).
19. Khatri, R., McKinney, A. M., Swenson, B. & Janardhan, V. Blood–brain barrier, reperfusion injury, and hemorrhagic transformation in acute ischemic stroke. *Neurology* **79**, S52–S57 (2012).
20. Sandoval, K. E. & Witt, K. A. Blood-brain barrier tight junction permeability and ischemic stroke. *Neurobiol Dis* **32**, 200–219, https://doi.org/10.1016/j.nbd.2008.08.005 (2008).
21. Fiala, M. *et al.* Cyclooxygenase-2-positive macrophages infiltrate the Alzheimer's disease brain and damage the blood–brain barrier. *European journal of clinical investigation* **32**, 360–371 (2002).
22. Zlokovic, B. V. Neurovascular pathways to neurodegeneration in Alzheimer's disease and other disorders. *Nat Rev Neurosci* **12**, 723–738, https://doi.org/10.1038/nrn3114 (2011).
23. Desai, B. S., Monahan, A. J., Carvey, P. M. & Hendey, B. Blood–brain barrier pathology in Alzheimer's and Parkinson's disease: implications for drug therapy. *Cell transplantation* **16**, 285–299 (2007).
24. Persidsky, Y. *et al.* Rho-mediated regulation of tight junctions during monocyte migration across the blood-brain barrier in HIV-1 encephalitis (HIVE). *Blood* **107**, 4770–4780 (2006).
25. Oby, E. & Janigro, D. The blood–brain barrier and epilepsy. *Epilepsia* **47**, 1761–1774 (2006).
26. Remy, S. & Beck, H. Molecular and cellular mechanisms of pharmacoresistance in epilepsy. *Brain* **129**, 18–35 (2006).
27. Correale, J. & Villa, A. The blood–brain-barrier in multiple sclerosis: functional roles and therapeutic targeting. *Autoimmunity* **40**, 148–160 (2007).
28. de Vries, H. E. & Dijkstra, D. Mononuclear phagocytes at the blood-brain barrier in multiple sclerosis. *Blood-Spinal Cord and Brain Barriers in Health and Disease*, 409–417 (2004).
29. Opdenakker, G., Nelissen, I. & Van Damme, J. Functional roles and therapeutic targeting of gelatinase B and chemokines in multiple sclerosis. *The Lancet Neurology* **2**, 747–756 (2003).
30. Abdul-Muneer, P. M. *et al.* Induction of oxidative and nitrosative damage leads to cerebrovascular inflammation in an animal model of mild traumatic brain injury induced by primary blast. *Free Radic Biol Med* **60**, 282–291, https://doi.org/10.1016/j.freeradbiomed.2013.02.029 (2013).
31. Chen, Y. & Huang, W. Non-impact, blast-induced mild TBI and PTSD: concepts and caveats. *Brain injury* **25**, 641–650 (2011).
32. Haorah, J. *et al.* Ethanol-Induced Activation of Myosin Light Chain Kinase Leads to Dysfunction of Tight Junctions and Blood-Brain Barrier Compromise. *Alcoholism: Clinical and Experimental Research* **29**, 999–1009 (2005).
33. Haorah, J. *et al.* Oxidative stress activates protein tyrosine kinase and matrix metalloproteinases leading to blood–brain barrier dysfunction. *Journal of neurochemistry* **101**, 566–576 (2007).
34. Hue, C. D. *et al.* Time Course and Size of Blood-Brain Barrier Opening in a Mouse Model of Blast-Induced Traumatic Brain Injury. *J Neurotrauma*, https://doi.org/10.1089/neu.2015.4067 (2015).
35. Baldwin, S. A., Fugaccia, I., Brown, D. R., Brown, L. V. & Scheff, S. W. Blood-brain barrier breach following cortical contusion in the rat. *Journal of neurosurgery* **85**, 476–481 (1996).
36. Başkaya, M. K., Rao, A. M., Doğan, A., Donaldson, D. & Dempsey, R. J. The biphasic opening of the blood–brain barrier in the cortex and hippocampus after traumatic brain injury in rats. *Neuroscience letters* **226**, 33–36 (1997).
37. Hicks, R. R., Baldwin, S. A. & Scheff, S. W. Serum extravasation and cytoskeletal alterations following traumatic brain injury in rats. *Molecular and chemical neuropathology* **32**, 1–16 (1997).
38. Higashida, T. *et al.* The role of hypoxia-inducible factor-1α, aquaporin-4, and matrix metalloproteinase-9 in blood-brain barrier disruption and brain edema after traumatic brain injury: laboratory investigation. *Journal of neurosurgery* **114**, 92–101 (2011).
39. Shapira, Y., Setton, D., Artru, A. A. & Shohami, E. Blood-brain barrier permeability, cerebral edema, and neurologic function after closed head injury in rats. *Anesthesia & Analgesia* **77**, 141–148 (1993).
40. Elder, G. A. *et al.* Vascular and inflammatory factors in the pathophysiology of blast-induced brain injury. *Front Neurol* **6**, 48, https://doi.org/10.3389/fneur.2015.00048 (2015).
41. Hue, C. D. *et al.* Dexamethasone potentiates *in vitro* blood-brain barrier recovery after primary blast injury by glucocorticoid receptor-mediated upregulation of ZO-1 tight junction protein. *Journal of Cerebral Blood Flow & Metabolism* **35**, 1191–1198 (2015).
42. Kawoos, U., Gu, M., Lankasky, J., McCarron, R. M. & Chavko, M. Effects of Exposure to Blast Overpressure on Intracranial Pressure and Blood-Brain Barrier Permeability in a Rat Model. *PloS one* **11**, e0167510 (2016).
43. Readnower, R. D. *et al.* Increase in blood-brain barrier permeability, oxidative stress, and activated microglia in a rat model of blast-induced traumatic brain injury. *J Neurosci Res* **88**, 3530–3539, https://doi.org/10.1002/jnr.22510 (2010).
44. Shetty, A. K., Mishra, V., Kodali, M. & Hattiangady, B. Blood brain barrier dysfunction and delayed neurological deficits in mild traumatic brain injury induced by blast shock waves. *Frontiers in cellular neuroscience* **8** (2014).
45. Yeoh, S., Bell, E. D. & Monson, K. L. Distribution of blood-brain barrier disruption in primary blast injury. *Ann Biomed Eng* **41**, 2206–2214, https://doi.org/10.1007/s10439-013-0805-7 (2013).

46. Kabu, S. *et al.* Blast-associated shock waves result in increased brain vascular leakage and elevated ROS levels in a rat model of traumatic brain injury. *PloS one* **10**, e0127971 (2015).

47. Sosa, M. A. G. *et al.* Selective vulnerability of the cerebral vasculature to blast injury in a rat model of mild traumatic brain injury. *Acta neuropathologica communications* **2**, 67 (2014).

48. Sosa, M. A. G. *et al.* Blast overpressure induces shear-related injuries in the brain of rats exposed to a mild traumatic brain injury. *Acta neuropathologica communications* **1**, 51 (2013).

49. Stokum, J. A. *et al.* Glibenclamide pretreatment protects against chronic memory dysfunction and glial activation in rat cranial blast traumatic brain injury. *Behavioural brain research* **333**, 43–53 (2017).

50. Needham, C. E., Ritzel, D., Rule, G. T., Wiri, S. & Young, L. Blast testing issues and TBI: experimental models that lead to wrong conclusions. *Frontiers in neurology* **6**, 72 (2015).

51. Skotak, M., Alay, E. & Chandra, N. On the accurate determination of shock wave time-pressure profile in the experimental models of blast induced neurotrauma. *Frontiers in Neurology* **9**, 52 (2018).

52. Skotak, M. *et al.* Rat injury model under controlled field-relevant primary blast conditions: acute response to a wide range of peak overpressures. *J Neurotrauma* **30**, 1147–1160, https://doi.org/10.1089/neu.2012.2652 (2013).

53. Hyde, D. W. *ConWep: Conventional Weapon Effects (software)* (1991).

54. Chandra, N., Sundaramurthy, A. & Gupta, R. K. Validation of Laboratory Animal and Surrogate Human Models in Primary Blast Injury Studies. *Military medicine* **182**, 105–113, https://doi.org/10.7205/milmed-d-16-00144 (2017).

55. Kuriakose, M. *et al.* Tailoring the Blast Exposure Conditions in the Shock Tube for Generating Pure, Primary Shock Waves: The End Plate Facilitates Elimination of Secondary Loading of the Specimen. *PloS one* **11**, e0161597 (2016).

56. Mishra, V. *et al.* Primary blast causes mild, moderate, severe and lethal TBI with increasing blast overpressures: Experimental rat injury model. *Scientific reports* **6**, 26992 (2016).

57. Chandra, N. *et al.* Evolution of blast wave profiles in simulated air blasts: experiment and computational modeling. *Shock Waves* **22**, 403–415, https://doi.org/10.1007/s00193-012-0399-2 (2012).

58. Garman, R. H. *et al.* Blast exposure in rats with body shielding is characterized primarily by diffuse axonal injury. *Journal of neurotrauma* **28**, 947–959 (2011).

59. Li, W. *et al.* A quantitative MRI method for imaging blood-brain barrier leakage in experimental traumatic brain injury. *PloS one* **9**, e114173 (2014).

60. Su, E. J. *et al.* Imatinib treatment reduces brain injury in a murine model of traumatic brain injury. *Frontiers in cellular neuroscience* **9** (2015).

61. Tanno, H., Nockels, R. P., Pitts, L. H. & Noble, L. Breakdown of the blood–brain barrier after fluid percussive brain injury in the rat. *Part 1: distribution and time course of protein extravasation. Journal of neurotrauma* **9**, 21–32 (1992).

62. Candelario-Jalil, E., Yang, Y. & Rosenberg, G. Diverse roles of matrix metalloproteinases and tissue inhibitors of metalloproteinases in neuroinflammation and cerebral ischemia. *Neuroscience* **158**, 983–994 (2009).

63. Nishioku, T. *et al.* Detachment of brain pericytes from the basal lamina is involved in disruption of the blood–brain barrier caused by lipopolysaccharide-induced sepsis in mice. *Cell. Mol. Neurobiol.* **29**, 309–316 (2009).

64. Armulik, A., Abramsson, A. & Betsholtz, C. Endothelial/pericyte interactions. *Circ Res* **97**, 512–523, https://doi.org/10.1161/01.RES.0000182903.16652.d7 (2005).

65. Armulik, A. *et al.* Pericytes regulate the blood-brain barrier. *Nature* **468**, 557–561, https://doi.org/10.1038/nature09522 (2010).

66. Abbott, N. J. Astrocyte–endothelial interactions and blood–brain barrier permeability. *Journal of anatomy* **200**, 523–534 (2002).

67. Abbott, N. J., Rönnbäck, L. & Hansson, E. Astrocyte-endothelial interactions at the blood-brain barrier. *Nature reviews. Neuroscience* **7**, 41 (2006).

68. Benarroch, E. E. *Mayo Clinic Proceedings* **10**, 1326–1338. Elsevier (2005).

69. Polavarapu, R. *et al.* Tissue-type plasminogen activator–mediated shedding of astrocytic low-density lipoprotein receptor–related protein increases the permeability of the neurovascular unit. *Blood* **109**, 3270–3278 (2007).

70. Banks, W. A. From blood-brain barrier to blood-brain interface: new opportunities for CNS drug delivery. *Nature Reviews Drug Discovery* (2016).

71. Hue, C. D. *et al.* Blood-brain barrier dysfunction after primary blast injury *in vitro*. *Journal of neurotrauma* **30**, 1652–1663 (2013).

72. Lucke-Wold, B. P. *et al.* Bryostatin-1 Restores Blood Brain Barrier Integrity following Blast-Induced Traumatic Brain Injury. *Mol Neurobiol* **52**, 1119–1134, https://doi.org/10.1007/s12035-014-8902-7 (2015).

73. Blyth, B. J. *et al.* Validation of serum markers for blood-brain barrier disruption in traumatic brain injury. *Journal of neurotrauma* **26**, 1497–1507 (2009).

74. Burda, J. E., Bernstein, A. M. & Sofroniew, M. V. Astrocyte roles in traumatic brain injury. *Experimental neurology* **275**, 305–315 (2016).

75. Vajtr, D. *et al.* Correlation of Ultrastructural Changes of Endothelial Cells and Astrocytes Occurring during Blood Brain Barrier Damage after Traumatic Brain Injury with Biochemical Markers of Blood Brain Barrier Leakage and Inflammatory Response. *Physiological Research* **58**, 263–268 (2009).

76. Fernández-López, D. & Vexler, Z. S. In *The Blood Brain Barrier (BBB)* 91–116 (Springer, 2013).

77. Louboutin, J.-P., Chekmasova, A., Marusich, E., Agrawal, L. & Strayer, D. S. Role of CCR5 and its ligands in the control of vascular inflammation and leukocyte recruitment required for acute excitotoxic seizure induction and neural damage. *The FASEB Journal* **25**, 737–753 (2011).

78. Szmydynger-Chodobska, J., Fox, L. M., Lynch, K. M., Zink, B. J. & Chodobski, A. Vasopressin amplifies the production of proinflammatory mediators in traumatic brain injury. *Journal of neurotrauma* **27**, 1449–1461 (2010).

79. Cavaglia, M. *et al.* Regional variation in brain capillary density and vascular response to ischemia. *Brain research* **910**, 81–93 (2001).

80. Brown, R. C., Egleton, R. D. & Davis, T. P. Mannitol opening of the blood–brain barrier: regional variation in the permeability of sucrose, but not 86Rb+ or albumin. *Brain Research* **1014**, 221–227, https://doi.org/10.1016/j.brainres.2004.04.034 (2004).

81. Johanson, C. E. Permeability and vascularity of the developing brain: cerebellum vs cerebral cortex. *Brain research* **190**, 3–16 (1980).

82. LaManna, J. C. & Harik, S. I. Regional studies of blood—brain barrier transport of glucose and leucine in awake and anesthetized rats. *Journal of Cerebral Blood Flow & Metabolism* **6**, 717–723 (1986).

83. Pluta, R., Tomida, S., Ikeda, J., Nowak, T. S. Jr & Klatzo, I. Cerebral vascular volume after repeated ischemic insults in the gerbil: comparison with changes in CBF and brain edema. *Journal of Cerebral Blood Flow & Metabolism* **9**, 163–170 (1989).

84. Holash, J., Sugamori, K. & Stewart, P. The difference in vascular volume between cerebrum and cerebellum is in the pia mater. *Journal of Cerebral Blood Flow & Metabolism* **10**, 432–434 (1990).

85. Allt, G. & Lawrenson, J. G. Is the pial microvessel a good model for blood-brain barrier studies? *Brain Research Reviews* **24**, 67–76, https://doi.org/10.1016/S0165-0173 (1997).

86. Huber, B. R. *et al.* Blast exposure causes dynamic microglial/macrophage responses and microdomains if brain microvessel dysfunction. *Neuroscience* **319**, 206–220, https://doi.org/10.1016/j.neuroscience.2016.01.022 (2016).

87. Chandra, N., Holmberg, A. & Feng, R. Controlling the shape of the shock wave profile in a blast facility. *US Provisional patent application* **61542354** (2011).

88. Jiang, Z. *et al.* Role of hydrogen sulfide in early blood-brain barrier disruption following transient focal cerebral ischemia. *PloS one* **10**, e0117982 (2015).

89. Yen, L. F., Wei, V. C., Kuo, E. Y. & Lai, T. W. Distinct patterns of cerebral extravasation by Evans blue and sodium fluorescein in rats. *PloS one* **8**, e68595 (2013).
90. Kaya, M. & Ahishali, B. In *Permeability Barrier* 369–382 (Springer, 2011).
91. Sandel, W. R., Hubbard, R. W. & Schehl-Geiger, D. Indocyanine Green (ICG) and Evans Blue: Comparative Study of Plasma Volume Measurement. (Army Research Inst Of Environmental Medicine Natick Ma, 1982).
92. Wolman, M. *et al.* Evaluation of the dye-protein tracers in pathophysiology of the blood-brain barrier. *Acta neuropathologica* **54**, 55–61 (1981).

Acknowledgements

Author Contributions

M.K., K.V.R. and N.C. wrote the main manuscript text, M.K. and K.V.R. conducted experiments described in this work and M.K. and D.Y. prepared the figures. All authors reviewed the manuscript.

Additional Information

Competing Interests: The authors declare no competing interests.

Publisher's note: Springer Nature remains neutral with regard to jurisdictional claims in published maps and institutional affiliations.

SCIENTIFIC REP⚙RTS

Electrophysiological Correlates of Blast-Wave Induced Cerebellar Injury

Gokhan Ordek[1], Ahmet S. Asan[1], Esma Cetinkaya[1], Maciej Skotak[1,2], Venkata R. Kakulavarapu[1,2], Namas Chandra[1,2] & Mesut Sahin[1]

Understanding the mechanisms underlying traumatic neural injury and the sequelae of events in the acute phase is important for deciding on the best window of therapeutic intervention. We hypothesized that evoked potentials (EP) recorded from the cerebellar cortex can detect mild levels of neural trauma and provide a qualitative assessment tool for progression of cerebellar injury in time. The cerebellar local field potentials evoked by a mechanical tap on the hand and collected with chronically implanted micro-ECoG arrays on the rat cerebellar cortex demonstrated substantial changes both in amplitude and timing as a result of blast-wave induced injury. The results revealed that the largest EP changes occurred within the first day of injury, and partial recoveries were observed from day-1 to day-3, followed by a period of gradual improvements (day-7 to day-14). The mossy fiber (MF) and climbing fiber (CF) mediated components of the EPs were affected differentially. The behavioral tests (ladder rung walking) and immunohistological analysis (calbindin and caspase-3) did not reveal any detectable changes at these blast pressures that are typically considered as mild (100–130 kPa). The results demonstrate the sensitivity of the electrophysiological method and its use as a tool to monitor the progression of cerebellar injuries in longitudinal animal studies.

The devastating consequences of severe head injuries are well known to the public. It is also known that undetected mild TBI can be a high risk factor for subsequent injuries and repeated mTBI, whether identified or not, leads to much more serious injuries[1]. Time of intervention is a critical parameter to achieve the best results in the treatment of TBI patients. This requires the knowledge of the time course of injury and its severity. To this end, animal models have been developed to generate better controllable results such as injury severity, type, and location, as well as the age, gender and genetic composition of the subjects, for investigations of immunohistochemical and biomechanical aspects of TBI. Although animal models continue to provide valuable insights into the mechanisms of brain injury, the need to terminate the animals for histological evaluation introduces a significant source of variability by preventing data collection at multiple time points in the same animals during injury progression. Thus, post-mortem techniques rely on statistics to account for inter-animal variations. Cascaded sequelae of the initial and delayed phases of neural injury make it further difficult to determine the temporal course of the injury. Secondary (or delayed) injury mechanisms can last minutes to months including cascaded metabolic, cellular and molecular events that lead to brain cell and tissue damage[2–4]. On the other hand, the electrophysiological technique can provide a powerful tool for multi-point measurements or continuous monitoring of the biomarkers correlated with injury while cascaded changes are taking place in live animals. We developed a novel approach to monitoring various phases of injury using multi-electrode arrays (MEAs) implanted on the cerebellar surface (micro-ECoG technique) to detect any subtle changes in the cortical network excitability. Implanting the rats with MEAs before the blast exposure provided a baseline within the same subject for comparison.

Traditionally, the cerebellum has been considered as a brain center for sensorimotor integration and motor coordination. In recent years the cerebellum has been implicated in cognitive functions and emotions[5,6]. Despite numerous studies, there is still no consensus either on the nature of the information provided by the cerebellar outputs to other brain centers, or how the disruption of these outputs leads to the observed functional deficits

[1]Department of Biomedical Engineering, New Jersey Institute of Technology, Newark, 07102-1982, NJ, USA. [2]Center for Injury Biomechanics, Materials, and Medicine (CIBM3), New Jersey Institute of Technology, Newark, 07103-3540, NJ, USA. Correspondence and requests for materials should be addressed to N.C. (email: namas.chandra@njit.edu) or M.Sahin (email: sahin@njit.edu)
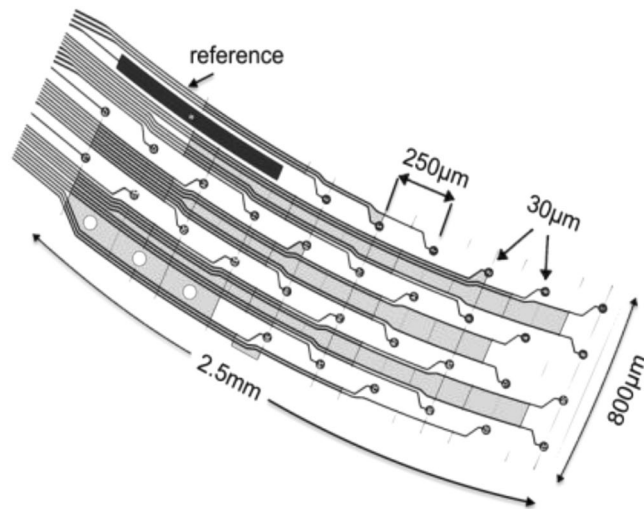
Figure 1. Custom-design multi-electrode array contained 32 Pt contacts (30 μm diam.) that were arranged in 4 rows and 10 columns that cover most of the right PML. The first four contacts are missing in the design on the first row, where the reference contact is, and also on the fourth row.

after head trauma. The neurologic disabilities that result from a direct insult to the cerebellum include ataxias, tremors, loss of balance and motor skills, and cognitive deficits[7–10].

To date, the cerebellum has been understudied in the field of TBI research because of the notion that majority of cerebellar deficits occur only by direct impacts on the cerebellum, which rarely occurs in accidents. However, a recent report showed functional and structural cerebellar deficits as a result of blast induced repeated mTBI where the entire brain was affected[11]. Another report suggested a lower threshold for cerebellar injuries in veterans exposed to repetitive blasts[12]. Although diffuse axonal injury (DAI) is the main focus of mTBI research, recent evidence also indicated vulnerability of the synaptic mechanisms to blast injuries[13–16]. Other findings in cerebellar injuries included Purkinje cell (PC) deterioration[17–19], synaptic disruptions[11,20] and behavioral deficits[8,17,18].

Scientific evidence is building up to suggest that mild head injuries, including concussions, can leave permanent damage in the brain especially if they reoccur before the person completely recovers from the first injury[21]. These mild injuries are difficult to study in experimental animals because the damage may not cause the brain cells to show any anatomical changes or complete degenerations, but rather slowing down of their communication with other cells. Furthermore, mild injuries cannot be detected using behavioral measures since the impairments may be too subtle to affect the motor function or cognition or need a prohibitively large sample size to be detected. Here, we propose a highly sensitive electrophysiological method as a tool to monitor the state of on-going cerebellar injury with repeated or continuous recordings of evoked potentials in anesthetized animals.

Results

We first studied the effects of blast injury on the cerebellar local field potentials evoked by dorsal hand and whisker mechanical stimulation using a custom-design multi-electrode array (Fig. 1). Changes in the EP waveforms were shown on the post-injury days compared to the control day for a sample rat (Fig. 2). In general, the cerebellar EPs demonstrated characteristic waveforms that are reproducible. The amplitudes of evoked potentials (EPAs) were in the 120 ± 10 μV-160 ± 20 μV range for the largest deflections (latency of 8–10 ms) as a response to whisker stimulation in the pre-injury period. The largest deflection amplitude drastically dropped down to 10 ± 5 μV immediately after the blast injury (<10 min). The EPs evoked by hand stimulation persisted around the same amplitudes immediately after injury (paired t-test, n = 4 trials, p > 0.5) but decreased substantially on the next day (day-1). The EPs for both hand and whisker stimulations were very small and barely above the baseline noise on day-1 (red traces, 5–8 $\pm$ 2–4 μV). On day-3 of injury, both signals showed larger and multiple volleys compared to day-1, which suggested a partial recovery from injury (green trace, 60–80 $\pm$ 8–13 μV).

The changes in EPAs were quantified by calculating the area under the curve (AUC) as a measure, which reflects both the amplitude and duration information of a deflection in the EPs. An illustrative example from a control (pre-injury) animal was shown for a single channel of the MEA (Fig. 3A) and in multiple animals for hand and whisker stimulations (Fig. 3B, N = 7 rats). The raw AUC values were normalized by the maximum AUC that was observed in the pre-injury period within each animal individually and then averaged across all animals. The AUC values decreased significantly after the blast exposure during the 7 days after injury (N = 7 rats). Most drastic changes occurred within one hour after injury for the whisker EPs and on the next day for the hand EPs (a decline by ~56% in whisker AUCs at 1 h, p < 0.001 and by 43% in hand AUCs on day-1, p < 0.01; Dunnett's test). On day-3, AUCs increased slightly compared to day-1 measurements (Whisker ~13%, p < 0.44; Hand ~%24, p < 0.16) similar to the trend in EP amplitude measures in Fig. 2, which suggested a partial recovery. On day-7, the average AUCs were still lower than the control values by ~44% (p = 0.003, Dunnett's test) and ~32% (p = 0.07, Dunnett's test) for whisker and hand stimulation respectively. However, the AUC measures that were obtained from day-3 (73.1 $\pm$ 10%) and day-7 (58.3 $\pm$ 17.1%) for the hand EPs were not significantly different from pre-injury values (90.3 $\pm$ 4.3%).
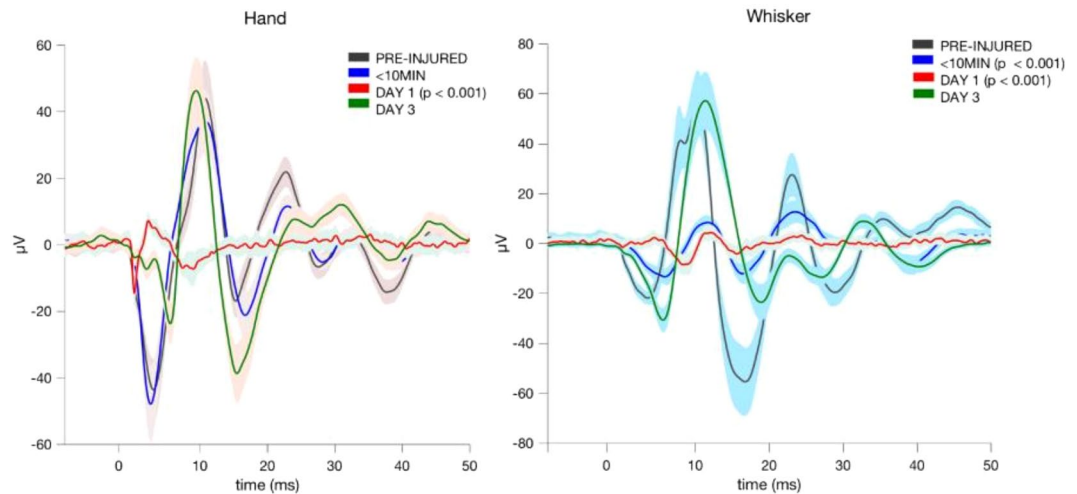
Figure 2. Sample evoked potential (EP) waveforms for hand and whisker stimulations before and after injury in a rat. Stimulus-trigger averaged (STA) signals were filtered at 10–500 Hz, and then averaged across channels. Multiple recordings (4–5 STAs) were averaged for each time point (i.e. each trace) and plotted as mean (solid) $\pm$ s.d (shades) from the time of stimulus arrival (t = 0 ms). While pronounced changes in EPs to whisker stimulations occurred immediately after injury (<10 min, T = 9 recordings, p < 0.001), hand EPs indicated significant changes only on the next day (T = 10, p < 0.001).

Next, the EPs were segregated into MF and CF mediated potentials as identified by their characteristic latencies from the time of stimulus (Fig. 4A), i.e. 2–10 ms for MF (red) and 12–20 ms for CF (blue). Because hand EPs were more reproducible than that of whiskers, we used only the hand evoked signals in the rest of the analysis. For precise measurements of arrival times, the EPs were spike-trigger averaged across multiple trials in each day for individual channels of the recording array separately. Consequently, each dot in the x-y plots of Fig. 4B represents a single contact out of 31 contacts of the array for the specified day of recording (color coded) in one of the animals. The histograms on the top and the right side of each plot show distributions of the MF and CF arrival times (latencies) across the array contacts in all animals as group data. The results suggest that there was a transient lengthening of MF onset latencies from the control values of 5.5–6.5 ms to 6–8 ms within the first hour of injury, which was followed by a decrease to the 4–6 ms range on day-1. On the following days, there was a progressive increase in MF delays with mean values of 6.05 ms, 6.6 ms, and 7.05 ms on days 3, 7, and 14 respectively. The variance of the MF latencies across the channels was much wider on the post-injury days compared to the pre-injury values. Conversely, the CF peak delays started increasing immediately after injury (1 h) from a range of 15–16 ms and reached to 16–20 ms with a mean of ~19 ms, and stayed higher for the rest of the study period without a specific pattern in the trend. Most notably, significant changes were observed both in MF and CF arrival times within the first hour, although they moved in different directions specifically on day-1. Overall, these results suggest that the injury induces differential effects on the MF and CF arrival times.

As a measure of excitability in the cerebellar network, we used z-scores of the normalized amplitudes (nEPAs) of the MF- and CF-EPs (Fig. 5). In each animal, the majority of supra-threshold CF responses occurred before the injury (Fig. 5A; control, 90% or 19/21 trials in the pooled data). Conversely, none of the MF responses reached the excitability threshold on the day before the injury (Fig. 5A; $Z_{score} > 2.05$, no blue markers <10 ms, a gray area excluded). After the injury, the ratio of supra-threshold CF components declined to 66% (63/95 trials for all time points) from 90% (pre-injury), showing the sharpest decline within the hour (Fig. 5A; red markers). While all of the supra-threshold MF-nEPAs were registered in the post-injury period for all animals (Most heightened at ~1 hour; red markers, $Z_{score} = 2.25 \pm 0.11$), CF-nEPAs were much stronger in the pre-injury period in comparison (blue markers in $t \geq 10$ ms area, $Z_{score} = 2.56 \pm 0.13$).

All supra-threshold responses (shown in Fig. 5A) were averaged for each day across animals and replotted (Fig. 5B). The z_{score} threshold was lowered to 1.55 for this particular analysis in order to include at least one data point per day. In each animal, the data set was normalized to the largest amplitude that was recorded during pre- or post-injury periods, following z-score qualification. Significant changes were detected in nEPAs of both MF and CF responses from pre- to post-injury (MF; $F_{(6,522)} = 7.12$, CF; $F_{(6,593)} = 14.51$) recordings. Within the first hour, CF-nEPAs were diminished almost completely down from 0.89 ± 0.09 in pre-injury. After day-1 of injury, the magnitudes of CF-nEPAs were still nearly 3-fold smaller (0.27 ± 0.2) than the pre-injury values and did not differ significantly on day-14 from day-7 (p = 0.22, one tailed t-test). Contrarily, MF-nEPAs increased to 0.22 ± 0.12 (p < 0.01; single data point from the pre-injury period in each rat) in the first hour and sustained higher magnitudes than the controls during the two weeks of the post-injury period (nEPAs = 0.14 ± 0.08 on day-14). These results suggest that the MF and CF amplitudes were also affected differentially by the injury, and analogous to the trend in their arrival times. Note that the overall effect of injury on the EP amplitudes was a net decrease by the AUC measures before separating the MF and CF components (Fig. 3).
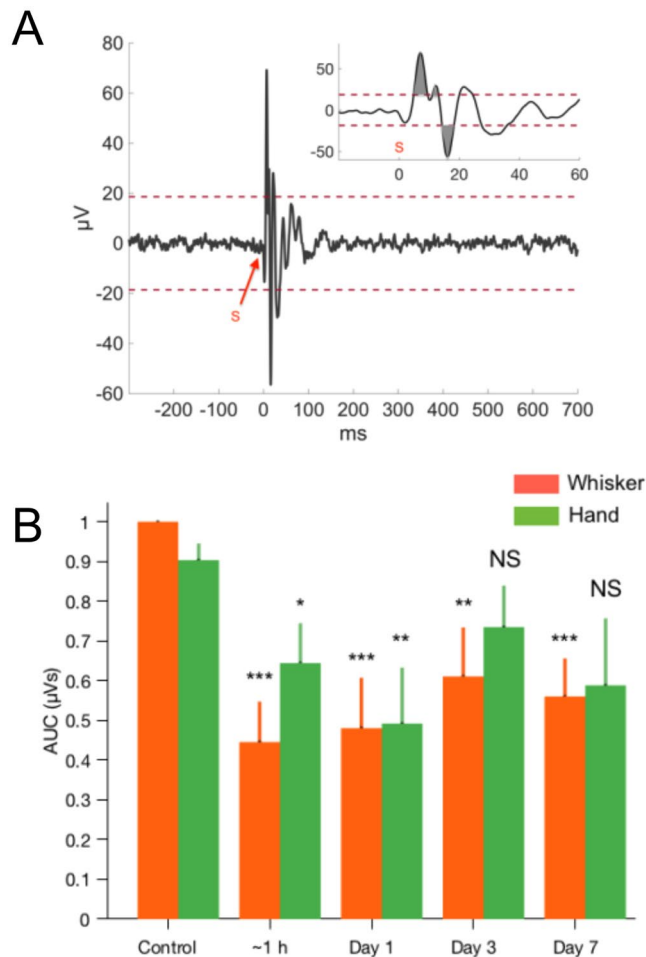
Figure 3. EP quantification by the area under the curve (AUC) method. (**A**) An example of AUC calculation is shown on a stimulus-trigger averaged signal that had a sufficient amplitude to be included in the analysis (threshold $\pm 20\,\mu V$). (**B**) Mean EP changes during the 7 days following blast injury (N = 7 rats). AUCs showed significant drops for both whisker (F(4, 30) = 5.69, p = 0.0016; rmANOVA) and hand evoked potentials (F(4, 30) = 2, p = 0.011; rmANOVA). Bars indicate $\pm$ s.d. Significance vs. control (pre-injury) is indicated by the asterisks according to Dunnett's test. ***P < 0.001, **P < 0.01, *P < 0.05. NS: not significant.

Ladder Walking. The functional impact of injury was assessed using the skilled locomotion test on the horizontal ladder rung (HLR) in a group of rats that were exposed to the same blast-pressures as the rats with array electrode implants (Fig. 6A, N = 3 rats). The walking performances improved during one-week of pre-injury training period as indicated by the lower number of foot slips (1.33 $\pm$ 0.28, p = 0.001; Tukey test, day-1 vs. day-4) and the body falls (1.44 $\pm$ 0.37, p = 0.009, Tukey test, day-1 vs. day-6). Interestingly, HLR scores did not present any significant differences after the blast injury ($F_{(2,32)} = 0.909$, p = 0.512; from day 4 to day 12). In fact, they showed nearly the same number of misses and falls on day-1 (Tukey test, p > 0.99; Day 7 vs Day 8) and day-2 (Tukey test, p > 0.95; Day 7 vs. Day 9) of the post-injury period. Results indicated no behavioral deficits in the limb functions during the learned HLR walking due to blast-exposure.

Rotarod tests. As another method to assess motor coordination in animals exposed to blast injury, rotarod testing was done in animals 24 h, 3 days and 7 days post-injury. Similar to ladder walking performance test, at any time point after the injury, latency times between control and injured animals did not display any statistically significant differences (Fig. 6B). These results are consistent with the ladder performance tests, and further confirms that electrophysiological measures are more sensitive tools to identify progressive cerebellar injuries following mild blast injury.

Assessment of Neuronal Loss. In order to identify any potential neuronal loss contributing to electrophysiological disturbances at 24 h and 7 day post-injury, immunohistochemical analysis of calbindin D28K, an intracellular Ca^{2+} binding protein and a marker of Purkinje cells, as well as cleaved caspase-3, a marker of apoptosis was performed. Results indicate immunoreactivity (intensity) of calbindin D28K or a number of calbindin D-28K positive cells did not change in the paramedian lobule of cerebella in rats exposed to 130 kPa over pressure compared to controls (Fig. 7). Likewise, a number of caspase-3 positive cells did not change following injury. Calbindin D-28K and caspase-3 immunostaining were also performed 7 days post-injury and similar to 24 h data,
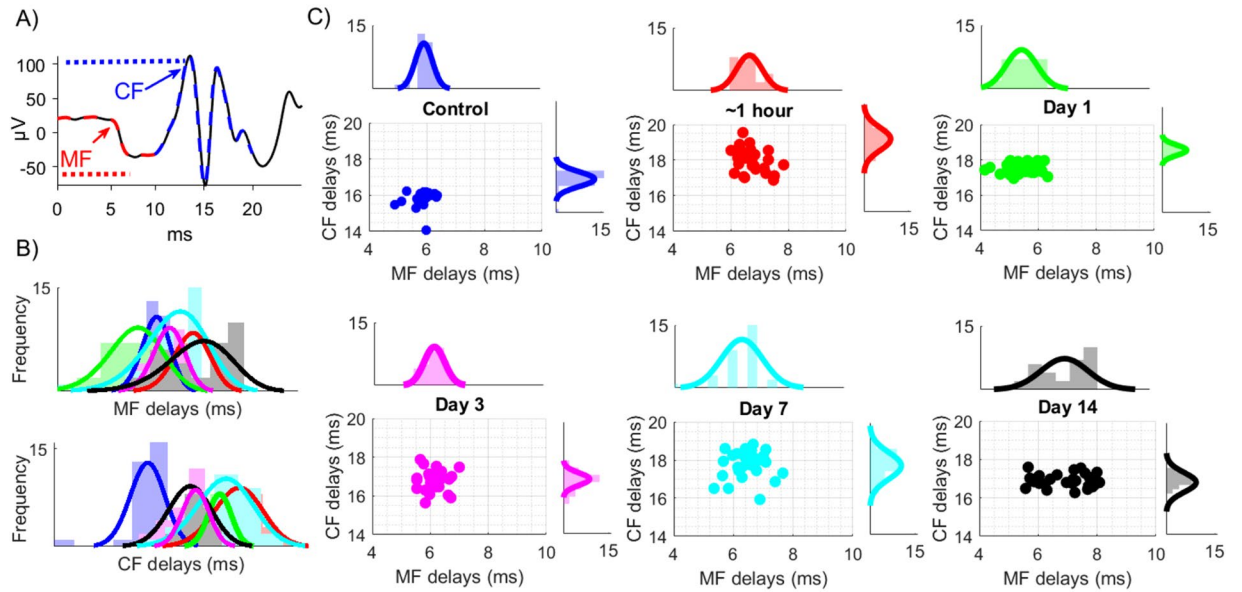
Figure 4. Arrival times of MF and CF mediated local field potentials evoked by mechanical hand stimulation before and after injury. (**A**) Identification of the MF onset and the CF peak, based on arrival times (arrows). Stimulus is at 0 ms. (**B**) MF and CF delays for each array contact were averaged across multiple trials (2–3 trials per day) separately in each day and animal (3 rats indicated by different symbols) and plotted against each other as an x-y chart to show the variation across 31-channels of the recording array. Histograms show day-by-day (color coded) changes in the mean and distribution of the delays. All statistical significances were performed with paired comparisons between pre-injury (control) vs. each day of post-injury. N = 3, Mann-Whitney; *P < 0.01, **P < 0.001, ***P < 0.0001. (**C**) All histograms from different days are merged into a single plot to demonstrate the trends in MF and CF delays day-by-day.
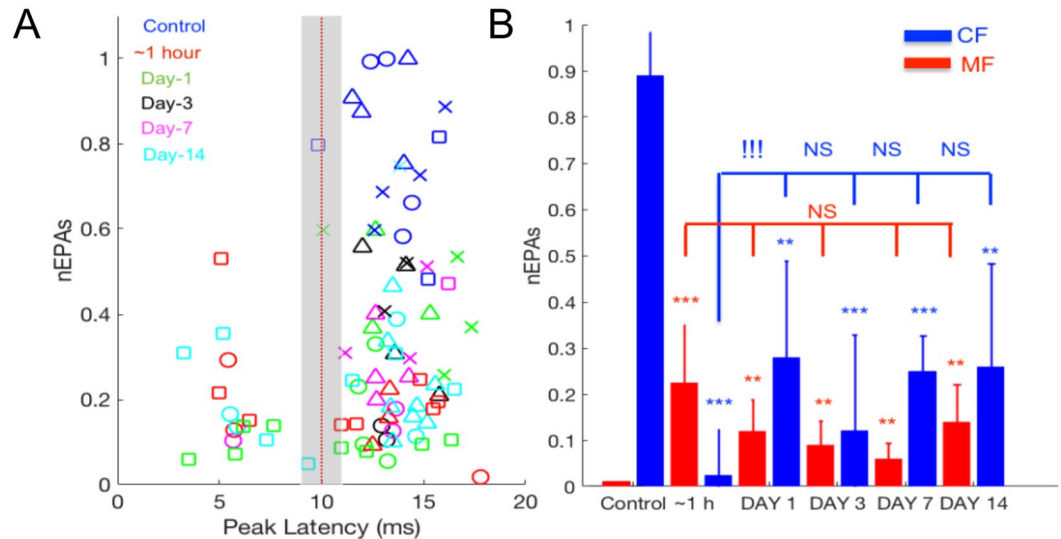
Figure 5. Excitability changes after injury in EP components by hand stimulation. (**A**) Amplitude distribution of MF (latency < 10 ms) and CF (latency > 10 ms) components. EPAs were normalized (nEPA) to a maximum recorded amplitude on any day throughout the pre-/post injury period in each rat, and then a z-score value was applied as a threshold (Zscore > 2.05, 15 MFs and 71 CFs). The data were gathered from 4 rats as indicated by different marker shapes. While CF-EPAs indicated the strongest responses in the pre-injury (control) recordings in all animals (blue markers, T = 14/19 trials; Zscore > 2.05), MF-EPAs showed supra-threshold responses only in the post-injury period (T = 15/89 Trials, Zscore > 2.05), except day-3. (**B**) Same data with a lower threshold (Zscore > 1.55) were averaged and shown as mean ± s.d for MF (red) and CF (blue), respectively. Statistical analysis indicated significant increases in MF-nEPAs, and significant decreases in CF-nEPAs in the post-injury period (ANOVA followed by Dunnett's test; control vs. post-injury time points, n = 5 days, n = 32 MF-nEPAs, n = 105 CF-nEPAs; ***P < 0.001, **P < 0.01, *P < 0.05). Individual days were compared using pairwise t-test (CF ~1 h vs. day-1; !!!P = 0.0013, NS: Not significant).
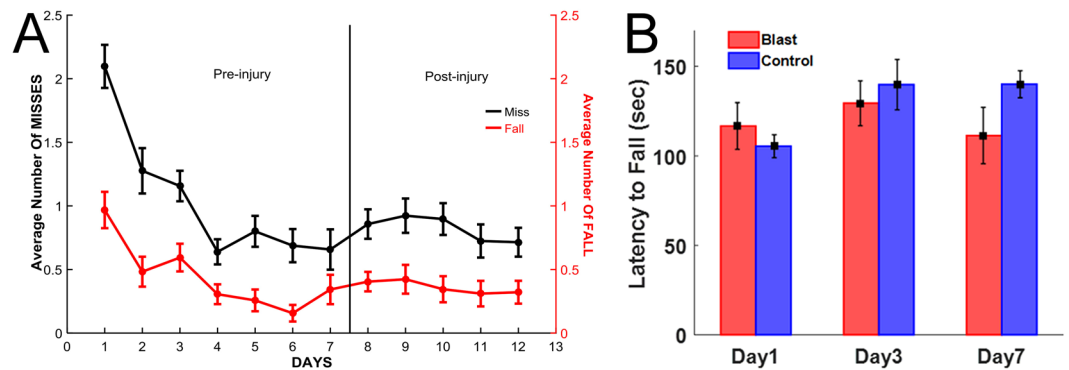
Figure 6. (**A**) Walking performances during repeated horizontal ladder crossings. Number of slips (misses) and falls in any of the four feet were scored in three rats. Rats demonstrated improved walking skills during the training period of one week with lowered number of falls and misses prior to injury (Days 1–7). Animals showed no statistically significant changes in motor performance scores with nearly the same miss and fall scores on day-1 (Day 8) and day-2 (Day 9) of injury. (**B**) Effect of mild blast injury on rotarod performance. Values were recorded from control and blast-injured animals on day 1, day 3 and day post-injury. Results are the mean ± SEM of the time animals remained on the rotarod before falling. There was no significant difference between control and injured animal groups at any time point (p > 0.05).

no significant changes were observed between controls and 7-day post-injury animals. Additionally, to evaluate whether purkinje cells were undergoing apoptosis, we performed double immunostaining of calbindin-D28K and caspase-3. We did not observe any colocalization of caspase-3 positive staining in purkinje cells. These results indicate that Purkinje cell loss does not contribute to the observed disturbances in electrophysiological functions in this study.

Discussion

Electrophysiological Correlates of TBI. Electrophysiological detection of TBI related neurological abnormalities has been investigated in humans[22,23] and animal models[24,25]. While researchers and clinicians mostly focused on the cerebral regions such as the neocortex[24,25] and hippocampus[26–28], reports on the cerebellum also presented strong evidence for the use of electrophysiology in TBI detection[20,29–31]. A wide spectrum of electrophysiological classifiers has been investigated. Nevertheless, amplitude and frequency analyses remain as the most sensitive parameters to identify abnormalities in the altered electrophysiology of the injured cerebellum. Amplitude variations in the electrical activity has previously been correlated to the cell loss in the cerebellum[20], while the frequency[32] and coherence spectra[33] of the cerebellar oscillations have also been shown to change due to the injury.

Recently, we introduced the use of evoked potentials for detection of cerebellar injury in focal fluid percussion model with chronic implantation of multi-electrode arrays in rodents[30]. Our published data demonstrated the sensitivity of the electrophysiological assessment method in detection of cerebellar injuries earlier than the onset of molecular degeneration in fluid percussion injured (FPI) rats. Despite the differences in the injury mechanism between FPI-induced (both focal and locally diffuse) and blast-exposed (whole-brain diffuse) TBI models, cerebellar recordings showed a number of akin findings that support the sensitivity of the electrophysiological method. As a result of EPA amplitude variations between the animals, the recovery on day-3 (and day-7) was not statistically strong in the group data (Fig. 3) to unambiguously confirm the distinct recovery shown in the sample animal of Fig. 2. The amplitude analysis in conjunction with the time of arrivals (Fig. 5) suggests that the recovery is not complete within our observation window after injury. In contrast, we did not observe any signs of recovery in our previous FPI work within one week, which may be explained by different injury mechanisms.

Our definition of the MF time window was relaxed to account for additional propagation delays from periphery and we essentially used the first volley after the stimulus for the analysis. Here, we strictly defined the MF component with latencies less than 10 ms and extended our previous findings by separating the EP components into MF and CF mediated components. The former showed an increased and the latter showed a decreased excitability after the injury. Increased excitability in mossy fiber responses after FPI induction has been reported before. In Ai and Baker[20,29], FPI applied over the posterior fossa immediately behind the lambda line in the center resulted in presynaptic hyperexcitability within mossy fiber granule cell synapses at 3 days post-injury along with by hyperexcitability of the parallel fiber-Purkinje cell synapses at 3–7 days post-injury. The major discrepancy between our and Ai and Baker's results is that they did not observe any significant changes in neither of these synaptic strengths at 1 day after injury, a finding that was clearly suggested by our data with both FPI[30] and blast injury mechanisms. A potential explanation was offered by our observation that the whisker EPs declined within the first hour post-injury as opposed to the hand EPs showing major changes on the next day. This suggests that different cerebellar networks may have varying time windows to respond to the injury depending on whether they are affected directly or indirectly.

The pre-implantation of an MEA may be a risk factor that the presence of the MEA on the cerebellar cortex during exposure to the blast wave may augment the impact and exacerbate the resulting injury. This concern was invalidated to a large extent by the fact that the whisker and hand evoked potentials were affected differentially
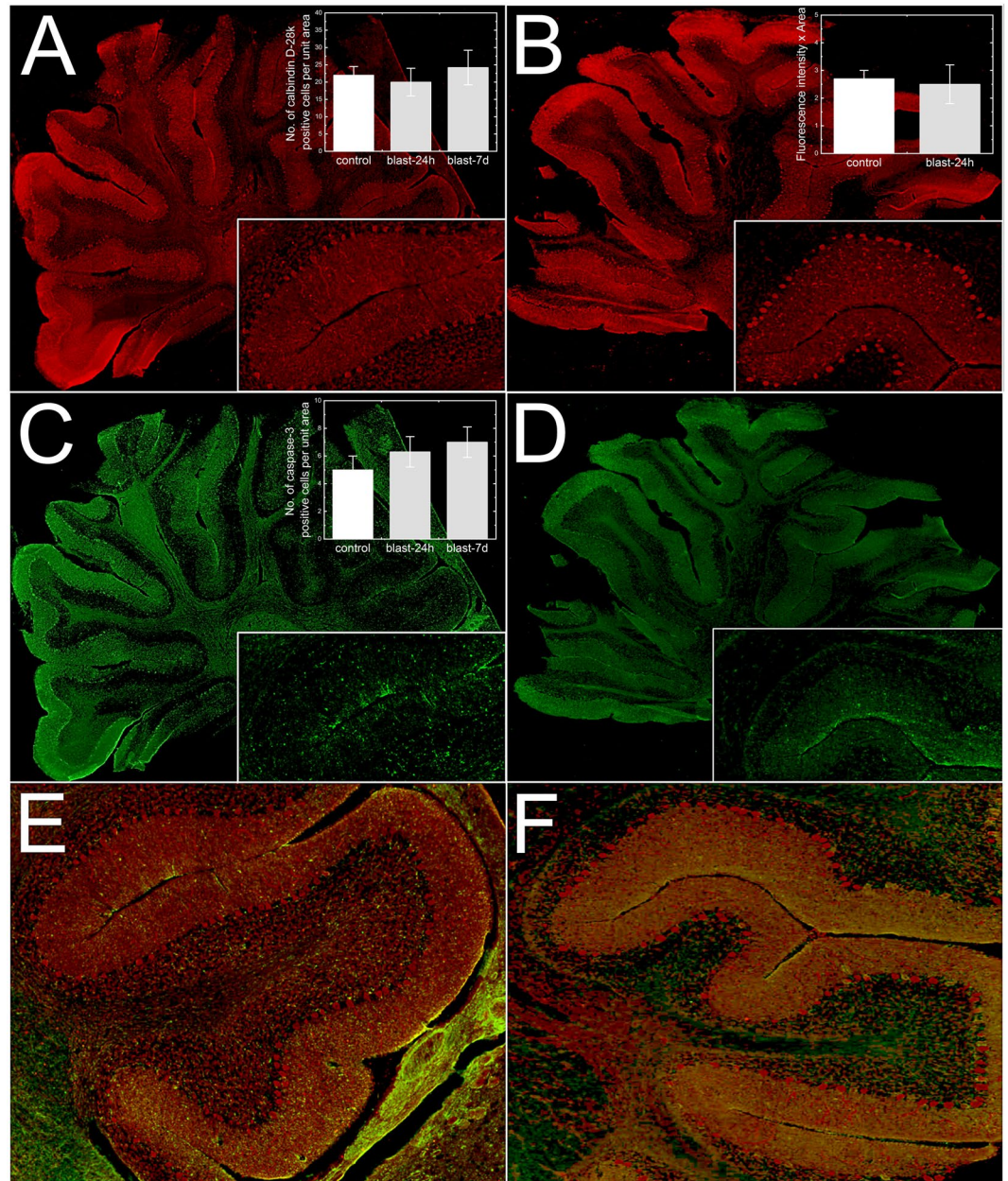
Figure 7. Immunofluorescence images of calbindin-D28K (**A,B**) and cleaved caspase-3 (**C,D**) in control, 24 hours and 7 days after blast injury. Sagittal sections with enlarged fragments from the paramedian lobules (insets) captured at 40x magnification and quantification results are presented. Paramedial lobules double stained for calbindin-D28K (red) and caspase-3 (green) showing no colocalization of caspase-3 in Purkinje cells (**E,F**). Bar plots present quantification of: 1) a cell count for: calbindin-28k (**A**), and capsase-3 (**C**) positive cells, and 2) calbindin-28k fluorescence signal (**B**). No appreciable changes in the levels of calbindin-D28K or cleaved caspase-3 were observed between control and the injured cerebella ($p > 0.05$).

and that the hand evoked signals did not differ significantly in recordings immediately after the injury. The deterioration of the signal amplitudes may still be occurring due to tissue encapsulation around the electrode until the chronic tissue response is complete in about two to three months[34–36]. The stability of the signals in a group of uninjured control animals with implantation times up to 21 days suggested that the signals do not deteriorate significantly within this time window[30]. The subdural implantation of the MEA can also provide a sub millimeter level spatial resolution for localization of injury if needed, as demonstrated by EP amplitude distributions from whisker and hand stimulation in uninjured animals[37].

Hand vs. Whisker Stimulation. Unlike the hand stimulation, the EPAs by whisker stimulation were significantly lower at each measurement point as seen in the pooled data from all animals (Fig. 3). This may be due to several factors. Cerebellar cortex contains multimodal functional topography[38–41] that is defined by discrete

clusters of neurons, which may receive multi-variant projections during stimulation of different body parts[38]. For instance afferent information from whisker activation is transmitted through a more direct and shorter pathway that involves trigeminal nuclei and inferior olive via middle cerebellar peduncle before reaching granule cells and PCs in the cerebellar cortex[42]; while inputs from the hand are mediated by spino-olivary pathways ascending via inferior cerebellar peduncle to activate the same type of neurons in the cerebellum[43–45]. Biomechanical factors during blast injury might induce differential effects on the hand and whisker networks of the cerebellum that are defined by different ascending pathways. This is supported by studies indicating a higher sensitivity of the vestibular nucleus to shock-wave induced blast injuries in humans and rats[46–48], although we cannot confirm a similar effect since we did not include behavioral tests to verify balance and coordination deficits in our experimental animals. Nevertheless, it is possible that an adjacent structure to the vestibular fibers, the trigeminal tract, may also have a higher sensitivity to the blast-waves.

Additionally, we observed large differences in EPAs, particularly in those from the hand, between the animals that were exposed to blast pressures with lower (100 psi) and higher (130 psi) pressure peaks (data not shown). While the whisker EPAs showed rapid drops within hours of injury, only at higher pressures the hand EPAs presented discernible deteriorations. While the differences in the measured peak pressures explain the variations in our pooled data, this observation also suggests the sensitivity of the cerebellar EPs to graded levels of injury severity. In our blast experiments the animals were held in prone position with shock waves traveling from rostral to caudal direction and reaching the cerebellum last. In FPI experiments, the injury is usually induced just above the cerebellum. Though the blast loading is biomechanically distinct from FPI, the subtle electrophysiological changes were measurable in both injury types.

MF vs. CF Mediated Components. Cerebellar evoked potentials were previously investigated with penetrating as well as surface electrodes and characteristic waves (amplitude, onset time, duration, etc.) were linked to cerebellar morphology[37,49–52]. The sole output of the cerebellar cortex, the Purkinje cells (PCs), receive inputs through two major pathways. First, the mossy fibers (MF) that project on PCs via granule cell (GC)-parallel fiber (Pf) pathway and generate an early (2–6 ms; onset latency, P1-N1, N2) excitatory post synaptic potentials (EPSPs) in the evoked potential waveform. Second, the climbing fibers (CF) that originate from the inferior olive (IO) and make strong excitatory connections with the PCs and give rise to local field deflections with 8–20 ms latencies in response to a sensory stimulus[52,53].

The evoked potentials, identified by their anatomical origins within the cerebellar cortex, were shown to detect changes of excitability[54,55]. We separated the cerebellar EPs into mossy and climbing fiber components with respect to their arrival times (Figs 4 and 5). While the CF components presented delayed arrival times (up to ~4 ms) for all days of post-injury, the MF responses had a changing trend. We noted that the MF onsets were initially increased (~1 h), then decreased (day 1) and finally increased again from day-3 to day-14 of the injury period. Finally, the increasing standard deviation of the CF delays between the recording channels indicated a wider spatial distribution of arrival times across the cerebellar cortex.

Differential effects in the timing of the MF and CF signals prompted a similar analysis to be performed on the amplitudes. Typically, the MF deflections exhibited smaller amplitudes with negative polarity, which is plausible considering the weakness of PF-PC synapses. The effect of the CF pathway on PC dendrites is much stronger with hundreds of synapses[56], and thus the CF component is recorded with larger amplitudes and positive polarity. Figure 5 suggests an increase in the MF mediated volleys and a decrease in the CF mediated components during the post-injury period, particularly at early stages, from 1 hour to a day. The higher z-score threshold yielded many more MF component detections after the injury suggests hyperexcitability. Increased excitability of pre-synaptic inputs at the mossy fibers-granule cell terminals was reported before[20]. Although our findings suggested a similar trend, we argue that the time window for MF hyperexcitability may be occurring in the earlier acute stage (hours to a day) rather than in the delayed phase (day-3 to day-7) of injury.

Behavioral Tests. We hypothesized that electrophysiological approach could be sensitive enough to investigate mild injuries that would be too subtle to detect with conventional methods. To confirm this hypothesis, we first evaluated the behavioral scores during a skilled walking task on a horizontal ladder rung. The cerebellum plays a major role in motor learning tasks when the predictive timing and coordination is essential[57,58]. Animal models suggest that cerebellar injury can lead to Purkinje cell losses and behavioral deficits in moderate to severe head injuries[17,59]. We implemented a horizontal ladder rung test to evaluate skilled walking parameters such as foot slips, step cycle, limb coordination to complement foot fault scorings in pre- and post-injury periods. Although multiple parameters were analyzed (not shown), we observed only clear improvements in the reduction of foot slips and partial (or complete) falls in the learning period prior to injury induction. After blast exposure, animals showed no differences in their walking performance on the ladder. In our previous study, FPI at 15–30 psi induced detectable changes in step duration, suggesting that the HLR task is a proper behavioral paradigm to demonstrate cerebellar injuries[60]. The absence of walking alterations in the HLR task among blast injury cohort suggests that the cerebellum is affected only mildly. These results show that the electrophysiological method can detect changes in the cerebellar circuits even in the absence of behavioral deficits.

Immunohistochemistry. Neuronal loss, particularly the Purkinje cell loss has been reported in different forms of TBI with different injury severities[18]. Earlier, employing fluid percussion model of TBI, we also observed that mild injury (~15 psi) caused a significant Purkinje cell loss (decreased calbindin D28K immunoreactivity and increased Fluoro-Jade C staining) in parasagittal sections of cerebellar cortex 7 days post-injury[30]. Our previous observation is in contrast with our present study showing no Purkinje cell loss following blast injury at 24 h or 7 days post-injury, although the peak over pressure appear to be similar (15 psi = 103 kPa). It is possible that the injury outcomes may be dictated by the mode of injury (e.g., blast vs. blunt injury). Accordingly, direct tissue

injury at the epicenter in the blunt TBI could trigger a cascade of events (neuroinflammation, local blood brain barrier breakdown) that may be different from blast injury. Additionally, a single blast at moderate levels may not be sufficient to trigger neurodegeneration whereas a single blunt impact and associated direct tissue damage could render Purkinje neurons more vulnerable. In fact, employing a repetitive blast model in mice (3 blasts at 19 psi over 24 h interval) chronic Purkinje cell loss and persistent synaptic disturbances occurred[12], which supports our tenet. Nevertheless, electrophysiological disturbances observed in the present study appear to be not due to neuronal loss.

Methods

Implant Surgery. Custom-design flexible multi-electrode arrays (E32_250_25_30_PML, NeuroNexus, MI) were implanted using sterile surgical techniques in 10 Long Evans rats (male, 250–275 g) one week prior to blast exposure. Data from 7 rats that were collected at matching time points in the post-injury period are presented here. All procedures were approved and performed in accordance to the guidelines of the Institutional Animal Care and Use Committee, Rutgers University, Newark, NJ. Anesthesia was induced using isoflurane (4% in 100% O_2) and maintained with lower doses of the same (1.5–2.5%). Dexamethasone sodium phosphate was administered (2 mg/kg, IM) before surgery to reduce cerebellar edema. A craniotomy of ~2 mm² was made over the right cerebellum (corner at 1.7 mm lateral from midline and 2.5 mm caudal from the posterior edge of the skull) in order to implant the flexible MEA subdurally on the paramedian lobule (PML). The platinum contacts (30 μm diam.) of the MEA had a pitch of 200 μm and 250 μm in AP and ML directions respectively in 4 × 10 configuration (Fig. 1). The MEA substrate was a thin polymer (polyimide, thickness 12 μm) and fabricated in a slightly curved shape to fit between the blood vessels without occluding them and cover most of the PML. Contact impedances varied between 800 kΩ–1.2 MΩ in saline prior to implantation and stabilized around 1–1.5 MΩ after the first week of surgery. A large reference electrode was incorporated into the MEA at one corner to suppress common-mode signals originating from subcortical locations within the cerebellum. The leftmost edge of the array was juxtaposed to the paravermal vein on the right PML. Trace amounts of octyl cyanoacrylate tissue adhesive (Nexaband, WPI, Inc., FL) was applied on the edges of the MEA to fix it on the pia surface before covering it with autologous connective tissue for sealing the dural opening. The micro connector at the end of the MEA ribbon cable was fixed to the skull using octyl cyanoacrylate first as an adhesive layer over the skull followed by dental acrylic.

Blast-Wave Injury. Seven to ten days were allowed for the animals to recover from the surgery and the evoked potentials to stabilize before the injury. Then, the rats were exposed to a single blast wave in a 6 m long shock tube with 9-inch square cross-section located in the Center of Injury Biomechanics, Materials and Medicine, NJIT[61]. The shock tube generates blast overpressure vs. time pulses that have been validated against live-fire explosions so that the experimental conditions reported here are both field-validated and realistic[62]. Rats were anesthetized with a cocktail of ketamine and xylazine (100 mg/10 mg/kg, IP) before mounting them inside the test chamber located 2.80 m from the point where the shock-wave was generated at one end of the tube and 3.05 m from its exit. The incident blast pressures, as measured near the test subject, varied between 110 and 130 kPa, had a duration of 5.7 ± 0.3 ms, and corresponding impulse values, i.e. the area under the overpressure curve, of 234 ± 27 Pa·s[63,64], animals were exposed to the blast in a horizontal head-on position while strapped to an aerodynamic aluminum holder with a thin cotton cloth wrapped around the body. By this experimental setting the gross head motion was eliminated almost entirely as confirmed by high-speed video recording. The high-speed videos were recorded on Photron FASTCAM Mini UX100 camera equipped with Tokina 100 mm f/2.8 macro lens and operating at a frame rate of 5000 fps. Typically, 8000 frames of video footage were recorded in a single experiment and subsequently saved via Photron FASTCAM Viewer 3.3.5 software. The incident overpressure was recorded at the location of the specimen in the test chamber using a LabView program running on a customized data acquisition system based on National Instruments PXI-6133 S-Series DAQ Module. The pressure waveform was recorded using PCB Piezotronics sensors model 134A24 (Depew, NY) at 1.0 MHz sampling frequency for a duration of 100 ms.

Electrophysiological Signals. This study utilized the sensory evoked potentials as a measure of electrophysiological intactness of the cerebellar cortex in a rat model. Sensory evoked potentials were elicited by a mechanical stimulation device, a 1 mm diameter cylindrical wood stick attached to the center of an audio speaker and activated by a short-pulse through a computer with milli-second accuracy. The control pulse was passed through a high-voltage solenoid driver circuit (SDM840, Magnetic Sensor Systems, CA) to achieve a fast and large displacement (3–4 mm) of the speaker coil. A train of mechanical stimuli (20 stimuli at 1 pps) were delivered to ipsilateral whiskers (not necessary the same one in each session) and the back of the hand to evoke local field potentials in the PML cortex of the cerebellum also under ketamine/xylazine anesthesia (30 mg/kg and 2 mg/kg, IP). The neural recordings were performed in a large Faraday cage through a 34-channel headstage amplifier (Gain 800, 0.8 Hz–3 kHz, Triangular Biosystems, NC). Signals were sampled at 16 kHz and filtered at 10 Hz-500 Hz in Matlab (Mathworks). Stimulus-triggered averaging (STA) was employed to suppress the background noise. Further details of electrophysiological methods were previously described elsewhere[30,37].

Characterization of EPs. Evoked potentials were characterized by amplitude (EPA) and latencies following the time of stimulus arrival, marked as 0 ms in Fig. 2A. Two different methods were followed for EPA quantification. First, we calculated the area under the curve (AUC) of any potential deflections that is above five times the standard deviation of the baseline activity in the post-stimulus time window, i.e. 0–50 ms (shaded areas of top right panel in Fig. 3A). Any signal component arriving 50 ms after the stimulus was discarded since these may be

the responses to the stimuli relayed through the brain centers outside the cerebellar network, such as those from the cerebral cortex[65,66].

In the second method, evoked volleys were first identified as either mossy fiber (MF) or climbing fiber (CF) mediated potentials based on the timing of their peaks (before or after 10 ms, left Figs 4–5). Then, it was determined whether the MF and CF volleys were significantly greater ($Z_{score} > 2.05$) than the baseline fluctuation. Those peak values that exceeded three times the background standard deviation was taken. If there was more than one volley for each type, only the largest deflection was included in the analysis. All quantitative measures used the EPAs normalized (nEPA) by the maximum EPA ever recorded before or after injury in that given animal.

Behavioral Testing. Three additional rats of the same size, strain, and gender as in the MEA implants were used for the behavioral testing. Walking on horizontal ladder rung (HLR) was chosen as the behavioral paradigm in order to investigate the impact of blast injury on the motor function. The HLR method is sensitive to the injury of the cerebellum[67]. The custom-designed ladder was assembled by 90×19 cm Plexiglas side walls that were separated by metal rungs of 3 mm diameter. The spacing between the rungs was set to 1 cm (regular) for habituation and 1–3 cm (irregular) in the training sessions. The ladder was elevated to 30 cm from the ground and two video cameras (220×330 pixels, 100 fps, Allied Vision) were installed to image the entire terrain while being able to see the hands and the feet without obstruction. Both ends of the ladder had a chamber where the animal could receive a food reward. During the first week, animals became accustomed to the environment and slowly learned to cross the ladder. Each rat had two ~10 min sessions per day for 7 days, at which point all animals learned to cross the ladder without hesitation. After this pre-training, the ladder rung pattern was changed by removing some of the rungs randomly and their walking was scored by counting the steps in which they missed the rung momentarily but corrected quickly (miss) or lost their balance before placing the hand correctly (fall). The same random rung pattern was used for all rats. Then, the animals were injured using a single blast wave at ~130 kPa, as in the other group of rats for electrophysiological recordings. Behavioral data collection sessions consisted of 10 crossings on each day of pre- and post-injury periods. The video recordings were analyzed frame-by-frame using VirtualDub software. The number of missed steps and falls were counted for each crossing and used for statistical analysis in IBM SPSS Statistics software.

Rotarod tests. We also performed rotarod performance test as an additional measure to investigate the effect of blast injury on motor function. A set of 12 rats were subjected to pretraining for 3 days twice daily (with 30 min resting period) to acclimate to the testing procedures before exposing the animals to blast injury. During the testing phase, rotarod was set in the accelerated mode with increasing number of revolutions from 4–40 rpm reaching within 90 s (2.5 s intervals for 1 rpm increment). The average time each rat spent on the rotarod during the 3-day pertaining was calculated and the values were statistically validated using nonparametric test to meet non-gaussian distribution to eliminate bias in the distribution of animals (with approximately equal latency times in control and experimental groups) before exposing the animals to blast injury. Rats were then exposed to blast injury and rotarod testing was performed at 24 hours, 3- and 7-days post-injury and results were expressed as mean ± SEM of latency time.

Immunohistochemistry. Three rats Long Evans rats (male, 250–275 g) were subjected to a single blast injury with 130 kPa peak overpressure and animals were euthanized 24 hours post-TBI for the immunological analysis. Three sham control rats of the same size, strain and gender received anesthesia and noise exposure but without blast exposure, i.e. anesthetized animals were placed next to the shock tube on the outside and then a single shot was fired. Following blast injury, animals were monitored closely for any signs of trauma-related distress such as apnea.

Immunofluorescence and microscopy. Twenty-four-hour and 7 days post-injury, both sham and TBI animals (4 animals in each group for 24 h study and 6 animals in each group for 7-day study) were transcardially perfused with PBS followed by 4% paraformaldehyde. Cerebella were dissected and post-fixed in 4% paraformaldehyde (PFA) for additional 48 h and cryoprotected by immersing in 30% sucrose. Fixed cerebellum was vertically cut into two halves and left half of the cerebellum from control or blast animals was embedded in OCT (Optimal Cutting Temperature) in sagittal orientation and quickly frozen in isopentane cooled to liquid nitrogen temperature. 15 μm thick slices were collected 3 mm from the surface of the embedded frozen cerebellum blocks, using Leica CM3050 cryostat and mounted on glass slides. At least 3 sections from each animal cut serially were mounted on each slide. Sections were washed with 10 mM phosphate buffered saline (PBS), fixed in ice-cold methanol (100%) solution for 10 min at −20 °C. The tissue sections were blocked with 10% donkey serum at room temperature for 1 hour in PBS containing 0.03% Triton X-100. Fixed tissues were incubated with anti-calbindin D-28K (rabbit polyclonal, Calbiochem, 1:300) or anti-cleaved caspase-3 (rabbit polyclonal, Millipore Inc, 1:100) overnight at 4 °C, followed by incubation (1 h) with Alexa Fluor 594 secondary antibody. We also performed a double immunostaining of calbindin D-28K (mouse monoclonal, Calbiochem, 1:400) and caspase-3 (Rabbit polyclonal, Millipore 1:100). The tissue was counterstained with DAPI (Invitrogen, Carlsbad, CA) to visualize cellular nuclei and facilitate quantification (cell count).

Image acquisition and analysis. Slides were digitized (40x magnification) using a Leica Aperio Versa 200 fluorescent microscope. For fluorescence intensity quantification, exposure times and grey scale balance were adjusted manually for each channel prior to scanning. Fluorescence intensity of calbindin D-28K cerebellar sections (2–3 in each slide) derived from 3 individual animals/group was quantitated using a FLAreaQuantV1 algorithm (Leica Biosystems) and expressed as average fluorescence intensity per unit area. Briefly, in each image, a minimum intensity threshold value was set that will exclude any background fluorescence caused by nonspecific binding of the fluorescent secondary antibody. This was followed by setting a maximum intensity threshold as

to remove any oversaturation due to excess fluorescent dye. The area quantification algorithm then determines if the intensity value of each pixel within the specified region falls between the minimum and maximum intensity thresholds. The algorithm outputs the area of positive stain for each brain region, the average intensity of each channel, and expression profile of the protein. For visualization of calbindin D-28K and caspase-3 positive cells, ImageJ software (NIH) was used. Briefly, color images were converted to gray scale and different regions of interest (ROIs, 10–15 random areas of approximately $4\,mm^2$ diameter) were drawn in the paramedian lobe, and the images were thresholded to separate background from particles of interest, in this instance, number of calbindin D-28K and caspase-3 positive particles which different ROIs with varying area were counted, averaged and represented as total number of cells/unit area.

Conclusions

The acute phases of injury were monitored *in vivo* using local field potentials recorded with chronically implanted micro-electrode arrays. The results demonstrate the sensitivity of the electrophysiological measures for detection of cerebellar injuries at levels of blast pressure that are not detectable by behavioral (ladder walking) or immunohistological assays. The two main findings are: First, the largest modulations of the EP amplitudes were seen within the first 24 hours after injury, which was followed by a slower pace of recovery period. Second, blast-wave injury produced differential effects both on the amplitudes and arrival times of the MF and CF mediated components. Taken together, we can conclude that micro EcoG method can identify subtle neurological changes triggered by mTBI conditions.

References

1. Slemmer, J. E., Matser, E. J., De Zeeuw, C. I. & Weber, J. T. Repeated mild injury causes cumulative damage to hippocampal cells. *Brain* **125**, 2699–2709 (2002).
2. Bramlett, H. M. & Dietrich, W. D. Progressive damage after brain and spinal cord injury: pathomechanisms and treatment strategies. *Prog. Brain Res.* **161**, 125–141 (2007).
3. Marklund, N., Bakshi, A., Castelbuono, D. J., Conte, V. & McIntosh, T. K. Evaluation of pharmacological treatment strategies in traumatic brain injury. *Curr. Pharm. Des.* **12**, 1645–1680 (2006).
4. Thompson, H. J. *et al.* Lateral fluid percussion brain injury: a 15-year review and evaluation. *J. Neurotrauma* **22**, 42–75 (2005).
5. Adamaszek, M. *et al.* Consensus Paper: Cerebellum and Emotion. *Cerebellum (London, England)* (2016).
6. Schmahmann, J. D. & Sherman, J. C. The cerebellar cognitive affective syndrome. *Brain: A Journal of Neurology* **121**(Pt 4), 561–579 (1998).
7. Basford, J. R. *et al.* An assessment of gait and balance deficits after traumatic brain injury. *Arch Phys Med Rehabil* **84**, 343–349 (2003).
8. Braga, L. W., Souza, L. N., Najjar, Y. J. & Dellatolas, G. Magnetic resonance imaging (MRI) findings and neuropsychological sequelae in children after severe traumatic brain injury: the role of cerebellar lesion. *Journal of Child Neurology* **22**, 1084–1089 (2007).
9. Kuhtz-Buschbeck, J. P. *et al.* Sensorimotor recovery in children after traumatic brain injury: analyses of gait, gross motor, and fine motor skills. *Developmental Medicine and Child Neurology* **45**, 821–828 (2003).
10. Louis, E. D. *et al.* Delayed-onset cerebellar syndrome. *Archives of Neurology* **53**, 450–454 (1996).
11. Mautes, A. E., Fukuda, K. & Noble, L. J. Cellular response in the cerebellum after midline traumatic brain injury in the rat. *Neuroscience Letters* **214**, 95–98 (1996).
12. Meabon, J. S. *et al.* Repetitive blast exposure in mice and combat veterans causes persistent cerebellar dysfunction. *Science Translational Medicine* **8**, 321ra326 (2016).
13. Miller, D. R., Hayes, J. P., Lafleche, G., Salat, D. H. & Verfaellie, M. White matter abnormalities are associated with overall cognitive status in blast-related mTBI. *Brain Imaging Behav* (2016).
14. Przekwas, A., Somayaji, M. R. & Gupta, R. K. Synaptic Mechanisms of Blast-Induced Brain Injury. *Front. Neurol.*, 2 (2016).
15. Taber, K. H. *et al.* White matter compromise in veterans exposed to primary blast forces. *J Head Trauma Rehabil* **30**, E15–25 (2015).
16. Taber, K. H., Warden, D. L. & Hurley, R. A. Blast-Related TraumaticBrain Injury: What Is Known? *JNP* **18**, 141–145 (2006).
17. Hallam, T. M. *et al.* Comparison of behavioral deficits and acute neuronal degeneration in rat lateral fluid percussion and weight-drop brain injury models. *J. Neurotrauma* **21**, 521–539 (2004).
18. Park, E., McKnight, S., Ai, J. & Baker, A. J. Purkinje cell vulnerability to mild and severe forebrain head trauma. *Journal of Neuropathology and Experimental Neurology* **65**, 226–234 (2006).
19. Sato, M., Chang, E., Igarashi, T. & Noble, L. J. Neuronal injury and loss after traumatic brain injury: time course and regional variability. *Brain Res.* **917**, 45–54 (2001).
20. Ai, J. & Baker, A. Presynaptic hyperexcitability at cerebellar synapses in traumatic injury rat. *Neurosci Lett* **332**, 155–158 (2002).
21. DeKosky, S. T., Ikonomovic, M. D. & Gandy, S. Traumatic Brain Injury — Football, Warfare, and Long-Term Effects. *New England Journal of Medicine* **363**, 1293–1296 (2010).
22. Kershman, J., Elvidge, A. & Jasper, H. H. Electroencephalographic studies of injury to the head. *Archives of Neurology & Psychiatry* **328**, 44 (1940).
23. Williams, D. The Electro-encephalogram in acute head injuries. *Journal of Neurology and Psychiatry* **4**, 107–130 (1941).
24. D'Ambrosio, R. *et al.* Progression from frontal-parietal to mesial-temporal epilepsy after fluid percussion injury in the rat. *Brain* **128**, 174–188 (2005).
25. Sanders, M. J., Dietrich, W. D. & Green, E. J. Behavioral, electrophysiological, and histopathological consequences of mild fluid-percussion injury in the rat. *Brain Res* **904**, 141–144 (2001).
26. Witgen, B. M. *et al.* Regional hippocampal alteration associated with cognitive deficit following experimental brain injury: a systems, network and cellular evaluation. *Neuroscience* **133**, 1–15 (2005).
27. Reeves, T. M., Zhu, J., Povlishock, J. T. & Phillips, L. L. The effect of combined fluid percussion and entorhinal cortical lesions on long-term potentiation. *Neuroscience* **77**, 431–444 (1997).
28. Miyazaki, S. *et al.* Enduring suppression of hippocampal long-term potentiation following traumatic brain injury in rat. *Brain Res* **585**, 335–339 (1992).
29. Ai, J. & Baker, A. Presynaptic excitability as a potential target for the treatment of the traumatic cerebellum. *Pharmacology* **71**, 192–198 (2004).
30. Ordek, G., Proddutur, A., Santhakumar, V., Pfister, B. J. & Sahin, M. Electrophysiological monitoring of injury progression in the rat cerebellar cortex. *Frontiers in Systems Neuroscience* **8**, 197 (2014).
31. Watase, K. *et al.* Motor discoordination and increased susceptibility to cerebellar injury in GLAST mutant mice. *Eur J Neurosci* **10**, 976–988 (1998).
32. Culic, M. *et al.* Spectral analysis of cerebellar activity after acute brain injury in anesthetized rats. *Acta neurobiologiae experimentalis* **65**, 11–17 (2005).

33. Thatcher, R. W., Walker, R. A., Gerson, I. & Geisler, F. H. EEG discriminant analyses of mild head trauma. *Electroencephalography and clinical neurophysiology* **73**, 94–106 (1989).
34. Sankar, V. *et al*. Electrode impedance analysis of chronic tungsten microwire neural implants: understanding abiotic vs. biotic contributions. *Frontiers in neuroengineering* **7**, 13 (2014).
35. Liu, X. *et al*. Stability of the interface between neural tissue and chronically implanted intracortical microelectrodes. *IEEE transactions on rehabilitation engineering: a publication of the IEEE Engineering in Medicine and Biology Society* **7**, 315–326 (1999).
36. Polikov, V. S., Tresco, P. A. & Reichert, W. M. Response of brain tissue to chronically implanted neural electrodes. *Journal of neuroscience methods* **148**, 1–18 (2005).
37. Ordek, G., Groth, J. D. & Sahin, M. Differential effects of ketamine/xylazine anesthesia on the cerebral and cerebellar cortical activities in the rat. *Journal of Neurophysiology* **109**, 1435–1443 (2013).
38. Apps, R. & Garwicz, M. Anatomical and physiological foundations of cerebellar information processing. *Nature Reviews Neuroscience* **6**, 297–311 (2005).
39. Dietrichs, E. The cerebellar corticonuclear and nucleocortical projections in the cat as studied with anterograde and retrograde transport of horseradish peroxidase: IV. The paraflocculus. *Experimental Brain Research* **44** (1981).
40. Ji, Z. & Hawkes, R. Topography of purkinje cell compartments and mossy fiber terminal fields in lobules ii and iii of the rat cerebellar cortex: Spinocerebellar and cuneocerebellar projections. *Neuroscience* **61**, 935–954 (1994).
41. Shambes, G. M., Gibson, J. M. & Welker, W. Fractured Somatotopy in Granule Cell Tactile Areas of Rat Cerebellar Hemispheres Revealed by Micromapping; pp. 116–140. *Brain, Behavior and Evolution* **15**, 116–140 (2008).
42. Mehler, W. R. & Nauta, W. J. Connections of the basal ganglia and of the cerebellum. *Confin Neurol* **36**, 205–222 (1974).
43. Oscarsson, O. Functional Organization of Spinocerebellar Paths, In *Somatosensory System*, Vol. 2. (ed. Iggo, A.) 339–380 (Springer Berlin Heidelberg, Berlin, Heidelberg; 1973).
44. Jörntell, H., Ekerot, C., Garwicz, M. & Luo, X. L. Functional organization of climbing fibre projection to the cerebellar anterior lobe of the rat. *The Journal of Physiology* **522**(Pt 2), 297–309 (2000).
45. Zucca, R., Rasmussen, A. & Bengtsson, F. Climbing Fiber Regulation of Spontaneous Purkinje Cell Activity and Cerebellum-Dependent Blink Responses. *eNeuro* **3** (2016).
46. Awwad, H. O. *et al*. Blast Overpressure Waves Induce Transient Anxiety and Regional Changes in Cerebral Glucose Metabolism and Delayed Hyperarousal in Rats. *Frontiers in Neurology* **6** (2015).
47. Myers, P., Wilmington, D., Gallun, F., Henry, J. & Fausti, S. Hearing Impairment and Traumatic Brain Injury among Soldiers: Special Considerations for the Audiologist. *Seminars in Hearing* **30**, 005–027 (2009).
48. Scherer, M. R. & Schubert, M. C. Traumatic Brain Injury and Vestibular Pathology as a Comorbidity After Blast Exposure. *Physical Therapy* **89**, 980–992 (2009).
49. Eccles, J. C., Hubbard, J. I. & Oscarsson, O. Intracellular recording from cells of the ventral spinocerebellar tract. *The Journal of Physiology* **158**, 486–516 (1961).
50. Eccles, J., Llinas, R. & Sasaki, K. Excitation of cerebellar purkinje cells by the climbing fibres. *Nature* **203**, 245–246 (1964).
51. Armstrong, D. M., Harvey, R. J. & Schild, R. F. Climbing fibre pathways from the forelimbs to the paramedian lobule of the cerebellum. *Brain Research* **25**, 199–202 (1971).
52. Armstrong, D. M. & Drew, T. Responses in the posterior lobe of the rat cerebellum to electrical stimulation of cutaneous afferents to the snout. *The Journal of Physiology* **309**, 357–374 (1980).
53. Bengtsson, F. & Jörntell, H. Ketamine and xylazine depress sensory-evoked parallel fiber and climbing fiber responses. *Journal of Neurophysiology* **98**, 1697–1705 (2007).
54. Ding, M.-C., Wang, Q., Lo, E. H. & Stanley, G. B. Cortical excitation and inhibition following focal traumatic brain injury. *J. Neurosci.* **31**, 14085–14094 (2011).
55. Alwis, D. S., Yan, E. B., Morganti-Kossmann, M.-C. & Rajan, R. Sensory cortex underpinnings of traumatic brain injury deficits. *PloS One* **7**, e52169 (2012).
56. Palay, S. L. & Chan-Palay, V. The Purkinje Cell, in *Cerebellar Cortex* 11–62 (Springer Berlin Heidelberg, Berlin, Heidelberg; 1974).
57. Manto, M. *et al*. Consensus Paper: Roles of the Cerebellum in Motor Control—The Diversity of Ideas on Cerebellar Involvement in Movement. *The Cerebellum* **11**, 457–487 (2012).
58. Mauk, M. D., Medina, J. F., Nores, W. L. & Ohyama, T. Cerebellar function: coordination, learning or timing? *Curr. Biol.* **10**, R522–525 (2000).
59. Joyal, C. C. *et al*. Effects of midline and lateral cerebellar lesions on motor coordination and spatial orientation. *Brain Research* **739**, 1–11 (1996).
60. Binion, D. J., Keller, S. B., Ordek, G. & Sahin, M. In Annual Meeting of Biomedical Engineering Society (San Antonio, TX; 2014).
61. Kuriakose, M. *et al*. Tailoring the Blast Exposure Conditions in the Shock Tube for Generating Pure, Primary Shock Waves: The End Plate Facilitates Elimination of Secondary Loading of the Specimen. *PLoS One* **11**, e0161597 (2016).
62. Chandra, N., Sundaramurthy, A. & Gupta, R. K. Validation of Laboratory Animal and Surrogate Human Models in Primary Blast Injury Studies. *Military medicine* **182**, 105–113 (2017).
63. Mishra, V. *et al*. Primary blast causes mild, moderate, severe and lethal TBI with increasing blast overpressures: Experimental rat injury model. *Scientific reports* **6**, 26992 (2016).
64. Skotak, M. *et al*. Rat injury model under controlled field-relevant primary blast conditions: acute response to a wide range of peak overpressures. *Journal of neurotrauma* **30**, 1147–1160 (2013).
65. Watson, T. C. Electrophysiological mapping of novel prefrontal - cerebellar pathways. *Frontiers in Integrative Neuroscience* **3** (2009).
66. Watson, T. C., Becker, N., Apps, R. & Jones, M. W. Back to front: cerebellar connections and interactions with the prefrontal cortex. *Frontiers in Systems Neuroscience* **8** (2014).
67. Van Der Giessen, R. S. *et al*. Role of olivary electrical coupling in cerebellar motor learning. *Neuron* **58**, 599–612 (2008).

Acknowledgements

Author Contributions

Ma.S. and G.O. carried out blast exposure experiments, G.O. and A.S.A. performed electrophysiological and behavioral tests, E.C., A.S.A. and V.R.K. performed histological evaluation, N.C. and Me.S. designed the study and critically evaluated the data, G.O., A.S.A., Me.S., Ma.S., V.R.K. and N.C. wrote the manuscript, Me.S. supervised the execution the experiments. All authors read and approved the final version of manuscript.

Additional Information

Competing Interests: The authors declare no competing interests.

Publisher's note: Springer Nature remains neutral with regard to jurisdictional claims in published maps and institutional affiliations.

Molecular Neurobiology

Microglia Receptors in Traumatic Brain Injury
--Manuscript Draft--

Manuscript Number:	
Full Title:	Microglia Receptors in Traumatic Brain Injury
Article Type:	Reviews
Keywords:	Microglia; brain injury; receptors; Fractalkine receptor; Purinergic receptor; Toll-like receptor; Tumor necrosis factor receptor; Interleukin receptor; Peroxisome proliferator-activated receptor
Corresponding Author:	Namas Chandra New Jersey Institute of Technology Newark, NJ UNITED STATES
Corresponding Author Secondary Information:	
Corresponding Author's Institution:	New Jersey Institute of Technology
Corresponding Author's Secondary Institution:	
First Author:	Daniel Younger, B.S.
First Author Secondary Information:	
Order of Authors:	Daniel Younger, B.S.
	Madhuvika Murugan
	Kakulavarapu V Rama Rao, Ph.D
	Long-Jun Wu, Ph.D
	Namas Chandra, Ph.D
Order of Authors Secondary Information:	

Abstract:	Microglia have been implicated as the primary contributors of chronic inflammation following traumatic brain injury (TBI). The animal models of TBI vary significantly based on the type of brain injury (focal versus diffuse). This has made it extremely difficult to assess the role of microglia and the window of microglia activation. Hence, the focus of this review is to summarize the time course of microglia activation in various animal models of TBI. The review explores the repertoire of secondary injury mechanisms such as aberrant neurotransmitter release, oxidative stress, blood brain barrier disruption and neuroinflammation that follow microglia activation. Since receptors act as sensors for activation, we highlight certain microglia receptors that have been implicated in TBI pathology, including Fractalkine receptor (CX3CR1), Purinergic receptor (P2Y12R), Toll-like receptor (TLR4) and Tumor necrosis factor receptor (TNF-1R), Interleukin receptor (IL-1R) and Peroxisome proliferator-activated receptor (PPAR). In addition to describing their downstream signaling pathways in TBI, we describe the functional consequences of their activation and the implication in behavioral outcomes. Further, we discuss classical, as well as recently developed techniques used to investigate microglia receptors. Taken together, this review will provide a holistic view of the role of microglia in TBI based on animal studies.

Microglia Receptors in Traumatic Brain Injury

Daniel Younger[1#], Madhuvika Murugan[1#], Kakulavarapu V. Rama Rao, Long-Jun Wu[2] and Namas Chandra[1*]

[1]Department of Bioengineering, New Jersey Institute of Technology, Newark, NJ 07102

[2]Department of Neurology, Mayo Clinic, Rochester, MN 55905

# Equally contributed

* Corresponding Author

Abbreviated Title: Microglia in TBI

Text Pages: 15, **Figures**: 3, **Tables:** 1, **Supplementary table**: 1

Keywords: Microglia, brain injury, receptors.

Word Count: Abstract -200; Text- 7400

Conflict of Interest: The authors declare no competing financial interests.

*Correspondence:

Dr. Namas Chandra

Dept. of Bioengineering

New Jersey Institute of Technology

111 Lock Street, Room105 CHEN bldg, Newark, NJ 07102

TEL: (732) 445-2182;

FAX: (732) 445-5870

E-MAIL: namas.chandra@njit.edu

Abstract

Microglia have been implicated as the primary contributors of chronic inflammation following traumatic brain injury (TBI). The animal models of TBI vary significantly based on the type of brain injury (focal versus diffuse). This has made it extremely difficult to assess the role of microglia and the window of microglia activation. Hence, the focus of this review is to summarize the time course of microglia activation in various animal models of TBI. The review explores the repertoire of secondary injury mechanisms such as aberrant neurotransmitter release, oxidative stress, blood brain barrier disruption and neuroinflammation that follow microglia activation. Since receptors act as sensors for activation, we highlight certain microglia receptors that have been implicated in TBI pathology, including Fractalkine receptor (CX3CR1), Purinergic receptor (P2Y12R), Toll-like receptor (TLR4) and Tumor necrosis factor receptor (TNF-1R), Interleukin receptor (IL-1R) and Peroxisome proliferator-activated receptor (PPAR). In addition to describing their downstream signaling pathways in TBI, we describe the functional consequences of their activation and the implication in behavioral outcomes. Further, we discuss classical, as well as recently developed techniques used to investigate microglia receptors. Taken together, this review will provide a holistic view of the role of microglia in TBI based on animal studies.

Introduction

Traumatic brain injury (TBI) is one of the leading causes of mortality and morbidity around the world. In 2013, in the US alone there were about 2.8 million emergency room visits, among which there were 282,000 hospitalizations, and 56,000 deaths related to TBI. The three leading causes of TBI related hospitalizations include falls (47%), impact by striking objects (15%), and automobile accidents (14%) [1]. TBI accounts for approximately 30.5% of all injury-related deaths in the US. Over the past decade, there has been a sharp increase in incidents of TBI resulting from combat related injuries as well as insurgent activities on civilian population [2] . In 2010, the direct medical costs of TBI was 76.5 billion dollars [3]. Although there has been a lot of effort focusing on treatment modalities for TBI, there has not been much success in developing a therapeutic strategy to treat TBI-associated deficits. Accordingly, over 30 stage III clinical trials failed to show significant improvement in TBI patients [4]. This is probably due to lack of clear understanding of the secondary mechanisms in the evolution of injury pathology and due to highly heterogeneous nature of TBI phenotype[4]. This has led scientists and researchers to look for novel methods to delay and prevent TBI induced pathology.

Microglia are the immune cells in the brain and have been implicated in pathogenesis following TBI. In this review, we highlight the response of microglia to injury, specifically, the involvement in secondary injury mechanisms such as neurotransmitter release, oxidative stress, and blood brain barrier (BBB) breakdown after TBI. We then describe some of the receptors that are known to be critical in microglia activation and response following TBI. Moreover, we provide a brief summary of the tools and techniques that are used to study microglia receptors.

Microglia response to brain injury

Microglia constantly survey the central nervous system (CNS) microenvironment for any changes in homeostasis using their highly motile processes. In their resting state, microglia possess a rod shaped soma with processes extending out symmetrically in all direction [5]. Processes are motile with an average extension and retraction rate of 1.47 μm per minute and ranging from 0.4 and 3.8 μm per minute, respectively. Upon microglia activation a series of characteristic morphological changes occur. Usually, the motility change of their processes from undirected to targeted movement towards the injury site [5]. The processes begin to retract and the soma enlarges and become spherical in shape [6]. Finally microglia begin to migrate to the site of injury at a rate of 1-2 μm per hour [5].

Classically, microglial activation was categorized as M1 (proinflammatory) state or M2 (anti-inflammatory) state [7]. The M1state is initiated by events such as TBI, wherein, the microglia synthesize and release excess superoxide, nitric oxide, proinflammatory cytokines and chemokines. Although, the secretion of these compounds by microglia are primarily for host defense, often an exaggerated response follows an insult resulting in by-stander injury of the surrounding tissue [8]. When in M2 state, microglia produces anti-inflammatory cytokines (IL-4, IL-10, IL-13, IL-18) which promotes matrix remodeling, angiogenesis, tissue repair and

regeneration among other functions [9]. Recent studies have shown that activated microglia can exist in both states simultaneously where individual cells produce danger associated molecular patterns (DAMPS) or pathogen associated molecular patterns (PAMPS) [10].

There are currently 4 major animal models used to simulate the heterogeneous pathology of human TBI. These include weight drop injury (WD), control cortical impact injury, (CCI), fluid percussion injury (FPI), and blast / diffuse brain injury [11]. The WD model mimics closed head injuries frequently associated with falls, dropping of heavy objects in construction sites which lead to cerebral contusions found in TBI. It is performed by dropping a weight from a predetermined height onto the skull or exposed dura. In a modified version of WD model, also known as the closed head injury model, a metal plate is placed above the skull to distribute weight over a larger area and prevent skull fracture. WD model in mice showed signs of diffuse neuronal loss, neuroinflammation, markers of apoptosis, and short and long term cognitive impairments [12].Similar to the WD model CCI injury uses a solid impactor to damage exposed dura. To increase the reproducibility of the injury a pneumatic or electrochemical device is used. This mechanism also reduces rebound injury produced by gravity driven devices [13]. By adjusting location, shape of impactor, velocity, and the depth of brain deformation different types of injuries can be produced. CCI injuries are typically manifest as cortical tissue loss, axonal injury, BBB dysfunction, and/ or subdural hematoma [14-17].

In FPI injury model, a craniotomy is performed to expose a portion of the dura. The injury is inflicted by directing a fluid pulse, produced by a pendulum striking a piston of fluid reservoir, against the exposed dural surface [13]. The injury model is characterized by a locally diffuse injury producing vascular and axonal damage and produces an amalgamation of cortical contusion and diffuse subcortical neuronal injury [11]. Studies have varied the location of injury site, but most commonly, the injury is performed lateral to the sagittal suture (LFPI) or medially (CFPI) [13]. The blast/ diffuse injury attempts to replicate the shockwaves from explosive devices to cause a diffuse brain injury. To recreate the Freelander waveform produced in explosion either live explosives or gas driven shock tubes are used. Blast/ diffuse injury is characterized by diffuse cerebral brain edema, extreme hyperemia, a delayed vasospasm, and diffuse axonal injury [2, 18].

Microglia activation follows a different temporal pattern depending upon the type and severity of brain injury (**Figure 1**). CCI and FPI are the most studied among different injury mechanisms and therefore microglia activity state have been thoroughly investigated. Markers such arginase (Arg-1)[19], CD206[20, 21], and YM-1[20, 22] are used to identify M2 activated microglia versus CD16[20], CD 86[20, 21], which are markers for M1 activated microglia. In TBI models such as blast and weight drop only the time profile of microglia activation have been studied. For instance, following CCI injury M2 like microglia increase in the first week following injury. The number of M2 microglia peak at 5 days post injury but decreases rapidly in number immediately afterwards [21, 23]. M1 microglia begin to increase in the cortex, striatum and corpus callosum at 1 week [23], peaking at 4 weeks following injury [21]. M2 type microglia predominate in the acute phase of injury while the M1 phase of microglia remain during the chronic phase after focal injury produced by CCI. Similar to focal injury, diffuse injury produced

by FPI induced transient activation of M2 type of microglia that resolved within 7 days after injury, whereas, M1 type microglia remained in their activated amoeboid morphology for up to 30 days following injury [23].

It is interesting to note that microglia activation patterns differ not only temporally but also spatially following brain injury. The spatial variability in microglia response to injury may depend upon regional differences in mechanical loading and/ or the intrinsic property of the tissue. Despite the limited studies on mechanical signaling in microglia, a recent study showed cultured microglia cells were susceptible to mechanical changes [24]. In line with this, another study showed that mechanical loading was capable of modulating microglia proliferation, activation and chemotaxis [25]. The response of microglia to injury may also depend on the intrinsic property of the tissue such as microglia/ blood vessel distribution and neuronal vulnerability within the region. There is a lower occurrence of microglia in grey matter areas compared to the white matter. Regionally, the lowest of occurrence is the cerebellum (0.3%), frontal (4.7%), parietal (3.6%) and occipital (2.9%) lobes of the cerebrum with highest expression levels in the white matter track of the medulla oblongata (16.9%) [26]. A recent study showed that microglia activation paralleled the pattern of neuronal loss in a mouse model of CCI injury [27] which is in line with another study that observed prominent occurrence of activated microglia in regions of neuronal loss including the ipsilateral cortex, hippocampus, and thalamus after injury [28]. In a blast model of brain injury, microglia activation was found to be closely associated around the blood vessels suggesting that the difference in the distribution of microglia and blood vessels may underlie some of the regional vulnerabilities to injury [6].

Microglia mediated secondary mechanisms in brain injury

Depending on the type of TBI, the secondary injury may involve a wide array of mechanisms including oxidative stress, neuroinflammation, BBB disruption, cell death, mitochondrial dysfunction and neurotransmitter release [29, 30]. Studies conducted thus far, have reported the involvement of microglia receptor activation in not only altering microglia morphology and motility, but also in neurotransmitter release, modulating neuron-glia synaptic transmission, secretion of cytokines, generation of reactive oxygen species and production of nitric oxide. Here, we summarize the microglia mediated secondary mechanisms following brain injury.

Aberrant neurotransmitter release

Activated microglia contribute to neuronal excitotoxicity by releasing neurotransmitters in response to several external stimuli. The known neurotransmitters released by microglia include glutamate and ATP. Glutamate release by microglia can be triggered by activation through multiple receptor systems. For instance, microglia release of glutamate may be induced by secreted amyloid precursor protein (APP) [31] or amyloid β [32]. Similarly, TNF-α can induce the release of glutamate by up regulating glutaminase. Microglia are capable of releasing sufficient amount of glutamate to contribute to neural degeneration [33]. Such excess release of glutamate has been reported following ischemic brain injury [34]. However, there has been no study investigating the microglia release of glutamate in TBI models. The excess glutamate may

activate pre and post-synaptic glutamate receptors in neurons leading to excitotoxicity. Alternatively, they can activate microglia glutamate receptors including AMPA receptor [35-37], metabotropic glutamate receptors [38-41] and NMDAR [42-44], resulting in a cascade of secondary events.

Adenosine triphosphate (ATP) is the other commonly released neurotransmitter by microglia. ATP release from microglia cells can be induced by bacterial endotoxin lipopolysaccharide (LPS) [45, 46]. Lysophosphatidic acid (LPA) induces the release of ATP via activation of the LPA_3 receptor [47]. High intracellular calcium levels have been shown to induce ATP release in microglia [48]. Extracellular ATP was shown to enhance radiation-induced brain injury through microglial activation and paracrine signaling via P2X7 receptor [49]. Microglia abundantly express ATP-mediated purinergic receptors. Although the ATP release by in brain injury has not been shown, the microglia response via purinergic signaling has been well-studied in brain injury models [50]. The purinergic receptors in microglia are abundant and are implicated in important functions such as cytokine production (P2X receptors), motility (P2Y12 receptor) and in phagocytosis (P2Y6 receptors) [51-53]. The expression and function of these receptors in neuronal/glial cells in neuropathologies have been reviewed previously [54] and their role in TBI and is worthy of investigation.

Oxidative stress

Under normal physiological conditions there is a delicate balance between reactive oxygen/ nitrogen species (ROS/ RNS) and their removal via antioxidants. Following TBI, the balance can be disrupted leading to an excess buildup of ROS [55, 56]. Accumulation of ROS/RNS is known to mediate cellular damage via lipid peroxidation, protein modification, and/or DNA strand breaks [57]. Activated microglia produce superoxide by the enzymatic activity of NADPH oxidase (NOX), a multi-subunit enzyme that catalyzes the production of superoxide from oxygen [58]. Microglia, like all phagocytic cells express NOX2 [59]. NOX 2 generates superoxide molecules which help in the neutralization of foreign pathogens [60]. It was shown that NOX2 mediated ROS production was strongly upregulated in M1 but not M2 polarized microglia in CCI injury. Inhibiting NOX2, by using selective peptide inhibitor gp91ds-tat or NOX2 knockout mice, reduced markers for M1 activated microglia, limited tissue loss, and improved motor recovery. Inhibition of NOX2 also promoted M2 like activation in microglia [61]. In FPI injury, inhibition of NOX with apocyanin had no effect on neuromotor function but reduced the release the proinflammatory cytokines IL-1β, and TNF-α at 3 and 24 h after injury [62]. Recently, it was shown that NOX2 expression was increased at 24 h after moderate blast injury (180 kPa) and this directly correlated with elevated ROS production [63]. Activation of cytokine receptors such as IL-2R [64, 65], IL-15R [66], TNFR1 [67], INF-γR and thrombin receptor [68] in microglia have also been implicated in ROS production. ROS production by microglia may also be mediated by Notch-1 receptor [69, 70], dopamine receptor D_1, D_2 [71, 72], and Angiotensin II receptor [73].

BBB disruption

The CNS vasculature differs from the rest of the vasculature in that it has intricate connections and innervations with neural cells particularly astrocytes (astrocyte end feet), pericytes and

microglia to form the functional BBB, a specialized structure that selectively separates the brain parenchyma from the peripheral blood. Studies on the interaction between microglia and BBB in both physiological and pathological conditions are limited and have recently gained more attention [74, 75]. The perivascular microglia communicate with the ECs and survey the influx of blood-borne components into the CNS. Hence, any disruption of the BBB as reported following brain injury, can prime, and attract microglia [6].

Microglia activation dependent alterations to BBB after TBI is thought to be predominantly mediated by neuroinflammation and oxidative stress [76-78]. Therefore, most TBI studies that investigate both microglia activation and BBB disruption focus on shifting microglia from their proinflammatory M1state to their anti-inflammatory M2 state. For instance, following CCI injury binding of 2 arachidonylglycerol (2-AG) (agonist) to the cannabinoid receptor in microglia shifted microglia at 3 and 7 days from M1 to M2 activated phenotypes. This shift in activation was coupled with the reduction of BBB permeability at the same time point [79]. Reduction in the release of pro-inflammatory cytokines and reduction of inducible ROS production prevented further degradation of BBB [79]. Pretreatment with apocynin (NOX inhibitor) prevented BBB disruption following WD injury [80] , as well as in blast injury model [81]. Microglia as the major source of NOX mediated ROS production are implicated as the cause for the increase permeability of the BBB following injury [80]. In a mouse model of mild blast injury, microglia activation was restricted to regions close to the blood vessel microdomains, as evidenced by rapid microglial process retraction and increased amoeboid morphology [6]. Taken together, these TBI studies confirm that there is a close association between microglia activation and BBB disruption and vice-versa following injury.

Neuroinflammation

Neuroinflammation is one of the key mediators of secondary injuries following brain injury. The acute response includes secretion of pro-inflammatory cytokines within minutes following injury. The activation of resident microglial cells, alongside the infiltration of peripheral macrophages, are key mediators of neuroinflammatory responses after TBI. Several studies have attempted to discriminate the differential roles of resident microglia and infiltrated monocytes after brain/ spinal cord injury [82-84]. In this review, we highlight the contribution of microglia to inflammation, however, the role of infiltrating monocytes/ macrophages in neuroinflammation and overall TBI pathology cannot be overlooked.

Upon the detection of foreign macromolecules such as DAMPS/PAMPS, microglia can release a wide range of cytokines and chemokines. These molecules guide the expression of adhesion molecules, signal peripheral immune cells to infiltrate the injury site, and further release of pro-inflammatory mediators and growth factors that regulate neuronal death or regeneration [85]. Many studies have investigated cytokines and chemokines expression following TBI. These studies have focused on levels of cytokines found in homogenized tissue section or CSF. These studies attribute the increased expression of cytokine to the activity of activated microglia. This assertion may be correct, but microglia's contribution to the inflammatory environment is unlikely to be exclusive [86].

Following CCI injury, levels of IL-1β and IL-18 increased in brain homogenates surrounding the contusion site. Levels of IL-1β peaked at 6 h post injury and decreased to control level by 7 days.

IL-18 levels gradually increased over the 7 d observation period. Microglia specific release was confirmed by colocalization of NLRP-3 inflammasome and its associated components (ASC and caspase1) in microglia cells but not with astrocytes or neurons [87]. Chio et al found that administration of Etanercept, a TNF-α receptor antagonist, attenuated the release of TNF-α following FPI leading to reduced motor and neurological deficits as compared to the control and saline treated groups. At 72 hours after injury, TNF-α secreted by microglia increased in ischemic cortex, white matter, hippocampus, and hypothalamus. Double immunostaining confirmed that neuronal and astrocytic TNF-α levels were not significantly different between control, saline and etanercept treated groups leading to the conclusion that microglia was the prominent source of TNF-α production following diffuse TBI [88].

Bachstetter et al showed that p38α (MAPK14) protein kinase plays a role in the production of TNF-α and IL-1β by cultured microglia cells [89]. Using midline FPI model they investigated whether myeloid specific deletion of p38α influenced microglia cytokine production following injury. Unexpectedly they found that during the acute phase (0-12 h), release of IL-1β, IL-6, and TNFα was greater in the p38α knockout (KO) compared to the wild type injured animal. This increase could not be accounted for by the increase in infiltrating immune cells (macrophages and neutrophils) or by astrogliosis, as cell number were decreased in the KO animals relative to the WT. In the chronic phase (7 d), levels of IL-1 were significantly reduced in the p38α KO animals as compared to the WT injured animals. These findings suggest that microglia may not contribute significantly to inflammation in the acute phase but is responsible for the pro-inflammatory environment found in the chronic phase of injury [90].

Microglia release proinflammatory cytokines such as IL-1β upon ligand binding to the NMDAR [42], angiotensin II receptor [73], and IFN-γR [85]. Release of TNF-α has been reported upon activation of AMPA receptor [35, 36], NMDAR [42], kainate receptor [37, 43], metabotropic glutamate receptor [39, 41, 91, 92] α_{1a}, α_{2a}, β_1 adrenergic receptor [93], IFN-γR [85], TLR2 [94], TLR3 [95], TLR9 [96], CD-14 [97] and thrombin receptors [97]. Release of IL-6 upon GABAR [98] α_{1a}, α_{2a}, $\beta_1$adrenergic receptor [93], TNFR1 [99], IFN-γ [85], IL-1R1 [100], TLR2 [94], TLR3 [95], TLR5 [96], TLR9 [96], CD-14 [97], Thrombin receptor [68] activation. Release of IL-12 was noted upon activation of GABAR [98], IFNγR [101], TLR3 [95], TLR9 [96], CD-14 [97], and thrombin receptors [68].

Microglia are also capable of releasing chemokines such as release of CCL2 upon IFN-γR [101] TLR2 [94] activation. Release of CCL3 upon IL-13R [102, 103] CD-14 activation. Release of CCL5 upon IL-3R [102, 103] activation Release of CXCL-10 upon TLR3 [95] and TLR4 [95] activation. Release of CXCL2 upon CD-14 [97] activation. Once released these factors affect adjacent cells such as astrocytes and/or neurons in a paracrine manner since these cells possess receptors for these factors. Additionally, these factors could also affect microglia in an autocrine manner. In both scenarios the net effect exerted by these factors include lipid peroxidation, immune cell recruitment, BBB disruption, and the development of cerebral edema [104-106]

Microglial Receptors in brain injury

The microglia express a repertoire of receptors which act as sensors for specific ligands in the neuronal parenchyma. A comprehensive list of receptors expressed in microglia, the known

receptor agonists/ antagonists, their physiological function and the functional relevance of receptor activation is provided in **Supplementary Table 1**. Although many receptors have been indicated to be part of microglia sensor system only a fraction of them are activated during TBI (**Table 1**). In the following section, we summarize some of the microglia receptors most investigated in TBI, their downstream signaling pathway (**Figure 2**), the functional consequences of their activation and the implication in behavioral outcomes.

Chemokine receptor (CX3CR1)

Microglia in the CNS are characterized by the prominent expression of the chemokine receptor 1 (CX3CR1). The sole ligand for the receptor is fractalkine (CX3CL1) which is produced by neurons. CX3CL1 is known to induce microglia activation and release of proinflammatory factors [148]. Following brain injury, affected neurons release CX3CL1 allowing for microglia activation [149]. The schematic in Figure 1, summarizes the known intracellular signaling pathways associated with CX3CR1 receptor activation in microglia. It has been shown that CX3CL1 induces chemotaxis of microglia cells via chemokine macrophage inflammatory protein-1α (MIP-1α) to the site of neuronal damage [150]. CX3CL1 is also known to induce microglia activation through intracellular phosphorylation of microglial p38 mitogen-activated protein kinase (MAPK) [151, 152]. Further, treatment of cultured microglia with CX3CL1 promoted cell survival and inhibited Fas ligand-induced cell death via the Akt signaling pathway [153].

In a mouse model of CCI, they found that CX3CR1 KO mice had reduced cellular damage in the cortex and fewer sensorimotor deficits at 4 d post injury. In contrast, at 5 w, the CX3CR1 KO mice showed greater sensory motor deficits than that of control mice [112]. These results suggest that microglia-mediated fractalkine receptor signaling is associated with early toxicity but subsequent protection against TBI-induced pathology [112]. Drawing from this study, microglia seem to exacerbate injury outcome at the acute phase, however, it plays a more neuroprotective role at the chronic phase after injury. This was supported by another report that demonstrated a time-dependent role for CX3CL1/CX3CR1 signaling after TBI [86]. They showed that microglia exhibited M2 phenotypic markers (Ym1, CD206, and TGFβ) in the acute phase and predominantly exhibited M1 phenotypic markers CD68 in the chronic phase, owing to the differential outcomes to CX3CR1 deletion after TBI [86]. Moreover, CX3CR1 signaling has been implicated in the infiltration of peripheral immune cells and the resultant neurodegeneration [111]. Taken together, CX3CL1/CX3CR1 signaling modulates microglia activation, and depending upon the type and time of injury, either protects or exacerbates the injury response following TBI.

Purinergic receptor (P2Y12R)

Microglia respond to extracellular changes in ATP concentration via numerous purinergic receptors. Microglia expresses both P2Y receptors coupled to G-proteins, as well as, P2X receptors coupled to ligand gated cation channels [154]. In this review, we focus on purinergic receptor P2Y12R, a microglia-specific receptor [155] that mediates microglial chemotaxis towards site of injury [156]. Activation of P2Y12R results in the opening of K+ channel and

increased cAMP levels that is implicated in microglia surveillance and chemotaxis towards injury site [157, 158] (**Figure 2**). A recent study identified a two-pore domain channel, namely, THIK-1 as the potassium channel involved in microglia ramification and surveillance [157]. However, THIK-1 did not account for site-directed chemotaxis of microglia processes suggesting that another K+ channel may be coupled with P2Y12R and warrants further investigation [157, 158].

In addition to promoting microglia dynamic properties, ATP strongly activates microglia P2Y12R and stimulates the production of cytokines (IL-4, IL-6, IL13 and TNF-α) and chemokines (CCL3) by elevating the intracellular calcium levels [159, 160]. P2Y12R expression in activated microglia is controversial. A number of studies report increased expression of P2Y12R in activated microglia [161-163]. However, there are equally compelling studies that claim that P2Y12R is expressed exclusively in non-activated microglia [164] or alternatively activated microglia [159]. This discrepancy can be explained by the direct correlation between P2Y12R expression and ramified state of microglia [165]. Hence, although these studies claim microglia activation, the expression levels of P2Y12R is a good indication of level and direction of transformation that occurs to the microglia morphological and dynamic state (hyperramified with chemotactic processes versus hyporamified microglia with amoeboid soma).

Microglia P2Y12R is well known for its role as facilitator of process extension and migration following focal injury [165, 166]. In a pig model of diffuse central FPI, microglia processes converged on axonal swellings and exacerbated diffuse axonal injury [167]. Microglia process convergence towards swollen axons and dendrites are mediated by P2Y12R [168, 169]. Recently, P2Y12R-dependant microglial closure of injured blood-brain barrier was shown [50]. Given the cellular specificity of P2Y12R in microglia, it would be the ideal target for targeting microglia activation after TBI.

Toll like Receptor 4 (TLR4)

Toll-like receptors (TLRs) are first-line molecules for initiating immune responses. Microglia being the only innate immune cells in the CNS, they highly express TLRs, particularly TLR4. Some of the known ligands of TLR4 include lipopolysaccharide (LPS) [170], fibrinogen, heat shock proteins (HSP), high mobility group box protein 1 (HMGB-1) and monosodium urate [171]. TLR signaling initiates acute inflammatory response by promoting the release of proinflammatory cytokines. Ligand binding to TLR4 activates either a MyD88-dependent NF-κB activation or MyD88-independent activation of interferon regulatory factor–3 (IRF-3) activation and the subsequent expression of IFNβ [172] (Figure 1). In MyD88 deficient mice, Esen and Kielian found that the microglia was only partially inhibited, implying that both MyD88 dependent and independent pathways are functional in microglia [170].

The expression of TLR4 has been shown to be upregulated in various animal models of TBI [134]. Administration of pituitary adenylate cyclase-activating polypeptide (PACAP30), a known TLR4 antagonist, reduced the cognitive and motor decline, neural apoptosis and reduced brain edema in a WD model of TBI [134]. The effects of PACAP30 were strongly associated

with microglia mediated release of IL-1β, and TNF-α, implicating TLR4 in microglia activation and inflammation [134]. Release of excess ~~(HMGB1)~~, a ligand for TLR4 was reported in TBI patients, as well as in CCI animal model [116]. Genetic or pharmacological (VGX-1027) inhibition of TLR4 attenuated the microglial neuroinflammatory response (IL-6) and limited post-traumatic edema [116]. In line with this, another study demonstrated that deletion of TLR4 (TLR4 KO) resulted in lower M1 phenotypic genes and higher expression of M2 phenotypic markers in microglia [117]. Consequently, the TLR4 KO mice exhibited decreased infarct volumes and improved outcomes in behavioral tests after TBI [117]. Taken together, TLR4 deficiency contributes to regulating microglia to switch to the M2 phenotype, which ameliorates neurological impairment after TBI.

Interleukin-1 Receptor1 (IL-1R1)

Microglia are the prominent source of cytokine interleukin-1 (IL-1) production, yet little is known about the expression of the receptor IL-1R1 in them. Highest expression of IL-1R1 is found on endothelial cells with low expression in microglia and astrocytes [173]. The ligands of the IL-1R1 include IL-1α and IL-1β. The activation of IL-1R1 is transduced through both the NF-kB and the mitogen activated protein kinase (MAPK) pathways [174]. Upon ligand binding IL-1R accessory protein (IL-1RAP) is recruited. Similar to TLR4 signaling, the formation of the IL11R1 and IL-1RAP heterodimer initiated signal transduction by allowing for recruitment of MyD88 and IL‑1R associated kinase 4 (IRAK4), TNFR‑associated factor 6 (TRAF6) [174] (**Figure 2**).

It has been shown that proliferating microglia express high amounts of IL-1R1 [175]. IL-1β exacerbated, whereas IL-1R agonist attenuated neuronal injury and microglial activation after excitotoxic damage in organotypic hippocampal slice cultures [176]. In a CCI model, neutralization of IL-1β prevented the activation of IL-1R and reduced the activation of microglia at 3d and 7d post injury [108]. Subsequently, a reduction in lesion volume, attenuated cognitive deficits and decreased hemispheric tissue loss [108]. In mice lacking IL-1R1, fewer amoeboid microglia/macrophages appeared adjacent to the injured brain tissue and those microglia present at early post-injury intervals retained their resting morphology in a penetrating brain injury model [177]. This was followed by a significant reduction in inflammatory response such as Cox-2, IL-1, and IL-6 release [177]. These results implicate IL-1R1 in microglial activation after TBI. Since microglia are not the sole expressers of IL-1R1, the recently developed IL1R1[loxP/loxP] transgenic mouseline [178] can be used to study the microglia-specific role of IL-1R1 in TBI pathology.

NLRP3 inflammasome is a major mediator of IL-1β production via activation of caspase-1. Studies have reported the-activation of NLRP3 inflammasome in blunt models of TBI, whereas very few studies were performed in blast TBI [179, 180]. Our interest focus on the NLRP3 inflammasome is due to its known expression in microglia cells [181-183] and that microglial activation is well known in various forms of TBI. NLRP3 the most studied inflammasome is typically found in innate immune cells and is found to be activated by a wide range of stimuli such as viral, bacterial, and fungal components [184, 185], endogenous danger signals such as

extracellular ATP[186-188], amyloid‑β [181], uric acid crystals [181, 188, 189], and environmental micro particles such as silica crystals [190]. Originally thought to be expressed exclusively in microglia NLRP3 is now found to be expressed in neurons. The time course for expression following TBI differ among the two cell types. Whereas early (acute) expression is found in neurons and later (subacute) expression to be found in microglia [191]. Weight drop model measured colocalization at 3 days post injury. Liu et found that the mRNA levels of NLRP3 increase at 6h, 3 days and 7 days post injury but was at control levels at 24 hours after injury. In line with mRNA levels protein levels increased at all time points except the 6 hour time point. NLRP3 was coexpressed in neurons astrocytes and microglia at the 3 day time point. IL-1β peaked at 6 hours and decreased by to sham levels by day 7 [192].

CCI injury in mice Quian et al found that IL-1beta levels peaked at 6 hours and decreased steadily to control levels by day 7. IL-18 levels were at control concentration at 6 hours but increased at all time points peaking at 7 days. mRNA levels for NLRP3, ASC, and caspase-1 levels increased at 6 hours and maximal at 7 days. Although both astrocytes and microglia were activated following injury only microglia were accompanied by strong NLRP3 expression. [87]

Tumor necrosis factor receptor (TNFR1)

Microglia express both tumor necrosis factor-α (TNFα), as well as its receptors, TNFR1 (p55) and TNFR2 (p75) [193]. The two native receptors have differential intracellular signaling pathways. In this section we focus on TNFR1, which contains a death domain. Activation of TNFR1 normally leads to cellular apoptosis; however, under specific conditions, receptor activation can also lead to the activation of NFκB and contribute to cell survival. These divergent outcomes have been linked to receptor localization with receptor internalization leading to cell death and membrane localization supporting cell survival [194]. Upon ligand binding with TNFR1, the signal is transduced via transcription factors such as NF-κB and c-Jun which in turn are involved in immune, stress and inflammatory responses [195] (**Figure 2**).

The expression levels of TNF- α and its associated receptors have been correlated with trauma severity in patients admitted with TBI [196]. Genetic deletion of TNFR1 (TNFR1 KO) showed attenuation of motor deficits at 4-weeks following CCI [121]. In contrast, absence of TNFR2 (TNFR2 KO) resulted in worsening of motor deficits as compared to the control [121]. The study showed that TNF-α-TNFR1 signaling was proinflammatory in nature whereas, TNF-α-TNFR2 signaling was anti-inflammatory in nature [121]. Surprisingly, an independent study observed no differences in motor or cognitive outcome in either TNFR1, TNFR2 KO or TNFR1/TNFR2/Fas mice, versus wild type mice following CCI [197]. These conflicting data may be attributable to differences in the severity of the CCI models used, as well as anesthetic agent, differences in background strain genetics in TNFR KO mice, and other model-specific factors in the studies [198].

As mentioned earlier, the downstream signaling of TNFR1 may be neuroprotective or neurotoxic depending upon the sub-cellular localization of the receptor. In the normal rat cortex, a portion of TNFR1 is located in lipid raft microdomains, where it is associated with the adaptor proteins TRADD (TNF receptor-associated death domain), TNF receptor-associated factor-2 (TRAF-2),

the Ser/Thr kinase RIP (receptor-interacting protein), TRAF1, and cIAP-1 (cellular inhibitor of apoptosis protein-1), forming a survival signaling complex. Moderate TBI resulted in rapid recruitment of TNFR1, but not TNFR2 or Fas, to lipid rafts and induced alterations in the composition of signaling intermediates. Activation of TNFR1 after TBI induced the expression of caspase-8, thus initiating apoptosis and transient activation of NF-κB [199]. In CCI model, studies have identified co-expression of TNFR1 and TNFR2 in both microglia and endothelial cells, thereby implicating TNFR signaling in the pathogenesis of TBI [200, 201]. In brain injury models such as FPI and CCI , elevated TNF- α levels are found in the injured brain and inhibition of TNF- α and its receptors has been beneficial to postinjury cell death and functional outcome [124, 202]. However, in WD / concussive brain injury model, inhibition of TNF- α and Fas receptor resulted in cognitive decline independent of neuronal loss [140]. Hence, a better understanding of TNF-α -TNF1R signaling in the various injury models is needed to develop therapies targeting TNF1R for treatment of TBI.

Peroxisome proliferator-activated receptor (PPAR)

The peroxisome proliferator-activated receptors (PPAR) are a member of nuclear membrane receptor family and have been shown to be important for inflammatory signaling in microglia [105]. There are three isoforms of the receptor PPARα, PPAR δ/β, and PPARγ [203]. Of the three isoforms only PPARα and PPARγ are implicated in inflammation. The numerous agonists and antagonists of PPARs are listed in **Supplementary Table1**. Upon activation, the PPARs regulate inflammation via trans-reexpression of multiple inflammatory signaling systems such as nuclear factor-kappa B (NFκB), activator protein-1 (AP-1), signal transducer and activator of transcription (STAT) [204]. Although the endogenous ligand may not achieve critical concentration to activate the receptor a lot of research has gone into its role in TBI treatment.

Following CCI, mRNA levels of PPARγ have been reported to be elevated surrounding the injury site [126]. Agonists for both PPARα and PPARγ have been studied due to their ability to affect multiple signaling pathways and reduce TBI induced neuropathology. Fenofibrate, a PPARα agonist, has been shown to reduce oxidative stress and inflammation after TBI [205, 206]. Similarly, Pioglitazone and Rosiglitazone, both PPARγ agonists, have been shown to reduce oxidative stress [126], inflammation [207-209], mitochondrial dysfunction [125, 210] and cell death [124, 207, 211] following CNS injury. Using rosiglitazone, a known PPAR-γ agonist, Liu et al observed a decrease in expression of TNF-α, decreased microglia activation, increased neuronal survival and improved performance in motor function tasks at 24 h after CCI [124]. Pioglitazone also reduced lesion volume by 55% and prevented microglial activation in the tissue surrounding lesion after TBI [125]. In FPI injury model, a single dose of Pioglitazone administration reduced oxidative damage, decreased microglia activation, decreased neural degeneration, and reduced edema formation [130]. However, Pioglitazone administration was not found to have an influence on reactive astrogliosis [130]. It is important to note that PPAR expression in the brain in not exclusive to microglia [212]. Hence, whether the effect of the PPAR agonist/antagonists are due to the direct/ indirect action on microglia PPAR remains unclear. However, the pharmacological studies consistently show the involvement of PPAR signaling in microglial activation after TBI, making it a worthy therapeutic target.

Tools for examining microglial receptor activation

Recent advances in genetic, molecular and imaging techniques have tremendously improved our understanding of microglial receptor activation. Here we summarize some of the key techniques used to study microglia receptor activation (**Figure 3**) and highlight their advantages and limitations.

Cell culture studies

The discovery of receptor types expressed on microglia come from 1) cell culture 2) slice culture, and 3) live animal model studies. The most extensively used immortalized microglial cell-lines include BV2 and N9, which are derived from rat and mouse, respectively [213, 214]. The other highly proliferating non-genetically modified lines include the colony stimulating factor-1 dependent EOC cells [215] and the Highly Aggressively Proliferating Immortalized (HAPI) cell line [216]. A more detailed account of the advantages and disadvantages of various microglial cell lines and their specific appropriateness in a particular research context has been reviewed previously [217]. The cell cultures have the advantage of being highly prolific allowing easy harvest, faster study time and eliminates the need for live animals, while providing microglia-specific information. However, the cell-lines do not accurately represent microglia receptor expression, hence experts in the field often prefer primary microglia cell cultures for such studies.

Primary microglia cultures are very prevalent in neuro-inflammatory research due to the similarities in phenotype to *in vivo* cells. These cells are most often derived from the cortex of a rat or mouse before or early after birth and purified culture of approximately 95% enriched microglia can be obtained [218]. Cultured microglia cells are amoeboid and can be transitioned into ramified microglia by incubation with retinoic acid, an agent known to increase cellular differentiation [218]. Although, this induced ramified state is comparable to *in vivo* conditions, the cultured microglial cells are still under a certain degree of basal activation. The ability to study microglia receptor proteins in primary cell culture model is beneficial. Yet, the extensive preparations needed for each experiment makes this model more time consuming and perhaps less attractive as compared to other microglia lines that have shorter prep-time but maintain similar cell properties. One such way of obtaining cells that have faster proliferation rates, have a more homogeneous population, and at a lower cost, is by genetically immortalizing the primary microglia [217]. In spite of the limitations, cell culture studies are the most-widely used model to understand receptor signaling pathways specific to microglia.

Animal studies

Since microglia are very sensitive to any stimulation, the ideal method to investigate microglia is to study them *in situ* conditions. Immunolabeling and in-situ hybridization are common techniques used to identify localization of receptors on microglial surface. With the advent of recent developments in genetics and transgenic mice lines, it has become easier to study microglial receptors *in vivo*. Most commonly, fluorescent protein tagged to microglia- specific promoters such as CX_3CR1, Cd11b, Lys [219-221], have been used to monitor morphological and dynamic properties of microglia. Improvements in imaging technology such as two-photon

imaging has led to a better understanding of microglial dynamic properties in slice cultures, as well as, *in vivo* imaging. Moreover, the availability of microglia-specific constitutive (CX$_3$CR1 Cre) and inducible cre (CX$_3$CR1 CreER)-lines have allowed the generation of transgenic mice lacking the gene of interest in microglia-alone right from birth or at a particular time point, respectively [222]. When these cre lines are crossed with flox/lox line of the receptor of interest, the offspring lacks the receptor specifically in microglia, enabling the study of the role of the particular receptor in physiology and disease. Recently, TLR4 flox mice were crossed with PDGFRα-Cre mice to eliminate TLR4 in retinal Müller cells to investigate the signaling pathway underlying cytokine production [223]. Notably, studies of microglia depletion through genetic targeting or pharmacological therapies are gaining interest. It was shown that selective depletion of proliferating microglia resulted in markedly increased brain injury following ischemia [224, 225]. Such studies are yet to be conducted in brain injury models and would provide direct evidence on the detrimental / neuroprotective role of microglia in injury pathology.

mRNA and Protein Analysis

mRNA expression changes have been used to determine whether a receptor is upregulated or downregulated after TBI. The fold change in mRNA expression levels in control versus injury samples are usually estimated by performing a quantitative PCR. Since the mRNA expression does not always translate to protein expression, an enzyme-linked immunosorbent assay or western blot assay is performed for quantitative and semi-quantitative estimates of protein levels of the microglial receptors. To further confirm the cellular co-localization of the receptor on microglia surface, double immunostaining of the target receptor protein is performed with a standard microglial marker such as Iba1 [20, 90, 127, 143, 226-231] , CD11b [19, 232-234]+, CD45 [232], CD68 [86, 90, 232, 235, 236], to name a few.

More recently, RNA-Seq (RNA sequencing), a technique used to identify the presence and quantity of RNA in an entire transcriptome of a biological sample at a given moment, is gaining popularity. Hickman et al, was the first to demonstrate that microglia have a distinct transcriptomic signature and express a unique cluster of receptor proteins for sensing endogenous ligands [237]. This technique has also been used to establish differences between resident microglia and infiltrating monocytes and their distinct properties in neuroinflamatory conditions [238]. RNA-Seq analysis of microglia revealed the time-dependent activation of specific genetic programs following spinal cord injury [239]. Such a transcriptome-wide study in microglia has not performed in TBI conditions and would be worthy of investigation. The extensive datasets of such genomic studies in microglia and other glial cells are available for easy access to researchers via the Gila Open Access Database (GOAD) [240]. Although, these techniques provide adequate information on the expression levels, it does not shed light on the degree of functional activity of the receptors in injury pathology. Hence, functional studies of microglia receptor activation are highly preferred which are currently lacking in the TBI field.

Live Tissue Imaging

The advent of transgenic animal models with fluorescent tagged microglia has enabled major advancements in live imaging studies in both *ex vivo,* as well as, *in vivo* conditions. Microglia

motility and their ability to respond to injury site has been well-investigated by performing time-lapse imaging using two-photon microscopy [168, 241, 242]. Since microglia receptors act as "on" "off" switches to sense stimulus, these imaging studies often use genetic or pharmacological approach to investigate the role of the receptor in microglia response to injury [158, 243].

Calcium Imaging

Although calcium imaging has been used to study neurons and astrocytes, the role of intracellular Ca^{2+} dynamics in microglia was not investigated until recently. The microglia cells are exceptionally difficult to load with synthetic dyes thereby posing a technical issue [244, 245]. The Ca^{2+} signaling data from *in vivo* would be very valuable since microglia receptor activation invariably mediates secondary mechanisms such as inflammation and motility via $[Ca^{2+}]_i$ as a secondary messenger. The recent development of tools such as viral vectors and transgenic mice models have enabled the insertion of intracellular Ca^{2+} indicators such as GCaMP and Twitch-2B specifically in microglia [246-248]. A detailed account of calcium imaging studies in microglia was previously reported [249]. One study showed that 67% of microglia responding to a focal laser lesion displayed Ca2+ transients and was mediated by purinergic receptors [248]. These studies provide valuable insights into the physiology of microglia and its relationship to motility in response to TBI.

Electrophysiology

Despite being electrically inert, whole-cell patch recordings have been carried out in microglial cells to investigate the expression and function of ion channels. A detailed report of microglia ion channels have been summarized previously [100]. Microglia in the resting state display a distinct linear IV current as opposed to dramatic rectifying K+ currents in the activated states [162, 250]. Since, a number of microglia receptors are coupled to ion channels, whole-cell electrophysiological recordings are an ideal tool to investigate whether the functional activation of the receptor is enhanced after brain injury[162, 250]. Further, electrophysiology is an extremely sensitive technique and can be used to test the ability of drugs / blockers in preventing microglia activation [162]. Hence, this is an extremely valuable tool that can be exploited to test the ameliorating effect of drugs on microglia activation for the treatment of TBI.

Pharmacological approach

The use of receptor agonist/ inhibitor is the most common method used to determine the effects and functional relevance of a receptor. A complete list of ligands, agonist and inhibitors of various microglial receptors are provided in **Supplementary Table 1**. Pharmacological studies are often crude, due to non-specific target binding. Hence, the results of pharmacological studies hare difficult to interpret when trying to identify the role of a receptor expressed in a specific cell type. Hence, drugs attenuating overall microglia activation have been employed in

TBI studies such as – minocycline [251, 252], etanercept [88, 253, 254], statins [255], resveratrol [256], mGluR5 agonist and positive allosteric modulator [119, 120, 257], gp91ds-tat [61, 258], rosiglitazone [124, 126], alpha-7 nicotinic acetylcholine receptor agonists [259], interleukin-1 receptor antagonist[108]. Hence, a pharmacological approach is extremely effective and highly relevant, making it a potent tool of investigation.

Conclusion

In the various models of TBI, microglia activation varies based on the type and severity of injury. Microglia receptors act as sensors for identifying these subtle changes in the neuronal parenchyma and lead to various modes of microglia activation. Hence, the expression pattern of microglia receptors can be used as a signature to identify the injury severity/ mechanism following TBI. In the light of the above, it is evident that microglia receptor activation plays an important role in post-injury pathology and may be a sensitive diagnostic tool. Moreover, pharmacologically targeting microglia-specific receptors will prevent alterations in neuronal physiology and hence reduce unwanted side-effects. Hence, microglia receptors may be a potent therapeutic target for the treatment of brain injury. An ideal therapeutic strategy would be to potentiate the protective properties of microglia and attenuate its neurotoxic behavior by activating and inhibiting the appropriate anti-inflammatory and pro-inflammatory receptors, respectively.

Abbreviations

Akt	Protein Kinase B
AP-1	Activator protein-1
APP	Amyloid precursor protein
Arg-1	Arginase-1
ATP	Adenosine triphosphate
BBB	Blood brain barrier
CCI	Controlled cortical impact/injury
cFPI	Central FPI
cIAP-1	Cellular inhibitor of apoptosis protein-1
CNS	Central nervous system
CX3CR1	Chemokine receptor 1
CXCL1	Fractalkine
DAMPS	Danger associated molecular patterns
EC	Endothelial cells
FPI	Fluid Percussion Injury
GOAD	Gila open access database
HAPI	Highly aggressively proliferating immortalized
HMGB1	High mobility group box protein 1
HSP	Heat shock protein
IL-1R1	Interleukin 1 receptor
IL-1β	Interleukin 1β
IRAK4	IL‑1R associated kinase 4
IRF-3	Interferon regulatory factor–3
KO	Knockout
LFPI	Lateral FPI
LPA	Lysophosphatidic acid
LPS	Lipopolysaccharide
MAPK	Mitogen activated protein kinase
MIP-1α	Macrophage inflammatory protein-1α
mRNA	Messenger RNA
NADPH	Nicotinamide adenine dinucleotide phosphate
NFκB	Nuclear factor-kappa B
NOX	NADPH oxidase
PACAP30	Adenylate cyclase-activating polypeptide
PAMPS	Pathogens associated molecular patterns
PCR	Polymerase chain reaction
PPAR	Peroxisome proliferator-activated receptors
RIP	Receptor-interacting protein
RNA	Ribonucleic acid
RNA-seq	RNA sequencing
RNS	Reactive nitrogen species
ROS	Reactive oxygen species

STAT	Signal transducer and activator of transcription
TBI	Traumatic brain injury
TLR4	Toll like receptor 4
TNF α	Tumor necrosis factor α
TNF-R1	TNFα receptor 1
TRADD	TNF receptor-associated death domain
TRAF-2	TNF receptor-associated factor-2
TSPO	Translocator protein
WD	Weight drop

References

1. Taylor, C.A., J.M. Bell, M.J. Breiding, and L.K. Xu, *Traumatic Brain Injury-Related Emergency Department Visits, Hospitalizations, and Deaths - United States, 2007 and 2013.* Mmwr Surveillance Summaries, 2017. **66**(9): p. 1-18.
2. Cernak, I. and L.J. Noble-Haeusslein, *Traumatic brain injury: an overview of pathobiology with emphasis on military populations.* Journal of Cerebral Blood Flow and Metabolism, 2010. **30**(2): p. 255-266.
3. Faul, M.X., Likang; Wald, Marlena; Coronado, Victor, *Traumatic Brain Injury in the United States: Emergency Department Visits, Hospitalizations and Deaths 2002–2006*, C.f.D.C.a. Prevention, Editor 2010, National Center for Injury Prevention and Control: Atlanta.
4. Maas, A.I.R., B. Roozenbeek, and G.T. Manley, *Clinical Trials in Traumatic Brain Injury: Past Experience and Current Developments.* Neurotherapeutics, 2010. **7**(1): p. 115-126.
5. Nimmerjahn, A., F. Kirchhoff, and F. Helmchen, *Resting microglial cells are highly dynamic surveillants of brain parenchyma in vivo.* Science, 2005. **308**(5726): p. 1314-1318.
6. Huber, B.R., J.S. Meabon, Z.S. Hoffer, J. Zhang, J.G. Hoekstra, K.F. Pagulayan, P.J. McMillan, C.L. Mayer, W.A. Banks, B.C. Kraemer, M.A. Raskind, D.B. McGavern, E.R. Peskind, and D.G. Cook, *Blast exposure causes dynamic microglial/macrophage responses and microdomains if brain microvessel dysfunction.* Neuroscience, 2016. **319**: p. 206-220.
7. Loane, D.J. and A. Kumar, *Microglia in the TBI brain: The good, the bad, and the dysregulated.* Experimental Neurology, 2016. **275**: p. 316-327.
8. Ding, A.H., C.F. Nathan, and D.J. Stuehr, *Release of Reactive Nitrogen Intermediates and Reactive Oxygen Intermediates from Mouse Peritoneal-Macrophages - Comparison of Activating Cytokines and Evidence for Independent Production.* Journal of Immunology, 1988. **141**(7): p. 2407-2412.
9. Sica, A., T. Schioppa, A. Mantovani, and P. Allavena, *Tumour-associated macrophages are a distinct M2 polarised population promoting tumour progression: Potential targets of anti-cancer therapy.* European Journal of Cancer, 2006. **42**(6): p. 717-727.
10. Butovsky, O., M.P. Jedrychowski, C.S. Moore, R. Cialic, A.J. Lanser, G. Gabriely, T. Koeglsperger, B. Dake, P.M. Wu, C.E. Doykan, Z. Fanek, L.P. Liu, Z.X. Chen, J.D. Rothstein, R.M. Ransohoffl, S.P. Gygi, J.P. Antel, and H.L. Weiner, *Identification of a unique TGF-beta dependent molecular and functional signature in microglia.* Nature Neuroscience, 2014. **17**(1): p. 131-143.
11. Chiu, C.C., Y.E. Liao, L.Y. Yang, J.Y. Wang, D. Tweedie, H.K. Karnati, N.H. Greig, and J.Y. Wang, *Neuroinflammation in animal models of traumatic brain injury.* Journal of Neuroscience Methods, 2016. **272**: p. 38-49.
12. Deselms, H., N. Maggio, V. Rubovitch, J. Chapman, S. Schreiber, D. Tweedie, D.S. Kim, N.H. Greig, and C.G. Pick, *Novel pharmaceutical treatments for minimal traumatic brain injury and evaluation of animal models and methodologies supporting their development.* Journal of Neuroscience Methods, 2016. **272**: p. 69-76.
13. Xiong, Y., A. Mahmood, and M. Chopp, *Animal models of traumatic brain injury.* Nature Reviews Neuroscience, 2013. **14**(2): p. 128-142.
14. Dixon, C.E., G.L. Clifton, J.W. Lighthall, A.A. Yaghmai, and R.L. Hayes, *A Controlled Cortical Impact Model of Traumatic Brain Injury in the Rat.* Journal of Neuroscience Methods, 1991. **39**(3): p. 253-262.
15. Lighthall, J.W., *Controlled Cortical Impact: A New Experimental Brain Injury Model.* Journal of Neurotrauma, 1988. **5**(1): p. 1-15.

16. Smith, D.H., H.D. Soares, J.S. Pierce, K.G. Perlman, K.E. Saatman, D.F. Meaney, C.E. Dixon, and T.K. McIntosh, *A Model of Parasagittal Controlled Cortical Impact in the Mouse - Cognitive and Histopathologic Effects.* Journal of Neurotrauma, 1995. **12**(2): p. 169-178.

17. Lighthall, J.W., H.G. Goshgarian, and C.R. Pinderski, *Characterization of Axonal Injury Produced by Controlled Cortical Impact.* Journal of Neurotrauma, 1990. **7**(2): p. 65-76.

18. Garman, R.H., L.W. Jenkins, R.C. Switzer, 3rd, R.A. Bauman, L.C. Tong, P.V. Swauger, S.A. Parks, D.V. Ritzel, C.E. Dixon, R.S. Clark, H. Bayir, V. Kagan, E.K. Jackson, and P.M. Kochanek, *Blast exposure in rats with body shielding is characterized primarily by diffuse axonal injury.* J Neurotrauma, 2011. **28**(6): p. 947-59.

19. Truettner, J.S., H.M. Bramlett, and W.D. Dietrich, *Posttraumatic therapeutic hypothermia alters microglial and macrophage polarization toward a beneficial phenotype.* Journal of Cerebral Blood Flow and Metabolism, 2017. **37**(8): p. 2952-2962.

20. Wen, L., W.-D. You, H. Wang, Y. Meng, J.-F. Feng, and X. Yang, *Polarization of microglia to the M2 phenotype in a PPAR-gamma dependent manner attenuates axonal injury induced by traumatic brain injury in mice.* Journal of neurotrauma, 2018.

21. Jin, X.M., H. Ishii, Z.B. Bai, T. Itokazu, and T. Yamashita, *Temporal Changes in Cell Marker Expression and Cellular Infiltration in a Controlled Cortical Impact Model in Adult Male C57BL/6 Mice.* Plos One, 2012. **7**(7): p. 13.

22. Loane, D.J., A. Kumar, B.A. Stoica, R. Cabatbat, and A.I. Faden, *Progressive Neurodegeneration After Experimental Brain Trauma: Association With Chronic Microglial Activation.* Journal of Neuropathology and Experimental Neurology, 2014. **73**(1): p. 14-29.

23. Wang, G.H., J. Zhang, X.M. Hu, L.L. Zhang, L.L. Mao, X.Y. Jiang, A.K.F. Liou, R.K. Leak, Y.Q. Gao, and J. Chen, *Microglia/macrophage polarization dynamics in white matter after traumatic brain injury.* Journal of Cerebral Blood Flow and Metabolism, 2013. **33**(12): p. 1864-1874.

24. Bollmann, L., D.E. Koser, R. Shahapure, H.O.B. Gautier, G.A. Holzapfel, G. Scarcelli, M.C. Gather, E. Ulbricht, and K. Franze, *Microglia mechanics: immune activation alters traction forces and durotaxis.* Frontiers in Cellular Neuroscience, 2015. **9**: p. 16.

25. Navone, S.E., M. Peroglio, L. Guarnaccia, M. Beretta, S. Grad, M. Paroni, C. Cordiglieri, M. Locatelli, M. Pluderi, P. Rampini, R. Campanella, M. Alini, and G. Marfia, *Mechanical loading of intervertebral disc modulates microglia proliferation, activation, and chemotaxis.* Osteoarthritis and cartilage, 2018. **26**(7): p. 978-987.

26. Mittelbronn, M., K. Dietz, H.J. Schluesener, and R. Meyermann, *Local distribution of microglia in the normal adult human central nervous system differs by up to one order of magnitude.* Acta Neuropathologica, 2001. **101**(3): p. 249-255.

27. Igarashi, T., T.T. Huang, and L.J. Noble, *Regional vulnerability after traumatic brain injury: Gender differences in mice that overexpress human copper, zinc superoxide dismutase.* Experimental Neurology, 2001. **172**(2): p. 332-341.

28. Tong, W., T. Igarashi, D.M. Ferriero, and L.J. Noble, *Traumatic brain injury in the immature mouse brain: Characterization of regional vulnerability.* Experimental Neurology, 2002. **176**(1): p. 105-116.

29. Prins, M., T. Greco, D. Alexander, and C.C. Giza, *The pathophysiology of traumatic brain injury at a glance.* Disease Models & Mechanisms, 2013. **6**(6): p. 1307-1315.

30. Werner, C. and K. Engelhard, *Pathophysiology of traumatic brain injury.* British Journal of Anaesthesia, 2007. **99**(1): p. 4-9.

31. Barger, S.W. and A.D. Harmon, *Microglial activation by Alzheimer amyloid precursor protein and modulation by apolipoprotein E.* Nature, 1997. **388**(6645): p. 878-881.

32. Noda, M., H. Nakanishi, and N. Akaike, *Glutamate release from microglia via glutamate transporter is enhanced by amyloid-beta peptide.* Neuroscience, 1999. **92**(4): p. 1465-1474.

33. Barger, S.W. and A.S. Basile, *Activation of microglia by secreted amyloid precursor protein evokes release of glutamate by cystine exchange and attenuates synaptic function.* Journal of Neurochemistry, 2001. **76**(3): p. 846-854.

34. Faden, A.I., P. Demediuk, S.S. Panter, and R. Vink, *The Role of Excitatory Amino-Acids and Nmda Receptors in Traumatic Brain Injury.* Science, 1989. **244**(4906): p. 798-800.

35. Christensen, R.N., B.K. Ha, F. Sun, J.C. Bresnahan, and M.S. Beattie, *Kainate induces rapid redistribution of the actin cytoskeleton in ameboid microglia.* Journal of Neuroscience Research, 2006. **84**(1): p. 170-181.

36. Hagino, Y., Y. Kariura, Y. Manago, T. Amano, B. Wang, M. Sekiguchi, K. Nishikawa, S.U. Aoki, K. Wada, and M. Noda, *Heterogeneity and potentiation of AMPA type of glutamate receptors in rat cultured microglia.* Glia, 2004. **47**(1): p. 68-77.

37. Noda, M., H. Nakanishi, J. Nabekura, and N. Akaike, *AMPA-kainate subtypes of glutamate receptor in rat cerebral microglia.* Journal of Neuroscience, 2000. **20**(1): p. 251-258.

38. Biber, K., D.J. Laurie, A. Berthele, B. Sommer, T.R. Tolle, P.J. Gebicke-Harter, D. van Calker, and H. Boddeke, *Expression and signaling of group I metabotropic glutamate receptors in astrocytes and microglia.* Journal of Neurochemistry, 1999. **72**(4): p. 1671-1680.

39. Taylor, D.L., L.T. Diemel, M.L. Cuzner, and J.M. Pocock, *Activation of group II metabotropic glutamate receptors underlies microglial reactivity and neurotoxicity following stimulation with chromogranin A, a peptide up-regulated in Alzheimer's disease.* Journal of Neurochemistry, 2002. **82**(5): p. 1179-1191.

40. Taylor, D.L., L.T. Diemel, and J.M. Pocock, *Activation of microglial group III metabotropic glutamate receptors protects neurons against microglial neurotoxicity.* Journal of Neuroscience, 2003. **23**(6): p. 2150-2160.

41. Taylor, D.L., F. Jones, E. Kubota, and J.M. Pocock, *Stimulation of microglial metabotropic glutamate receptor mGlu2 triggers tumor necrosis factor alpha-induced neurotoxicity in concert with microglial-derived fas ligand.* Journal of Neuroscience, 2005. **25**(11): p. 2952-2964.

42. Murugan, M., V. Sivakumar, J. Lu, E.A. Ling, and C. Kaur, *Expression of N-Methyl D-Aspartate Receptor Subunits in Amoeboid Microglia Mediates Production of Nitric Oxide Via NF-kappa B Signaling Pathway and Oligodendrocyte Cell Death in Hypoxic Postnatal Rats.* Glia, 2011. **59**(4): p. 521-539.

43. Liu, G.J., A. Kalous, E.L. Werry, and M.R. Bennett, *Purine release from spinal cord microglia after elevation of calcium by glutamate.* Molecular Pharmacology, 2006. **70**(3): p. 851-859.

44. Gottlieb, M. and C. Matute, *Expression of ionotropic glutamate receptor subunits in glial cells of the hippocampal CA1 area following transient forebrain ischemia.* Journal of Cerebral Blood Flow and Metabolism, 1997. **17**(3): p. 290-300.

45. Ferrari, D., P. Chiozzi, S. Falzoni, M. DalSusino, G. Collo, G. Buell, and F. DiVirgilio, *ATP-mediated cytotoxicity in microglial cells.* Neuropharmacology, 1997. **36**(9): p. 1295-1301.

46. Ferrari, D., P. Chiozzi, S. Falzoni, S. Hanau, and F. DiVirgilio, *Purinergic modulation of interleukin-1 beta release from microglial cells stimulated with bacterial endotoxin.* Journal of Experimental Medicine, 1997. **185**(3): p. 579-582.

47. Fujita, R., Y. Ma, and H. Ueda, *Lysophosphatidic acid-induced membrane ruffling and brain-derived neurotrophic factor gene expression are mediated by ATP release in primary microglia.* Journal of Neurochemistry, 2008. **107**(1): p. 152-160.

48. Ballerini, P., P. Di Iorio, R. Ciccarelli, F. Caciagli, A. Poli, A. Beraudi, S. Buccella, I. D'Alimonte, M. D'Auro, E. Nargi, P. Patricelli, D. Visini, and U. Traversa, *P2Y(1) and cysteinyl leukotriene receptors mediate purine and cysteinyl leukotriene co-release in primary cultures of rat microglia.* International Journal of Immunopathology and Pharmacology, 2005. **18**(2): p. 255-268.

49.   Xu, P.F., Y.T. Xu, B. Hu, J. Wang, R. Pan, M. Murugan, L.J. Wu, and Y.M. Tang, *Extracellular ATP enhances radiation-induced brain injury through microglial activation and paracrine signaling via P2X7 receptor.* Brain Behavior and Immunity, 2015. **50**: p. 87-100.

50.   Lou, N.H., T. Takano, Y. Pei, A.L. Xavier, S.A. Goldman, and M. Nedergaard, *Purinergic receptor P2RY12-dependent microglial closure of the injured blood-brain barrier.* Proceedings of the National Academy of Sciences of the United States of America, 2016. **113**(4): p. 1074-1079.

51.   Koizumi, S., Y. Shigemoto-Mogami, K. Nasu-Tada, Y. Shinozaki, K. Ohsawa, M. Tsuda, B.V. Joshi, K.A. Jacobson, S. Kohsaka, and K. Inoue, *UDP acting at P2Y(6) receptors is a mediator of microglial phagocytosis.* Nature, 2007. **446**(7139): p. 1091-1095.

52.   Koizumi, S., K. Ohsawa, K. Inoue, and S. Kohsaka, *Purinergic receptors in microglia: Functional modal shifts of microglia mediated by P2 and P1 receptors.* Glia, 2013. **61**(1): p. 47-54.

53.   Hidetoshi, T.S., T. Makoto, and K. Inoue, *P2Y receptors in microglia and neuroinflammation.* Wiley Interdisciplinary Reviews: Membrane Transport and Signaling, 2012. **1**(4): p. 493-501.

54.   del Puerto, A., F. Wandosell, and J.J. Garrido, *Neuronal and glial purinergic receptors functions in neuron development and brain disease.* Frontiers in Cellular Neuroscience, 2013. **7**: p. 15.

55.   Ozdemir, D., N. Uysal, S. Gonenc, O. Acikgoz, A. Sonmez, A. Topcu, N. Ozdemir, M. Duman, I. Semin, and H. Ozkan, *Effect of melatonin on brain oxidative damage induced by traumatic brain injury in immature rats.* Physiological Research, 2005. **54**(6): p. 631-637.

56.   Solaroglu, I., O. Okutan, E. Kaptanoglu, E. Beskonakli, and K. Kilinc, *Increased xanthine oxidase activity after traumatic brain injury in rats.* Journal of Clinical Neuroscience, 2005. **12**(3): p. 273-275.

57.   Lewen, A., P. Matz, and P.H. Chan, *Free radical pathways in CNS injury.* Journal of Neurotrauma, 2000. **17**(10): p. 871-890.

58.   Bedard, K. and K.H. Krause, *The NOX family of ROS-generating NADPH oxidases: Physiology and pathophysiology.* Physiological Reviews, 2007. **87**(1): p. 245-313.

59.   Sankarapandi, S., J.L. Zweier, G. Mukherjee, M.T. Quinn, and D.L. Huso, *Measurement and characterization of superoxide generation in microglial cells: Evidence for an NADPH oxidase-dependent pathway.* Archives of Biochemistry and Biophysics, 1998. **353**(2): p. 312-321.

60.   Nauseef, W.M., *How human neutrophils kill and degrade microbes: an integrated view.* Immunological Reviews, 2007. **219**: p. 88-102.

61.   Kumar, A., J.P. Barrett, D.M. Alvarez-Croda, B.A. Stoica, A.I. Faden, and D.J. Loane, *NOX2 drives M1-like microglial/macrophage activation and neurodegeneration following experimental traumatic brain injury.* Brain Behavior and Immunity, 2016. **58**: p. 291-309.

62.   Ferreira, A.P.O., F.S. Rodrigues, I.D. Della-Pace, B.C. Mota, S.M. Oliveira, C.D.V. Gewehr, F. Bobinski, C.V. de Oliveira, J.S. Brum, M.S. Oliveira, A.F. Furian, C.S.L. de Barros, J. Ferreira, A.R.S. dos Santos, M.R. Fighera, and L.F.F. Royes, *The effect of NADPH-oxidase inhibitor apocynin on cognitive impairment induced by moderate lateral fluid percussion injury: Role of inflammatory and oxidative brain damage.* Neurochemistry International, 2013. **63**(6): p. 583-593.

63.   Rao, K.V.R., S. Iring, D. Younger, M. Kuriakose, M. Skotak, E. Alay, R.K. Gupta, and N. Chandra, *A Single Primary Blast-Induced Traumatic Brain Injury in a Rodent Model Causes Cell-Type Dependent Increase in Nicotinamide Adenine Dinucleotide Phosphate Oxidase Isoforms in Vulnerable Brain Regions.* Journal of Neurotrauma: p. 14.

64.   Petitto, J.N., Z. Huang, J. Lo, and W.J. Streit, *IL-2 gene knockout affects T lymphocyte trafficking and the microglial response to regenerating facial motor neurons.* Journal of Neuroimmunology, 2003. **134**(1-2): p. 95-103.

65.   Sakai, N., S. Kaufman, and S. Milstien, *Parallel Induction Of Nitric-Oxide And Tetrahydrobiopterin Synthesis By Cytokines In Rat Glial-Cells.* Journal of Neurochemistry, 1995. **65**(2): p. 895-902.

66. Hanisch, U.K., S.A. Lyons, M. Prinz, C. Nolte, J.R. Weber, H. Kettenmann, and F. Kirchhoff, *Mouse brain microglia express interleukin-15 and its multimeric receptor complex functionally coupled to janus kinase activity.* Journal of Biological Chemistry, 1997. **272**(46): p. 28853-28860.

67. Bruce, A.J., W. Boling, M.S. Kindy, J. Peschon, P.J. Kraemer, M.K. Carpenter, F.W. Holtsberg, and M.P. Mattson, *Altered neuronal and microglial responses to excitotoxic and ischemic brain injury in mice lacking TNF receptors.* Nature Medicine, 1996. **2**(7): p. 788-794.

68. Moller, T., U.K. Hanisch, and B.R. Ransom, *Thrombin-induced activation of cultured rodent microglia.* Journal of Neurochemistry, 2000. **75**(4): p. 1539-1547.

69. Cao, Q., J. Lu, C. Kaur, V. Sivakumar, F. Li, P.S. Cheah, S.T. Dheen, and E.A. Ling, *Expression of Notch-1 receptor and its ligands Jagged-1 and Delta-1 in amoeboid microglia in postnatal rat brain and murine BV-2 cells.* Glia, 2008. **56**(11): p. 1224-1237.

70. Grandbarbe, L., A. Michelucci, T. Heurtaux, K. Hemmer, E. Morga, and P. Heuschling, *Notch signaling modulates the activation of microglial cells.* Glia, 2007. **55**(15): p. 1519-1530.

71. Farber, K., U. Pannasch, and H. Kettenmann, *Dopamine and noradrenaline control distinct functions in rodent microglial cells.* Molecular and Cellular Neuroscience, 2005. **29**(1): p. 128-138.

72. Mastroeni, D., A. Grover, B. Leonard, J.N. Joyce, P.D. Coleman, B. Kozik, D.L. Bellinger, and J. Rogers, *Microglial responses to dopamine in a cell culture model of Parkinson's disease.* Neurobiology of Aging, 2009. **30**(11): p. 1805-1817.

73. Miyoshi, M., K. Miyano, N. Moriyama, M. Taniguchi, and T. Watanabe, *Angiotensin type 1 receptor antagonist inhibits lipopolysaccharide-induced stimulation of rat microglial cells by suppressing nuclear factor kappa B and activator protein-1 activation.* European Journal of Neuroscience, 2008. **27**(2): p. 343-351.

74. Zhao, X., U.B. Eyo, M. Murugan, and L.-J. Wu, *Microglial interactions with the neurovascular system in physiology and pathology.* Developmental neurobiology, 2018.

75. Stankovic, N.D., M. Teodorczyk, R. Ploen, F. Zipp, and M.H.H. Schmidt, *Microglia-blood vessel interactions: a double-edged sword in brain pathologies.* Acta Neuropathologica, 2016. **131**(3): p. 347-363.

76. Thal, S.C. and W. Neuhaus, *The blood-brain barrier as a target in traumatic brain injury treatment.* Arch Med Res, 2014. **45**(8): p. 698-710.

77. Chodobski, A., B.J. Zink, and J. Szmydynger-Chodobska, *Blood–brain barrier pathophysiology in traumatic brain injury.* Translational stroke research, 2011. **2**(4): p. 492-516.

78. Shlosberg, D., M. Benifla, D. Kaufer, and A. Friedman, *Blood-brain barrier breakdown as a therapeutic target in traumatic brain injury.* Nature Reviews Neurology, 2010. **6**(7): p. 393-403.

79. Tchantchou, F. and Y.M. Zhang, *Selective Inhibition of Alpha/Beta-Hydrolase Domain 6 Attenuates Neurodegeneration, Alleviates Blood Brain Barrier Breakdown, and Improves Functional Recovery in a Mouse Model of Traumatic Brain Injury.* Journal of Neurotrauma, 2013. **30**(7): p. 565-579.

80. Choi, B.Y., B.G. Jang, J.H. Kim, B.E. Lee, M. Sohn, H.K. Song, and S.W. Suh, *Prevention of traumatic brain injury-induced neuronal death by inhibition of NADPH oxidase activation.* Brain Research, 2012. **1481**: p. 49-58.

81. Kuriakose, M., R.R.V. Kakulavarapu, D. Younger, A.R. Ravula, E. Alay, M. Murugan, and N. Chandra, *Synergistic Roles of oxidative stress and blood-brain barrier permeability as injury mechanisms in the acute pathophysiology of blast-induced neurotrauma.* Journal of Neurotrauma, 2018 - under review.

82. Trahanas, D.M., C.M. Cuda, H. Perlman, and S.J. Schwulst, *Differential Activation of Infiltrating Monocyte-Derived Cells After Mild and Severe Traumatic Brain Injury.* Shock, 2015. **43**(3): p. 255-260.

83.   Gyoneva, S., D. Kim, A. Katsumoto, O.N. Kokiko-Cochran, B.T. Lamb, and R.M. Ransohoff, *Ccr2 deletion dissociates cavity size and tau pathology after mild traumatic brain injury.* Journal of Neuroinflammation, 2015. **12**: p. 12.

84.   Shechter, R., A. London, C. Varol, C. Raposo, M. Cusimano, G. Yovel, A. Rolls, M. Mack, S. Pluchino, G. Martino, S. Jung, and M. Schwartz, *Infiltrating Blood-Derived Macrophages Are Vital Cells Playing an Anti-inflammatory Role in Recovery from Spinal Cord Injury in Mice.* Plos Medicine, 2009. **6**(7): p. 17.

85.   Hanisch, U.K., *Microglia as a source and target of cytokines.* Glia, 2002. **40**(2): p. 140-155.

86.   Febinger, H.Y., H.E. Thomasy, M.N. Pavlova, K.M. Ringgold, P.R. Barf, A.M. George, J.N. Grillo, A.D. Bachstetter, J.A. Garcia, A.E. Cardona, M.R. Opp, and C. Gemma, *Time-dependent effects of CX3CR1 in a mouse model of mild traumatic brain injury.* Journal of Neuroinflammation, 2015. **12**: p. 16.

87.   Qian, H.H., Q.H. Li, and W.D. Shi, *Hyperbaric oxygen alleviates the activation of NLRP-3-inflammasomes in traumatic brain injury.* Molecular Medicine Reports, 2017. **16**(4): p. 3922-3928.

88.   Chio, C.C., C.H. Chang, C.C. Wang, C.U. Cheong, C.M. Chao, B.C. Cheng, C.Z. Yang, and C.P. Chang, *Etanercept attenuates traumatic brain injury in rats by reducing early microglial expression of tumor necrosis factor-alpha.* Bmc Neuroscience, 2013. **14**: p. 12.

89.   Bachstetter, A.D., B. Xing, L. de Almeida, E.R. Dimayuga, D.M. Watterson, and L.J. Van Eldik, *Microglial p38α MAPK is a key regulator of proinflammatory cytokine up-regulation induced by toll-like receptor (TLR) ligands or beta-amyloid (Aβ).* Journal of Neuroinflammation, 2011. **8**(1): p. 79.

90.   Bachstetter, A.D., R.K. Rowe, M. Kaneko, D. Goulding, J. Lifshitz, and L.J. Van Eldik, *The p38 alpha MAPK Regulates Microglial Responsiveness to Diffuse Traumatic Brain Injury.* Journal of Neuroscience, 2013. **33**(14): p. 6143-6153.

91.   Pinteaux-Jones, F., I.G. Sevastou, V.A.H. Fry, S. Heales, D. Baker, and J.M. Pocock, *Myelin-induced microglial neurotoxicity can be controlled by microglial metabotropic glutamate receptors.* Journal of Neurochemistry, 2008. **106**(1): p. 442-454.

92.   McMullan, S.M., B. Phanavanh, G.G. Li, and S.W. Barger, *Metabotropic glutamate receptors inhibit microglial glutamate release.* Asn Neuro, 2012. **4**(5): p. 323-330.

93.   Mori, K., E. Ozaki, B. Zhang, L.H. Yang, A. Yokoyama, I. Takeda, N. Maeda, M. Sakanaka, and J. Tanaka, *Effects of norepinephrine on rat cultured microglial cells that express alpha 1, alpha 2, beta 1 and beta 2 adrenergic receptors.* Neuropharmacology, 2002. **43**(6): p. 1026-1034.

94.   Farez, M.F., F.J. Quintana, R. Gandhi, G. Izquierdo, M. Lucas, and H.L. Weiner, *Toll-like receptor 2 and poly(ADP-ribose) polymerase 1 promote central nervous system neuroinflammation in progressive EAE.* Nature Immunology, 2009. **10**(9): p. 958-U44.

95.   Jack, C.S., N. Arbour, J. Manusow, V. Montgrain, M. Blain, E. McCrea, A. Shapiro, and J.P. Antel, *TLR signaling tailors innate immune responses in human microglia and astrocytes.* Journal of Immunology, 2005. **175**(7): p. 4320-4330.

96.   Suuronen, T., J. Huuskonen, T. Nuutinen, and A. Salminen, *Characterization of the pro-inflammatory signaling induced by protein acetylation in microglia.* Neurochemistry International, 2006. **49**(6): p. 610-618.

97.   Kielian, T., P. Mayes, and M. Kielian, *Characterization of microglial responses to Staphylococcus aureus: effects on cytokine, costimulatory molecule, and Toll-like receptor expression.* Journal of Neuroimmunology, 2002. **130**(1-2): p. 86-99.

98.   Charles, K.J., J. Deuchars, C.H. Davies, and M.N. Pangalos, *GABA(B) receptor subunit expression in glia.* Molecular and Cellular Neuroscience, 2003. **24**(1): p. 214-223.

99. Harry, G.J., C.L. d'Hellencourt, C.A. McPherson, J.A. Funk, M. Aoyama, and R.N. Wine, *Tumor necrosis factor p55 and p75 receptors are involved in chemical-induced apoptosis of dentate granule neurons.* Journal of Neurochemistry, 2008. **106**(1): p. 281-298.

100. Kettenmann, H., U.K. Hanisch, M. Noda, and A. Verkhratsky, *Physiology of Microglia.* Physiological Reviews, 2011. **91**(2): p. 461-553.

101. Hausler, K.G., M. Prinz, C. Nolte, J.R. Weber, R.R. Schumann, H. Kettenmann, and U.K. Hanisch, *Interferon-gamma differentially modulates the release of cytokines and chemokines in lipopolysaccharide- and pneumococcal cell wall-stimulated mouse microglia and macrophages.* European Journal of Neuroscience, 2002. **16**(11): p. 2113-2122.

102. Lee, Y.B., A. Nagai, and S.U. Kim, *Cytokines, chemokines, and cytokine receptors in human microglia.* Journal of Neuroscience Research, 2002. **69**(1): p. 94-103.

103. van Rossum, D., S. Hilbert, S. Strassenburg, U.K. Hanisch, and W. Bruck, *Myelin-phagocytosing macrophages in isolated sciatic and optic nerves reveal a unique reactive phenotype.* Glia, 2008. **56**(3): p. 271-283.

104. McIntosh, T.K., D.H. Smith, D.F. Meaney, M.J. Kotapka, T.A. Gennarelli, and D.I. Graham, *Neuropathological sequelae of traumatic brain injury: Relationship to neurochemical and biomechanical mechanisms.* Laboratory Investigation, 1996. **74**(2): p. 315-342.

105. Kumar, A. and D.J. Loane, *Neuroinflammation after traumatic brain injury: Opportunities for therapeutic intervention.* Brain Behavior and Immunity, 2012. **26**(8): p. 1191-1201.

106. Loane, D.J. and A.I. Faden, *Neuroprotection for traumatic brain injury: translational challenges and emerging therapeutic strategies.* Trends in Pharmacological Sciences, 2010. **31**(12): p. 596-604.

107. Basrai, H.S., K.J. Christie, A. Turbic, N. Bye, and A.M. Turnley, *Suppressor of Cytokine Signaling-2 (SOCS2) Regulates the Microglial Response and Improves Functional Outcome after Traumatic Brain Injury in Mice.* Plos One, 2016. **11**(4): p. 24.

108. Clausen, F., A. Hanell, M. Bjork, L. Hillered, A.K. Mir, H. Gram, and N. Marklund, *Neutralization of interleukin-1 beta modifies the inflammatory response and improves histological and cognitive outcome following traumatic brain injury in mice.* European Journal of Neuroscience, 2009. **30**(3): p. 385-396.

109. Dong, H., Y.F. Ma, Z.X. Ren, B. Xu, Y.H. Zhang, J. Chen, and B. Yang, *Sigma-1 Receptor Modulates Neuroinflammation After Traumatic Brain Injury.* Cellular and Molecular Neurobiology, 2016. **36**(5): p. 639-645.

110. Elliott, M.B., R.F. Tuma, P.S. Amenta, M.F. Barbe, and J.I. Jallo, *Acute Effects of a Selective Cannabinoid-2 Receptor Agonist on Neuroinflammation in a Model of Traumatic Brain Injury.* Journal of Neurotrauma, 2011. **28**(6): p. 973-981.

111. Erturk, A., S. Mentz, E.E. Stout, M. Hedehus, S.L. Dominguez, L. Neumaier, F. Krammer, G. Llovera, K. Srinivasan, D.V. Hansen, A. Liesz, K.A. Scearce-Levie, and M. Sheng, *Interfering with the Chronic Immune Response Rescues Chronic Degeneration After Traumatic Brain Injury.* Journal of Neuroscience, 2016. **36**(38): p. 9962-9975.

112. Zanier, E.R., F. Marchesi, F. Ortolano, C. Perego, M. Arabian, T. Zoerle, E. Sammali, F. Pischiutta, and M.G. De Simoni, *Fractalkine Receptor Deficiency Is Associated with Early Protection but Late Worsening of Outcome following Brain Trauma in Mice.* Journal of Neurotrauma, 2016. **33**(11): p. 1060-1072.

113. Haselkorn, M.L., D.K. Shellington, E.K. Jackson, V.A. Vagni, K. Janesko-Feldman, R.K. Dubey, D.G. Gillespie, D.M. Cheng, M.J. Bell, L.W. Jenkins, G.E. Homanics, J. Schnermann, and P.M. Kochanek, *Adenosine A(1) Receptor Activation as a Brake on the Microglial Response after Experimental Traumatic Brain Injury in Mice.* Journal of Neurotrauma, 2010. **27**(5): p. 901-910.

114. Koshinaga, M., Y. Katayama, M. Fukushima, H. Oshima, T. Suma, and T. Takahata, *Rapid and widespread microglial activation induced by traumatic brain injury in rat brain slices.* Journal of Neurotrauma, 2000. **17**(3): p. 185-192.

115. Kumar, A., B.A. Stoica, B. Sabirzhanov, M.P. Burns, A.I. Faden, and D.J. Loane, *Traumatic brain injury in aged animals increases lesion size and chronically alters microglial/macrophage classical and alternative activation states.* Neurobiology of Aging, 2013. **34**(5): p. 1397-1411.

116. Laird, M.D., J.S. Shields, S. Sukumari-Ramesh, D.E. Kimbler, R.D. Fessler, B. Shakir, P. Youssef, N. Yanasak, J.R. Vender, and K.M. Dhandapani, *High Mobility Group Box Protein-1 Promotes Cerebral Edema After Traumatic Brain Injury via Activation of Toll-Like Receptor 4.* Glia, 2014. **62**(1): p. 26-38.

117. Yao, X.L., S.W. Liu, W. Ding, P.J. Yue, Q. Jiang, M. Zhao, F. Hu, and H.Q. Zhang, *TLR4 signal ablation attenuated neurological deficits by regulating microglial M1/M2 phenotype after traumatic brain injury in mice.* Journal of Neuroimmunology, 2017. **310**: p. 38-45.

118. Lenzlinger, P.M., V.H.J. Hans, H.I. Joller-Jemelka, O. Trentz, M.C. Morganti-Kossmann, and T. Kossmann, *Markers for cell-mediated immune response are elevated in cerebrospinal fluid and serum after severe traumatic brain injury in humans.* Journal of Neurotrauma, 2001. **18**(5): p. 479-489.

119. Loane, D., B. Stoica, F. Tchantchou, A. Kumar, J. Barrett, T. Akintola, F. Xue, P. Conn, and A. Faden, *Novel mGluR5 Positive Allosteric Modulator Improves Functional Recovery, Attenuates Neurodegeneration, and Alters Microglial Polarization after Experimental Traumatic Brain Injury.* Neurotherapeutics, 2014. **11**(4): p. 857-869.

120. Loane, D.J., B.A. Stoica, K.R. Byrnes, W. Jeong, and A.I. Faden, *Activation of mGluR5 and Inhibition of NADPH Oxidase Improves Functional Recovery after Traumatic Brain Injury.* Journal of Neurotrauma, 2013. **30**(5): p. 403-412.

121. Longhi, L., C. Perego, F. Ortolano, S. Aresi, S. Fumagalli, E.R. Zanier, N. Stocchetti, and M.G. De Simoni, *Tumor necrosis factor in traumatic brain injury: effects of genetic deletion of p55 or p75 receptor.* Journal of Cerebral Blood Flow and Metabolism, 2013. **33**(8): p. 1182-1189.

122. Rao, V.L.R., A. Dogan, K.K. Bowen, and R.J. Dempsey, *Traumatic brain injury leads to increased expression of peripheral-type benzodiazepine receptors, neuronal death, and activation of astrocytes and microglia in rat thalamus.* Experimental Neurology, 2000. **161**(1): p. 102-114.

123. Venneti, S., A.K. Wagner, G. Wang, S.L. Slagel, X. Chen, B.J. Lopresti, C.A. Mathis, and C.A. Wiley, *The high affinity peripheral benzodiazepine receptor ligand DAA1106 binds specifically to microglia in a rat model of traumatic brain injury: Implications for PET imaging.* Experimental Neurology, 2007. **207**(1): p. 118-127.

124. Liu, H., M.E. Rose, S. Culver, X.C. Ma, C.E. Dixon, and S.H. Graham, *Rosiglitazone attenuates inflammation and CA3 neuronal loss following traumatic brain injury in rats.* Biochemical and Biophysical Research Communications, 2016. **472**(4): p. 648-655.

125. Sauerbeck, A., J.X. Gao, R. Readnower, M. Liu, J.R. Pauly, G.Y. Bing, and P.G. Sullivan, *Pioglitazone attenuates mitochondrial dysfunction, cognitive impairment, cortical tissue loss, and inflammation following traumatic brain injury.* Experimental Neurology, 2011. **227**(1): p. 128-135.

126. Yi, J.H., S.W. Park, N. Brooks, B.T. Lang, and R. Vemuganti, *PPAR gamma agonist rosiglitazone is neuroprotective after traumatic brain injury via anti-inflammatory and anti-oxidative mechanisms.* Brain Research, 2008. **1244**: p. 164-172.

127. Cao, T., T.C. Thomas, J.M. Ziebell, J.R. Pauly, and J. Lifshitz, *Morphological and Genetic Activation of Microglia After Diffuse Traumatic Brain Injury in the Rat.* Neuroscience, 2012. **225**: p. 65-75.

128. Gao, W.W., Z.L. Zhao, G.J. Yu, Z.W. Zhou, Y. Zhou, T.T. Hu, R.C. Jiang, and J.N. Zhang, *VEGI attenuates the inflammatory injury and disruption of blood-brain barrier partly by suppressing*

the TLR4/NF-kappa B signaling pathway in experimental traumatic brain injury. Brain Research, 2015. **1622**: p. 230-239.

129. Ekmark-Lewen, S., J. Flygt, G.A. Fridgeirsdottir, O. Kiwanuka, A. Hanell, B.J. Meyerson, A.K. Mir, H. Gram, A. Lewen, F. Clausen, L. Hillered, and N. Marklund, *Diffuse traumatic axonal injury in mice induces complex behavioural alterations that are normalized by neutralization of interleukin-1.* European Journal of Neuroscience, 2016. **43**(8): p. 1016-1033.

130. Pilipovic, K., Z. Zupan, P. Dolenec, J. Mrsic-Pelcic, and G. Zupan, *A single dose of PPAR gamma agonist pioglitazone reduces cortical oxidative damage and microglial reaction following lateral fluid percussion brain injury in rats.* Progress in Neuro-Psychopharmacology & Biological Psychiatry, 2015. **59**: p. 8-20.

131. Bye, N., M.D. Habgood, J.K. Callaway, N. Malakooti, A. Potter, T. Kossmann, and M.C. Morganti-Kossmann, *Transient neuroprotection by minocycline following traumatic brain injury is associated with attenuated microglial activation but no changes in cell apoptosis or neutrophil infiltration.* Experimental Neurology, 2007. **204**(1): p. 220-233.

132. Chang, C.Z., S.C. Wu, A.L. Kwan, and C.L. Lin, *Magnesium Lithospermate B Implicates 3 '-5 '-Cyclic Adenosine Monophosphate/Protein Kinase A Pathway and N-Methyl-D-Aspartate Receptors in an Experimental Traumatic Brain Injury.* World Neurosurgery, 2015. **84**(4): p. 954-963.

133. Hellewell, S.C., E.B. Yan, D.S. Alwis, N. Bye, and M.C. Morganti-Kossmann, *Erythropoietin improves motor and cognitive deficit, axonal pathology, and neuroinflammation in a combined model of diffuse traumatic brain injury and hypoxia, in association with upregulation of the erythropoietin receptor.* Journal of Neuroinflammation, 2013. **10**: p. 21.

134. Mao, S.S., R. Hua, X.P. Zhao, X. Qin, Z.Q. Sun, Y. Zhang, Y.Q. Wu, M.X. Jia, J.L. Cao, and Y.M. Zhang, *Exogenous Administration of PACAP Alleviates Traumatic Brain Injury in Rats through a Mechanism Involving the TLR4/MyD88/NF-kappa B Pathway.* Journal of Neurotrauma, 2012. **29**(10): p. 1941-1959.

135. Zhang, Z.R., Z.Y. Zhang, Y.Z. Wu, and H.J. Schluesener, *Immunolocalization of Toll-Like Receptors 2 and 4 as well as Their Endogenous Ligand, Heat Shock Protein 70, in Rat Traumatic Brain Injury.* Neuroimmunomodulation, 2012. **19**(1): p. 10-19.

136. Semple, B.D., N. Bye, M. Rancan, J.M. Ziebell, and M.C. Morganti-Kossmann, *Role of CCL2 (MCP-1) in traumatic brain injury (TBI): evidence from severe TBI patients and CCL2-/- mice.* Journal of Cerebral Blood Flow and Metabolism, 2010. **30**(4): p. 769-782.

137. Wang, J.W., H.D. Wang, Z.X. Cong, X.S. Zhang, X.M. Zhou, and D.D. Zhang, *Activation of metabotropic glutamate receptor 5 reduces the secondary brain injury after traumatic brain injury in rats.* Biochemical and Biophysical Research Communications, 2013. **430**(3): p. 1016-1021.

138. Wang, J.W., H.D. Wang, W.Z. Zhong, N. Li, and Z.X. Cong, *Expression and cell distribution of metabotropic glutamate receptor 5 in the rat cortex following traumatic brain injury.* Brain Research, 2012. **1464**: p. 73-81.

139. Zhang, Z.Y., Z.R. Zhang, M. Artelt, M. Burnet, and H.J. Schluesener, *Dexamethasone attenuates early expression of three molecules associated with microglia/macrophages activation following rat traumatic brain injury.* Acta Neuropathologica, 2007. **113**(6): p. 675-682.

140. Khuman, J., W.P. Meehan, X.X. Zhu, J.H. Qiu, U. Hoffmann, J. Zhang, E. Giovannone, E.H. Lo, and M.J. Whalen, *Tumor necrosis factor alpha and Fas receptor contribute to cognitive deficits independent of cell death after concussive traumatic brain injury in mice.* Journal of Cerebral Blood Flow and Metabolism, 2011. **31**(2): p. 778-789.

141. Bu, W., H.L. Ren, Y.P. Deng, N. Del Mar, N.M. Guley, B.M. Moore, M.G. Honig, and A. Reiner, *Mild Traumatic Brain Injury Produces Neuron Loss That Can Be Rescued by Modulating*

Microglial Activation Using a CB2 Receptor Inverse Agonist. Frontiers in Neuroscience, 2016. **10**: p. 17.

142.	Reiner, A., S.A. Heldt, C.S. Presley, N.H. Guley, A.J. Elberger, Y.P. Deng, L. D'Surney, J.T. Rogers, J. Ferrell, W. Bu, N. Del Mar, M.G. Honig, S.N. Gurley, and B.M. Moore, *Motor, Visual and Emotional Deficits in Mice after Closed-Head Mild Traumatic Brain Injury Are Alleviated by the Novel CB2 Inverse Agonist SMM-189.* International Journal of Molecular Sciences, 2015. **16**(1): p. 758-787.

143.	Kaur, C., J. Singh, M.K. Lim, B.L. Ng, E.P.H. Yap, and E.A. Ling, *The Response of Neurons and Microglia to Blast Injury in the Rat-Brain.* Neuropathology and Applied Neurobiology, 1995. **21**(5): p. 369-377.

144.	Beschorner, R., T.D. Nguyen, F. Gozalan, I. Pedal, R. Mattern, H.J. Schluesener, R. Meyermann, and J.M. Schwab, *CD14 expression by activated parenchymal microglia/macrophages and infiltrating monocytes following human traumatic brain injury.* Acta Neuropathologica, 2002. **103**(6): p. 541-549.

145.	Franke, H., C. Parravicini, D. Lecca, E.R. Zanier, C. Heine, K. Bremicker, M. Fumagalli, P. Rosa, L. Longhi, N. Stocchetti, M.G. De Simoni, M. Weber, and M.P. Abbracchio, *Changes of the GPR17 receptor, a new target for neurorepair, in neurons and glial cells in patients with traumatic brain injury.* Purinergic Signalling, 2013. **9**(3): p. 451-462.

146.	Helmy, A., M.R. Guilfoyle, K.L.H. Carpenter, J.D. Pickard, D.K. Menon, and P.J. Hutchinson, *Recombinant human interleukin-1 receptor antagonist promotes M1 microglia biased cytokines and chemokines following human traumatic brain injury.* Journal of Cerebral Blood Flow and Metabolism, 2016. **36**(8): p. 1434-1448.

147.	Robinson, S., J.B. Berglass, J.L. Denson, J. Berkner, C.V. Anstine, J.L. Winer, J.R. Maxwell, J.H. Qiu, Y.R. Yang, L.O. Sillerud, W.P. Meehan, R. Mannix, and L.L. Jantzie, *Microstructural and Microglial Changes After Repetitive Mild Traumatic Brain Injury in Mice.* Journal of Neuroscience Research, 2017. **95**(4): p. 1025-1035.

148.	Cardona, A.E., E.P. Pioro, M.E. Sasse, V. Kostenko, S.M. Cardona, I.M. Dijkstra, D.R. Huang, G. Kidd, S. Dombrowski, R. Dutta, J.C. Lee, D.N. Cook, S. Jung, S.A. Lira, D.R. Littman, and R.M. Ransohoff, *Control of microglial neurotoxicity by the fractalkine receptor.* Nature Neuroscience, 2006. **9**(7): p. 917-924.

149.	Tarozzo, G., M. Campanella, M. Ghiani, A. Bulfone, and M. Beltramo, *Expression of fractalkine and its receptor, CX(3)CR1, in response to ischaemia-reperfusion brain injury in the rat.* European Journal of Neuroscience, 2002. **15**(10): p. 1663-1668.

150.	Harrison, J.K., Y. Jiang, S.Z. Chen, Y.Y. Xia, D. Maciejewski, R.K. McNamara, W.J. Streit, M.N. Salafranca, S. Adhikari, D.A. Thompson, P. Botti, K.B. Bacon, and L.L. Feng, *Role for neuronally derived fractalkine in mediating interactions between neurons and CX3CR1-expressing microglia.* Proceedings of the National Academy of Sciences of the United States of America, 1998. **95**(18): p. 10896-10901.

151.	Clark, A.K., P.K. Yip, J. Grist, C. Gentry, A.A. Staniland, F. Marchand, M. Dehvari, G. Wotherspoon, J. Winter, J. Ullah, S. Bevan, and M. Malcangio, *Inhibition of spinal microglial cathepsin S for the reversal of neuropathic pain.* Proceedings of the National Academy of Sciences of the United States of America, 2007. **104**(25): p. 10655-10660.

152.	Zhuang, Z.Y., Y. Kawasaki, P.H. Tan, Y.R. Wen, J. Huang, and R.R. Ji, *Role of the CX3CR1/p38 MAPK pathway in spinal microglia for the development of neuropathic pain following nerve injury-induced cleavage of fractalkine.* Brain Behavior and Immunity, 2007. **21**(5): p. 642-651.

153.	Boehme, S.A., F.M. Lio, D. Maciejewski-Lenoir, K.B. Bacon, and P.J. Conlon, *The chemokine fractalkine inhibits Fas-mediated cell death of brain microglia.* Journal of Immunology, 2000. **165**(1): p. 397-403.

154. Abbracchio, M.P. and G. Burnstock, *Purinoceptors - Are There Families Of P2X And P2Y Purinoceptors.* Pharmacology & Therapeutics, 1994. **64**(3): p. 445-475.

155. Sasaki, Y., M. Hoshi, C. Akazawa, Y. Nakamura, H. Tsuzuki, K. Inoue, and S. Kohsaka, *Selective expression of Gi/o-coupled ATP receptor P2Y(12) in microglia in rat brain.* Glia, 2003. **44**(3): p. 242-250.

156. Honda, S., Y. Sasaki, K. Ohsawa, Y. Imai, Y. Nakamura, K. Inoue, and S. Kohsaka, *Extracellular ATP or ADP induce chemotaxis of cultured microglia through G(i/o)-coupled P2Y receptors.* Journal of Neuroscience, 2001. **21**(6): p. 1975-1982.

157. Madry, C., V. Kyrargyri, I.L. Arancibia-Carcamo, R. Jolivet, S. Kohsaka, R.M. Bryan, and D. Attwell, *Microglial Ramification, Surveillance, and Interleukin-1 beta Release Are Regulated by the Two-Pore Domain K+ Channel THIK-1.* Neuron, 2018. **97**(2): p. 299-+.

158. Swiatkowski, P., M. Murugan, U.B. Eyo, Y. Wang, S. Rangaraju, S.B. Oh, and L.J. Wu, *Activation of Microglial P2Y12 Receptor is Required for Outward Potassium Currents in Response to Neuronal Injury.* Neuroscience, 2016. **318**: p. 22-33.

159. Moore, C.S., A.R. Ase, A. Kinsara, V.T.S. Rao, M. Michell-Robinson, S.Y. Leong, O. Butovsky, S.K. Ludwin, P. Seguela, A. Bar-Or, and J.P. Antel, *P2Y12 expression and function in alternatively activated human microglia.* Neurology-Neuroimmunology & Neuroinflammation, 2015. **2**(2): p. 10.

160. Tozaki-Saitoh, H., H. Miyata, T. Yamashita, K. Matsushita, M. Tsuda, and K. Inoue, *P2Y12 receptors in primary microglia activate nuclear factor of activated T-cell signaling to induce C-C chemokine 3 expression.* Journal of Neurochemistry, 2017. **141**(1): p. 100-110.

161. Kobayashi, K., H. Yamanaka, T. Fukuoka, Y. Dai, K. Obata, and K. Noguchi, *P2Y(12) receptor Upregulation in activated microglia is a gateway of p38 signaling and neuropathic pain.* Journal of Neuroscience, 2008. **28**(11): p. 2892-2902.

162. Gu, N., U.B. Eyo, M. Murugan, J.Y. Peng, S. Matta, H.L. Dong, and L.J. Wu, *Microglial P2Y12 receptors regulate microglial activation and surveillance during neuropathic pain.* Brain Behavior and Immunity, 2016. **55**: p. 82-92.

163. Avignone, E., L. Ulmann, F. Levavasseur, F. Rassendren, and E. Audinat, *Status epilepticus induces a particular microglial activation state characterized by enhanced purinergic signaling.* Journal of Neuroscience, 2008. **28**(37): p. 9133-9144.

164. Sipe, G.O., R.L. Lowery, M.E. Tremblay, E.A. Kelly, C.E. Lamantia, and A.K. Majewska, *Microglial P2Y12 is necessary for synaptic plasticity in mouse visual cortex.* Nature Communications, 2016. **7**: p. 15.

165. Haynes, S.E., G. Hollopeter, G. Yang, D. Kurpius, M.E. Dailey, W.B. Gan, and D. Julius, *The P2Y(12) receptor regulates microglial activation by extracellular nucleotides.* Nature Neuroscience, 2006. **9**(12): p. 1512-1519.

166. Sieger, D., C. Moritz, T. Ziegenhals, S. Prykhozhij, and F. Peri, *Long-Range Ca2+ Waves Transmit Brain-Damage Signals to Microglia.* Developmental Cell, 2012. **22**(6): p. 1138-1148.

167. Lafrenaye, A.D., M. Todani, S.A. Walker, and J.T. Povlishock, *Microglia processes associate with diffusely injured axons following mild traumatic brain injury in the micro pig.* Journal of Neuroinflammation, 2015. **12**: p. 15.

168. Eyo, U.B., N. Gu, S. De, H.L. Dong, J.R. Richardson, and L.J. Wu, *Modulation of Microglial Process Convergence Toward Neuronal Dendrites by Extracellular Calcium.* Journal of Neuroscience, 2015. **35**(6): p. 2417-2422.

169. Kato, G., H. Inada, H. Wake, R. Akiyoshi, A. Miyamoto, K. Eto, T. Ishikawa, A.J. Moorhouse, A.M. Strassman, and J. Nabekura, *Microglial Contact Prevents Excess Depolarization and Rescues Neurons from Excitotoxicity.* Eneuro, 2016. **3**(3): p. 9.

170. Esen, N. and T. Kielian, *Central role for MyD88 in the responses of microglia to pathogen-associated molecular patterns.* Journal of Immunology, 2006. **176**(11): p. 6802-6811.

171. Zhang, Z. and H.J. Schluesener, *Mammalian toll-like receptors: from endogenous ligands to tissue regeneration.* Cellular and Molecular Life Sciences, 2006. **63**(24): p. 2901-2907.

172. Ock, J., J. Jeong, W.S. Choi, W.H. Lee, S.H. Kim, I.K. Kim, and K. Suk, *Regulation of toll-like receptor 4 expression and its signaling by hypoxia in cultured microglia.* Journal of Neuroscience Research, 2007. **85**(9): p. 1989-1995.

173. Zhang, Y., K.N. Chen, S.A. Sloan, M.L. Bennett, A.R. Scholze, S. O'Keeffe, H.P. Phatnani, P. Guarnieri, C. Caneda, N. Ruderisch, S.Y. Deng, S.A. Liddelow, C.L. Zhang, R. Daneman, T. Maniatis, B.A. Barres, and J.Q. Wu, *An RNA-Sequencing Transcriptome and Splicing Database of Glia, Neurons, and Vascular Cells of the Cerebral Cortex.* Journal of Neuroscience, 2014. **34**(36): p. 11929-11947.

174. Sims, J.E. and D.E. Smith, *The IL-1 family: regulators of immunity.* Nature Reviews Immunology, 2010. **10**(2): p. 89-102.

175. Bruttger, J., K. Karram, S. Wörtge, T. Regen, F. Marini, N. Hoppmann, M. Klein, T. Blank, S. Yona, Y. Wolf, M. Mack, E. Pinteaux, W. Müller, F. Zipp, H. Binder, T. Bopp, M. Prinz, S. Jung, and A. Waisman, *Genetic Cell Ablation Reveals Clusters of Local Self-Renewing Microglia in the Mammalian Central Nervous System.* Immunity, 2015. **43**(1): p. 92-106.

176. Stavridis, S., F. Dehghani, H.W. Korf, and N. Hailer, *Characterisation of transverse slice culture preparations of postnatal rat spinal cord: preservation of defined neuronal populations.* Histochemistry and Cell Biology, 2005. **123**(4-5): p. 377-392.

177. Basu, A., J.K. Krady, M. Malley, S.D. Styren, S.T. DeKosky, and S.W. Levison, *The Type 1 Interleukin-1 Receptor Is Essential for the Efficient Activation of Microglia and the Induction of Multiple Proinflammatory Mediators in Response to Brain Injury.* The Journal of Neuroscience, 2002. **22**(14): p. 6071.

178. Robson, M.J., C.B. Zhu, M.A. Quinlan, D.A. Botschner, N.L. Baganz, K.M. Lindler, J.G. Thome, W.A. Hewlett, and R.D. Blakely, *Generation and Characterization of Mice Expressing a Conditional Allele of the Interleukin-1 Receptor Type 1.* Plos One, 2016. **11**(3): p. 17.

179. Ma, J., W.J. Xiao, J.R. Wang, J. Wu, J.D. Ren, J. Hou, J.W. Gu, K.H. Fan, and B.T. Yu, *Propofol Inhibits NLRP3 Inflammasome and Attenuates Blast-Induced Traumatic Brain Injury in Rats.* Inflammation, 2016. **39**(6): p. 2094-2103.

180. Fan, K.H., J. Ma, W.J. Xiao, J.M. Chen, J. Wu, J.D. Ren, J. Hou, Y.H. Hu, J.W. Gu, and B.T. Yu, *Mangiferin attenuates blast-induced traumatic brain injury via inhibiting NLRP3 inflammasome.* Chemico-Biological Interactions, 2017. **271**: p. 15-23.

181. Halle, A., V. Hornung, G.C. Petzold, C.R. Stewart, B.G. Monks, T. Reinheckel, K.A. Fitzgerald, E. Latz, K.J. Moore, and D.T. Golenbock, *The NALP3 inflammasome is involved in the innate immune response to amyloid-beta.* Nature Immunology, 2008. **9**(8): p. 857-865.

182. Hanamsagar, R., V. Torres, and T. Kielian, *Inflammasome activation and IL-1 beta/IL-18 processing are influenced by distinct pathways in microglia.* Journal of Neurochemistry, 2011. **119**(4): p. 736-748.

183. Shi, F.S., Y. Yang, M. Kouadir, Y.Y. Fu, L.F. Yang, X.M. Zhou, X.M. Yin, and D.M. Zhao, *Inhibition of phagocytosis and lysosomal acidification suppresses neurotoxic prion peptide-induced NALP3 inflammasome activation in BV2 microglia.* Journal of Neuroimmunology, 2013. **260**(1-2): p. 121-125.

184. Duncan, J.A., X. Gao, M.T.H. Huang, B.P. O'Connor, C.E. Thomas, S.B. Willingham, D.T. Bergstralh, G.A. Jarvis, P.F. Sparling, and J.P.Y. Ting, *Neisseria gonorrhoeae Activates the Proteinase Cathepsin B to Mediate the Signaling Activities of the NLRP3 and ASC-Containing Inflammasome.* Journal of Immunology, 2009. **182**(10): p. 6460-6469.

185. Ichinohe, T., H.K. Lee, Y. Ogura, R. Flavell, and A. Iwasaki, *Inflammasome recognition of influenza virus is essential for adaptive immune responses.* Journal of Experimental Medicine, 2009. **206**(1): p. 79-87.

186. Cruz, C.M., A. Rinna, H.J. Forman, A.L.M. Ventura, P.M. Persechini, and D.M. Ojcius, *ATP activates a reactive oxygen species-dependent oxidative stress response and secretion of proinflammatory cytokines in macrophages.* Journal of Biological Chemistry, 2007. **282**(5): p. 2871-2879.

187. Hoegen, T., N. Tremel, M. Klein, B. Angele, H. Wagner, C. Kirschning, H.W. Pfister, A. Fontana, S. Hammerschmidt, and U. Koedel, *The NLRP3 Inflammasome Contributes to Brain Injury in Pneumococcal Meningitis and Is Activated through ATP-Dependent Lysosomal Cathepsin B Release.* Journal of Immunology, 2011. **187**(10): p. 5440-5451.

188. Mariathasan, S., D.S. Weiss, K. Newton, J. McBride, K. O'Rourke, M. Roose-Girma, W.P. Lee, Y. Weinrauch, D.M. Monack, and V.M. Dixit, *Cryopyrin activates the inflammasome in response to toxins and ATP.* Nature, 2006. **440**(7081): p. 228-232.

189. Martinon, F., V. Petrilli, A. Mayor, A. Tardivel, and J. Tschopp, *Gout-associated uric acid crystals activate the NALP3 inflammasome.* Nature, 2006. **440**(7081): p. 237-241.

190. Hornung, V., F. Bauernfeind, A. Halle, E.O. Samstad, H. Kono, K.L. Rock, K.A. Fitzgerald, and E. Latz, *Silica crystals and aluminum salts activate the NALP3 inflammasome through phagosomal destabilization.* Nature Immunology, 2008. **9**(8): p. 847-856.

191. Lee, S.W., S. Gajavelli, M.S. Spurlock, C. Andreoni, J.P.D. Vaccari, M.R. Bullock, R.W. Keane, and W.D. Dietrich, *Microglial Inflammasome Activation in Penetrating Ballistic-Like Brain Injury.* Journal of Neurotrauma, 2018: p. 13.

192. Liu, H.D., W. Li, Z.R. Chen, Y.C. Hu, D.D. Zhang, W. Shen, M.L. Zhou, L. Zhu, and C.H. Hang, *Expression of the NLRP3 Inflammasome in Cerebral Cortex After Traumatic Brain Injury in a Rat Model.* Neurochemical Research, 2013. **38**(10): p. 2072-2083.

193. Kuno, R., J.Y. Wang, J. Kawanokuchi, H. Takeuchi, T. Mizuno, and A. Suzumura, *Autocrine activation of microglia by tumor necrosis factor-alpha.* Journal of Neuroimmunology, 2005. **162**(1-2): p. 89-96.

194. Kraft, A.D., C.A. McPherson, and G.J. Harry, *Heterogeneity of microglia and TNF signaling as determinants for neuronal death or survival.* Neurotoxicology, 2009. **30**(5): p. 785-793.

195. Chen, G.Q. and D.V. Goeddel, *TNF-R1 signaling: A beautiful pathway.* Science, 2002. **296**(5573): p. 1634-1635.

196. Liu, C. and J.W. Tang, *Expression levels of tumor necrosis factor-alpha and the corresponding receptors are correlated with trauma severity.* Oncology Letters, 2014. **8**(6): p. 2747-2751.

197. Yang, J.S., Z.R. You, H.H. Kim, S.K. Hwang, J. Khuman, S.Z. Guo, E.H. Lo, and M.J. Whalen, *Genetic Analysis of the Role of Tumor Necrosis Factor Receptors in Functional Outcome after Traumatic Brain Injury in Mice.* Journal of Neurotrauma, 2010. **27**(6): p. 1037-1046.

198. Longhi, L., F. Ortolano, E.R. Zanier, C. Perego, N. Stocchetti, and M.G. De Simoni, *Effect of traumatic brain injury on cognitive function in mice lacking p55 and p75 tumor necrosis factor receptors*, in *Intracranial Pressure and Brain Monitoring Xiii: Mechanisms and Treatment*, G. Manley, C. Hemphill, and S. Stiver, Editors. 2008, Springer-Verlag Wien: Vienna. p. 409-+.

199. Lotocki, G., O.F. Alonso, W.D. Dietrich, and R.W. Keane, *Tumor necrosis factor receptor 1 and its signaling intermediates are recruited to lipid rafts in the traumatized brain.* Journal of Neuroscience, 2004. **24**(49): p. 11010-11016.

200. Yager, P.H., Z. You, T. Qin, H.H. Kim, K. Takahashi, A.B. Ezekowitz, G.L. Stahl, M.C. Carroll, and M.J. Whalen, *Mannose binding lectin gene deficiency increases susceptibility to traumatic brain injury in mice.* Journal of Cerebral Blood Flow and Metabolism, 2008. **28**(5): p. 1030-1039.

201.   Hailer, N.P., *Immunosuppression after traumatic or ischemic CNS damage: It is neuroprotective and illuminates the role of microglial cells.* Progress in Neurobiology, 2008. **84**(3): p. 211-233.

202.   Bermpohl, D., Z. You, E.H. Lo, H.H. Kim, and M.J. Whalen, *TNF alpha and Fas mediate tissue damage and functional outcome after traumatic brain injury in mice.* Journal of Cerebral Blood Flow and Metabolism, 2007. **27**(11): p. 1806-1818.

203.   Michalik, L. and W. Wahli, *Peroxisome proliferator-activated receptors: three isotypes for a multitude of functions.* Current Opinion in Biotechnology, 1999. **10**(6): p. 564-570.

204.   Delerive, P., J.C. Fruchart, and B. Staels, *Peroxisome proliferator-activated receptors in inflammation control.* Journal of Endocrinology, 2001. **169**(3): p. 453-459.

205.   Besson, V.C., X.R. Chen, M. Plotkine, and C. Marchand-Verrecchia, *Fenofibrate, a peroxisome proliferator-activated receptor alpha agonist, exerts neuroprotective effects in traumatic brain injury.* Neuroscience Letters, 2005. **388**(1): p. 7-12.

206.   Chen, X.R., V.C. Besson, B. Palmier, Y. Garcia, M. Plotkine, and C. Marchand-Leroux, *Neurological recovery-promoting, anti-inflammatory, and anti-oxidative effects afforded by fenofibrate, a PPAR alpha agonist, in traumatic brain injury.* Journal of Neurotrauma, 2007. **24**(7): p. 1119-1131.

207.   Park, S.W., J.H. Yi, G. Miranpuri, I. Satriotomo, K. Bowen, D.K. Resnick, and R. Vemuganti, *Thiazolidinedione class of peroxisome proliferator-activated receptor gamma agonists prevents neuronal damage, motor dysfunction, myelin loss, neuropathic pain, and inflammation after spinal cord injury in adult rats.* Journal of Pharmacology and Experimental Therapeutics, 2007. **320**(3): p. 1002-1012.

208.   Hyong, A., V. Jadhav, S. Lee, W. Tong, J. Rowe, J.H. Zhang, and J.P. Tang, *Rosiglitazone, a PPAR gamma agonist, attenuates inflammation after surgical brain injury in rodents.* Brain Research, 2008. **1215**: p. 218-224.

209.   Kapadia, R., J.H. Yi, and R. Vemuganti, *Mechanisms of anti-inflammatory and neuroprotective actions of PPAR-gamma agonists.* Frontiers in Bioscience-Landmark, 2008. **13**: p. 1813-1826.

210.   Hunter, R.L., N. Dragicevic, K. Seifert, D.Y. Choi, M. Liu, H.C. Kim, W.A. Cass, P.G. Sullivan, and G.Y. Bing, *Inflammation induces mitochondrial dysfunction and dopaminergic neurodegeneration in the nigrostriatal system.* Journal of Neurochemistry, 2007. **100**(5): p. 1375-1386.

211.   McTigue, D.M., R. Tripathi, P. Wei, and A.T. Lash, *The PPAR gamma agonist Pioglitazone improves anatomical and locomotor recovery after rodent spinal cord injury.* Experimental Neurology, 2007. **205**(2): p. 396-406.

212.   Warden, A., J. Truitt, M. Merriman, O. Ponomareva, K. Jameson, L.B. Ferguson, R.D. Mayfield, and R.A. Harris, *Localization of PPAR isotypes in the adult mouse and human brain.* Scientific Reports, 2016. **6**: p. 15.

213.   Blasi, E., B.J. Mathieson, L. Varesio, J.L. Cleveland, P.A. Borchert, and U.R. Rapp, *Selective Immortalization of Murine Macrophages from Fresh Bone-Marrow by a Raf/Myc Recombinant Murine Retrovirus.* Nature, 1985. **318**(6047): p. 667-670.

214.   Blasi, E., R. Barluzzi, V. Bocchini, R. Mazzolla, and F. Bistoni, *Immortalization of Murine Microglial Cells by a V-RAF/V-MYC Carrying Retrovirus.* Journal of Neuroimmunology, 1990. **27**(2-3): p. 229-237.

215.   Walker, W.S., J. Gatewood, E. Olivas, D. Askew, and C.E.G. Havenith, *Mouse microglial cell lines differing in constitutive and interferon-gamma-inducible antigen-presenting activities for naive and memory CD4(+) and CD8(+) T cells.* Journal of Neuroimmunology, 1995. **63**(2): p. 163-174.

216.   Cheepsunthorn, P., L. Radov, S. Menzies, J. Reid, and J.R. Connor, *Characterization of a novel brain-derived microglial cell line isolated from neonatal rat brain.* Glia, 2001. **35**(1): p. 53-62.

217.   Stansley, B., J. Post, and K. Hensley, *A comparative review of cell culture systems for the study of microglial biology in Alzheimer's disease.* Journal of Neuroinflammation, 2012. **9**: p. 8.

218. Giulian, D. and T.J. Baker, *CHARACTERIZATION OF AMEBOID MICROGLIA ISOLATED FROM DEVELOPING MAMMALIAN BRAIN.* Journal of Neuroscience, 1986. **6**(8): p. 2163-2178.

219. Jung, S., J. Aliberti, P. Graemmel, M.J. Sunshine, G.W. Kreutzberg, A. Sher, and D.R. Littman, *Analysis of fractalkine receptor CX(3)CR1 function by targeted deletion and green fluorescent protein reporter gene insertion.* Molecular and Cellular Biology, 2000. **20**(11): p. 4106-4114.

220. Duffield, J.S., S.J. Forbes, C.M. Constandinou, S. Clay, M. Partolina, S. Vuthoori, S.J. Wu, R. Lang, and J.P. Iredale, *Selective depletion of macrophages reveals distinct, opposing roles during liver injury and repair.* Journal of Clinical Investigation, 2005. **115**(1): p. 56-65.

221. Faust, N., F. Varas, L.M. Kelly, S. Heck, and T. Graf, *Insertion of enhanced green fluorescent protein into the lysozyme gene creates mice with green fluorescent granulocytes and macrophages.* Blood, 2000. **96**(2): p. 719-726.

222. Yona, S., K.W. Kim, Y. Wolf, A. Mildner, D. Varol, M. Breker, D. Strauss-Ayali, S. Viukov, M. Guilliams, A. Misharin, D.A. Hume, H. Perlman, B. Malissen, E. Zelzer, and S. Jung, *Fate Mapping Reveals Origins and Dynamics of Monocytes and Tissue Macrophages under Homeostasis.* Immunity, 2013. **38**(1): p. 79-91.

223. Liu, Y., S.S. McAfee, N.M. Guley, N. Del Mar, W. Bu, S.A. Heldt, M.G. Honig, B.M. Moore, 2nd, A. Reiner, and D.H. Heck, *Abnormalities in Dynamic Brain Activity Caused by Mild Traumatic Brain Injury Are Partially Rescued by the Cannabinoid Type-2 Receptor Inverse Agonist SMM-189.* eNeuro, 2017. **4**(4).

224. Szalay, G., B. Martinecz, N. Lenart, Z. Kornyei, B. Orsolits, L. Judak, E. Csaszar, R. Fekete, B.L. West, G. Katona, B. Rozsa, and A. Denes, *Microglia protect against brain injury and their selective elimination dysregulates neuronal network activity after stroke.* Nature Communications, 2016. **7**: p. 13.

225. Lalancette-Hebert, M., J. Faustino, S.S. Thammisetty, S. Chip, Z.S. Vexler, and J. Kriz, *Live imaging of the innate immune response in neonates reveals differential TLR2 dependent activation patterns in sterile inflammation and infection.* Brain Behavior and Immunity, 2017. **65**: p. 312-327.

226. Ziebell, J.M., S.E. Taylor, T.X. Cao, J.L. Harrison, and J. Lifshitz, *Rod microglia: elongation, alignment, and coupling to form trains across the somatosensory cortex after experimental diffuse brain injury.* Journal of Neuroinflammation, 2012. **9**: p. 11.

227. Morrison, H., K. Young, M. Qureshi, R.K. Rowe, and J. Lifshitz, *Quantitative microglia analyses reveal diverse morphologic responses in the rat cortex after diffuse brain injury.* Scientific Reports, 2017. **7**: p. 12.

228. Baalman, K.L., R.J. Cotton, S.N. Rasband, and M.N. Rasband, *Blast Wave Exposure Impairs Memory and Decreases Axon Initial Segment Length.* Journal of Neurotrauma, 2013. **30**(9): p. 741-751.

229. Sajja, V., W.B. Hubbard, C.S. Hall, F. Ghoddoussi, M.P. Galloway, and P.J. VandeVord, *Enduring deficits in memory and neuronal pathology after blast-induced traumatic brain injury.* Scientific Reports, 2015. **5**: p. 10.

230. Readnower, R.D., M. Chavko, S. Adeeb, M.D. Conroy, J.R. Pauly, R.M. McCarron, and P.G. Sullivan, *Increase in blood-brain barrier permeability, oxidative stress, and activated microglia in a rat model of blast-induced traumatic brain injury.* J Neurosci Res, 2010. **88**(16): p. 3530-9.

231. Acabchuk, R., D.I. Briggs, M. Angoa-Perez, M. Powers, R. Wolferz, Jr., M. Soloway, M. Stern, L.R. Talbot, D.M. Kuhn, and J.C. Conover, *Repeated mild traumatic brain injury causes focal response in lateral septum and hippocampus.* Concussion (London, England), 2016. **1**(3).

232. Kokiko-Cochran, O.N., M. Saber, S. Puntambekar, S.M. Bemiller, A. Katsumoto, Y.S. Lee, K. Bhaskar, R.M. Ransohoff, and B.T. Lamb, *Traumatic Brain Injury in hTau Model Mice: Enhanced*

Acute Macrophage Response and Altered Long-Term Recovery. Journal of Neurotrauma, 2018. **35**(1): p. 73-84.

233.   Huang, E.Y.K., T.H. Tsai, T.T. Kuo, J.J. Tsai, P.F. Tsui, Y.C. Chou, H.I. Ma, Y.H. Chiang, and Y.H. Chen, *Remote effects on the striatal dopamine system after fluid percussion injury.* Behavioural Brain Research, 2014. **267**: p. 156-172.

234.   Carbonnel, W.S. and M.S. Grady, *Regional and temporal characterization of neuronal, glial, and axonal response after traumatic brain injury in the mouse.* Acta Neuropathologica, 1999. **98**(4): p. 396-406.

235.   Webster, K.M., D.K. Wright, M.J. Sun, B.D. Semple, E. Ozturk, D.G. Stein, T.J. O'Brien, and S.R. Shultz, *Progesterone treatment reduces neuroinflammation, oxidative stress and brain damage and improves long-term outcomes in a rat model of repeated mild traumatic brain injury.* Journal of Neuroinflammation, 2015. **12**: p. 13.

236.   Xu, L.Y., M.L. Schaefer, R.M. Linville, A. Aggarwal, W. Mbuguiro, B.A. Wester, and V.E. Koliatsos, *Neuroinflammation in primary blast neurotrauma: Time course and prevention by torso shielding.* Experimental Neurology, 2016. **277**: p. 268-274.

237.   Hickman, S.E., N.D. Kingery, T.K. Ohsumi, M.L. Borowsky, L.C. Wang, T.K. Means, and J. El Khoury, *The microglial sensome revealed by direct RNA sequencing.* Nature Neuroscience, 2013. **16**(12): p. 1896-1905.

238.   Lewis, N.D., J.D. Hill, K.W. Juchem, D.E. Stefanopoulos, and L.K. Modis, *RNA sequencing of microglia and monocyte-derived macrophages from mice with experimental autoimmune encephalomyelitis illustrates a changing phenotype with disease course.* Journal of Neuroimmunology, 2014. **277**(1-2): p. 26-38.

239.   Noristani, H.N., Y.N. Gerber, J.C. Sabourin, M. Le Corre, N. Lonjon, N. Mestre-Frances, H.E. Hirbec, and F.E. Perrin, *RNA-Seq Analysis of Microglia Reveals Time-Dependent Activation of Specific Genetic Programs following Spinal Cord Injury.* Frontiers in Molecular Neuroscience, 2017. **10**: p. 16.

240.   I.R. Holtman, M.A.N., M. Bijlsma, K.N. Duong, M.A. van der Geest, P.T. Ketelaars, S. Boersma, M.L. Dubbelaar, N. Brouwer, I.D. Vainchtein, B.J.L. Eggen, H.W.G.M. Boddeke, *GOAD Glia Open Access Database*, 2014, Hanze University of Applied Sciences, Institute for LIfe Science & Technology

241.   Parkhurst, C.N., G. Yang, I. Ninan, J.N. Savas, J.R. Yates, J.J. Lafaille, B.L. Hempstead, D.R. Littman, and W.B. Gan, *Microglia Promote Learning-Dependent Synapse Formation through Brain-Derived Neurotrophic Factor.* Cell, 2013. **155**(7): p. 1596-1609.

242.   Thrane, V.R., A.S. Thrane, J. Chanag, V. Alleluia, E.A. Nagelhus, and M. Nedergaard, *Real-Time Analysis of Microglial Activation and Motility in Hepatic And Hyperammonemic Encephalopathy.* Neuroscience, 2012. **220**: p. 247-255.

243.   Pagani, F., R.C. Paolicelli, E. Murana, B. Cortese, S. Di Angelantonio, E. Zurolo, E. Guiducci, T.A. Ferreira, S. Garofalo, M. Catalano, G. D'Alessandro, A. Porzia, G. Peruzzi, F. Mainiero, C. Limatola, C.T. Gross, and D. Ragozzino, *Defective microglial development in the hippocampus of Cx3cr1 deficient mice.* Frontiers in Cellular Neuroscience, 2015. **9**: p. 14.

244.   Eichhoff, G., B. Brawek, and O. Garaschuk, *Microglial calcium signal acts as a rapid sensor of single neuron damage in vivo.* Biochimica Et Biophysica Acta-Molecular Cell Research, 2011. **1813**(5): p. 1014-1024.

245.   Garaschuk, O., *Imaging microcircuit function in healthy and diseased brain.* Experimental Neurology, 2013. **242**: p. 41-49.

246.   Seifert, S., M. Pannell, W. Uckert, K. Farber, and H. Kettenmann, *Transmitter- and hormone-activated Ca2+ responses in adult microglia/brain macrophages in situ recorded after viral transduction of a recombinant Ca2+ sensor.* Cell Calcium, 2011. **49**(6): p. 365-375.

247.   Brawek, B., Y.J. Liang, D. Savitska, K.Z. Li, N. Fomin-Thunemann, Y. Kovalchuk, E. Zirdum, J. Jakobsson, and O. Garaschuk, *A new approach for ratiometric in vivo calcium imaging of microglia.* Scientific Reports, 2017. **7**: p. 13.

248.   Pozner, A., B. Xu, S. Palumbos, J.M. Gee, P. Tvrdik, and M.R. Capecchi, *Intracellular calcium dynamics in cortical microglia responding to focal laser injury in the PC::G5-tdT reporter mouse.* Frontiers in Molecular Neuroscience, 2015. **8**: p. 10.

249.   Tvrdik, P. and M.Y.S. Kalani, *In Vivo Imaging of Microglial Calcium Signaling in Brain Inflammation and Injury.* International Journal of Molecular Sciences, 2017. **18**(11): p. 18.

250.   Boucsein, C., H. Kettenmann, and C. Nolte, *Electrophysiological properties of microglial cells in normal and pathologic rat brain slices.* European Journal of Neuroscience, 2000. **12**(6): p. 2049-2058.

251.   Adembri, C., V. Selmi, L. Vitali, A. Tani, M. Margheri, B. Loriga, M. Carlucci, D. Nosi, L. Formigli, and A.R. De Gaudio, *Minocycline But Not Tigecycline Is Neuroprotective and Reduces the Neuroinflammatory Response Induced by the Superimposition of Sepsis Upon Traumatic Brain Injury.* Critical Care Medicine, 2014. **42**(8): p. E570-E582.

252.   Haber, M., S.G.A. Baki, N.M. Grin'kina, R. Irizarry, A. Ershova, S. Orsi, R.J. Grill, P. Dash, and P.J. Bergold, *Minocycline plus N-acetylcysteine synergize to modulate inflammation and prevent cognitive and memory deficits in a rat model of mild traumatic brain injury.* Experimental Neurology, 2013. **249**: p. 169-177.

253.   Chio, C.C., M.T. Lin, and C.P. Chang, *Microglial Activation as a Compelling Target for Treating Acute Traumatic Brain Injury.* Current Medicinal Chemistry, 2015. **22**(6): p. 759-770.

254.   Chio, C.C., J.W. Lin, M.W. Chang, C.C. Wang, J.R. Kuo, C.Z. Yang, and C.P. Chang, *Therapeutic evaluation of etanercept in a model of traumatic brain injury.* Journal of Neurochemistry, 2010. **115**(4): p. 921-929.

255.   Li, B., A. Mahmood, D.Y. Lu, H.T. Wu, Y. Xiong, C.S. Qu, and M. Chopp, *Simvastatin Attenuates Microglial Cells and Astrocyte Activation and Decreases Interleukin-1b Level After Traumatic Brain Injury.* Neurosurgery, 2009. **65**(1): p. 179-186.

256.   Gatson, J.W., M.M. Liu, K. Abdelfattah, J.G. Wigginton, S. Smith, S. Wolf, and J.P. Minei, *Resveratrol decreases inflammation in the brain of mice with mild traumatic brain injury.* Journal of Trauma and Acute Care Surgery, 2013. **74**(2): p. 470-474.

257.   Byrnes, K.R., D.J. Loane, B.A. Stoica, J. Zhang, and A.I. Faden, *Delayed mGluR5 activation limits neuroinflammation and neurodegeneration after traumatic brain injury.* Journal of Neuroinflammation, 2012. **9**: p. 43.

258.   Zhang, Q.G., M.D. Laird, D. Han, K. Nguyen, E. Scott, Y. Dong, K.M. Dhandapani, and D.W. Brann, *Critical role of NADPH oxidase in neuronal oxidative damage and microglia activation following traumatic brain injury.* PLoS One, 2012. **7**(4): p. e34504.

259.   Dash, P.K., J. Zhao, N. Kobori, J.B. Redell, M.J. Hylin, K.N. Hood, and A.N. Moore, *Activation of Alpha 7 Cholinergic Nicotinic Receptors Reduce Blood-Brain Barrier Permeability following Experimental Traumatic Brain Injury.* Journal of Neuroscience, 2016. **36**(9): p. 2809-2818.

260.   Kust, B.M., K. Biber, D. Van Calker, and P.J. Gebicke-Haerter, *Regulation of K+ channel mRNA expression by stimulation of adenosine A(2a)-receptors in cultured rat microglia.* Glia, 1999. **25**(2): p. 120-130.

261.   Fiebich, B.L., K. Biber, K. Lieb, D. vanCalker, M. Berger, J. Bauer, and P.J. GebickeHaerter, *Cyclooxygenase-2 expression in rat microglia is induced by adenosine A(2a)-receptors.* Glia, 1996. **18**(2): p. 152-160.

262.   Heese, K., B.L. Fiebich, J. Bauer, and U. Otten, *Nerve growth factor (NGF) expression in rat microglia is induced by adenosine A(2a)-receptors.* Neuroscience Letters, 1997. **231**(2): p. 83-86.

263. Hammarberg, C., G. Schulte, and B.B. Fredholm, *Evidence for functional adenosine A(3) receptors in microglia cells.* Journal of Neurochemistry, 2003. **86**(4): p. 1051-1054.

264. Xiang, Z.H. and G. Burnstock, *Expression of P2X receptors on rat microglial cells during early development.* Glia, 2005. **52**(2): p. 119-126.

265. Horvath, R.J. and J.A. Deleo, *Morphine Enhances Microglial Migration through Modulation of P2X(4) Receptor Signaling.* Journal of Neuroscience, 2009. **29**(4): p. 998-1005.

266. Cavaliere, F., K. Dinkel, and K. Reymann, *Microglia response and P2 receptor participation in oxygen/glucose deprivation-induced cortical damage.* Neuroscience, 2005. **136**(3): p. 615-623.

267. Visentin, S., C.D. Nuccio, and G.C. Bellenchi, *Different patterns of Ca⁺ signals are induced by low compared to high concentrations of P2Y agonists in microglia.* Purinergic signalling, 2006. **2**(4): p. 605-17.

268. Light, A.R., Y. Wu, R.W. Hughen, and P.B. Guthrie, *Purinergic receptors activating rapid intracellular Ca2+ increases in microglia.* Neuron Glia Biology, 2006. **2**: p. 125-138.

269. Liu, G.J., R. Nagarajah, R.B. Banati, and M.R. Bennett, *Glutamate induces directed chemotaxis of microglia.* European Journal of Neuroscience, 2009. **29**(6): p. 1108-1118.

270. Drouin-Ouellet, J., A.L. Brownell, M. Saint-Pierre, C. Fasano, V. Emond, L.E. Trudeau, D. Levesque, and F. Cicchetii, *Neuroinflammation Is Associated with Changes in Glial mGluR5 Expression and the Development of Neonatal Excitotoxic Lesions.* Glia, 2011. **59**(2): p. 188-199.

271. Geurts, J.J.G., G. Wolswijk, L. Bo, P. van der Valk, C.H. Polman, D. Troost, and E. Aronica, *Altered expression patterns of group I and II metabotropic glutamate receptors in multiple sclerosis.* Brain, 2003. **126**: p. 1755-1766.

272. Byrnes, K.R., B. Stoica, D.J. Loane, A. Riccio, M.I. Davis, and A.I. Faden, *Metabotropic Glutamate Receptor 5 Activation Inhibits Microglial Associated Inflammation and Neurotoxicity.* Glia, 2009. **57**(5): p. 550-560.

273. Loane, D.J., B.A. Stoica, A. Pajoohesh-Ganji, K.R. Byrnes, and A.I. Faden, *Activation of Metabotropic Glutamate Receptor 5 Modulates Microglial Reactivity and Neurotoxicity by Inhibiting NADPH Oxidase.* Journal of Biological Chemistry, 2009. **284**(23): p. 15629-15639.

274. Kuhn, S.A., F.K.H. van Landeghem, R. Zacharias, K. Farber, A. Rappert, S. Pavlovic, A. Hoffmann, C. Nolte, and H. Kettenmann, *Microglia express GABA(B) receptors to modulate interleukin release.* Molecular and Cellular Neuroscience, 2004. **25**(2): p. 312-322.

275. De Simone, R., M.A. Ajmone-Cat, D. Carnevale, and L. Minghetti, *Activation of alpha 7 nicotinic acetylcholine receptor by nicotine selectively up-regulates cyclooxygenase-2 and prostaglandin E-2 in rat microglial cultures.* Journal of Neuroinflammation, 2005. **2**: p. 10.

276. Shytle, R.D., T. Mori, K. Townsend, M. Vendrame, N. Sun, J. Zeng, J. Ehrhart, A.A. Silver, P.R. Sanberg, and J. Tan, *Cholinergic modulation of microglial activation by alpha 7 nicotinic receptors.* Journal of Neurochemistry, 2004. **89**(2): p. 337-343.

277. Suzuki, T., I. Hide, A. Matsubara, C. Hama, K. Harada, K. Miyano, M. Andra, H. Matsubayashi, N. Sakai, S. Kohsaka, K. Inoue, and Y. Nakata, *Microglial alpha 7 nicotinic acetylcholine receptors drive a phospholipase C/IP3 pathway and modulate the cell activation toward a neuroprotective role.* Journal of Neuroscience Research, 2006. **83**(8): p. 1461-1470.

278. Rock, R.B., G. Gekker, R.N. Aravalli, S.X. Hu, W.S. Sheng, and P.K. Peterson, *Potentiation of HIV-1 expression in microglial cells by nicotine: Involvement of transforming growth factor-beta 1.* Journal of Neuroimmune Pharmacology, 2008. **3**(3): p. 143-149.

279. Liu, J., A.M. McGlinn, A. Fernandes, A.H. Milam, C.E. Strang, M.E. Andison, J.M. Lindstrom, K.T. Keyser, and R.A. Stone, *Nicotinic Acetylcholine Receptor Subunits in Rhesus Monkey Retina.* Investigative Ophthalmology & Visual Science, 2009. **50**(3): p. 1408-1415.

280. Fujita, H., J. Tanaka, N. Maeda, and M. Sakanaka, *Adrenergic agonists suppress the proliferation of microglia through beta 2-adrenergic receptor.* Neuroscience Letters, 1998. **242**(1): p. 37-40.

281. Mori, M., M. Aihara, K. Kume, M. Hamanoue, S. Kohsaka, and T. Shimizu, *Predominant expression of platelet-activating factor receptor in the rat brain microglia.* Journal of Neuroscience, 1996. **16**(11): p. 3590-3600.

282. Sattayaprasert, P., H.B. Choi, S. Chongthammakun, and J.G. McLarnon, *Platelet-activating factor enhancement of calcium influx and interleukin-6 expression, but not production, in human microglia.* Journal of Neuroinflammation, 2005. **2**: p. 8.

283. Wang, X., J.H. Bae, S.U. Kim, and J.G. McLarnon, *Platelet-activating factor induced Ca2+ signaling in human microglia.* Brain Research, 1999. **842**(1): p. 159-165.

284. Noda, M., Y. Kariura, T. Amano, Y. Manago, K. Nishikawa, S. Aoki, and K. Wada, *Kinin receptors in cultured rat microglia.* Neurochemistry International, 2004. **45**(2-3): p. 437-442.

285. Noda, M., Y. Kariura, U. Pannasch, K. Nishikawa, L.P. Wang, T. Seike, M. Ifuku, Y. Kosai, B. Wang, C. Nolte, S. Aoki, H. Kettenmann, and K. Wada, *Neuroprotective role of bradykinin because of the attenuation of pro-inflammatory cytokine release from activated microglia.* Journal of Neurochemistry, 2007. **101**(2): p. 397-410.

286. Ifuku, M., K. Faerber, Y. Okuno, Y. Yamakawa, T. Miyamoto, C. Nolte, V.F. Merrino, S. Kita, T. Iwamoto, I. Komuro, B. Wang, G. Cheung, E. Ishikawa, H. Ooboshi, M. Bader, K. Wada, H. Kettenmann, and M. Noda, *Bradykinin-induced microglial migration mediated by B-1-bradykinin receptors depends on Ca2+ influx via reverse-mode activity of the Na+/Ca2+ exchanger.* Journal of Neuroscience, 2007. **27**(48): p. 13065-13073.

287. Noda, M., Y. Kariura, T. Amano, Y. Manago, K. Nishikawa, S. Aoki, and K. Wada, *Expression and function of bradykinin receptors in microglia.* Life Sciences, 2003. **72**(14): p. 1573-1581.

288. Bader, M.F., L. Taupenot, G. Ulrich, D. Aunis, and J. Ciesielskitreska, *Bacterial-Endotoxin Induces Ca2+ I Transients and Changes the Organization of Actin in Microglia.* Glia, 1994. **11**(4): p. 336-344.

289. McLarnon, J.G., X. Wang, J.H. Bae, and S.U. Kim, *Endothelin-induced changes in intracellular calcium in human microglia.* Neuroscience Letters, 1999. **263**(1): p. 9-12.

290. Moller, T., O. Kann, M. Prinz, F. Kirchhoff, A. Verkhratsky, and H. Kettenmann, *Endothelin-induced calcium signaling in cultured mouse microglial cells is mediated through ETB receptors.* Neuroreport, 1997. **8**(9-10): p. 2127-2131.

291. Yamashita, K., M. Niwa, Y. Kataoka, K. Shigematsu, A. Himeno, K. Tsutsumi, M. Nakanonakashima, Y. Sakuraiyamashita, S. Shibata, and K. Taniyama, *Microglia With an Endothelin Et(B) Receptor Aggregate in Rat Hippocampus Ca1 Subfields Following Transient Forebrain Ischemia.* Journal of Neurochemistry, 1994. **63**(3): p. 1042-1051.

292. Cabral, G.A. and F. Marciano-Cabral, *Cannabinoid receptors in microglia of the central nervous system: immune functional relevance.* Journal of Leukocyte Biology, 2005. **78**(6): p. 1192-1197.

293. Facchinetti, F., E. Del Giudice, S. Furegato, M. Passarotto, and A. Leon, *Cannabinoids ablate release of TNF alpha in rat microglial cells stimulated with lypopolysaccharide.* Glia, 2003. **41**(2): p. 161-168.

294. Ramirez, B.G., C. Blazquez, T.G. del Pulgar, N. Guzman, and M.A.L. de Ceballos, *Prevention of Alzheimer's disease pathology by cannabinoids: Neuroprotection mediated by blockade of microglial activation.* Journal of Neuroscience, 2005. **25**(8): p. 1904-1913.

295. Maresz, K., E.J. Carrier, E.D. Ponomarev, C.J. Hillard, and B.N. Dittel, *Modulation of the cannabinoid CB2 receptor in microglial cells in response to inflammatory stimuli.* Journal of Neurochemistry, 2005. **95**(2): p. 437-445.

296. Feindt, J., A. Schmidt, and R. Mentlein, *Receptors and effects of the inhibitory neuropeptide somatostatin in microglial cells.* Molecular Brain Research, 1998. **60**(2): p. 228-233.

297. Tanaka, J., H. Fujita, S. Matsuda, K. Toku, M. Sakanaka, and N. Maeda, *Glucocorticoid- and mineralocorticoid receptors in microglial cells: The two receptors mediate differential effects of corticosteroids.* Glia, 1997. **20**(1): p. 23-37.

298. Chao, C.C., G. Gekker, S.X. Hu, W.S. Sheng, K.B. Shark, D.F. Bu, S. Archer, J.M. Bidlack, and P.K. Peterson, *kappa opioid receptors in human microglia downregulate human immunodeficiency virus 1 expression.* Proceedings of the National Academy of Sciences of the United States of America, 1996. **93**(15): p. 8051-8056.

299. Dobrenis, K., M.H. Makman, and G.B. Stefano, *Occurrence of the Opiate Alkaloid-Selective Mu(3) Receptor in Mammalian Microglia, Astrocytes and Kupffer Cells.* Brain Research, 1995. **686**(2): p. 239-248.

300. Lai, J.P., G.X. Zhan, D.E. Campbell, S.D. Douglas, and W.Z. Ho, *Detection of substance P and its receptor in human fetal microglia.* Neuroscience, 2000. **101**(4): p. 1137-1144.

301. Rasley, A., K.L. Bost, J.K. Olson, S.D. Miller, and I. Marriott, *Expression of functional NK-1 receptors in murine microglia.* Glia, 2002. **37**(3): p. 258-267.

302. Delgado, M. and D. Ganea, *Vasoactive intestinal peptide prevents activated microglia-induced neurodegeneration under inflammatory conditions: potential therapeutic role in brain trauma.* Faseb Journal, 2003. **17**(11): p. 1922-+.

303. Delgado, M., G.M. Jonakait, and D. Ganea, *Vasoactive intestinal peptide and pituitary adenylate cyclase-activating polypeptide inhibit chemokine production in activated microglia.* Glia, 2002. **39**(2): p. 148-161.

304. Gonzalez-Rey, E. and M. Delgado, *Vasoactive intestinal peptide inhibits cycloxygenase-2 expression in activated macrophages, microglia, and dendritic cells.* Brain Behavior and Immunity, 2008. **22**(1): p. 35-41.

305. Mizoguchi, Y., A. Monji, T. Kato, Y. Seki, L. Gotoh, H. Horikawa, S.O. Suzuki, T. Iwaki, M. Yonaha, S. Hashioka, and S. Kanba, *Brain-Derived Neurotrophic Factor Induces Sustained Elevation of Intracellular Ca2+ in Rodent Microglia.* Journal of Immunology, 2009. **183**(12): p. 7778-7786.

306. Cowell, R.M., H.Y. Xu, J.M. Parent, and F.S. Silverstein, *Microglial expression of chemokine receptor CCR5 during rat forebrain development and after perinatal hypoxia-ischemia.* Journal of Neuroimmunology, 2006. **173**(1-2): p. 155-165.

307. Boddeke, E., I. Meigel, S. Frentzel, N.G. Gourmala, J.K. Harrison, M. Buttini, O. Spleiss, and P. Gebicke-Harter, *Cultured rat microglia express functional beta-chemokine receptors.* Journal of Neuroimmunology, 1999. **98**(2): p. 176-184.

308. Bordey, A. and D.D. Spencer, *Chemokine modulation of high-conductance Ca2+-sensitive K+ currents in microglia from human hippocampi.* European Journal of Neuroscience, 2003. **18**(10): p. 2893-2898.

309. Rappert, A., K. Biber, C. Nolte, M. Lipp, A. Schubel, B. Lu, N.P. Gerard, C. Gerard, H. Boddeke, and H. Kettenmann, *Secondary lymphoid tissue chemokine (CCL21) activates CXCR3 to trigger a Cl- current and chemotaxis in murine microglial.* Journal of Immunology, 2002. **168**(7): p. 3221-3226.

310. Boddeke, E., I. Meigel, S. Frentzel, K. Biber, L.Q. Renn, and P. Gebicke-Harter, *Functional expression of the fractalkine (CX3C) receptor and its regulation by lipopolysaccharide in rat microglia.* European Journal of Pharmacology, 1999. **374**(2): p. 309-313.

311. Lacy, M., J. Jones, S.R. Whittemore, D.L. Haviland, R.A. Wetsel, and S.R. Barnum, *Expression of the Receptors for the C5a Anaphylatoxin, Interleukin-8 and Fmlp by Human Astrocytes and Microglia.* Journal of Neuroimmunology, 1995. **61**(1): p. 71-78.

312. Butovsky, O., S. Bukshpan, G. Kunis, S. Jung, and M. Schwartz, *Microglia can be induced by IFN-gamma or IL-4 to express neural or dendritic-like markers.* Molecular and Cellular Neuroscience, 2007. **35**(3): p. 490-500.

313.   Hanisch, U.K., M. Prinz, K. Angstwurm, K.G. Hausler, O. Kann, H. Kettenmann, and J.R. Weber, *The protein tyrosine kinase inhibits AG126 prevents the massive microglial cytokine induction by pneumococcal cell walls.* European Journal of Immunology, 2001. **31**(7): p. 2104-2115.

314.   Syed, M.M., N.K. Phulwani, and T. Kielian, *Tumor necrosis factor-alpha (TNF-alpha) regulates Toll-like receptor 2 (TLR2) expression in microglia.* Journal of Neurochemistry, 2007. **103**(4): p. 1461-1471.

315.   Michelucci, A., T. Heurtaux, L. Grandbarbe, E. Morga, and P. Heuschling, *Characterization of the microglial phenotype under specific pro-inflammatory and anti-inflammatory conditions: Effects of oligomeric and fibrillar amyloid-beta.* Journal of Neuroimmunology, 2009. **210**(1-2): p. 3-12.

316.   Stohwasser, R., J. Giesebrecht, R. Kraft, E.C. Muller, K.G. Hausler, H. Kettenmann, U.K. Hanisch, and P.M. Kloetzel, *Biochemical analysis of proteasomes from mouse microglia: Induction of immunoproteasomes by interferon-gamma and lipopolysaccharide.* Glia, 2000. **29**(4): p. 355-365.

317.   Butovsky, O., A.E. Talpalar, K. Ben-Yaakov, and M. Schwartz, *Activation of microglia by aggregated beta-amyloid or lipopolysaccharide impairs MHC-II expression and renders them cytotoxic whereas IFN-gamma and IL-4 render them protective.* Molecular and Cellular Neuroscience, 2005. **29**(3): p. 381-393.

318.   Prinz, M., H. Schmidt, A. Mildner, K.P. Knobeloch, U.K. Hanisch, J. Raasch, D. Merkler, C. Detje, I. Gutcher, J. Mages, R. Lang, R. Martin, R. Gold, B. Becher, W. Bruck, and U. Kalinke, *Distinct and nonredundant in vivo functions of IFNAR on myeloid cells limit autoimmunity in the central nervous system.* Immunity, 2008. **28**(5): p. 675-686.

319.   McNamee, E.N., K.M. Ryan, D. Kilroy, and T.J. Connor, *Noradrenaline induces IL-1ra and IL-1 type II receptor expression in primary glial cells and protects against IL-1 beta-induced neurotoxicity.* European Journal of Pharmacology, 2010. **626**(2-3): p. 219-228.

320.   Pinteaux, E., L.C. Parker, N.J. Rothwell, and G.N. Luheshi, *Expression of interleukin-1 receptors and their role in interleukin-1 actions in murine microglial cells.* Journal of Neurochemistry, 2002. **83**(4): p. 754-763.

321.   Andre, R., D. Lerouet, I. Kimber, E. Pinteaux, and N.J. Rothwell, *Regulation of expression of the novel IL-1 receptor family members in the mouse brain.* Journal of Neurochemistry, 2005. **95**(2): p. 324-330.

322.   Cunningham, E.T. and E.B. Desouza, *Interleukin-1 Receptors in the Brain and Endocrine Tissues.* Immunology Today, 1993. **14**(4): p. 171-176.

323.   Sawada, M., A. Suzumura, and T. Marunouchi, *Induction Of Functional Interleukin-2 Receptor In Mouse Microglia.* Journal of Neurochemistry, 1995. **64**(5): p. 1973-1979.

324.   Shimizu, E., K. Kawahara, M. Kajizono, M. Sawada, and H. Nakayama, *IL-4-Induced Selective Clearance of Oligomeric beta-Amyloid Peptide(1-42) by Rat Primary Type 2 Microglia.* Journal of Immunology, 2008. **181**(9): p. 6503-6513.

325.   Gonzalez, P., F. Burgaya, L. Acarin, H. Peluffo, B. Castellano, and B. Gonzalez, *Interleukin-10 and Interleukin-10 Receptor-I Are Upregulated in Glial Cells After an Excitotoxic Injury to the Postnatal Rat Brain.* Journal of Neuropathology and Experimental Neurology, 2009. **68**(4): p. 391-403.

326.   Huang, Z., G.K. Ha, and J.M. Petitto, *IL-15 and IL-15R alpha gene deletion: Effects on T lymphocyte trafficking and the microglial and neuronal responses to facial nerve axotomy.* Neuroscience Letters, 2007. **417**(2): p. 160-164.

327.   Prinz, M. and U.K. Hanisch, *Murine microglial cells produce and respond to interleukin-18.* Journal of Neurochemistry, 1999. **72**(5): p. 2215-2218.

328.   Bernardino, A.L.F., T.A. Myers, X. Alvarez, A. Hasegawa, and M.T. Philipp, *Toll-like receptors: Insights into their possible role in the pathogenesis of Lyme neuroborreliosis.* Infection and Immunity, 2008. **76**(10): p. 4385-4395.

329. Bsibsi, M., R. Ravid, D. Gveric, and J.M. van Noort, *Broad expression of Toll-like receptors in the human central nervous system.* Journal of Neuropathology and Experimental Neurology, 2002. **61**(11): p. 1013-1021.

330. Olson, J.K. and S.D. Miller, *Microglia initiate central nervous system innate and adaptive immune responses through multiple TLRs.* Journal of Immunology, 2004. **173**(6): p. 3916-3924.

331. Zuiderwijk-Sick, E.A., C. Van der Putten, M. Bsibsi, I.P. Deuzing, W. De Boer, C. Persoon-Deen, I. Kondova, L.A. Boven, J.M. Van Noort, B.A. Hart, S. Amor, and J.J. Bajramovic, *Differentiation of primary adult microglia alters their response to TLR8-mediated activation but not their capacity as APC.* Glia, 2007. **55**(15): p. 1589-1600.

332. Babcock, A.A., M. Wirenfeldt, T. Holm, H.H. Nielsen, L. Dissing-Olesen, H. Toft-Hansen, J.M. Millward, R. Landmann, S. Rivest, B. Finsen, and T. Owens, *Toll-like receptor 2 signaling in response to brain injury: An innate bridge to neuroinflammation.* Journal of Neuroscience, 2006. **26**(49): p. 12826-12837.

333. Chen, K.Q., P. Iribarren, J.Y. Hu, J.H. Chen, W.H. Gong, E.H. Cho, S. Lockett, N.M. Dunlop, and J.M. Wang, *Activation of toll-like receptor 2 on microglia promotes cell uptake of Alzheimer disease-associated amyloid beta peptide.* Journal of Biological Chemistry, 2006. **281**(6): p. 3651-3659.

334. Ebert, S., J. Gerber, S. Bader, F. Muhlhauser, K. Brechtel, T.J. Mitchell, and R. Nau, *Dose-dependent activation of microglial cells by Toll-like receptor agonists alone and in combination.* Journal of Neuroimmunology, 2005. **159**(1-2): p. 87-96.

335. Lehnardt, S., P. Henneke, E. Lien, D.L. Kasper, J.J. Volpe, I. Bechmann, R. Nitsch, J.R. Weber, D.T. Golenbock, and T. Vartanian, *A mechanism for neurodegeneration induced by group B streptococci through activation of the TLR2/MyD88 pathway in microglia.* Journal of Immunology, 2006. **177**(1): p. 583-592.

336. Town, T., D. Jeng, L. Alexopoulou, J. Tan, and R.A. Flavell, *Microglia recognize double-stranded RNA via TLR3.* Journal of Immunology, 2006. **176**(6): p. 3804-3812.

337. Qin, L.Y., G.R. Li, X. Qian, Y.X. Liu, X.F. Wu, B. Liu, J.S. Hong, and M.L. Block, *Interactive role of the toll-like receptor 4 and reactive oxygen species in LPS-induced microglia activation.* Glia, 2005. **52**(1): p. 78-84.

338. Lehnardt, S., C. Lachance, S. Patrizi, S. Lefebvre, P.L. Follett, F.E. Jensen, P.A. Rosenberg, J.J. Volpe, and T. Vartanian, *The toll-like receptor TLR4 is necessary for lipopolysaccharide-induced oligodendrocyte injury in the CNS.* Journal of Neuroscience, 2002. **22**(7): p. 2478-2486.

339. Butchi, N.B., M. Du, and K.E. Peterson, *Interactions Between TLR7 and TLR9 Agonists and Receptors Regulate Innate Immune Responses by Astrocytes and Microglia.* Glia, 2010. **58**(6): p. 650-664.

340. Cervantes, J.L., B. Weinerman, C. Basole, and J.C. Salazar, *TLR8: the forgotten relative revindicated.* Cellular & Molecular Immunology, 2012. **9**(6): p. 434-438.

341. Dalpke, A.H., M.K.H. Schafer, M. Frey, S. Zimmermann, J. Tebbe, E. Weihe, and K. Heeg, *Immunostimulatory CpG-DNA activates murine microglia.* Journal of Immunology, 2002. **168**(10): p. 4854-4863.

342. Prinz, M., O. Kann, H.J. Draheim, R.R. Schumann, H. Kettenmann, J.R. Weber, and U.K. Hanisch, *Microglial activation by components of Gram-positive and -negative bacteria: Distinct and common routes to the induction of ion channels and cytokines.* Journal of Neuropathology and Experimental Neurology, 1999. **58**(10): p. 1078-1089.

343. Bate, C., R. Boshuizen, and A. Williams, *Microglial cells kill prion-damaged neurons in vitro by a CD14-dependent process.* Journal of Neuroimmunology, 2005. **170**(1-2): p. 62-70.

344. Chattopadhyay, N., C.P. Ye, T. Yamaguchi, M. Nakai, O. Kifor, P.M. Vassilev, R.N. Nishimura, and E.M. Brown, *The extracellular calcium-sensing receptor is expressed in rat microglia and modulates an outward K+ channel.* Journal of Neurochemistry, 1999. **72**(5): p. 1915-1922.

345. Moller, T., C. Nolte, R. Burger, A. Verkhratsky, and H. Kettenmann, *Mechanisms of C5a and C3a complement fragment-induced Ca2+ (i) signaling in mouse microglia.* Journal of Neuroscience, 1997. **17**(2): p. 615-624.

346. Nolte, C., T. Moller, T. Walter, and H. Kettenmann, *Complement 5a controls motility of murine microglial cells in vitro via activation of an inhibitory G-protein and the rearrangement of the actin cytoskeleton.* Neuroscience, 1996. **73**(4): p. 1091-1107.

347. Ilschner, S., C. Nolte, and H. Kettenmann, *Complement factor C5a and epidermal growth factor trigger the activation of outward potassium currents in cultured murine microglia.* Neuroscience, 1996. **73**(4): p. 1109-1120.

348. Balcaitis, S., Y.H. Xie, J.R. Weinstein, H. Andersen, U.K. Hanisch, B.R. Ransom, and T. Moller, *Expression of proteinase-activated receptors in mouse microglial cells.* Neuroreport, 2003. **14**(18): p. 2373-2377.

349. Mitrasinovic, O.M. and G.M. Murphy, *Accelerated phagocytosis of amyloid-beta by mouse and human microglia overexpressing the macrophage colony-stimulating factor receptor.* Journal of Biological Chemistry, 2002. **277**(33): p. 29889-29896.

350. Mitrasinovic, O.M. and G.M. Murphy, *Microglial overexpression of the M-CSF receptor augments phagocytosis of opsonized A beta.* Neurobiology of Aging, 2003. **24**(6): p. 807-815.

351. Mitrasinovic, O.M., V.A.M. Vincent, D. Simsek, and G.M. Murphy, *Macrophage colony stimulating factor promotes phagocytosis by murine microglia.* Neuroscience Letters, 2003. **344**(3): p. 185-188.

352. Wang, X.J., M. Ye, Y.H. Zhang, and S.D. Chen, *CD200-CD200R regulation of microglia activation in the pathogenesis of Parkinson's disease.* Journal of Neuroimmune Pharmacology, 2007. **2**(3): p. 259-264.

353. Wright, G.J., H. Cherwinski, M. Foster-Cuevas, G. Brooke, M.J. Puklavec, M. Bigler, Y.L. Song, M. Jenmalm, D. Gorman, T. McClanahan, M.R. Liu, M.H. Brown, J.D. Sedgwick, J.H. Phillips, and A.N. Barclay, *Characterization of the CD200 receptor family in mice and humans and their interactions with CD200.* Journal of Immunology, 2003. **171**(6): p. 3034-3046.

354. Moller, T., J.J. Contos, D.B. Musante, J. Chun, and B.R. Ransom, *Expression and function of lysophosphatidic acid receptors in cultured rodent microglial cells.* Journal of Biological Chemistry, 2001. **276**(28): p. 25946-25952.

355. Tiffany, H.L., M.C. Lavigne, Y.H. Cui, J.M. Wang, T.L. Leto, J.L. Gao, and P.M. Murphy, *Amyloid-beta induces chemotaxis and oxidant stress by acting at formylpeptide receptor 2, a G protein-coupled receptor expressed in phagocytes and brain.* Journal of Biological Chemistry, 2001. **276**(26): p. 23645-23652.

356. Cui, Y.H., Y.Y. Le, W.H. Gong, P. Proost, J. Van Damme, W.J. Murphy, and J.M. Wang, *Bacterial lipopolysaccharide selectively up-regulates the function of the chemotactic peptide receptor formyl peptide receptor 2 in murine microglial cells.* Journal of Immunology, 2002. **168**(1): p. 434-442.

357. Hall, A.A., Y. Herrera, C.T. Ajmo, J. Cuevas, and K.R. Pennypacker, *Sigma Receptors Suppress Multiple Aspects of Microglial Activation.* Glia, 2009. **57**(7): p. 744-754.

358. Gekker, G., S.X. Hu, W.S. Sheng, R.B. Rock, J.R. Lokensgard, and P.K. Peterson, *Cocaine-induced HIV-1 expression in microglia involves sigma-1 receptors and transfonning growth factor-beta 1.* International Immunopharmacology, 2006. **6**(6): p. 1029-1033.

359. Urrea, C., D.A. Castellanos, J. Sagen, P. Tsoulfas, H.M. Bramlett, and W.D. Dietrich, *Widespread cellular proliferation and focal neurogenesis after traumatic brain injury in the rat.* Restorative Neurology and Neuroscience, 2007. **25**(1): p. 65-76.

360. Kelley, B.J., J. Lifshitz, and J.T. Povlishock, *Neuroinflammatory responses after experimental diffuse traumatic brain injury.* Journal of Neuropathology and Experimental Neurology, 2007. **66**(11): p. 989-1001.

361. Israel, I., A. Ohsiek, E. Al-Momani, C. Albert-Weissenberger, C. Stetter, S. Mencl, A.K. Buck, C. Kleinschnitz, S. Samnick, and A.L. Siren, *Combined F-18 DPA-714 micro-positron emission tomography and autoradiography imaging of microglia activation after closed head injury in mice.* Journal of Neuroinflammation, 2016. **13**: p. 13.

362. Kabadi, S.V., B.A. Stoica, D.B. Zimmer, L. Afanador, K.B. Duffy, D.J. Loane, and A.I. Faden, *S100B inhibition reduces behavioral and pathologic changes in experimental traumatic brain injury.* Journal of Cerebral Blood Flow and Metabolism, 2015. **35**(12): p. 2010-2020.

363. Morganti, J.M., L.K. Riparip, and S. Rosi, *Call Off the Dog(ma): M1/M2 Polarization Is Concurrent following Traumatic Brain Injury.* Plos One, 2016. **11**(1): p. 13.

364. Kumar, A., D.M. Alvarez-Croda, B.A. Stoica, A.I. Faden, and D.J. Loane, *Microglial/Macrophage Polarization Dynamics following Traumatic Brain Injury.* Journal of Neurotrauma, 2016. **33**(19): p. 1732-+.

Figure Legends

Figure 1: Microglia activation markers and time-course in various animal models of traumatic brain injury. The top panel depicts the two forms of microglia activation states: M1 and M2 and the markers used to identify each state. The lower panels illustrates how the expression levels of the microglia activation markers (Iba1, ED1, CD11b, CD16, CD68, YM-1, Arg-1. EMAP II and TSPO) change with t=0 representing time of injury in various animal injury models. Note that the y-axis denoting expression levels is arbitrary and is used to show the upregulated/ peak expression of the particular protein. Solid lines indicate proven studies, while dotted lines represent hypothetical expression. The numbers in superscript refers to the cited literature. In addition to portraying the stages of microglia activation, this illustration reveals that there is no absolute standard for defining microglia activation. Further, the evidence for long-term chronic activation of microglia following brain injury is lacking. [20-22, 90, 127, 135, 139, 143, 226, 227, 230, 233, 234, 236, 359-364]

Figure 2: A Schematic depicting various molecular signaling pathway of microglial receptors including CX3CR1, P2Y12R, TLR4, IL1R1, TNFR1 and PPAR.

Figure 3: Schematic depicting various molecular tools for examining microglial receptor activation. Illustration highlights classical as well as recently developed tools used to investigate microglia and its receptor activation.

Table Legends

Table 1. Microglia receptors in various TBI models.

Supplementary Table 1: Microglial receptors and their functional relevance.

Table 1: Microglia receptors in various TBI models.

Injury model	reference
CCI	SOCS2[107], IL-1b [108], Sigma-1 Receptor [109], Cannabinoid-2 Receptor [110], CX3CR1[86, 111, 112], Adenosine A1 Receptor [113], CR3[114], IL-4R[115], TLR4[116, 117], IL-2R [118], mGluR5[119, 120], TNFR [121], peripheral benzodiazepine receptor [122, 123], NLRP3[87], PPAR [124-126]
FPI	TSPO [127], TLR4[128], CCR2, CX3CR1[83], IL-1R [129], PPAR [130]
Weight drop	NMDAR[131, 132], Epo receptor [133], TLR4[134, 135], CCL2 (MCP-1)[136], metabotropic glutamate receptor 5[137, 138], TLR2 [135], P2X4[139], TNFR1 and Fas receptor [140]
Blast	CB2[141, 142], complement type three receptors (CR3), [143]
Human	CD14[144], GPR17[145], IL-1R[146], CCL2 (MCP-1)[136], TNFR1[147]

Figure 1   Click here to download Figure Figure 1.tif ⬇

Figure 2

Figure 2. Microglial Receptor Signaling Pathways

Figure 3
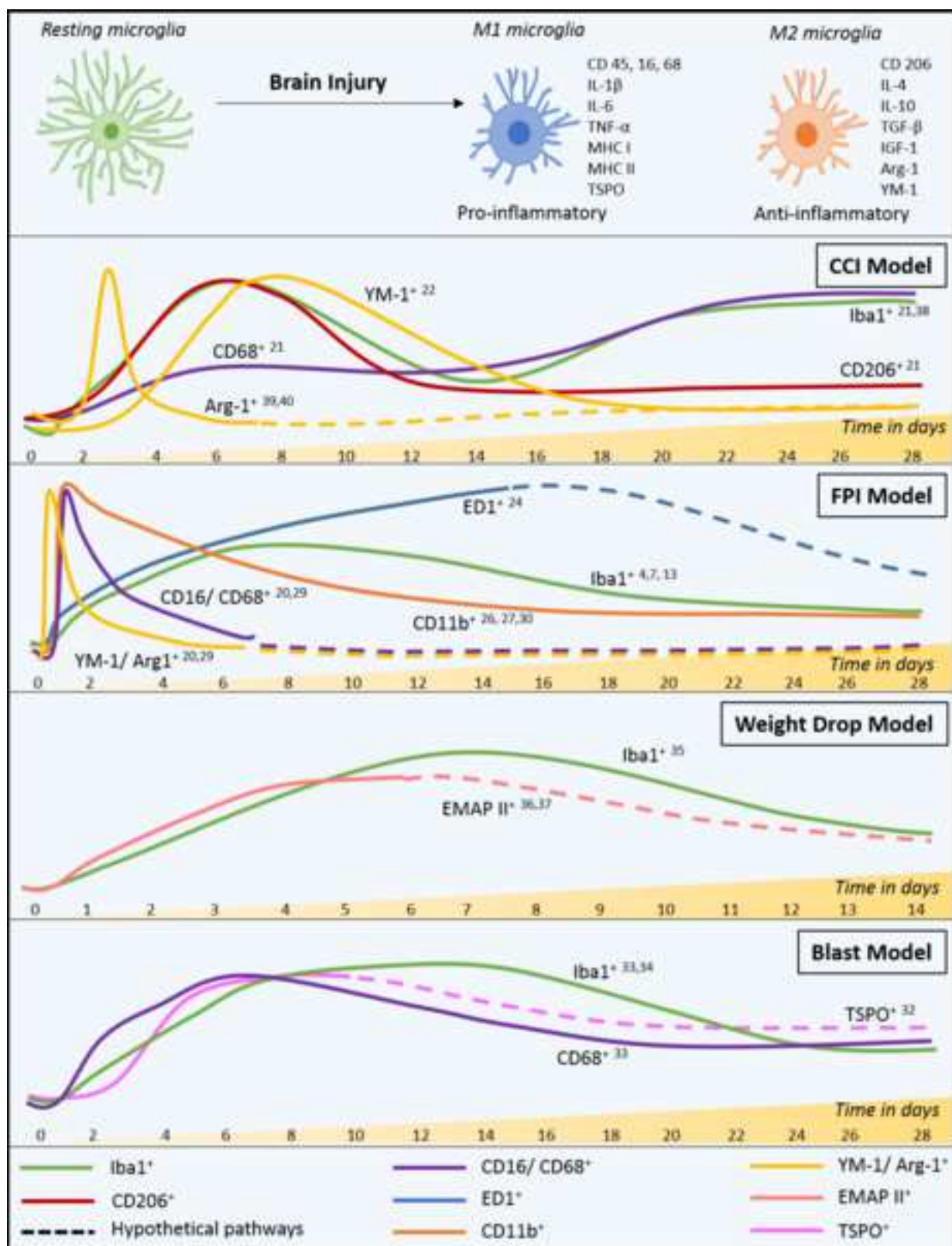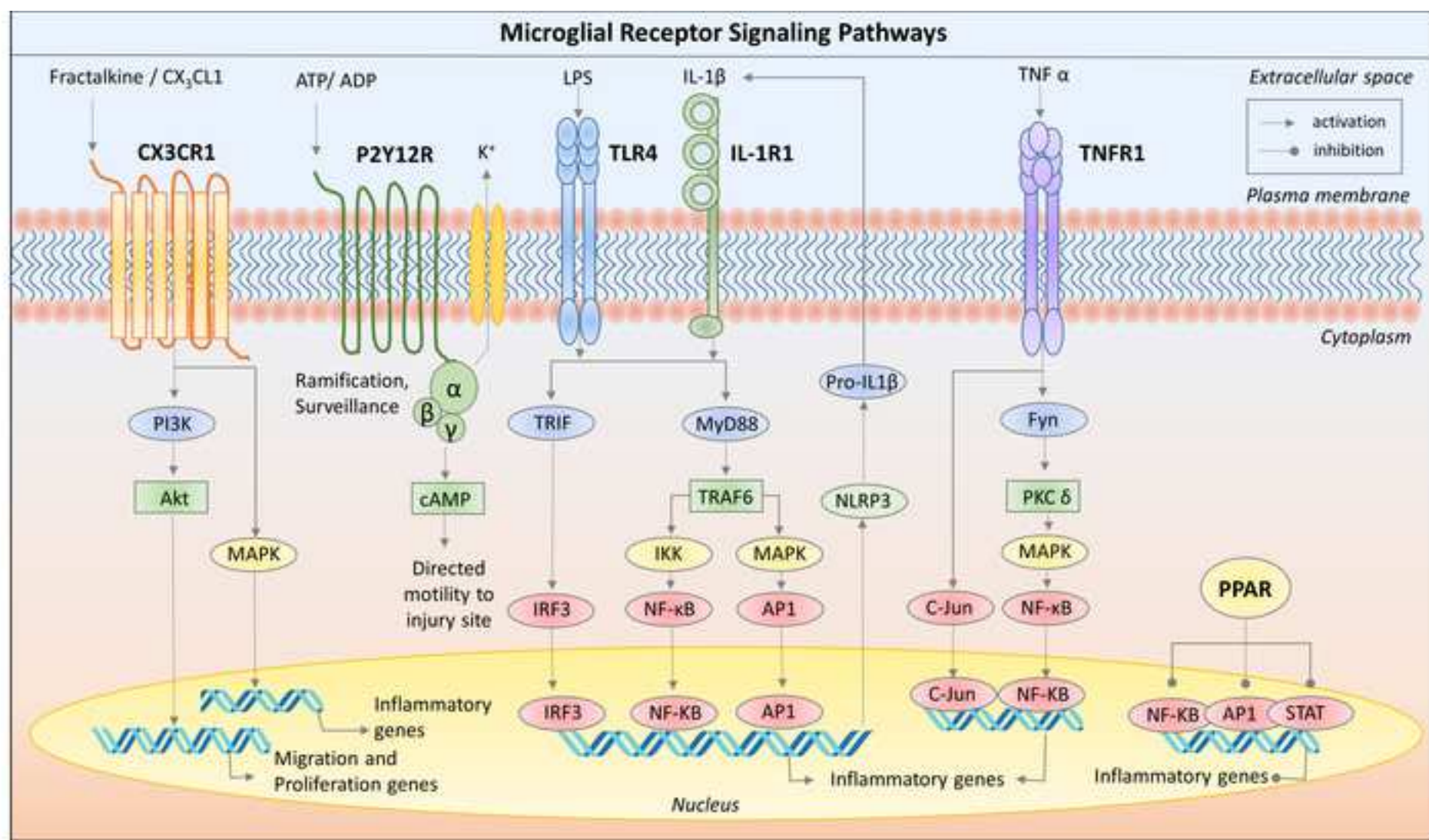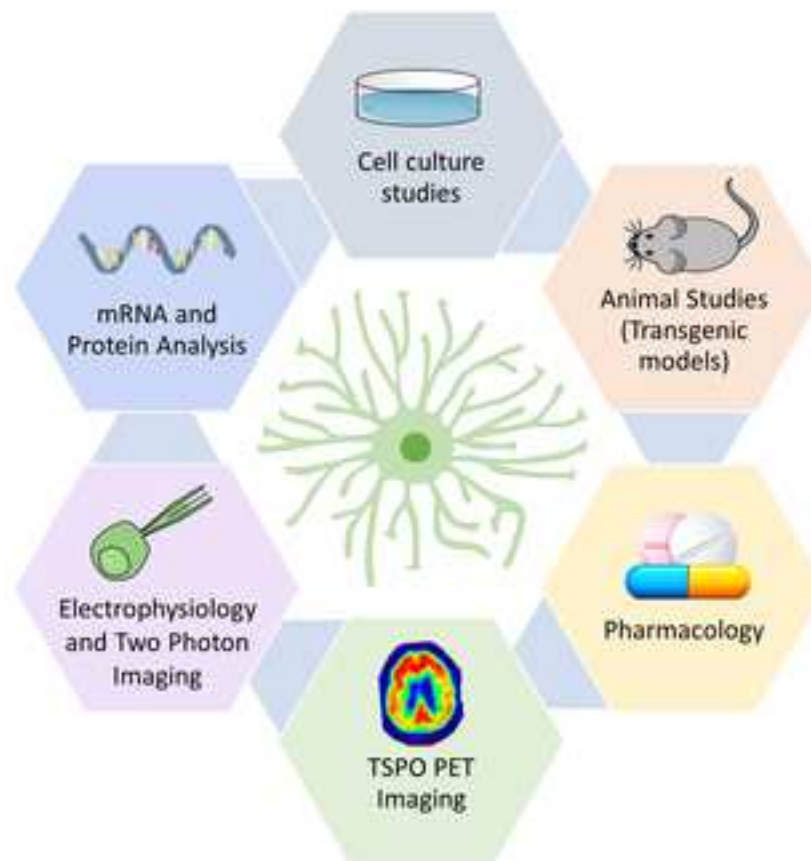
Conference Presentations

Abstracts

SOCIETY for NEUROSCIENCE

MEMBERSHIP | **MEETINGS** | CAREERS | INITIATIVES | ADVOCACY | OUTREACH | PUBLICATIONS | ABOUT

View Meeting Abstracts

NEUROSCIENCE **2017**

November 11-15
Washington, DC

Abstracts | Sessions & Events

Thank You For Attending Neuroscience 2017

Neuroscience 2017 was held November 11-15 at the Walter E. Washington Convention Center in Washington, DC. More than 30,300 attendees convened in the United States capital city for the world's largest marketplace of ideas and tools for global neuroscience.

Join or renew your SfN membership now to get the best savings for Neuroscience 2018, November 3-7 in San Diego, CA.

› Meeting abstracts

› Program

› Event recordings

392.18 / BB2 - Blast-induced traumatic brain injury displays a unique pattern of spatial neuropathology

📅 November 13, 2017, 1:00 PM - 5:00 PM | 📍 Halls A-C

Presenter at Poster
Mon, Nov. 13, 2017, 2:00 PM - 3:00 PM

Session Type
Poster

Grant Support
DOD W81XWH-15-1-0303

Authors
*N. CHANDRA[1], R. R. KAKULAVARAPU, 07102-1982[2], D. Y. YOUNGER, 07102-1982[2], A. A. ARAVIND, 07102-1982[2], B. P. PFISTER, 07102-1982[2], M. KURIAKOSE[2], M. SKOTAK[2];
[1]Biomed. Engin., New Jersey Inst. of Technol., Morris Plains, NJ; [2]Biomed. Engin., New Jersey Inst. of Technol., Newar, NJ

Disclosures
 N. Chandra: None. R.R. Kakulavarapu: None. D.Y. Younger: None. A.A. Aravind: None. B.P. Pfister: None. M. Kuriakose: None. M. Skotak: None.

Abstract

Blast-induced Traumatic brain injury (bTBI) is a leading cause of morbidity and mortality in soldiers in the combat and in training sites and is becoming an important public health issue. The bTBI simultaneously causes primary (shockwave), secondary (penetrating), and tertiary (blunt-accelerative forces) injuries causing different loading modalities and pathological outcomes compared to pure blunt injury. The brain injury patterns resulting from primary shockwave propagation across different brain structures has not been carefully investigated. We hypothesize that bTBI has a unique histopatholgy and pathophysiology different from blunt TBI. In bTBI all the regions of brain from prefrontal cortex to hippocampus to cerebellum to brain stem are all simultaneously biomechanically loaded as the shock wave propagates unimpeded across the brain. This is different from the blunt TBI, where the injuries are mostly confined to the site of injury and nearby areas, the extent of which is dictated by the severity of blunt loading. Since oxidative stress has been implicated as a major pathogenic factor in TBI, here we examined the brain spatial resolution and cellular distribution of changes in superoxide producing enzyme NADPH oxidase1 (NOX1) as well as neurodegeneration paradigm during the early phase (4h) of moderate blast TBI (180 Kpa) and compared these data with that of moderate blunt TBI (FPI). Immunofluorescence analysis displayed that NOX1 was upregulated in different brain regions and showed a differential vulnerability with the highest increase found in hippocampus and thalamus followed by frontal cortex and cerebellum. Among different cells, neurons exhibit highest amount of basal NOX1 and its increase was higher in hippocampal and cerebellar regions compared to astrocytes and microglia. Interestingly, blunt injury induced in the cortical region did not display any change in NOX1 expression in cerebellum suggesting that the spread of the injury in blunt TBI is localized. Blast did not display neurodegeneration in any region, while blunt TBI showed focal neurodegeneration in the cortical and hippocampus areas only in ipsilateral side. These studies indicate that the injury pattern and pathological changes in blast TBI are unique and spread across the entire brain compared to blunt injuries.

141.03 / CC1 - Characterization of a combined model of blast and blunt injury

📅 November 12, 2017, 8:00 AM - 12:00 PM | 📍 Halls A-C

Presenter at Poster
Sun, Nov. 12, 2017, 10:00 AM - 11:00 AM

Session Type
Poster

Grant Support
New Jersey Commission on Brain Injury Research CBIR17PIL021

Authors

A. ARVIND, *B. J. PFISTER, R. KAKULAVARAPU, M. LONG, N. CHANDRA;
Dept Biomed Engin., New Jersey Inst. Technol., Newark, NJ

Disclosures

A. Arvind: None. **B.J. Pfister:** None. **R. Kakulavarapu:** None. **M. Long:** None. **N. Chandra:** None.

Abstract

Soldiers are often exposed to both primary blast waves and blunt impacts due to falls or vehicle crashes. While the cumulative effects of repeated exposure to a blast or blunt traumatic brain injury (TBI) has been under investigation, a combination of blast and blunt impacts has yet to be examined. Our hypothesis is a blast exposure, while not necessarily leading to a diagnosable injury, will predispose the brain to greater injury upon a second blunt injury to the head. Here, rats were exposed to primary blasts (130 KPa - mild or 180 KPa - moderate) followed by a moderate fluid percussion injury (FPI - 29-32 psi) to examine if a blast exposure would exacerbate the injury outcome of FPI in rats. The animals were first subjected to the blast then a craniectomy was performed while still under anesthesia and 24 hrs later, the rats were subjected to the FPI. Control groups of blast +craniectomy, FPI only and craniectomy alone were also generated. Time-matched to 4hr after FPI, coronal sections from all experimental groups were stained with fluoro jade C. Acute neuronal degeneration was observed in the cortex, hippocampus and thalamus regions of the animals subjected to the blunt and blast +blunt group while blast alone group showed no neurodegeneration. Neurodegeneration was more pronounced in cortical region in the mild and moderate blast +blunt groups than the blunt impact group alone, while respective controls (blast +craniectomy or craniectomy alone) did not show any neuronal degeneration. Neuronal degeneration at the FPI site of impact was observed to be more pronounced in the mild blast+blunt group than the moderate blast+blunt group animals. Hemorrhage was also observed in the moderate blunt and combined impacts than the blast impacts. Potential changes in apnea and the righting reflex are so far inconclusive. Our data indicate that a prior blast impact increases the induced neuronal degeneration from a subsequent blunt impact. Ongoing studies aim to identify the longer term effects on cell death as well as behavioral and biochemical deficits present in the combined model.

NSSW 2018

5th NATIONAL SYMPOSIUM ON SHOCK WAVES

February 26-28, 2018

– Organized by –
SOCIETY FOR SHOCK WAVE RESEARCH (INDIA)
– In collaboration with –
HIGH ENERGY MATERIALS SOCIETY OF INDIA CHANDIGARH-DELHI CHAPTER
– at –
Terminal Ballistics Research Laboratory
Sector 30, Chandigarh, INDIA

ANNOUNCEMENTS: NEW   NSSW 2018 Brochure Accepte

NSSW 2018

NSSW brochure	**Accepted papers**
Send Registration form immediately	**Oral and Poster Papers**
Programme	**Accommodation and Transportation details**
Request to visit hemsichd.org regularly for more updates	

NSSW 2018: 5th National Symposium on Shock Waves

Duration: 26-28 February 2018

Organized by: Society for Shock Wave Research (India) & High Energy Materials Society of India, Chandigarh-Delhi Chapter

Venue: Terminal Ballistics Research Laboratory, Sector 30, Chandigarh, INDIA [The symposium will be organized in Manthan Auditorium at TBRL Ranges about 22 km from Chandigarh on Chandigarh- Yamuna Nagar Highway (NH 73)]

Society for Shock Wave Research (India)
The society was formulated by Department of Aerospace Engineering Indian Institute of Science, Bengaluru, India to create awareness about shock wave science and its applications in different fields. The society is conducting bi annual national symposium and has conducted four national symposia on shock wave so far. The interaction and deliberations in these symposia has given way to many partnerships among the academia, R&D organizations and industries.

Topics
- Shock Generation Devices & Techniques
- Diagnostics and High Speed Instrumentation
- Modeling and Simulation of Detonation, Shock & Hypersonic Flow
- Underwater Shock Waves and Tsunami
- Ballistics and Shock Waves
- Shock Waves in Condensed Media
- Shock Waves in Porous, Composite and Geological Media
- Detonation and Shock Induced Chemistry
- Shock Tubes and High Temperature Chemical Kinemetics
- Blast/ Shock Mitigation
- Medical and Biological Applications

Call for Papers: Authors are invited to submit papers for the symposium. Selection will be on the based of quality of abstract. Best paper awards instituted by Society for Shock Waves Research will be given to best papers by students working in the area of Shock Wave research. Abstract submission should include title of paper, authors name, affiliation, keywords. The MS word format to be used along with pdf version for clarity of symbols used. The abstracts should be mailed to **nssw2018@gmail.com**

Important Dates
- First announcement – 31st July 2017
- Submission of abstracts – 30th September 2017
- Notification of acceptance – 31st October 2017
- Full Paper submission – 31st December 2017
- Registration – 31st January 2018

Registration Fee (Registration form in downloads)
Delegates from scientific / academic institutes - Rs.5000/-
Students - Rs. 1500/-   Members of SSWR/ HEMSI - Rs. 4000/-

Souvenir: A souvenir will be published comprising of abstracts and advertisements. All industry partners are invited to advertise their products and give impetus to the seminar.

Advertisement rates
Front cover inside: Rs. 50,000,   Back cover outside: Rs. 50,000
Back cover inside: Rs. 40,000, Full page: Rs. 25,000 Half page: Rs. 10,000

Exhibition: Exhibition of industrial products and models made by student/researcher. Fee Rs. 20000 per cubical (Area 2.5m x 2.5m and height 2.4 m. 2 chairs, 1 table and electric supply).

Payment Details: The registration fee and advertisement/exhibition charges can be deposited **directly to a/c no. 37030950725 at SBI, Sec-30, Chandigarh (IFSC Code: SBIN0001443) or by demand draft in favour of "The Chairman, NSSW-2018" payable at Chandigarh**.

Chandigarh- The City Beautiful
Chandigarh, the dream city of India's first Prime Minister, Pt. Jawahar Lal Nahru, was planned by the famous French architect Le Corbusier. Chandigarh 'The City Beautiful' is situated 250km north of New Delhi and is well connected by road, train and air.

Climate: Chandigarh weather in February is pleasant, generally dry and the temperature in between 10^oC to 25^oC.

Places to Visit:
- Chandigarh : Beautiful gardens (Leisure Valley, Bougainvillea Park, Zakir Rose Garden, Shanti Kunj, Hibiscus Garden, Botanical Garden, Topiary Garden and Terraced Garden and World Famous Rock Garden), Sukhana Lake
- Moghul Garden at Pinjore (20 km)
- Mussoorie 160 km, linked via road
- Shimla 100 km, linked via Road and Heritage Train
- Kasauli 60 km, linked via Road
- Manali 300 km, linked via Road
- Dharamshala 250 km, linked via Road

Important Contacts

Inderpal Singh Sandhu, Sc E, 99142 12403, 0173-3307304
Dr P K Soni, Sc F, 0173-3307204, A C Sharma, Sc G, 0173-3307503
TBRL, Sector 30, Chandigarh, Ph: 0172-3957117, Fax: 0172-2657506

Email: nssw2018@gmail.com;   Website: **www.hemsichd.org**

Important Reservation Websites to Plan Journey

By Air: www.airindia.in   **By Train**: https://www.irctc.co.in
By AC Luxury Bus: http://hartrans.gov.in/ors/
By AC Luxury Bus: http://www.punbusonline.com/

Blast Induced Neurotrauma-Current state of clinical and experimental progress

Namas Chandra[1], Ajay K Singh[2], Subash Khushu[2] and Raj Gupta[3]

Department of Biomedical Engineering, New Jersey Institute of Technology, New Jersey, USA

Institute of Nuclear Medicine and Allied Sciences, Delhi, India

U.S. Army Medical Research and Material Command, 504 Scott Street, Fort Detrick, MD

Abstract

Blast-induced Traumatic brain injury (bTBI) is a leading cause of morbidity and mortality in soldiers in combat and in training sites; it is becoming an important public health issue. The bTBI simultaneously causes primary (shockwave), secondary (penetrating), and tertiary (blunt-accelerative forces) injuries causing different loading modalities and pathological outcomes compared to pure blunt injury[a]. In this presentation, we will give an overview of the relationship between a charged explosive, stand-off distance and the resulting shock-blast wave that propagates outwards and the effect of reflections of ground, structures on the shock profile. We will then present some clinical data on soldiers in the acute and short- and long-term chronic stages. We will then present the current progress in the design and findings of experimental animal models[b,c]. We will show that the biomechanical load causes blood-brain barrier compromise and excessive production of oxidative stress; in turn, these trigger many neuroinflammatory cascades leading to many observed clinical pathologies and neurodegenerative diseases. We will finally outline the path forward in the determination of injury mechanisms and treatment strategies.

[a]N. Chandra, A. Sundaramurthy, R.K. Gupta, Validation of laboratory animal and surrogate human models in the primary blast injury studies, **Journal of Military Medicine**, 182, 3/4:105, (2017).

[b]V. Mishra, M. Skotak, H. Schuetz, A. Heller, J. Haorah, N. Chandra, Primary blast causes mild, moderate, severe and lethal TBI with increasing blast overpressures: Experimental rat injury model, **Nature-Scientific Reports**, **6**, 26992, (2016)

[c]E. Alay, M. Skotak, A. Misistia, N. Chandra, Dynamic loads on human and animal surrogates at different locations in compressed-gas-driven shock tubes, **Shock Waves**, 1-12, (2018)

Role of Advanced Imaging Methods in Mild Traumatic Brain Injury

Maria M D'Souza[1], Richa Trivedi[1], Amit Bagchi[2], Namas Chandra[3], Raj Gupta[4], Subhash Khushu[1], and Ajay Kumar Singh[1]

[1]Institute of Nuclear Medicine and Allied Sciences, Delhi, India

[2]Naval Research Laboratory, Washington, USA

[3]Department of Biomedical Engineering, New Jersey Institute of Technology, New Jersey, USA

[4]U.S. Army Medical Research and Material Command, 504 Scott Street, Fort Detrick, MD

Abstract

Traumatic Brain Injury (TBI) occurs when an external object interacts with the head in the form of blunt, blast or ballistic loadings. Though the biomechanics of each of these forms may be different, the resulting pathophysiological changes and hence cognitive, motor and behavioral consequences may parallel each other. Mild TBI, reported in almost 80% of the cases often goes undetected by conventional CT and MRI, yet has the potential to produce long-term symptoms and cognitive deficits. However, in this paper we show based on clinical observations that advanced imaging techniques are capable of deciphering mild TBI even when conventional CT and MRI images appear normal. Since imaging is essentially non-invasive and readily accessible to clinicians there is a pressing need for the development of objective measures that are more sensitive to the subtle alterations in brain morphology.

The joint Indo-US collaboration seeks to assess the utility of advanced imaging techniques in better understanding the pathophysiology of TBI which would thus facilitate the accurate diagnosis and prognostication of injured individuals. Among the more promising of these tools are advanced MRI (magnetic resonance imaging) techniques, particularly DTI (diffusion tensor imaging), fMRI (functional MRI), MR spectroscopy and SWI (susceptibility weighted imaging).

Brain trauma leads to diffuse axonal injury secondary to abrupt acceleration/deceleration and/or rotational/vibrational forces which cause axonal shearing. This has been characterized in this study by DTI, which provides an objective, quantifiable measure of axonal integrity. The subsequent functional disruptions in neural network communication are being assessed by resting state functional MRI (fMRI). SWI has been found useful to visualize traumatic micro-hemorrhages which are invisible to CT and conventional MRI. This collaborative study also assesses the severity of post-concussive symptoms and the level of cognitive deficit sustained in the chronic phase of injury. The preliminary results based upon an initial analysis of the mild TBI population that has been recruited so far demonstrates alterations in the structural integrity of multiple axonal tracts in the mild TBI population compared to a healthy control group and these alterations are associated with the severity of post-concussive symptoms. Reduced functional communication within two resting state networks, the default mode network and the somatomotor network has been observed in this cohort. Ongoing recruitment and additional analysis of the data will hopefully provide greater insights into the intriguing pathophysiology of TBI.

Experimental Model of Blast Shows Whole-brain and Regional Variations in Histopathology and Metabolomics profile

Poonam Rana[1], Rama Rao V. Kakulavarapu[2], Matthew Kuriakose, Subash Khushu[2] Richa Trivedi[1] and Raj Gupta[3], Namas Chandra[2]

[1]Institute of Nuclear Medicine and Allied Sciences, Delhi, India

[2]Department of Biomedical Engineering, New Jersey Institute of Technology, New Jersey, USA

[3]U.S. Army Medical Research and Material Command, 504 Scott Street, Fort Detrick, MD, USA

Abstract

Blast-induced Traumatic brain injury (bTBI) is a leading cause of morbidity and mortality in soldiers in the battle field as well as training sites and becomes an important public health issue. The bTBI is different from blunt TBI in that the shockwave generated by the blast diffuses throughout the brain while injuries caused by the blunt trauma are highly local. Although the primary mechanical injury itself caused by direct impact of the shockwave may perturb brain physiological homeostasis, the brain injury pattern resulting from shockwave propagation across different brain structures are not known.We have recently identified changes in blood-brain barrier (BBB) permeability in a rat mode of blast TBI as determined by extravasation of sodium fluorescein (NaFl, 376kDa), Evan blue (EB, 66kDa when bound to albumin) as well as disruption of vascular tight junction proteins (occludin and claudin 5) at as low as 70 kPa (10 psi) blast over pressure and the magnitude of BBB breakdown increases with BOP from 70 kPa, 130 kPa, 180 kPa. Such BBB disruption peaked at 4h post injury suggesting that secondary mechanisms (e.g., oxidative stress, neuroinflammation) activated by blast exacerbate the initial BBB damage caused by the shockwave itself. Our studies identified increased levels of NADPH oxidase (NOX), a plasma membrane bound superoxide producing enzyme at moderate blast 4h post injury throughout the brain including cerebellum and such increase displayed a regional variation and hippocampus showed highest increase. The BBB disruption and oxidative damage appears to cause long term metabolic effects as ^{1}H NMR spectroscopy of brain extracts collected at 24h, 3 and 7 days after animals exposed to moderate blast (180 kPa) using 600 MHz NMR spectrometer (Bruker Biospin, Switzerland) showed changes in various metabolites associated with energy metabolism (lactate, alanine, AMP, creatinine), membrane metabolism (choline, glycerophosphoethanolamine, phosphocholine) and osmolytes (betaine, myoinositol).The study further shows maximum changes at day 3 post blast exposure which continued till day 7 Taken together, BBB disruption appears to be a "signature" wound and an earliest response to blast injury which is exacerbated by secondary mechanisms including oxidative stress and these abnormalities cumulatively impact on brain metabolomics and contribute to the pathophysiology of blastTBI.

Validation of a compressed-gas driven shocktube against free-field shocks and a computational model

Molly Townsend[1], Priyanka Sharma[2], Maceij Skotak[1], Ajay Kumar Singh[2], Maria D'Souza[2], Subhash Khushu[2], Raj Gupta[3] and Namas Chandra[1]

[1]Department of Biomedical Engineering, New Jersey Institute of Technology, New Jersey, USA

[2]Institute of Nuclear Medicine and Allied Sciences, Delhi, India

[3]U.S. Army Medical Research and Material Command, 504 Scott Street, Fort Detrick, MD

Abstract

Compressed gas drive shock tube has been extensively used for the generation of shock-blast loading conditions, occurring in the field. There are numerous variations in the design and operation shock tubes to conduct animal experiments; and only a few of them are capable of replicating primary blast loading conditions[a]. Only a properly validated shock tube experimental platform can enable the controlled study of blast-induced traumatic brain injury. Robust validation of a compressed-gas driven shock tube entails comparison of the produced static and dynamic pressures with free-field shockwaves. The shock tube at the NJIT in the CIBM[3] has been validated for shockwaves synonymous with mild and moderate traumatic brain injury. This shock tube has been duplicated by INMAS under a joint US-India collaborative program. Although similar in construction, differences in available materials, ambient conditions, and animal origin may result in natural variability in shockwave propagation. Therefore, a computational model of the shock tubes has been developed and validated against the shock tube at CIBM[3]. With an accurate measurement of the burst pressure, the static and dynamic pressures can be accurately calculated, compared to experimental measurements, and validated with theoretical free-field experiments. The Eulerian finite element model is accurate for moderate blast overpressures (130 kPa) with errors less than 10%. With validation of this tool, validation of the new shock tube can be completed efficiently and inexpensively.

[a]N. Chandra, A. Sundaramurthy, R.K. Gupta, Validation of laboratory animal and surrogate human models in the primary blast injury studies, **Journal of Military Medicine**, 182, 3/4:105, (2017).

Altered Diffusion Indices of the Rat Brain Parenchyma after Mild Blast Induced Traumatic Neurotrauma (BINT)

Richa Trivedi[1], Priyanka Sharma[1], Maria M D'souza[1], Namas Chandra[2], Subash Khushu[1], Raj K Gupta[3], Ajay K Singh[1]

[1]NMR research Centre, Institute of Nuclear Medicine and Allied Sciences (INMAS), Delhi, INDIA;
[2]Department of Bio-Medical Engineering, New Jersey, USA;
[3]U.S. Army Medical Research and Matrial Command, Detrick, USA

Introduction: Blast injury has become the major cause of mortality and morbidity in recent warfares. It manifest as a complex of neuro-somatic damage, including blast induced traumatic neurotrauma (BINT). Early assessment and identification of extent of injury in reproducible experimental models of primary blast wave exposure is vital to the development of therapeutic strategies for blast victims. In vivo conventional MRI (magnetic resonance imaging) studies have failed to show any apparent cell death and tissue damage in mild BINT. But animal models of BINT have demonstrated resultant cellular dysfunction and behavioral short- and long- term deficits. Owing to neuropathological alterations and neuropsychological deficits in presence of normal conventional imaging, the present study aims to assess advanced imaging findings in acute phase of mild BINT.

Methods and Materials: Ten adult, male Sprague-Dawley rats (8-10 weeks, 200-250gms), housed (23°C±1°C, 50% ±5% humidity, and 12 h light/dark cycle) with free access to food and water were used during the study. All the 10 rats were exposed to 10 psi overpressure using an in-house developed shock tube.

MRI was performed in rats before blast exposure at day 0 (each rat served as its own control) and post exposer at 4 hours, 1 day, 3 days, and 5 days. All MR imaging was performed at a Bruker Biospec 7.0 Tesla. The MRI protocol included axial multislice Turbo RARE T2-weighted and DTI images. DTI measures were calculated from the brain parenchyma of exposed animals at all time points.

Results: A repeated measure ANOVA was performed to assess alterations in diffusion indices with time in different regions of brain. Injury induced decreased fractional anisotropy (FA) and mean diffusivity (MD) values were observed in the hippocampal region as compared to controls at all time points post exposure.

Discussion & Conclusion: To conclude, in absence of any signal abnormality on conventional T2 image of mild BINT rodent model, we found successive decreases in diffusion measures at acute time points in the hippocampal region as compared to controls. This may be due to trauma induced hypoxic- ischemic injury, cytotoxic edema and reactive astrogliosis. These findings support the use of mild BINT as a model to evaluate putative therapeutic options.

Military Health System Research Symposium

Medical Innovation for Warfighter Readiness: The Future Starts Now

Thank you for attending!

August 20-23, 2018
Gaylord Palms Resort & Convention Center | Kissimmee, FL

Join the Mailing List

Microglia-Vascular interactions with the Blood Brain Barrier following blast TBI

Daniel Younger[1], Kakulavarapu V. Rama Rao[1], Namas Chandra[1]
[1]Center for Injury Biomechanics, Materials, and Medicine, Department of Biomedical Engineering,
New Jersey Institute of Technology, Newark, NJ

Background

Traumatic brain injury (TBI) is a leading cause of death and disability in individuals due to variety of head injuries resulting from blast waves generated by detonation of explosives in combat zones, automobile accidents as well as injuries caused by a variety of sports events. Among these, blast-induced TBI is becoming a leading cause of morbidity and mortality in soldiers in the battle field as well as training sites. While primary mechanical injury caused by direct impact may perturb brain physiological homeostasis, down-stream propagation of various biochemical events leading to brain injury are not fully understood. Studies have revealed that Blood Brain Barrier disruption is a "signature wound" that initiates various pathological factors secondary to blast injury. Earlier it has been demonstrated that the injury severity of singular blast-induced traumatic brain injury (bTBI) increases with blast over pressures in a dose-response manner. The response to multiple blasts have not been studied in detail following injury, the central nervous systems innate immune system, composed of microglia cells, detect homeostatic changes to the brain parenchyma in response to mechanical damage through a diverse receptor system. Upon detection of danger associated molecules in the brain parenchyma through the compromised BBB, these cells activate and undergo morphological and biochemical changes that initiate several biochemical cascades such as oxidative stress and neuroinflammation. These biochemical cascades induce further damage to the neurons not caused by the initial mechanical insult.

Of several factors that induce brain pathology in TBI, neuroinflammation is an important pathway triggered by upstream factors including the activation of Toll-like receptor4 (TLR4) that transcriptionally activates the synthesis of pro-IL-1β, a precursor of inflammatory cytokine IL-1β. The resulting activation of NLRP3 inflammasome, an assembly of several proteins including apoptosis-associated speck-like protein (ASC1) and caspase-1 (IL-1β converting enzyme), induces the production of functional IL-1β. IL1-β promotes a variety of neuroinflammatory responses by altering cellular homeostatic events such as autophagy, a physiological process responsible for lysosomal-dependent degradation of senescent cytoplasmic proteins, intra-cellular organelles as well as toxic protein aggregates. A hallmark of defective autophagy is the accumulation of autophagosome marker LC3, a Microtubule-associated protein that fuses with autophagosome and promotes its degradation. Here we examined regional variations in the brain (frontal cortex, hippocampus, thalamus, visual cortex and cerebellum) levels of TLR4, pro-IL-1β, NLRP3 as well as the levels of autophagy marker LC-3 in acute phase (4h) of severe-blast TBI (180 Kpa) in rats. We hypothesized that the pathophysiological outcomes, particularly neuroinflammation in response to TBI, is initiated by microglia interaction with the BBB and is

dependent on the extent of blast over pressures and /or differential vulnerability of various brain structures.

Methods

Sprague-dawley rats (n=16, male, 350 ± 50g) were allocated into three groups (control, single blast, repeated blast) and exposed to a moderate shock wave of 180kPa or mild 5x 35 kPa in the helium-driven shock tube housed in CIBM3 at NJIT. Following blast injury, animals were closely monitored for any signs of trauma-related distress (apnea, loss of motor coordination). Neurological severity score was assessed five minutes' post exposure and none of the animals included in this study displayed scores that differed from control animals. All animals were euthanized via transcardial perfusion-fixation either four hours, 24 hours, and 28 days' post-exposure.

To evaluate the activation of microglia near blood vessels and the following blast injury, double immunofluorescence studies were conducted for Iba-1 and RECA-1 in the frontal cortex hippocampus, thalamus, visual cortex and cerebellum. Brains were extracted from cranial vaults and incubated in 4% PFA for additional 48 hours and cryoprotected by immersion in 30% sucrose before sectioning with Leica VT 1000S vibratome. Tissue sections (20 µm thick) were mounted on glass slides prepared from individual animals in each group were washed with 10 mM phosphate buffered saline (PBS), fixed in ice-cold methanol (100%) solution for 10 minutes at –20 °C. The tissue sections were blocked with 10% donkey serum at room temperature for 1 hour in PBS containing 0.03% Triton X-100. Fixed tissues were incubated overnight at 4 °C with respective primary antibodies to Iba-1 (goat polyclonal, Invitrogen, 1:250) and RECA-1 (Mouse monoclonal, Abcam, 1:50). The tissues were incubated in goat biotin from one hour. Double immunofluorescence was performed using streptavidin 488 for Iba-1 and Alexafluor 594 for RECA-1. Slides containing different brain regions were digitized (20x magnification) using Leica Aperio Versa 200 fluorescent microscope and slide scanner. Morphological changes and migration of microglia cells were analyzed manually by calculating soma size, processes length and number of cells near the compromised BBB.

To assess the downstream products of microglia activation levels of TLR4, pro-IL-1β, NLRP3 as well as the levels of autophagy marker LC-3 were assessed via western blot. Following perfusion with PBS, brains were excised from the cranial vaults, and micro dissected for individual regions and homogenized in ice using CellLytic-M (Sigma) using sonicator with probe amplitude set to 45%. Samples were then centrifuged at 14,000× g at 4^{0}C. The protein concentration in the samples was estimated by BCA method. Subsequently, 20 µg of protein per lane was loaded into 4–15% SDS-PAGE gradient gels (Bio Rad). Proteins separated according to their molecular size were then transferred onto PVDF membranes using Turbo Protein Transfer instrument (Bio Rad Laboratories) using manufacturer's instructions. Membranes were blocked with 5% milk dissolved in Tris-Buffered saline containing 0.1% Tween-20 (TBS-T) and incubated overnight at 4^{0}C with TLR4, antibody (Sigma-Aldrich) or Pro IL-1β antibody (Novus Biologicals) or NLRP3 (Abcam), ASC1, or LC-3 at a dilution of 1:1000. Bands were visualized using Western Pico Chemiluminescence Substrate (Thermo Scientific) on Chemi Doc Imaging System (Bio Rad Laboratories). For densitometric quantitation of western blots, images were digitized using a BioRad GS800 calibrated densitometer, and analyzed with BioRad Quantity One software.

Results

        Upon detection of compromised blood brain barrier microglia begin to activate which is characterized by a retraction of their radial processes, increase in soma size, and migration to the site of injury. As early as 4 hours following single moderate blast exposure (180 kPa) cells accumulated around the blood vessels of all sizes (10 – 120 microns in diameter) and remained in their active state for at least 7 days' post injury. Following repeated mild blast microglia remain in their active amoeboid state chronically 28 days following injury. Immunoblot analysis showed a regional variability in the protein levels of these markers with hippocampus displaying highest increase in TLR4, Pro-IL1 and NLRP3 protein levels. Additionally, bTBI caused a pronounced accumulation of LC3 protein in hippocampus, which suggests a defective autophagy, process likely mediated by increased neuroinflammation.

Conclusion

 These results build a connection between the breakdown of the BBB and microglia role in the production of the neuroinflammatory state found following bTBI. This data collectively suggests that moderate bTBI induces acute neuroinflammatory response by triggering a cascade of events potentially resulting in perturbations in autophagy that may represent an important neuropathological event in bTBI.

Role of Oxidative Stress on Blood-Brain Barrier Permeability Following Blast-Induced Traumatic Brain Injury

Matthew Kuriakose[1], Kakulavarapu V. Rama Rao[1], Namas Chandra[1]
[1]Center for Injury Biomechanics, Materials, and Medicine, Department of Biomedical Engineering, New Jersey Institute of Technology, Newark, NJ

Background

Blast-induced traumatic brain injuries (bTBIs) have become the most prevalent form of neurotrauma amongst military soldiers and a growing cause of injury in civilian populations due to increased acts of terrorism domestically and abroad. However, in spite of the increase in BINT studies, there are still significant gaps in understanding of how primary mechanical injury and subsequent secondary injuries manifest and contribute to the pathophysiology following blast. A recent survey reported that more than 30 phase III clinical trials aimed at targeting TBI have failed due to lack of a thorough understanding of blast injury pathology. Our group has attempted to elucidate the temporal and spatial neuropathology of bTBI as it pertains to two commonly identified pathological factors: oxidative stress and blood-brain barrier breakdown.

Oxidative stress has been implicated in multiple modes of TBI and is mainly induced by reactive oxidative species (ROS). These include, but are not limited to, superoxide ($O2\cdot-$), hydroxyl radical ($HO\cdot$), and hydrogen peroxide (H_2O_2). While a basal level of ROS participate in many physiological functions (cell growth, gene expression and signal transduction), an excess amount, as seen after injury, can be harmful. NADPH oxidase (NOX) is a multi-subunit enzyme that catalyzes the formation of superoxide radicals, from present molecular oxygen. Our recent studies have shown NOX isoform upregulation in different brain regions following blast injury and that neurons display highest increase in hippocampus compared to other neural cells.

Oxidative stress has also been linked to the breakdown of the blood-brain barrier (BBB), which is a selectively-permeable membrane separating the brain from the circulatory system. The BBB consists of tight junction complexes, which attach adjacent endothelial cells together, as well as a host of dynamically modulating cells including pericytes and astrocytes, which wrap around the endothelium. Similarly to oxidative stress, increased permeability of the BBB has been observed in several modes of TBI including closed cortical injuries, weight drop models, and blast models. We recently identified that direct mechanical loading imparted by blast injury is able to compromise BBB integrity and such BBB disruption further enhanced 4 h post-injury, perhaps due to the contribution of secondary mechanisms. Damage to the BBB was established through extravasation of tracers Evans blue and sodium fluorescein, the dislodging of tight junction proteins, and leakage of blood-borne cells into the brain parenchyma and vice versa. Since our recent studies established increased expression of NADPH oxidase (NOX) and a concomitant increase in the production of superoxide, we sought to examine the role of oxidative stress in the compromise of BBB integrity following blast injury. Accordingly, we investigated whether apocynin, which inhibits the assembly of NOX subunits and prevents its activation, exerts a protective role against BBB disruption following blast injury.

Methods

Adult (10-week old), male Sprague-dawley rats (n = 42, 350 ± 50g) were divided into three groups (control, blast, blast + treatment) and exposed to a moderate shock wave of 180kPa in the helium-driven shock tube housed in CIBM3 at NJIT. Animals in treatment group received intraperitoneal injection of apocynin (5mg/kg, Sigma-Aldrich) 30 minutes prior to blast exposure. Following blast injury, animals were closely monitored for any signs of trauma-related distress (apnea, loss of motor coordination). Neurological severity score was assessed five minutes post exposure and none of the animals included in this study displayed scores that differed from control animals. All animals were euthanized via transcardial perfusion-fixation four hours post-exposure. For extravasation studies, Evans

blue (2% solution dissolved in PBS, 0.002g/ml, 0.7ml delivered) was injected intravenously through tail vein two hours prior to euthanasia (two hours post-blast).

In order to evaluate the increase in NOX1 expression in vascular endothelial cells following blast injury, double immunofluorescence studies were conducted for NOX1 and RECA-1 in the frontal cortex. Brains were extracted from cranial vaults and incubated in 4% PFA for additional 48 hours and cryoprotected by immersion in 30% sucrose before sectioning with Leica VT 1000S vibratome. Tissue sections (20 μm thick) mounted on glass slides were prepared from individual animals and washed with 10 mM phosphate buffered saline (PBS), fixed in ice-cold methanol (100%) solution for 10 minutes at –20 °C. The tissue sections were blocked with 10% donkey serum at room temperature for 1 hour in PBS containing 0.03% Triton X-100. Fixed tissues were incubated overnight at 4 °C with respective primary antibodies to NOX1 (Rabbit polyclonal, Sigma-Aldrich, 1:400) and RECA-1 (Mouse monoclonal, Abcam, 1:50). Double immunofluorescence was performed using Alexafluor 488 for NOX1 and Alexafluor 594 for RECA-1. Slides containing different brain regions were digitized (20x magnification) using Leica Aperio Versa 200 fluorescent microscope and slide scanner. Fluorescence intensities in each region were quantitated using AreaQuant software (Leica Biosystems) and expressed as average fluorescence intensity/unit area.

Superoxide levels in different brain regions were measured using dihydroethidium (DHE) following previously established methods. Briefly, animals were injected with 5mg/kg DHE (Molecular probes, MA, dissolved in DMSO). Sectioning proceeded as described and fluorescent intensitites in each region were quantitated using slide scanner.

As a means to determine the abundance of tight junction proteins and matrix metalloproteinases in the brain tissue, ELISAs were performed in the cerebral hemisphere. Following perfusion with PBS, cerebrum was homogenized in CellLytic-M (Sigma) using sonicator on ice. Samples were then centrifuged at 14,000g at 4°C. The protein concentration in the samples was estimated bicinochoninic acid (BCA) method (Thermo Scientific, Rockford, IL). Samples were diluted in PBS and loaded onto specific ELISA plates for MMP3, MMP9, occludin, and claudin-5 (LSBio, Seattle, WA). Plates were read in microplate reader (Spectra Max i3, Molecular Devices) at wavelength of 450nm. Steps of ELISA were conducted in accordance with manufacturer instructions.

Results

Based on double immunofluorescence studies (NOX1 and RECA-1, endothelial cell marker), NOX1 is significantly upregulated in neurovascular endothelial cells four hours following moderate blast injury. This corresponds to an increase in superoxide production at this time point; however, the pretreatment with apocynin substantially reduces superoxide production following blast, due to the neutralization of present NOX enzymes. In injured groups, concentration of matrix metalloproteinase III and IX robustly increase in brain homogenates, but in the treatment group present similarly as sham animals. Integrity of the BBB was assessed with ELISA for tight junction proteins occludin and claudin-5 as well as a functional extravasation assay using Evans blue tracer. In blast groups, a significant reduction in tight junction protein abundance was observed, which concomitantly resulted in increased BBB permeability. Use of apocynin was demonstrated to protect the integrity of the tight junction complexes and thusly maintain control-like levels of BBB integrity.

Conclusions

This work elucidates the relationship between two commonly studied secondary injury mechanisms of blast-induced neurotrauma: oxidative stress and blood brain barrier breakdown. In the present study, oxidative stress is responsible for degradation of tight junctions and breakdown of the BBB, via catalysis of superoxide production and subsequent matrix metalloproteinase upregulation. However, pretreatment with apocynin, a NOX-inhibitor was shown to prevent degradation of the BBB.

Computational and Experimental Methods to Understand Traumatic Brain Injury Mechanisms

MT Townsend[1], M Skotak[1], N Chandra[1]
[1]Department of Biomedical Engineering, Center for Injury Biomechanics, Materials and Medicine, New Jersey Institute of Technology

Background

Conventional traumatic brain injury mechanisms rely on gross motion of the head and to predict injuries from a loading event. These injury mechanisms fail to predict injuries resulting from exposure to a primary blast, as these mild blast-induced traumatic brain injuries (mbTBI) are not always manifested with head accelerations[1]. Current experimental limitations preclude an understanding of the mechanical load experienced in the human brain. As the field of computational simulation advances, there is a potential to simulate the mechanism of injury in an anatomically realistic human head, enabling the development of blast-specific injury metrics. An important preliminary step in the creation of a high-fidelity computational model is to validate the loading and boundary conditions that are used to represent the primary blast. Therefore, this work uses a combined experimental and computational approach to validate the loading experienced by an instrumented realistic explosive dummy (RED) human head surrogate within a shock tube at a variety of blast overpressures and head orientations.

Methods

A RED head form was mounted to a Hybrid III neck surrogate and exposed to shock waves within a field-validated shock tube. The surrogate was exposed to shock waves of varying intensities (20-200 kPa) at three orientations with the blast, where the shock wave was travelling from anterior to posterior, laterally, and from posterior to anterior. Surface pressures were recorded at ten regions of interest on the surface of the head. Surface-measured reflected pressures were used as validation criteria for a hydrodynamics model of the experimental setup. The model was generated from the geometry of the RED head and the twenty-eight-inch shock tube. Surface reflected pressures were compared with experimental measurements, matching the rise times, peak intracranial pressures, durations, frequency content, and impulses in all three orientations. This validated the simulation inputs, enabling for the investigation of pressure and impulse contours on the simulated RED head.

Results

We demonstrate that the hydrodynamic simulation is capable of matching, with a high degree of accuracy, surface reflected pressures at various blast overpressures and surrogate orientations. Surface pressure measurements were found to be dependent on the alignment of the RED head, exhibited by a mean 22%±2.7% difference between the pressure measurements of the left and right eyes. The highest pressures were seen at areas of concavity, i.e. the eyes when the shock wave travelled in the anterior-posterior direction. As expected, good agreement was achieved between the simulation and the experimental reflected pressures. This resulted in highly accurate contour maps depicting the reflected pressures and impulses normalized with the input test conditions.

Conclusions

A computational model of the loading and boundary conditions was validated against shock tube experimentation with a surrogate head model. With confidence, we can now simulate how a

shock wave interacts with the geometry of a human head. This enables the creation of finite element models depicting the internal complexity of the human brain with the confidence that loading and boundary conditions within the simulation accurately reflect the experimental testing conditions at a wide range of blast overpressures and impulses. This work is an important set to the development of mbTBI-specific injury mechanisms.

References

1. Skotak M, Wang F, Alai A, Holmberg A, Harris S, Switzer RC, et al. Rat injury model under controlled field-relevant primary blast conditions: acute response to a wide range of peak overpressures. J Neurotrauma [Internet]. 2013;30:1147–60. Available from: http://www.ncbi.nlm.nih.gov/pubmed/23362798

Institute for Brain and Neuroscience Research

Institute News

IBNR Graduate Student / Post Doctoral Research Showcase

Thursday, March 29 2018 at 10 am to 2 pm in the NJIT Wellness and Events Center

Come and see the graduate and post doctoral students showcase thier hard work.

IBNR- Inaugural Seminar

"Robustness, Variability and Modulation in Neurons and Networks"

<u>Eve Marder, Ph.D.</u>
Professor of Biology at Brandeis University
Member of the U.S. National Academy of Sciences
Monday, April 17, 2017 at 10 am to 11:30am in NJIT Eberhardt Hall Room 112

IBNR Faculty Member Wins Distinguished Research Award

2017 CSLA Awards Ceremony Recipient

Horacio Rotstein
Department of Mathematical Sciences
2017 Distinguished Research Award

Come join us in celebrating our IBNR Faculty member at the 2017 CSLA Awards Ceremony will take place on **Tuesday, May 2, 2017, at 2:30 PM in the Campus Center Ballroom**. Please save the date and join us to celebrate the accomplishments of the CSLA community.

2017 CSLA Awards Ceremony & Recipients

Inauguration of the Institute of Brain and Neuroscience Research (IBNR)

Monday, March 6, 2017
Campus Center Atrium

Col. Sidney Hinds, M.D., MC
Brain Health Research Program Coordinator

Mechanisms underlying epileptogenisis following blast induced traumatic brain injury in rat model

Madhuvika Murugan[1], Vijayalakshmi Santhakumar[2,3], Namas Chandra[1]

1. Department of Biomedical Engineering, Center for Injury Biomechanics, Materials and Medicine, New Jersey Institute of Technology, Newark, NJ; 2. Department of Pharmacology, Physiology and Neuroscience, Rutgers New Jersey Medical School, Newark, NJ; 3. Department of Molecular Cell and Systems Biology, University of California, Riverside, CA

Blast-related traumatic brain injury (bTBI) is the signature injury of combat troops in recent wars and leads to long-term physical, mental and cognitive deficits. bTBI is defined as an injury due to "primary" blast wave exposure which is distinct from impact TBI which is caused due to blunt-force or impact. Although brain injury is a known precursor for the development of post traumatic epilepsy (PTE), the singular contribution of the primary blast wave to PTE remains unknown. Hence, the primary aim of this study was to investigate the effect of bTBI on epileptogenisis in a military-relevant rat model of bTBI. Interestingly, we found that rats subject to mild bTBI (130 kPa) developed abnormal changes in EEG oscillations with a decreased in theta and increase in gamma frequency oscillations. We also demonstrated that behavioral seizures in blast-exposed animals occurred earlier than controls following kainic acid administration. Post-blast injury induced neuronal death in the cortex corresponded with the epileptogenic phenotype seen in bTBI rats. Our results suggest that bTBI causes neuronal loss and changes in the neuronal circuitry that enhance neuronal excitability and contribute to epileptogenesis. This study will further our understanding of the mechanisms underlying bTBI-induced seizures and help identify targets for improved therapeutic solutions.

Development, Convergence, and Validation of a Rat Finite Element Model Applicable to the Investigation of Blast-Induced Traumatic Brain Injury

Debrina Roy, Dr. Molly Townsend, Dr. Maciej Skotak, Dr. Namas Chandra

Experimental investigation into the complex nature of blast-induced traumatic brain injury is best accomplished using animal models. Additionally, concurrent and accurate use of the finite element method provides additional insights into the mechanics of injury that are difficult to investigate using experimental techniques alone. Therefore, a finite element model of a rat head and brain is under development for use in the understanding of injury mechanisms resulting from blast-induced traumatic brain injury. A three-dimensional geometrical model of the rat head, skull, and brain was developed by segmenting and combining several high-resolution magnetic resonance images and computed-tomography scans. Five major internal brain anatomical structures were partitioned based on scalable brain atlases. This resulted in a finite element model, which was subjected to an experimentally-relevant shockwave and the strain, pressure, and internal energy were converged. An extensive literature search was conducted to determine the appropriate constitutive material models and material properties of the rat brain at high strain rates. Ideal material properties were isolated using a sensitivity analysis, determining the parameters to which the model was most sensitive. Model validation was achieved through matching simulated intracranial pressure profiles with those obtained using experimental methods. The results of this work elucidate the relationship between the founded material properties and the biomechanical representation of differing brain regions and their responses to shockwave transmission. This work presents a high-fidelity model of a rat head under shock loading that will enable research into the connection between mechanical loading of brain regions and blast-induced traumatic brain injury.

The limitations of a modeling shockwave development in a shocktube using commercially available finite element tools

Molly T. Townsend, PhD and Namas Chandra, PhD

The compressed-air driven shocktube is a powerful research tool that, when properly designed, operated, validated, and calibrated, is capable of reliably replicating free-field primary blast waves. However, variations in design and experimental procedures between experimental facilities make the validation process arduous and expensive. To this end, a computational model capable of simulating various shocktube configurations is being developed, to enable validation of shocktube experimental setups with other shocktubes and minimizing the need for free-field validation. A finite element model of the CIBM[3] shocktube was created and the output of the model was compared to experimental data. The Eulerian model was developed that enables simulation of a shockwave, using only ambient atmospheric conditions, the driver gas, the shocktube shape, and the burst pressure. Methods of increasing the fidelity of the baseline model were investigated to improve validation by eliminating model assumptions. The baseline model matches (<10% error in pressure measurements) experimental conditions at 130 kPa overpressures. It proved to be limited in the prediction of lower and higher blast overpressures, unacceptably underpredicting pressures at lower blast overpressures (100 kPa) and overpredicting pressures at higher blast overpressures (240 kPa). Upon increasing model fidelity, results indicate that the assumptions investigated, including membrane inclusion, gas mixture ratio, and temperature variability, cause the model prediction to deviate from experimental results further. Initial conclusions indicate that the error may exist in the gas flow constitutive equations used by the commercial finite element solver. Work is ongoing to circumvent the native constitutive equations to implement a higher fidelity numerical approximation of the mechanics.

About Us   Centers   Faculty   Funding   Resources   Meetings & Seminars   Support BHI

Home   Meetings & Seminars   The Third Annual Rutgers Brain Health Institute Symposium

The 2017 BHI Symposium will be held at Raritan Valley Community College, 118 Lamington Road, Branchburg, NJ on Friday, December 1, 2017.

The day long-symposium will feature **Dr. Regina Carelli** from University of North Carolina at Chapel Hill as the Keynote speaker. Rutgers faculty awarded the 2016 BHI-RUN-NJIT Pilot Grant Awards will present their work. A poster session will be held at the end of the day; please submit no more than one poster from each lab. The top three posters will receive cash prizes ($150, $75 and $50).

The registration fee includes continental breakfast, buffet lunch and a wine & cheese reception at the end of the day. Round transportation will be provided from Newark and Piscataway for a fee.

On-site <u>**cash only**</u> **registration will be available (Faculty: $60; Student/Post-Doc/Staff: $25)**

Directions to Raritan Valley Community College (https://goo.gl/maps/weQa6L5uwq42)

Agenda for Third Annual Rutgers BHI Symposium

8.00 AM – 8.30 AM	**Registration and Breakfast**
8.15 AM- 8.30 AM	Welcome by Dr. Gary Aston-Jones (BHI Director), Dr. Nabil Adams (Vice-Provost for Research Rutgers-Newark), Dr. Robert Weider (Provost-New Jersey Medical), Dr. Atam Dhawan (Senior Vice Provost for Research, NJIT)
8.30 AM – 9.00 AM	**Gary Aston-Jones** *(Director, Brain Health Institute)* *BHI Overview and Updates*
9.00 AM - 9.10 AM	**Kelvin Kwan** (RU-SAS-Cell Biology & Neuroscience) *A Bio-Inspired Transcription Factor for Spiral Ganglion Neuron Regeneration*
9.15 AM – 9.25 AM	**Teresa Wood** (RBHS-NJMS-Pharmacology, Physiology & Neuroscience) *Delineating Oligodendrocyte Progenitor Subtypes and their Roles in CNS Remyelination*
9.30 AM – 9.40 AM	**Morgan James** (BHI) *Designer Receptors: A novel potential therapeutic for management of trigeminal neuropathic pain*
9.45 AM – 9.55 AM	**Viji Santhakumar** (RBHS-NJMS-Pharmacology, Physiology & Neuroscience) *Novel model targeting Semaphorin-Neuropilin Signaling in Inhibitory Circuit Development to examine mechanisms of Pediatric Epilepsy-Autism Comorbidity*
10.00 AM – 10.10 AM	***Madhuvika Murugan*** (NJIT) *Biomechanical differences in injury rate determine neurological outcomes after blast and impact TBI*
10.15 AM – 10.25 PM	**Neha Sinha** (RU-Newark)

Blast and brain injury research at the Center for Injury Biomechanics materials and medicine at NJIT

Madhuvika Murugan, Daniel Younger, Maciej Skotak, Rama Rao, Bryan Pfister, Namas Chandra
Department of Biomedical Engineering, Center for Injury Biomechanics, Materials and Medicine, New Jersey Institute of Technology, NJ

Brain injuries can be caused from impacts in automotive or sports accidents in the civilian world or blast related neurotrauma in the defense world. The injury produces short and long term neurological and behavioral dysfunctions and has serious economic and emotional consequences to the victim and their families. In our Center, we have developed unique facilities that accurately recreate impact and blast events using drop towers and field validated shock tubes. We have also developed animal injury models with capabilities to examine pathophysiological and behavioral effects of these injuries. Using these models, we have identified biomechanical and biochemical mechanisms. These findings have been used in the enhancement of better protection systems and in the development of new biomarkers, and therapeutics.

Mechanisms underlying epileptogenesis following blast induced traumatic brain injury in rat model

Madhuvika Murugan1, Bogumila Swietek2, Vijayalakshmi Santhakumar2, Namas Chandra1

1Biomedical Engineering, Center for Injury Biomechanics, Materials and Medicine, New Jersey Institute of Technology, NJ;
2Pharmacology, Physiology and Neuroscience, Rutgers New Jersey Medical School, NJ.

Blast-related traumatic brain injury (bTBI) is the signature injury of combat troops in recent conflicts and leads to acute and chronic physical, cognitive and behavioral dysfunctions. bTBI is defined here as an injury due to pure shock wave exposure and impact TBI (iTBI) as injury due to blunt body impact or inertia. Although iTBI is known to contribute to the development of post traumatic epilepsy (PTE), the risk for PTE following bTBI is not known. Hence, the primary aim of this study was to investigate the effect of bTBI on epileptogenesis in a military- relevant rat model of bTBI. bTBI can be classified as mild, moderate or severe based on the magnitude of blast
overpressure. In this work, we found that rats subject to mild bTBI developed abnormal EEG patterns and demonstrated behavioral seizures earlier than controls following kainic acid administration. Post-injury induced neuronal death and neuronal excitability changes in the dentate gyrus corresponded with the epileptogenic phenotype seen in bTBI rats. We further compared our results from bTBI model with a known model of iTBI- induced seizures (lateral fluid percussion injury- LFPI), in order to evaluate the effect of biomechanical differences in determining the neurological outcomes. Our results suggests that similar to the LFPI model, bTBI
causes an axonal and ischemic pathology that enhance hippocampal dentate excitability and contribute to epileptogenesis. This study will further our understanding of the mechanisms underlying bTBI-induced seizures and help identify targets for improved therapeutic solutions.

Name: Mid Atlantic Brain Research
Conference

Date: April 17, 2018

Time: 3:00 PM - 6:00 PM EDT

Event Description:

Registration is now closed--Walk-ins welcomed.

New Location: Please note the address is 675 Route 1 SOUTH not North

Commercialization Center for Innovative Technology
675 Route 1 SOUTH
North Brunswick, NJ 08902

This conference will give an overview of brain research in the region and begin to establish a network among researchers.

Agenda

3:00 to 4:15 - Call for Presentations

Presentations will be made in several groupings from the following companies and universities:

Brain Sensing Technologies
Arlene Ducao, CEO, Multimer, Brooklyn. NY
PainQx, Philadelphia, PA
Prof. Arnold Glass, Rutgers University

Neuro-Degenerative Therapies
Kira Sheinerman, Co-Founder & CEO, DiamiR Biosciences, Monmouth Junction, NJ
Jeffrey T Apoter, Medical Director, Princeton Medical Institute, Princeton, NJ
Dr. Ilena Soto, Rowan University

Traumatic Brain Injuries

Madhuvika Murugan, Postdoctoral Associate, New Jersey Institute of Technology
Dr. Milan Toma, Assistant Professor, New York Institute of Technology
David Devilbiss, Assistant Professor, Rowan University
Linda Edwards, ResilientMe, Inc./IASIS MicroCurrent, Rumson, NJ

Cutting Edge Advances

Lamar Mair, CTO, Neuroparticle Corporation, North Bethesda, MD
Dr. Mimi Phan, Professor, Rutgers University

4:15 PM to 4:30 PM - Break & Posters

4:30 to 5:15 pm - Panel 1

Future Opportunities and Challenges in Brain Science
Dr. Gary Aston-Jones, Director of the Rutgers Brain Health Institute
Hasan Ayaz, PhD, Associate Research Professor, School of Biomedical Engineering, Science and Health Systems, Drexel University
Michael Shelanski, MD, PhD, Henry Taub Professor of Pathology and Cell Biology, Co-Director of the Taub Institute for Research on Alzheimer's Disease and the Aging Brain & Senior Vice Dean for Research, Columbia University

5:15 - 6 pm - Panel 2:
Big Data: Analyzing High-Dimensional Brain Datasets
Konrad Kording, Penn Integrates Knowledge Prof in Neuroscience and Bioengineering, University of Pennsylvania
Jonathan Miller, PainQX
Eleftheria K Pissadaki, PhD, Computational Neuroscientist, Parkinson's Disease Etiopathology Expert, IBM T.J. Watson Research Center

Share:

To Current Calendar

Location:
New Location:

Commercialization Center for Innovative Technology
675 Route 1 SOUTH
North Brunswick, NJ 08902
View a Map

Contact Information:

Send an Email

Fees/Admission:

NJTC Members: $20
Future Members: $40

Set a Reminder:

Enter your email address below to receive a reminder message.

Enter Email Address

-- Select Days Before Event --

Go

To Current Calendar

Multidisciplinary Approach to Understand the Pathology of Blast induced Traumatic Brain Injury

Madhuvika Murugan1, Maciej Skotak1, Rama Rao1, Molly Townsend1, Bryan Pfister1, Namas Chandra1
1.   Department of Biomedical Engineering, Center for Injury Biomechanics, Materials and Medicine, New Jersey Institute of Technology, Newark, NJ

The goal of the Center for Injury Biomechanics, Materials and Medicine is to help understand the pathology underlying traumatic brain injury (TBI) using a multidisciplinary approach. A key focus is to identify the signature pattern for impact and blast injuries, which will help civilians, soldiers and athletes suffering from a particular form of injury. The Center is equipped with facilities that accurately recreate impact and blast events using drop towers and field validated shock tubes. Primarily, the research team conducts testing of protective equipment for protection against impact and blast injuries. In addition, the team has developed an array of biochemical, histology and molecular assays to quantify injury severity and investigate the extent of brain damage following TBI. Of particular interest is trauma-induced changes to the blood brain barrier permeability, which can be used as a biomarker for diagnosis of blast-induced mild TBI. Further, neurobehavioral and electrophysiological (EEG) studies show the manifestation of blast-TBI in pathologies such as post-traumatic mood-disorders and epilepsy, respectively. Computational models have been applied to various aspects of the studies, including generation of predictive tools to determine injury severity in blast-TBI patients based on biological experiments. Taken together, our findings have been used in the enhancement of better protection systems and in the development of new biomarkers and therapeutics.

Blast-induced Traumatic Brain Injury Displays a Unique Pattern of Spatial Resolution of Brain NADPH oxidase

Namas Chandra[1], K V Rama Rao[1], Stephanie Iring[2], Daniel Younger[1], Aswati Aravind[1], Bryan Pfister[1], and Maciej Skotak[1]
[1]New Jersey Institute of Technology, Newar, NJ, [2]New Jersey Institute of Technology, Newark, NJ

Introduction: Blast-induced Traumatic brain injury (bTBI) is a leading cause of morbidity and mortality in soldiers in the combat and in training sites and is becoming an important public health issue. The bTBI simultaneously causes primary (shockwave), secondary (penetrating), and tertiary (blunt-accelerative forces) injuries causing different loading modalities and pathological outcomes compared to pure blunt injury.

Materials and Methods: The blast loading on the rodent model was generated using a field-validated shock tube that is capable of producing shock blast overpressure-duration in the range of 60-400 kPa, 2-7 milli-seconds duration. 10-week old male Sprague-Dawley rats were subjected to a blast overpressure of 180kPa which falls within the range of mild-moderate bTBI as determined by our group. 6 animals were subjected to these pressures while 6 other animals served as sham. The protein levels of NOX1 in neurons, astrocytes and microglia in different brain regions (20 µm sections obtained from proximal to distal areas) including frontal cortex, striatum, somatosensory barrel cortex, thalamus, hippocampus and cerebellum was determined by double-immunofluorescence analysis. Image acquisitions were performed using Leica Aperio Versa 2000 fluorescent microscope attached with Digital Pathology Scanner and image quantitation was carried using FLAreaQuantV1 algorithm.

Results and Discussion: Immunofluorescence analysis of overall expression of NOX1 in different regions following bTBI showed the greatest increase in hippocampus (170%) followed by thalamus (140%), frontal cortex (48%) and cerebellum (35%). However, NOX1 levels did not change in striatum and brain stem. Evaluation of cell specific expression of NOX1 showed highest level of NOX1 in neurons as compared to astrocytes and microglia. Noteworthy that regions such as cerebellum and hippocampus which are known to contain higher density of neurons showed greatest increase in the levels of NOX1 following bTBI.
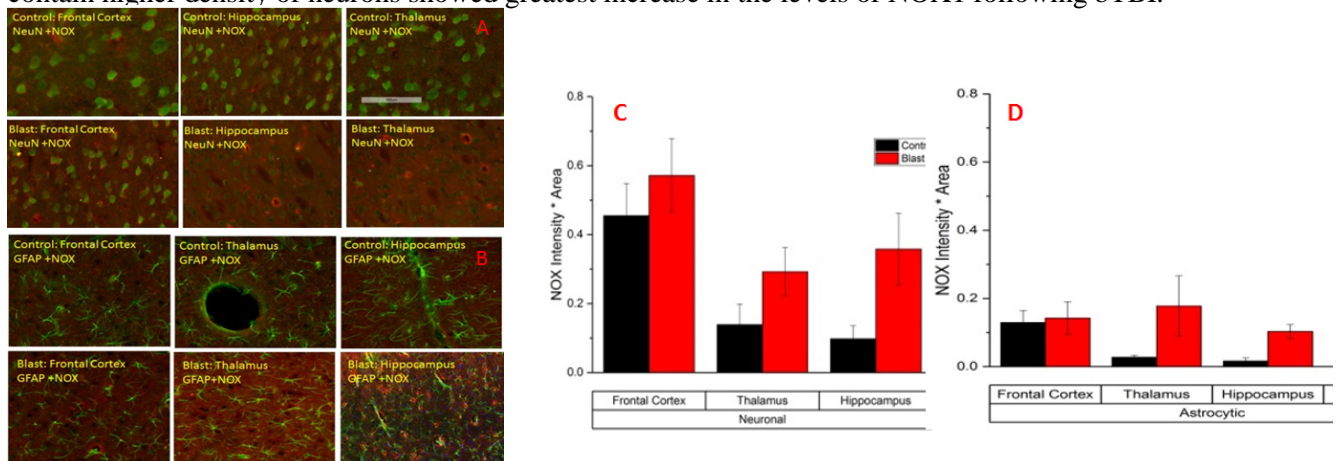

Figure 1: A &B. Doubleimmunofluorescence of NOX1 with NeuN (showing neuronal localization) and GFAP (showing astrocytic localization) in different brain regions following blast-TBI. C&D: Quantitation fluorescence intensities of co-localized NOX with NeN and GFAP showing NOX1 is mainly localized in neurons.

The regional vulnerability to oxidative damage (increased NOX1 expression) by bTBI is dictated not only by the uniform propagation of the shockwave throughout the brain regions, but also dependent on differential vulnerability of diffent brain structures to the injury. The cellular density and cell types distribution also play a vital role in the regional vulnerability in regions with greater density of neurons showed higher increase in NOX1. Further. Higher level of increase in NOX1 in neurons compared to glial cells (astrocytes and microglia) indicates that neurons are far more vulnerable to oxidative damage in bTBI. Such higher vulnerability for neurons may in part be due to lower antioxidant capacity of neurons as compared to glial cells.

Assessment of Cerebellar Injury in Rats Using Evoked Potentials and a Behavioral Task

Ahmet S. Asan[1], Gokhan Ordek[1], Esma Cetinkaya[1], Maciej Skotak[1,2], Venkata R. Kakulavarapu[1,2], Namas Chandra, and Mesut Sahin[1]
1 Department of Biomedical Engineering, NJIT, Newark, NJ 07102, USA
2 Center for Injury Biomechanics, Materials and Medicine, NJIT, Newark, NJ 07102, USA

Introduction: Understanding of the underlying cellular and pathophysiological mechanisms in traumatic brain injury (TBI) is important for deciding on therapeutic interventions. The cerebellum, in particular, can be affected during a TBI event even though the initial biomechanical loading is directed to a different region of the brain. Patients with cerebellar injury show motor and cognitive deficits. Electrophysiological and behavioral assessment tools can be utilized to detect acute and subacute phases of injury progression after the traumatic event. We hypothesized that evoked potentials (EPs) of the cerebellar cortex can be a sensitive measure capable of detecting even mild level cerebellar injuries before a functional deficit can be observed in behavioral tasks. The blast injury model was employed. In order to assess the impact of injury on the cerebellum, pre- and post-injury sensory EPs collected from the paramedian lobule (PML) of the cerebellum, and the horizontal ladder walking behavior were investigated.

Materials and Methods: A flexible 32-contact multi-electrode array (MEA, NeuroNexus) was implanted subdurally on the PML cortex of the right cerebellum under isoflurane anesthesia. Three Long Evans rats (250-350 g) were used in this study. All procedures were approved and performed in accordance to the guidelines of the Institutional Animal Care and Use Committee, Rutgers University, Newark, NJ. After completely recovering from surgery, the rats were anesthetized again with ketamine/xylazine cocktail (50/10 mg/kg, IP) for collection of EPs. A mechanical stimulation was applied to the animal's ipsilateral hand and the EP signals were recorded as a baseline before the blast injury. As the behavioral paradigm, horizontal ladder walking was employed. The rungs were arranged with irregular spacing to make the ladder walking a challenging task. The number of misses during the foot placements on the rungs and the falls were scored. Animals were trained until they crossed the ladder without hesitation in about one week. Then, the rats were exposed to a mild blast (overpressure of 130kPa) using a field validated shock tube at the Center of Biomechanics, Materials, and Medicine (CIMB[3]) of NJIT, and changes in the EPs as well as the behavioral performances were analyzed. The EP data collection under anesthesia was repeated 1, 3, and 7 days after injury. In a separate group of animals, the immunohistological evaluations were performed at one day post-injury.

Results: No significant differences were detected between pre- and post-injury measures using behavioral and histological assessments. On the contrary, evoke potentials allowed us to monitor the progression of cerebellar injury with reproducible signals and significant changes observed on different time points of the post-injury period. Amplitudes of the climbing fiber mediated EP components decreased and the latencies increased as a result of injury.

Conclusion: Mild cerebellar injuries that are too subtle to be detected in a behavioral task can be assessed using evoked potentials of the cerebellum recorded from its cortex, and can be used as a tool to identify TBI injury severity.

Blood-brain barrier permeability is a sensitive neurological marker for single and repeated occupational low-level blast exposures in a rodent model

Namas Chandra[*1], Rama Rao V. Kakulavarapu[1], Maciej Skotak[1], and Matthew Kuriakose[1]

[*]Distinguished Professor of Biomedical Engineering

[1]Center for Injury Biomechanics, materials and medicine, and Department of Biomedical Engineering, New Jersey Institute of Technology, Newark, New Jersey, 07950

Military service members are repeatedly exposed to blasts from a broad array of weapons (e.g., recoilless rifles, howitzers, rifles and hand grenades) during training and in combat. Additional threat of exposure exists in active war zones, from a variety of high-explosive sources: primarily the IEDs, a weapon of choice in the asymmetric warfare. Neurotrauma resulting from these blasts is caused by blast overpressures (BOP) in the range of 15 kPa to 300 kPa. Currently, there are no established diagnostic criteria for acute and chronic effects associated with occupational low-level multiple blasts due to lack of consistent clinical or experimental data. The design of diagnostic and protective measures calls for a dose-response curve that relates a single and multiple exposures to measurable and sensitive neurological marker(s). We have developed a dose-response curve for a rodent model in the range of a single BOP of 15 to 400 kPa based on 24-hour survival in a live-fire, field validated shock tube.

We hypothesize that injury severity is directly proportional to not only the intensity of BOP but also to the number of and the duration between exposures, i.e., there will be the higher propensity of severe injury outcome when a person has been exposed to the second blast early in the recovery phase. Accordingly, the pathological, cognitive and behavioral changes occurring in repeated blasts will be determined by the intensity of BOP, the number of and the time interval between exposures and post-injury elapsed time. We have recently identified changes in blood-brain barrier (BBB) permeability in a rat model of blast TBI using extravasation of sodium fluorescein (376 Da) and Evans blue (70 kDa, as albumin conjugate) disruption of vascular tight junction proteins (occludin and claudin-5) at 70 kPa (10 psi) BOP. The extent of BBB breakdown correlates with BOP intensity in the 70 kPa - 240 kPa range. We observed the BBB breakdown immediately (less than 15 minutes) after the injury, which indicates it is a direct result of biomechanical force can cause the vascular rupture mediated by dislodging of tight junction proteins. Such BBB breakdown right after exposure continues to persist for 24 hours triggering inflammatory cytokines and activating immune microglia/macrophage and oxidative damage pathways. The threshold for BBB permeability using extravasation of tracer molecules in a single blast exposure is 35 kPa BOP. However, exposure to five blasts with the same intensity within five minutes showed robust blood permeability into the brain comparable to the results observed at higher BOPs for a single exposure scenario. These results indicate that even exposure to a very low-level blast, when repeated successively will have a cumulative effect that can trigger measurable neurological events. In our innovative ongoing studies, we are modulating the injury severity by varying the blast overpressures, the number of repetitions and the time interval between exposures to understand and characterize repeated occupational low-level blast exposures.